LOW COST HYPERMIXING EJECTOR RAMJET PROGRAM

Joseph G. Bendot, et al

Marquardt Company

Prepared for:

Aerospace Research Laboratories

June 1975

UNCLASSIFIED

SECURITY CLASSIFICATION OF THIS PAGE (When Data Entered)

REPORT DOCUMENTATION PAGE		READ INSTRUCTIONS BEFORE COMPLETING FORM
1. REPORT NUMBER ARL 75-0219	2. GOVT ACCESSION NO.	3. RECIPIENT'S CATALOG NUMBER
4. TITLE (and Subtitle) LOW COST HYPERMIXING EJECTOR RAMJET PROGRAM		5. TYPE OF REPORT & PERIOD COVERED Final 15 June 1973-10 February 1975 6. PERFORMING ORG. REPORT NUMBER S-1322 A
7. AUTHOR(s) Joseph G. Fendot Wallace G. Harkins Thomas G. Piercy		8. CONTRACT OR GRANT NUMBER(s) F33615-73-C-4093
9. PERFORMING ORGANIZATION NAME AND ADDRESS The Marquardt Company 16555 Saticoy Street Van Nuys, California 91409		10. PROGRAM ELEMENT, PROJECT, TASK AREA & WORK UNIT NUMBERS Project No. 7116 0268 DOD Element 61102F
11. CONTROLLING OFFICE NAME AND ADDRESS Aerospace Research Laboratories /LE Building 450 - Area B Wright-Patterson Air Force Base, Ohio 45433		12. REPORT DATE June 1975 13. NUMBER OF PAGES 196
14. MONITORING AGENCY NAME & ADDRESS(if different from Controlling Office)		15. SECURITY CLASS. (of this report) Unclassified 15a. DECLASSIFICATION/DOWNGRADING SCHEDULE

16. DISTRIBUTION STATEMENT (of this Report)

Approved for public release; distribution unlimited.

17. DISTRIBUTION STATEMENT (of the abstract entered in Block 20, if different from Report)

18. SUPPLEMENTARY NOTES

19. KEY WORDS (Continue on reverse side if necessary and identify by block number)

Hypermixing
Ejector
Turbulent Mixing
Streamwise Vortices
Annular Ejector
Mixing Length
Ejector Ramjet

20. ABSTRACT (Continue on reverse side if necessary and identify by block number)

The Air Force Aerospace Research Laboratories (ARL) recently made a technology breakthrough in the field of turbulent mixing. ARL experiments indicated that the spreading rate of a subsonic jet may be increased dramatically by the introduction of streamwise vortices in the flow. These vortices promote efficient turbulent mixing within an extremely short distance, i.e., hypermixing. The basic objective of this program was to assess the payoff, if any, of applying hypermixing ejector technology to the design of a low cost ejector ramjet engine. Three variations of the ejector

DD FORM 1 JAN 73 1473 EDITION OF 1 NOV 65 IS OBSOLETE

UNCLASSIFIED

SECURITY CLASSIFICATION OF THIS PAGE (When Data Entered)

20. ramjet engine cycle were evaluated at the engine design point of Mach 0.75 @ 20000 feet altitude. The fuel addition-mix/diffuse/burn cycle variation was clearly superior. The selected fuel was UDMH. Engine performance was estimated for the specified flight envelope, Mo = 0.70 to 1.20 and sea level to 30000 feet altitude. An annular ring ejector which incorporated hypermixing technology was designed, fabricated, and experimentally evaluated. Test results showed no improvement with the hypermixing ejector as compared to a conventional annular ejector. The test ejector was then modified. A second test series showed this modification to be very effective. Full mixing (maximum mixer total pressure) was achieved in one half the length required for the annular/initial hypermixing ejector. At the ejector design point, full mixing was accomplished in 1.7 duct diameters.

PREFACE

The "Low Cost Hypermixing Ejector Ramjet Program" was performed for the Air Force/Aerospace Research Laboratories by The Marquardt Company under Contract F33615-73-C-4093. The basic objective of this program was to assess the payoff, if any, of applying hypermixing ejector technology to the design of a low cost ejector ramjet engine. The work described herein was accomplished during the period of June 15, 1973 to 10 February 1975.

Major Thomas Meier was largely responsible for initiating this program. Lt. Robert Boyle was the program manager through evaluation of the initial ejector design. Dr. Hermann Victs was the program manager of the highly successful modified ejector phase of this program.

The effort at The Marquardt Company was conducted under the supervision of Joseph G. Bendot. Thomas G. Piercy conducted the engine preliminary design studies and evaluated much of the test data. The development engineer was Wallace G. Harkins. William R. Hammill and Eric N. Gothric designed the flight engine and ejector test items.

Special acknowledgment is given to Jeanette A. Yocham who typed this report.

TABLE OF CONTENTS

LIST OF ILLUSTRATIONS

LIST OF TABLES

SECTION 1

INTRODUCTION

The Air Force Aerospace Research Laboratories (ARL) recently made a technology breakthrough in the field of turbulent mixing. Experiments at ARL indicated that the spreading rate of a subsonic jet may be increased dramatically by the introduction of streamwise vortices in the flow. See Figure 1. The vortices promote efficient turbulent mixing within an extremely short distance. One possible source of such a "hypermixing" jet is a segmented slot nozzle. Adjacent slots are skewed slightly from the flow direction to impart streamwise vorticity. To date the envisioned application of such nozzles has been in ejector flap and augmentor wing concepts for improved V/STOL aircraft designs.

The basic objective of this program was to assess the payoff, if any, of applying hypermixing ejector technology to the design of a low cost ejector ramjet engine. In this application, the ejector primary flow is supersonic. Hypermixing ejector nozzle technology offered the potential advantage of more rapid mixing with the ramjet engine airflow. If this were the case, mixer length could be reduced and/or the primary nozzle could be simplified by the reduction in the number of primary nozzles required to achieve full mixing. In either case, engine length, weight, and/or cost reductions could be realized through application of this technology.

Following a design and analysis phase to select the preferred ejector ramjet engine cycle/propellant(s), an experimental program was conducted to establish the rapidity of mixing downstream of a primary ejector nozzle system which incorporates the hypermixing technology developed by ARL.

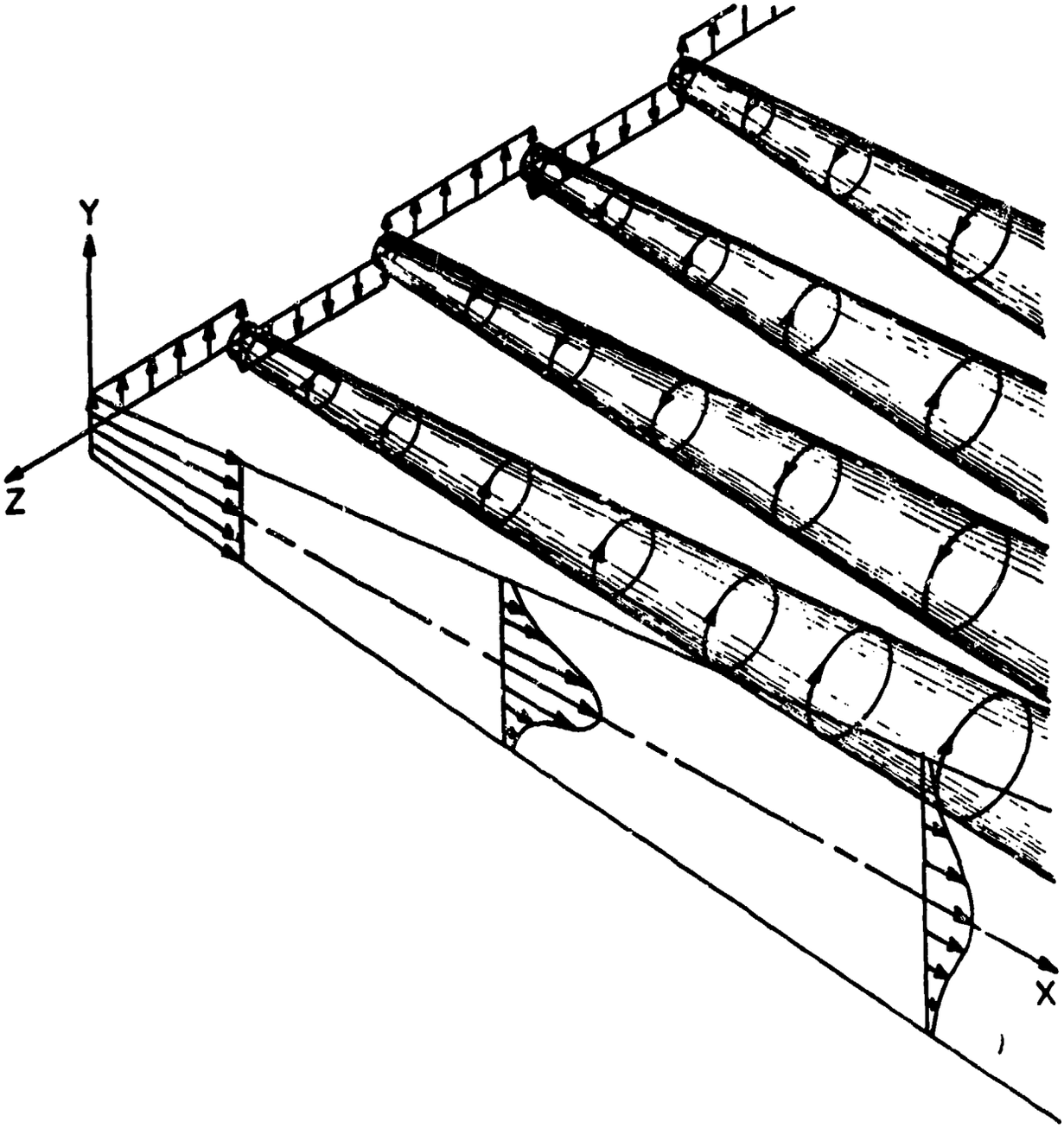

Figure 1. Streamwise Hypermixing Vortices in a Two-Dimensional Jet

SECTION II

ENGINE DESIGN CRITERIA

A design criteria selection coordination meeting was held with ARL personnel shortly after contract award. The following major design criteria were established:

- The 15-inch diameter Low Cost Ramjet Engine was the baseline engine size for this study (Air Force Contract F33615-72-C-1425).
- The primary flight envelope was Mach 0.7 to 0.9 at altitudes from sea level to 30,000 feet. Marquardt, however, would examine the performance characteristics of the selected ejector ramjet engine concept up to a Mach number of 1.2.
- Marquardt would examine both fuel and oxidizer addition ejector ramjet engine cycles. The fuel addition engine will use UDMH as the fuel, while the oxidizer addition engine will use hydrogen peroxide in the primary-mixer and JP-4 as the fuel to be injected into the afterburner.

SECTION III

ENGINE CYCLE SELECTION STUDIES

Mach 0.75 at 20,000 feet altitude was selected as the design point for determination of engine sizing. At this design point, each engine cycle was assumed to be operating at $\phi = 1.0$ (i.e., stoichiometric combustion) with the following component efficiencies:

Inlet pressure recovery	100.0%
Mixer efficiency	98.5%
Diffuser efficiency	99.0%
Primary nozzle efficiency	96.0%
Afterburner nozzle efficiency	96.0%
Combustion efficiency	95.0%

The primary pressure (delivering fuel or oxidizer to the ejector) was taken as 300 psia in keeping with the low cost objectives of this program. The heat of combustion of UDMH was taken as 12,939 Btu/lb, while the stoichiometric fuel/air ratio was 0.1088.

For the fuel addition engine (Figure 2), two cycle variations were considered. In the first cycle, it was assumed that the fuel-air mixing and combustion occurred simultaneously; the combustion products are then passed through a convergent nozzle whose exit pressure was equal to ambient pressure at the design condition, i.e., 6.76 psia at 20,000 feet. In the second cycle variation, it was assumed that mixing would occur without combustion. The mixed fuel-air was then diffused to the combustor area A_4 where flameholders and an ignition source would be required to initiate and sustain combustion at the assumed combustion efficiency level.

For the oxidizer addition engine (Figure 2), the incoming air and hydrogen peroxide are mixed, diffused, and JP-4 fuel is added in the afterburner to achieve combustion at a stoichiometric mixture ratio.

For each of these engine cycles, engine geometry and airflow were varied parametrically to obtain the maximum net jet thrust and minimum fuel consumption. This required an optimization which is described in the following paragraphs for each of the engine cycles.

1. FUEL ADDITION - SIMULTANEOUS MIX AND BURN

The effect of mixer area ratio A_3/A_2 is illustrated in Figure 3 for the case of simultaneous mixing and burning. For the case shown, the airflow Mach number at station 2 was taken as 0.15 for two different mixer inlet sizes, A_2. For the given flight condition, the combination of flow area A_2 and Mach number M_2 suffice to establish the engine airflow, W_s. For a $\phi = 1.0$, the fuel flow out of the primary nozzles is then established.

The variation shown in Figure 3, for each value of A_2, is to open up the mixer area A_3, starting at the condition where the mixer is constant area ($A_3 = A_2 + A_p$). As shown in the figure, the thrust increases and the fuel consumption decreases as the mixer is opened up to the maximum value possible (i.e., $A_3 = A3_b \cdot A_4$). By opening up the mixer, the total pressure losses due to combustion are reduced, yielding the noted results.

The effect of mixer inlet size A_2 is shown in Figure 4. As the mixer inlet area A_2 is increased, the thrust and specific fuel consumption increase. Also note that the area A_6 increases with A_2 in order to handle the increased air and fuel flow. It is generally desired to keep the exit nozzle area, A_6, equal to 60% or less of the combustor flow area A_4. This reduces the combustor flow Mach number and increases combustion efficiency and stability while reducing combustion total pressure losses. (A_6/A_4 will be set at 0.6 in this study.) Figure 3 includes the performance that would be predicted for a nozzle exit area ratio A_6/A_4 of 0.60 with an air entrance Mach number in the mixer of 0.15.

The effect of mixer inlet Mach number is shown in Figure 5. For a simultaneous mix and burn case a low entrance Mach number, M_2, is desired to reduce combustion pressure losses and maximize thrust. Note that the mixer inlet area A_2 is increasing

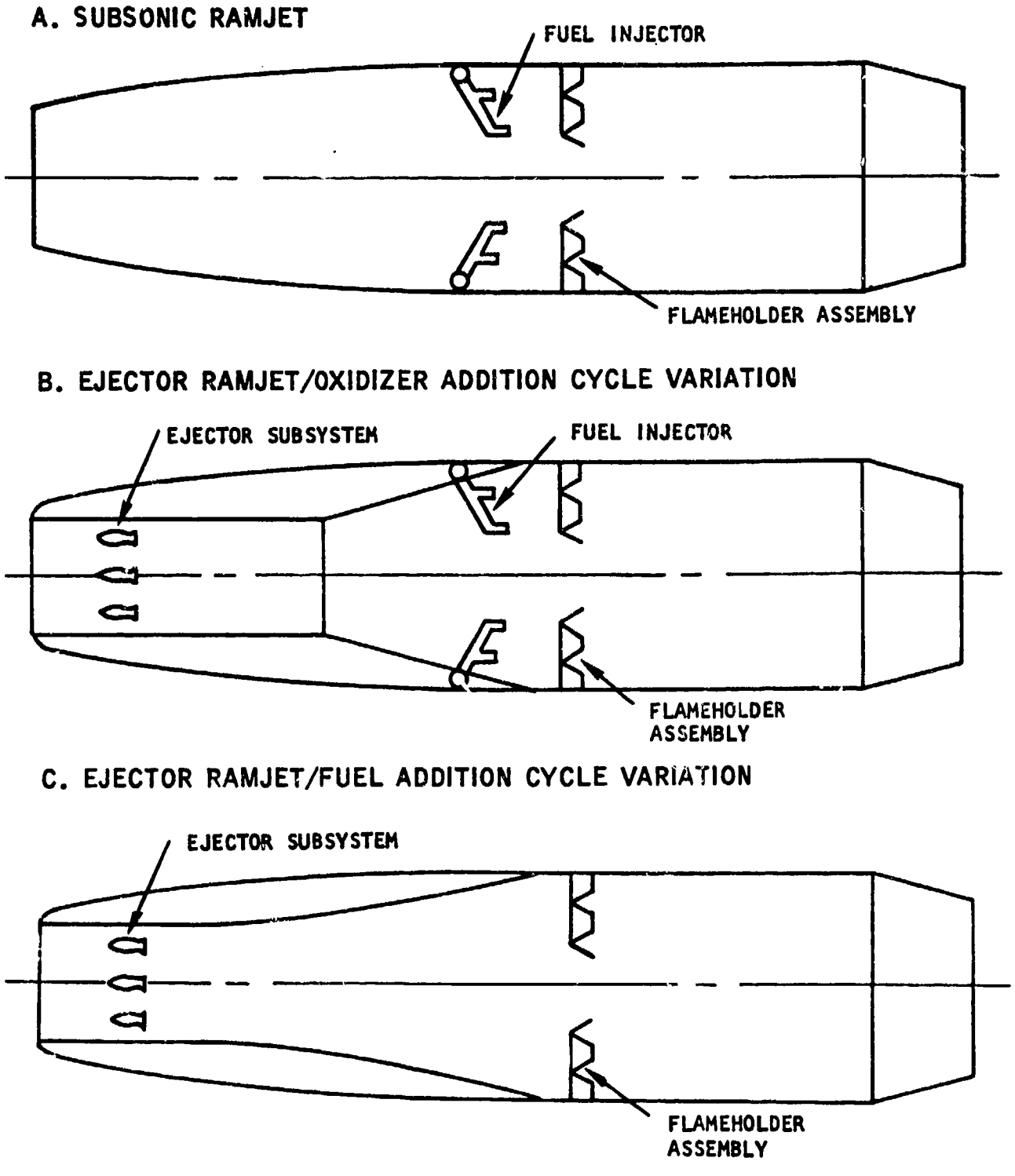

Figure 2. Ramjet/Ejector Ramjet Engine Concepts

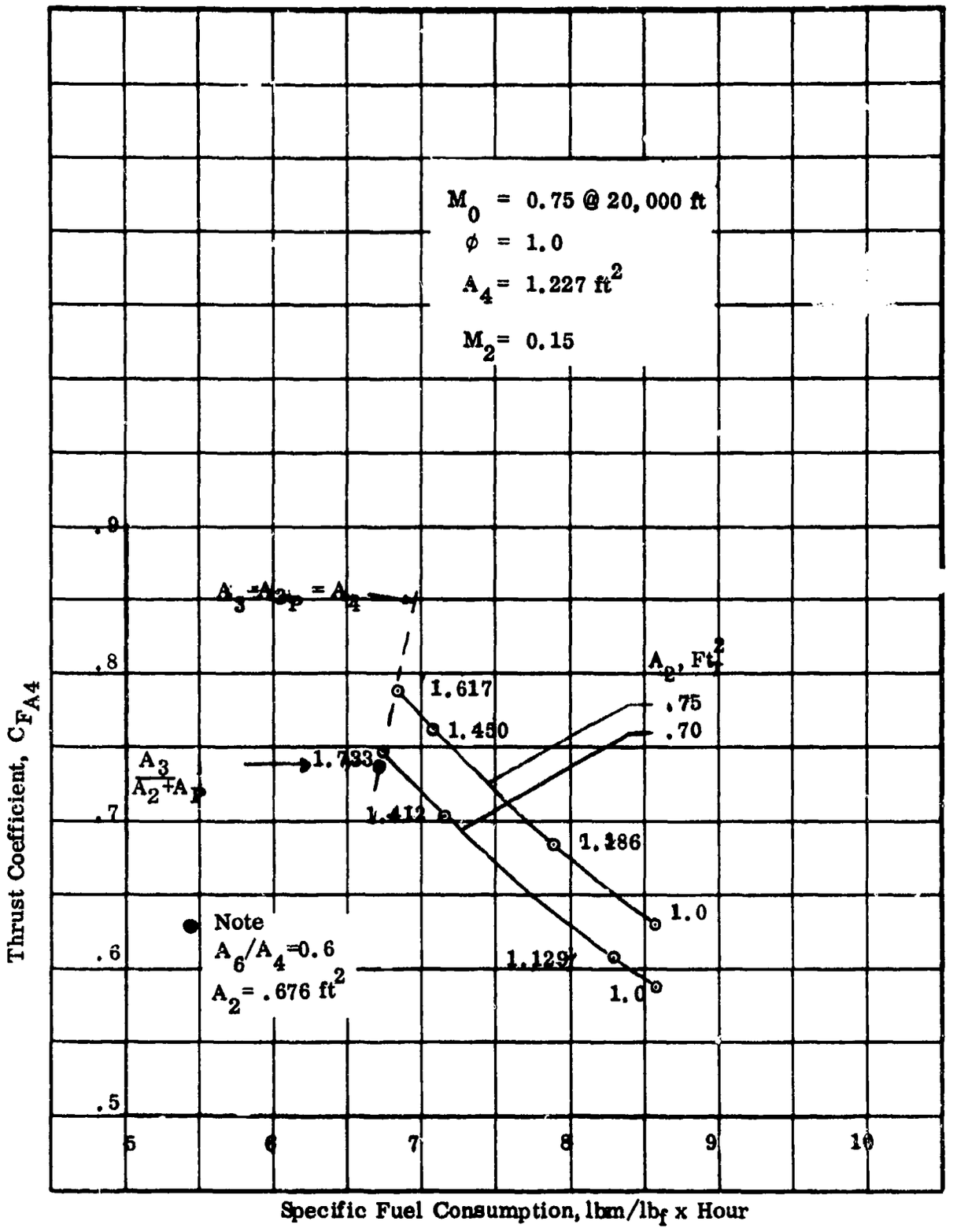

Figure 3. UDMH-Fueled Ejector Ramjet-Simultaneous Mix/Burn - Effect of Mixer Area Ratio

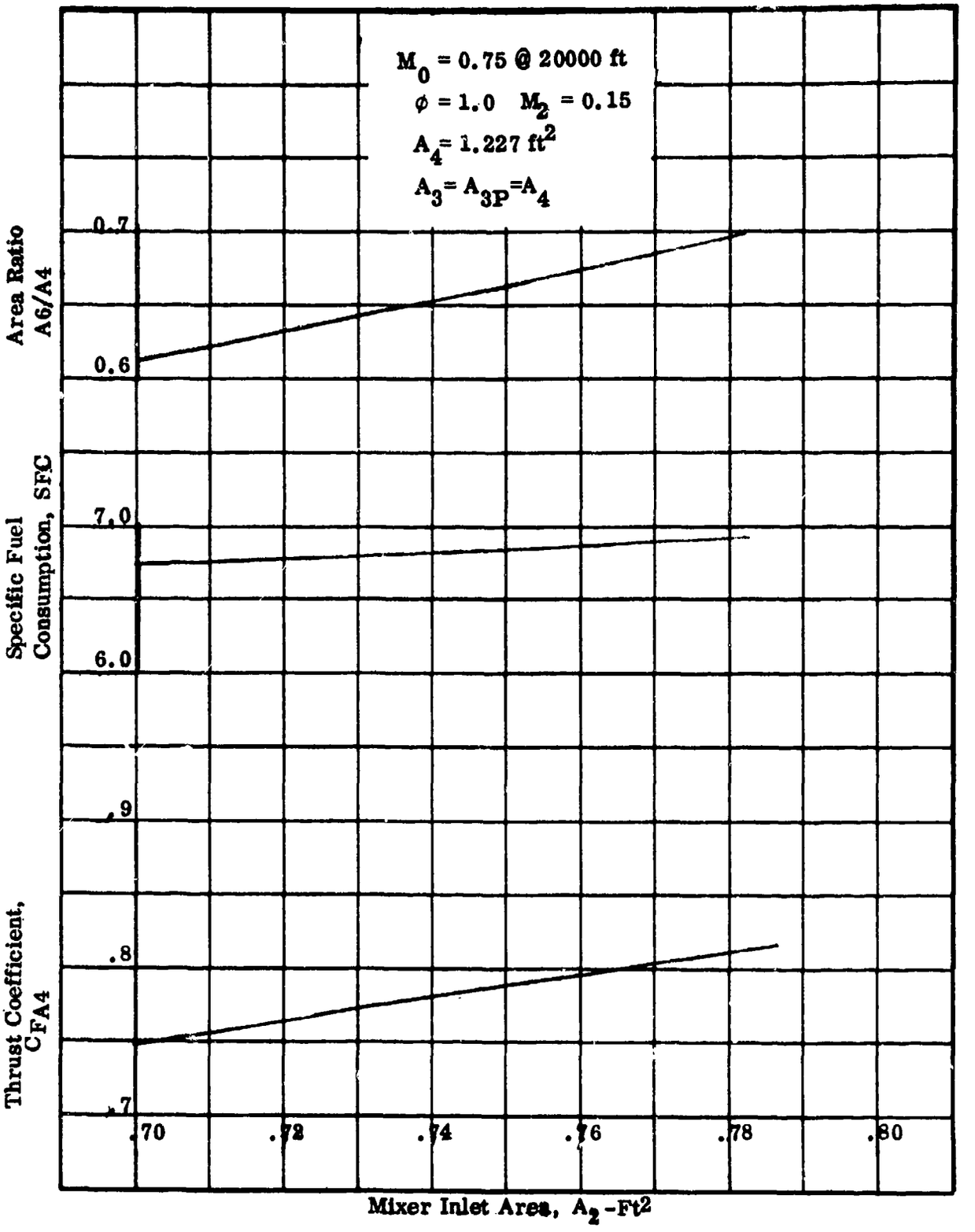

Figure 4. UDMH-Fueled Ejector Ramjet-Simultaneous Mix/Burn -Effect of Mixer Flow Area

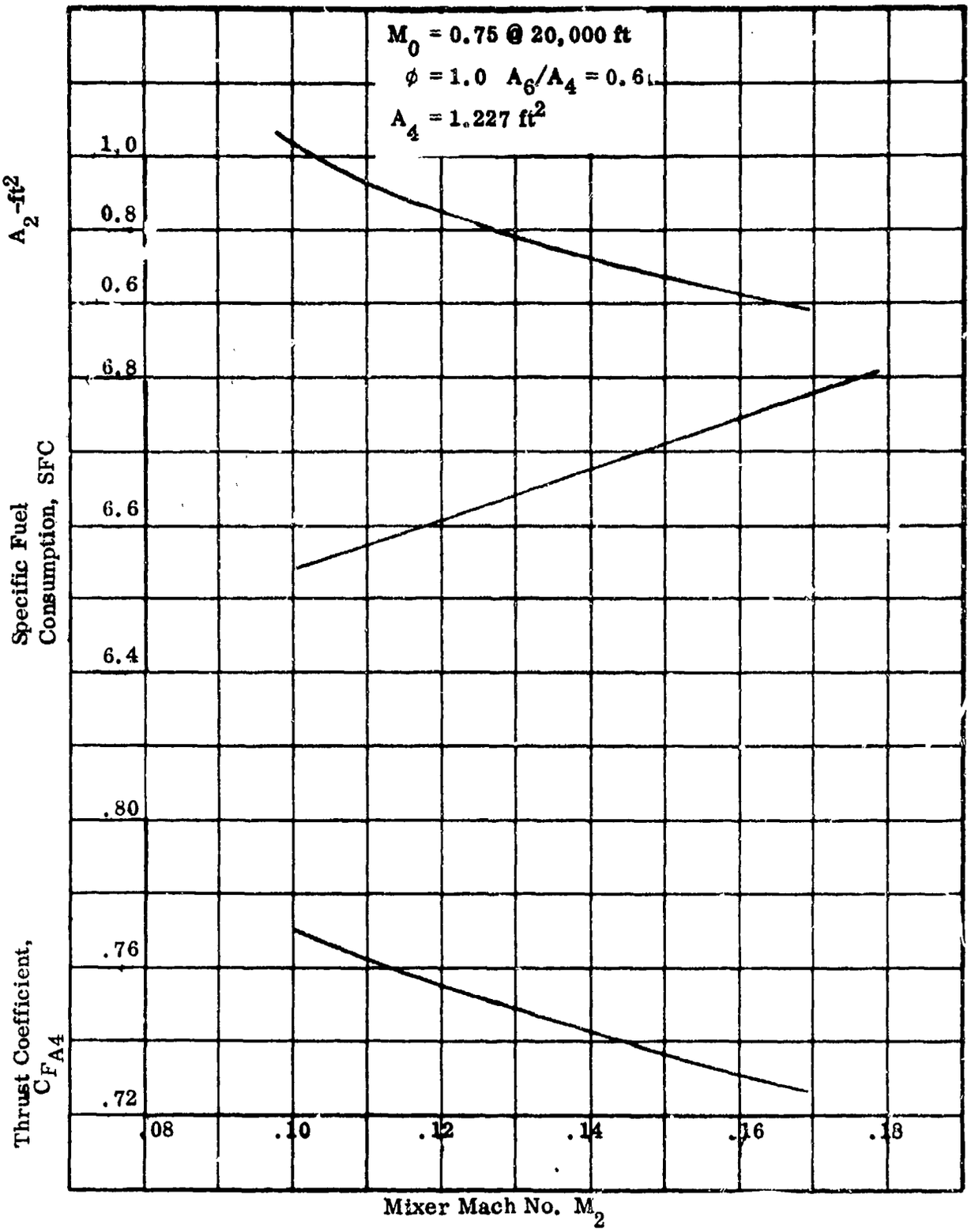

Figure 5. UDMH-Fueled Ejector Ramjet-Simultaneous Mix/Burn-Effect of Mixer Inlet Mach Number

as M_2 is reduced. Below a value of M_2 of 0.1, the required nozzle flow area is less than 60% of A_4, and the thrust coefficient begins to fall. The mixer and burner begin to approach a constant area cylinder of diameter equal to that of the combustor.

The final sizing and preliminary performance for the simultaneous mix and burn case is summarized in Table I, where it is compared to the other engine cycles. The performance of this engine for a range of fuel flows is discussed in a latter section of this report.

2. FUEL ADDITION - MIX/DIFFUSE/BURN

For this engine cycle, the air inlet Mach number M_2 and flow area A_2 were again varied in a systematic manner to determine the engine configuration yielding the maximum thrust coefficient. As with the simultaneous mix and burn cycle, the engine airflow is established by the combination of Mach number and size of the mixer for the given flight condition. Engine fuel flow through the primary nozzles is then about 11% of the engine airflow for stoichiometric combustion.

Figure 6 summarizes this engine cycle performance for nozzle exit areas of 50, 60, and 70% of the combustor flow area. For all exit nozzle sizes, the thrust and fuel consumption are optimized at a mixer inlet Mach number of about 0.35, compared to about 0.10 for the simultaneous mix and burn cycle. The thrust coefficient at M_2 of 0.35 and the selected value of nozzle area ratio A_6/A_4 of 60% is 0.991, representing a gain of 29% over the simultaneous mix and burn case. The preliminary performance and final sizing for this mix, diffuse, and burn case is summarized in Table I, where it may be compared with the other cycle variations. Performance with a range of fuel flows is discussed in another section of this report.

3. OXIDIZER ADDITION ENGINE CYCLE

The thrust coefficient of the oxidizer addition engine is not limited as with the fuel addition engine cycles. Thus the sizing of this engine is dependent upon the thrust level desired. For example, at low primary flow rates, the performance approaches that of the conventional ramjet, and optimum inlet Mach number M_2 for the flight conditions chosen is about 0.25 - 0.30. However, at high thrust levels corresponding to small ratios of secondary to primary flow rates, W_s/W_p, the optimum inlet Mach number M_2 is about 0.7, thus producing an essentially choked condition at the mixer outlet ($M_3 \cong 1.0$).

A typical optimization of the oxidizer addition engine is shown in Figure 7. The nozzle exit area was restricted to 60% of the combustor flow area A_4; for given values of entrance Mach number M_2, the mixer area A_2 and primary flow rate were varied to produce the variations of thrust coefficient and specific fuel consumption shown in Figure 7. The low thrust points of each curve correspond to ramjet performance (no primary flow). Increasing thrust is then achieved by increasing the primary flow rate. At high thrust levels, an entrance Mach number of 0.7 produces a minimum SFC. However, in the thrust coefficient range of 0.8 to 1.0, the minimum SFC is achieved with an

TABLE I. EJECTOR RAMJET ENGINE CYCLE SELECTION

Design Point: M_o = 0.75 @ 20,000 ft

A_6/A_4 = 0.6 fixed exit nozzle

ϕ = 1.0

A_4 = 1.227 ft^2

P_{T_P} = 300 psia

Engine parameter	Fuel addition simultaneous mix/burn	Fuel addition mix/diffuse/burn	Oxidizer addition (H_2O_2) mix/diffuse/burn
Fuel	UDMH	UDMH	JP-4
$C_{F_{A_4}}$	.77	.991	.796
M_2	.10	.35	0.60
A_2 (ft^2)	1.042	.359	.225
A_3 (ft^2)	1.2272	.3717	.2285
A_{3P}(ft^2)	1.2272	1.2272	1.2272
SFC	6.54	5.73	7.70
ϕ	1.0	1.0	1.0
W_s/W_p	9.1912	9.1912	19.326

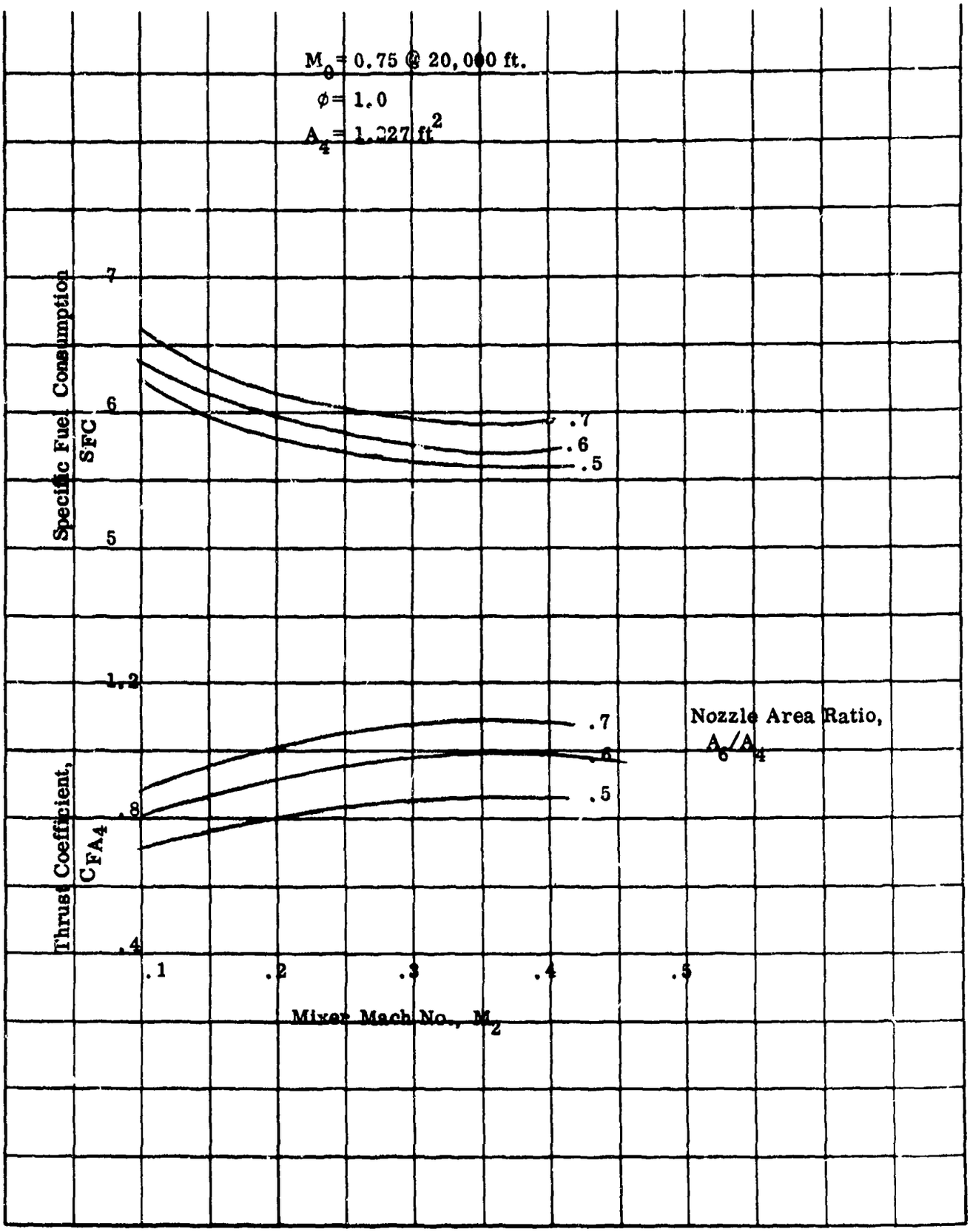

Figure 6. UDMH-Fueled Ejector Ramjet-Mix/Diffuse/Burn-Effect of Exit Nozzle Size

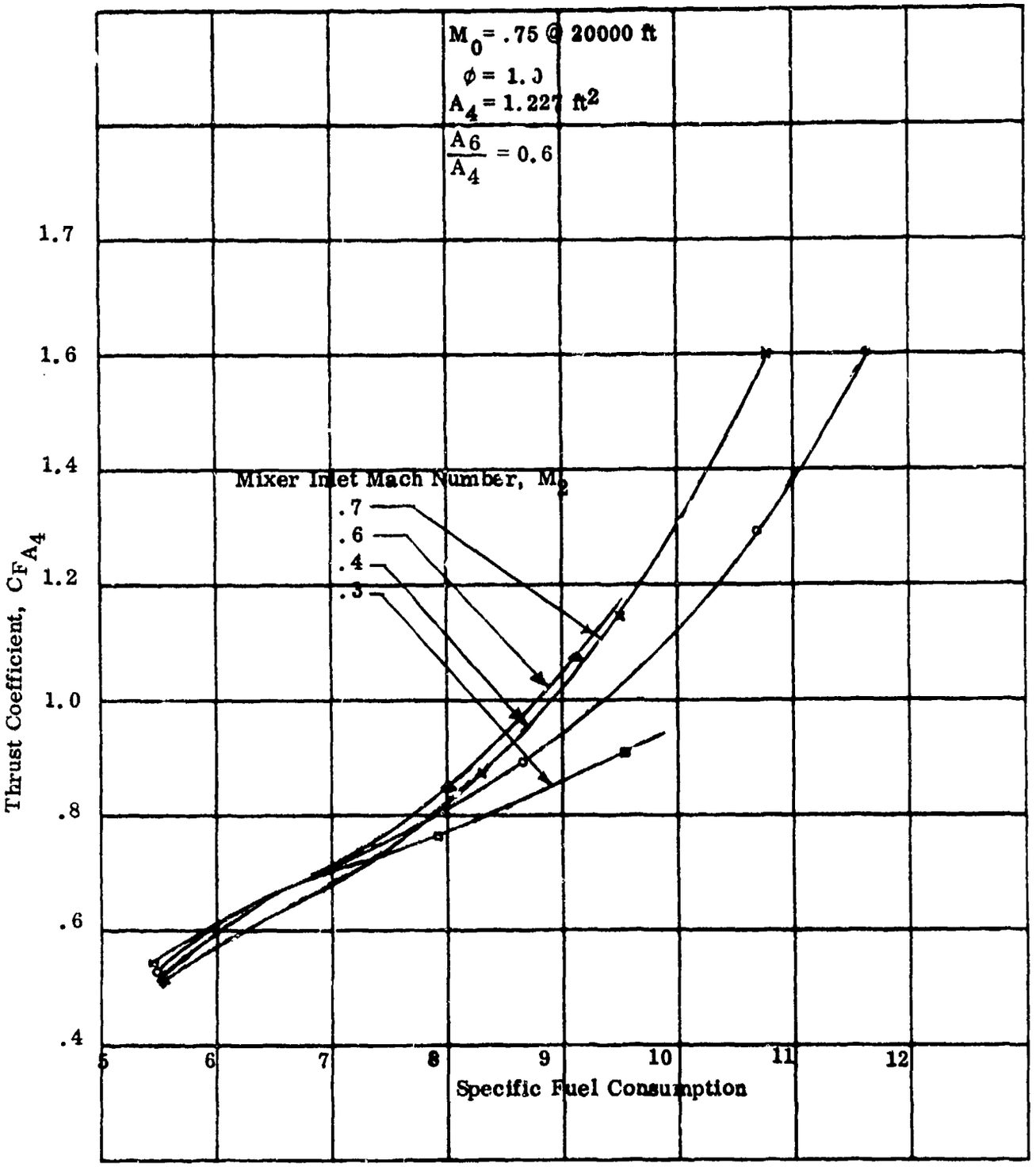

Figure 7. Oxidizer Addition Engine Cycle-Effect of Mixer Inlet Mach Number

entrance Mach number of about 0.6. This lower range of thrust coefficient was chosen for sizing of the oxidizer addition engine since this is the order of magnitude of the thrust coefficients produced by the fuel addition engine cycles previously discussed. The preliminary performance and sizing of the oxidizer addition engine is summarized in Table I.

SECTION IV

ENGINE CYCLE SELECTION

The performance of the three engine cycles is presented in Figure 8, wherein engine thrust coefficient is plotted versus specific fuel or propellant consumption. The primary flow rate for each engine cycle was varied to achieve the thrust variation noted, with solid circle points corresponding to optimized design points for each cycle variation (Table I). The lowest point on the oxidizer addition cycle corresponds to zero primary flow and thus is a simple, but not optimum geometry, ramjet engine.

These results were reviewed with the ARL Program Manager, and the fuel addition cycle with mixing, diffusion, and burning (afterwards designated MDB) was selected as the configuration for continued engine preliminary design. The high thrust and low specific fuel consumption of the MDB engine cycle made it an obvious choice, producing a thrust almost twice that of the ramjet at approximately the same fuel consumption levels. A review of the combustion environment indicated that combustion would not occur in the mixer, and that flame stabilization devices plus igniter would be required to promote burning with the desired efficiency in the afterburner. The simultaneous mixing and burning cycle, by the same token, is thus somewhat academic and is not a likely configuration.

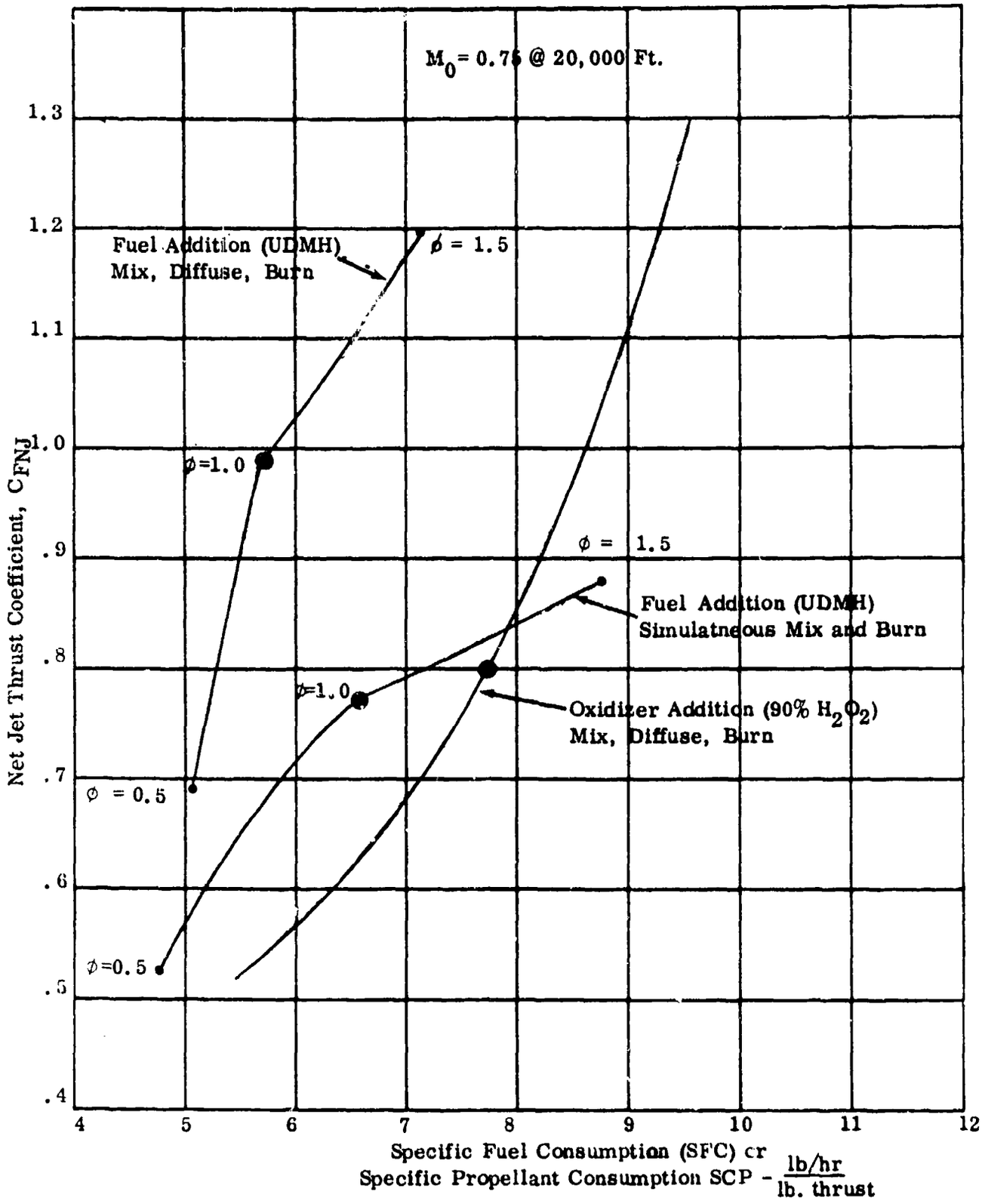

Figure 8. Low Cost Ejector Ramjet Engine Cycle Variation Comparison

SECTION V

UNSYMMETRICAL DIMETHYLHYDRAZINE (UDMH) PROPERTIES

UDMH was selected as the ejector ramjet fuel because of its ready availability, excellent storage capabilities, low cost, while providing substantial performance gains over propane and JP-4. However, in spite of its wide use as a rocket propellant, there is little information about its thermal properties as a monopropellant and the combustion of decomposed UDMH with air as required in the ejector ramjet cycle. For example, the Rocket Propellant Handbook (Reference 1) lists the heat of formation of UDMH as -187.3 cal/g (-11.27 K cal/mole) while the Callery Chemical Company (Reference 2) gives +12.74 K cal/mole. Similarly, the heat of combustion varies from 14160 Btu/lb to 12939 Btu/lb between these two references. Inasmuch as the design of the primary ejector subsystem and subsequent combustion in the afterburner is highly dependent upon the temperature, products of decomposition, and specific heat ratio in the expansion, mixing, and combustion processes, it was decided before proceeding further to collect and review as much data as possible on UDMH.

A visit was made to the USAF Rocket Propulsion Laboratory at Edwards Air Force Base, California, and discussions were held with Mr. W. Forbes/Rocket Propellants Section. RPL's UDMH decomposition data were very limited, particularly with regard to decomposition temperature; however, three references were identified as potential sources of design information. These references were obtained by Marquardt, and Reference 3, in particular, was outstanding. This report describes an experimental program conducted by the Jet Propulsion Laboratory of Pasadena, which evaluated UDMH as a monopropellant. The JPL report is included as Appendix A to this report.

The results of this experimental study indicate that decomposition of UDMH can be accomplished thermally. (Thermal decomposition has been assumed in keeping with the low cost objectives of this engine program.) However, the thermal decomposition temperature depends on whether the UDMH is injected as a liquid or as a vapor, and if as a vapor, how much heat is added to the UDMH before being injected into the decomposition chamber. JPL predicted a decomposition temperature of 1467°F (1927°R) at a chamber pressure of 300 psia. This result is based upon a heat of formation of +12.72 K cal/mole and chemical equilibrium upon assuming final products of H_2, N_2, CH_2, NH_3, HCN, and C. Marquardt analyses based upon a heat of formation of +12.74 K cal/mole show a reaction temperature of 1073°K (1931°R) as shown in Table II; thus the JPL and Marquardt results are quite comparable. JPL test results are summarized for convenience in Table III. With unheated UDMH injected into a preheated chamber, a decomposition temperature of 1262°F was achieved at 300 psia, compared to the theoretical value of 1467°F. A small increase in UDMH temperature, achieved by picking up a small amount of heat regeneratively, increased the measured C* and chamber temperature slightly. Finally, by adding supplementary heat and injecting the UDMH into the chamber as a vapor, the measured decomposition temperature reached 1373°F. These results indicate that with care in design and with suitable heat addition, the theoretical decomposition temperatures and chemical products can be approached.

TABLE II. DECOMPOSED UDMH THEORETICAL EJECTOR NOZZLE PERFORMANCE EQUILIBRIUM COMPOSITION

$T_{T_P} = 1073°K = 1931°R$

PC = 300.0 PSIA
CASE NO. 1

	CHEMICAL FORMULA			WT FRACTION (SEE NOTE)	ENTHALPY CAL/MOL	STATE	TEMP DEG K	DENSITY G/CC
FUEL	C 2.00000	H 8.00000	N 2.00000	1.00000	12740.000	L	298.15	0.0

O/F= 0.0 PERCENT FUEL=100.0000 EQUIVALENCE RATIO= ******* DENSITY= 0.0

	CHAMBER	THROAT	EXIT	EXIT	EXIT	EXIT	EXIT	EXIT	EXIT	EXIT	EXIT	EXIT	EXIT
PC/P	1.0000	1.7571	2.5000	2.7500	3.0000	3.2500	3.5000	4.0000	10.000	15.000	20.000	25.000	30.000
P, ATM	20.414	11.618	8.1655	7.4232	6.8046	6.2811	5.8325	5.1034	2.0414	1.3609	1.0207	0.8165	0.6805
T, DEG K	1073	1000	959	948	938	929	922	907	820	785	762	745	731
H, CAL/G	212.0	135.0	90.1	78.4	67.8	58.2	49.4	33.8	-65.6	-105.7	-132.8	-153.1	-169.2
S, CAL/(G)(K)	3.1069	3.1069	3.1069	3.1069	3.1069	3.1069	3.1069	3.1069	3.1069	3.1069	3.1069	3.1069	3.1069
M, MOL WT	14.967	15.202	15.358	15.401	15.441	15.478	15.513	15.576	16.028	16.237	16.388	16.507	16.604
(DLV/DLPT	-1.09133	-1.09060	-1.08976	-1.08948	-1.08920	-1.08894	-1.08867	-1.08816	-1.08347	-1.08075	-1.07859	-1.07680	-1.07526
(DLV/DLTP	1.9242	1.9767	2.0050	2.0119	2.0179	2.0232	2.0279	2.0359	2.0711	2.0752	2.0735	2.0696	2.0647
CP, CAL/(G)(K)	2.0029	2.1190	2.1862	2.2035	2.2189	2.2327	2.2452	2.2670	2.3864	2.4199	2.4357	2.4431	2.4459
GAMMA (S)	1.1822	1.1771	1.1739	1.1731	1.1723	1.1716	1.1709	1.1697	1.1620	1.1588	1.1567	1.1551	1.1538
SON VEL,M/SEC	839.4	802.4	780.5	774.7	769.5	764.8	760.5	752.7	702.9	682.6	668.7	658.3	649.9
MACH NUMBER	0.0	1.000	1.294	1.365	1.427	1.483	1.534	1.622	2.168	2.389	2.540	2.655	2.748
CSTAR, FT/SEC		3930	3930	3930	3930	3930	3930	3930	3930	3930	3930	3930	3930
CF		0.670	0.843	0.883	0.917	0.947	0.974	1.019	1.272	1.361	1.418	1.459	1.491
AE/AT		1.0000	1.0726	1.1111	1.1519	1.1962	1.2373	1.3247	2.3292	3.0880	3.8002	4.4794	5.1335
IVAC,LB-SEC/LB		151.3	155.4	157.2	158.9	160.6	162.1	165.0	183.9	191.4	196.4	200.1	203.0
I, LB-SEC/LB		81.8	103.0	107.8	112.0	115.7	118.9	124.5	155.4	166.3	173.2	178.2	182.1

MOLE FRACTIONS

C(S)	0.20270	0.19505	0.18989	0.18845	0.18711	0.18587	0.18470	0.18258	0.16706	0.15970	0.15431	0.15004	0.14649
CH4	0.19439	0.21215	0.22414	0.22750	0.23060	0.23349	0.23619	0.24112	0.27722	0.29435	0.30590	0.31685	0.32512
HCN	0.00001	0.00000	0.00000	0.00000	0.00000	0.00000	0.00000	0.00000	0.00000	0.00000	0.00000	0.00000	0.0
H2	0.40380	0.38874	0.37854	0.37568	0.37304	0.37059	0.36829	0.36408	0.33330	0.31868	0.30796	0.29948	0.29239
NH3	0.00109	0.00092	0.00083	0.00081	0.00079	0.00077	0.00075	0.00072	0.00055	0.00048	0.00044	0.00041	0.00039
N2	0.19801	0.20314	0.20660	0.20757	0.20846	0.20929	0.21007	0.21149	0.22187	0.22678	0.23038	0.23324	0.23561

ADDITIONAL PRODUCTS WHICH WERE CONSIDERED BUT WHOSE MOLE FRACTIONS WERE LESS THAN .000005 FOR ALL ASSIGNED CONDITIONS

C	CH	CH2	CH3	CN	CN2	C2	C2H	C2H2	C2H4
C2N	C2N2	C3	H	N	NH	NH2	N2C	N2H4	

NOTE. WEIGHT FRACTION OF FUEL IN TOTAL FUELS AND OF OXIDANT IN TOTAL OXIDANTS

TABLE III. UDMH DECOMPOSITION/JPL TEST RESULTS

Decomposition method	L*-Inch	P_{T_P} - psia	C*-ft/sec	T_{T_P} - °F	Comments
Thermal-Unheated Fuel	5110	300	3220	1262	Equilibrium flow analysis predicted T_{T_P} = 1467°F (1927°R) and C* = 3690 ft/sec
Thermal-Liquid UDMH Preheated by Regeneration to 170-300°F - Chamber Preheated 1100-1200°F	~5000	300 200	3333 3250	1268 1246	Small increase in C* and T_{T_P}. UDMH injected as liquid into chamber
Thermal-Vaporized UDMH-Supplemental External Heat	4810	310	3327	1373	Significant increase in T_{T_P} No improvement in C* UDMH injected as vapor into chamber

After review of these experimental data, a decomposition temperature of 1340°F (1800°R) was assumed with a chamber pressure of 300 psia. These conditions were used with Marquardt's chemical equilibrium program to establish total enthalpy, the process γ, and exit velocity for exapsnion through the primary nozzle through various pressure ratios. The results of this computer run are shown in Table IV. These results were then used to establish an effective γ across the primary nozzle such that, for a given primary pressure ratio and total enthalpy, Marquardt's ejector ramjet engine performance computer program give the same primary exit velocity as the chemical equilibrium program.

The chemical equilibrium program was then run for stoichiometric combustion of UDMH and air at 10 psia. This pressure is representative of the combustion chamber conditions at the Mach 0.75 at 20,000 foot altitude design point. The results of this computer run are shown in Table V. Only the chamber and throat conditions are of interest in this tabulation inasmuch as there is not enough pressure ratio to choke the engine exit nozzle. This computer run also served to determine combustion chamber exit total enthalpy and γ for use in combustion chamber and exit nozzle analysis.

TABLE IV. DECOMPOSED UDMH THEORETICAL EJECTOR NOZZLE PERFORMANCE
EQUILIBRIUM COMPOSITION
T_{T_P} = 1000°K = 1800°R

THEORETICAL ROCKET PERFORMANCE ASSUMING EQUILIBRIUM COMPOSITION DURING EXPANSION

PC = 300.0 PSIA
CASE NO. 1

	CHEMICAL FORMULA	WT FRACTION (SEE NOTE)	ENTHALPY CAL/MOL	STATE	TEMP DEG K	DENSITY G/CC
FUEL	C 2.00000 H 8.00000 N 2.00000	1.00000	4009.000	L	298.15	0.0

O/F= 0.0 PERCENT FUEL=100.0000 EQUIVALENCE RATIO= ******* DENSITY= 0.0

	CHAMBER	THROAT	EXIT	EXIT	EXIT	EXIT	EXIT	EXIT	EXIT	EXIT	EXIT	EXIT	EXIT
PC/P	1.0000	1.7525	2.5000	2.7500	3.0000	3.2500	3.5000	4.0000	10.000	15.000	20.000	25.000	30.000
P, ATM	20.414	11.648	8.1655	7.4232	6.8046	6.2811	5.8325	5.1034	2.0414	1.3609	1.0207	0.8165	0.6805
T, DEG K	1000	935	893	888	879	871	864	851	770	738	716	700	687
H, CAL/G	66.7	-5.3	-40.0	-50.3	-59.6	-68.0	-75.7	-89.5	-177.1	-212.5	-236.4	-256.4	-268.7
S, CAL/(G)(K)	2.9667	2.9667	2.9667	2.9667	2.9667	2.9667	2.9667	2.9667	2.9667	2.9667	2.9667	2.9667	2.9667
M, MOL WT	15.975	16.218	16.391	16.425	16.465	16.504	16.539	16.603	17.059	17.267	17.417	17.533	17.629
(DLV/DLP)T	-1.08431	-1.08117	-1.07885	-1.07819	-1.07756	-1.07697	-1.07642	-1.07539	-1.06747	-1.06353	-1.06059	-1.05823	-1.05626
(DLV/DLT)P	1.0084	1.0282	1.0349	1.0359	1.0365	1.0367	1.0368	1.0363	1.0129	1.0014	1.0720	1.0545	1.0388
CP, CAL/(G)(K)	1.0529	2.0158	2.0470	2.0562	2.0632	2.0653	2.0697	2.0766	2.0900	2.0756	2.0572	2.0384	2.0159
GAMMA (S)	1.1732	1.1693	1.1669	1.1662	1.1656	1.1651	1.1646	1.1637	1.1580	1.1558	1.1544	1.1534	1.1526
SON VEL,M/SEC	781.4	748.8	729.1	723.9	719.3	715.1	711.2	704.2	659.3	640.8	628.2	618.6	611.0
MACH NUMBER	0.0	1.000	1.296	1.367	1.429	1.485	1.535	1.623	2.166	2.385	2.536	2.659	2.762
CSTAR, FT/SEC		3682	3682	3682	3682	3682	3682	3682	3682	3682	3682	3682	3682
CF		0.667	0.842	0.882	0.916	0.946	0.973	1.019	1.273	1.362	1.419	1.451	1.473
AE/AT		1.0000	1.0742	1.1131	1.1544	1.1971	1.2406	1.3288	2.3419	3.1270	3.8249	4.5033	5.1651
IVAC,LB-SEC/LB		141.6	145.5	147.2	148.9	150.4	151.9	154.6	172.4	179.6	184.9	187.9	190.5
I, LB-SEC/LB		76.4	96.3	100.9	104.8	108.3	111.3	116.6	145.6	155.9	162.4	167.2	170.8

MOLE FRACTIONS

C(S)	0.16953	0.16089	0.15504	0.15343	0.15194	0.15055	0.14926	0.14690	0.12982	0.12180	0.11596	0.11135	0.10754
CH4	0.27198	0.29200	0.30555	0.30930	0.31278	0.31597	0.31898	0.32446	0.36417	0.38282	0.39642	0.40715	0.41613
H2	0.33708	0.32012	0.30861	0.30543	0.30249	0.29975	0.29720	0.29254	0.25470	0.24278	0.23318	0.22202	0.21443
NH3	0.00132	0.00110	0.00098	0.00095	0.00093	0.00090	0.00088	0.00085	0.00063	0.00055	0.00050	0.00046	0.00043
N2	0.22009	0.22589	0.22981	0.23089	0.23183	0.23281	0.23368	0.23526	0.24668	0.25284	0.25694	0.25972	0.26167

ADDITIONAL PRODUCTS WHICH WERE CONSIDERED BUT WHOSE MOLE FRACTIONS WERE LESS THAN .000005 FOR ALL ASSIGNED CONDITIONS

TABLE V. UDMH/AIR COMBUSTION PERFORMANCE EQUILIBRIUM COMPOSITION

PC = 10.0 PSIA
CASE NO. 1

	CHEMICAL FORMULA						WT FRACTION (SEE NOTE)	ENTHALPY CAL/MOL	STATE	TEMP DEG K	DENSITY G/CC
FUEL	C	2.00000	H	8.00000	N	2.00000	1.00000	4009.030	L	298.15	0.0
OXIDANT	AR	0.00930	N	1.56240	O	0.41900	1.00000	-155.000	G	497.00	0.0

O/F= 9.1743 PERCENT FUEL= 9.8287 EQUIVALENCE RATIO= 1.0028 DENSITY= 0.0

	CHAMBER	THROAT	EXIT	EXIT	EXIT	EXIT	EXIT	EXIT	EXIT
PC/P	1.0000	1.7701	2.5000	2.7500	3.0000	3.2500	3.5000	4.0000	10.000
P, ATM	0.6805	0.3844	0.2722	0.2474	0.2268	0.2094	0.1944	0.1701	0.0680
T, DEG K	2282	2098	1983	1951	1922	1895	1870	1825	1520
H, CAL/G	1.[illegible]	-84.6	-139.3	-152.7	-164.8	-175.8	-185.8	-203.5	-313.3
S, CAL/(G)(K)	2.3876	2.3876	2.3876	2.3876	2.3876	2.3876	2.3876	2.3876	2.3876
M, MOL WT	27.452	27.590	27.648	27.661	27.671	27.680	27.687	27.698	27.729
(DLV/DLP)T	-1.00343	-1.00178	-1.00109	-1.00093	-1.00081	-1.00070	-1.00061	-1.00047	-1.00002
(DLV/DLT)P	1.0997	1.0567	1.0366	1.0319	1.0280	1.0247	1.0219	1.0174	1.0010
CP, CAL/(G)(K)	0.5722	0.4866	0.4618	0.4308	0.4213	0.4130	0.4058	0.3938	0.3402
GAMMA (S)	1.1759	1.1955	1.2102	1.2146	1.2185	1.2222	1.2256	1.2317	1.2675
SON VEL,M/SEC	901.4	669.3	849.6	844.0	838.9	834.1	829.6	821.4	760.1
MACH NUMBER	0.0	1.000	1.279	1.347	1.407	1.461	1.510	1.596	2.136
CSTAR, FT/SEC		4223	4223	4223	4223	4223	4223	4223	4223
CF		0.675	0.844	0.883	0.917	0.947	0.973	1.018	1.261
AE/AT		1.0000	1.0664	1.1022	1.1401	1.1792	1.2189	1.2989	2.1812
IVAC,LB-SEC/LB		162.8	166.7	168.5	170.3	171.9	173.5	176.3	194.2
I, LB-SEC/LB		88.6	110.8	115.9	120.4	124.3	127.7	133.6	165.6

MOLE FRACTIONS

AR	0.00795	0.00799	0.00801	0.00801	0.00801	0.00802	0.00802	0.00802	0.00803
CO	0.01244	0.00673	0.00423	0.00367	0.00321	0.00283	0.00251	0.00201	0.00061
CO2	0.07735	0.08351	0.08621	0.08680	0.08730	0.08771	0.08805	0.08859	0.09009
H	0.00076	0.00027	0.00012	0.00010	0.00008	0.00006	0.00005	0.00003	0.00000
H2	0.00507	0.00292	0.00196	0.00174	0.00155	0.00140	0.00126	0.00105	0.00046
H2O	0.17211	0.17647	0.17830	0.17871	0.17904	0.17932	0.17955	0.17992	0.18092
NO	0.00254	0.00124	0.00072	0.00060	0.00051	0.00044	0.00038	0.00028	0.00001
N2	0.71138	0.71561	0.71738	0.71776	0.71808	0.71834	0.71856	0.71890	0.71984
O	0.00041	0.00012	0.00005	0.00004	0.00003	0.00002	0.00002	0.00001	0.00000
OH	0.00404	0.00190	0.00107	0.00090	0.00076	0.00065	0.00055	0.00041	0.00002
O2	0.00595	0.00323	0.00196	0.00167	0.00143	0.00123	0.00106	0.00078	0.00001

ADDITIONAL PRODUCTS WHICH WERE CONSIDERED BUT WHOSE MOLE FRACTIONS WERE LESS THAN .000005 FOR ALL ASSIGNED CONDITIONS

C(S)	C	CH	CH2	CH3	CH4	CN	CN2	C2	C2H
C2H2	C2H4	C2N	C2N2	C2O	C3	C3O2	HCN	HCO	HO2
H2O(S)	H2O(L)	N	NH	NH2	NH3	NO2	N2C	N2H4	N2O
N2O4									

NOTE. WEIGHT FRACTION OF FUEL IN TOTAL FUELS AND OF OXIDANT IN TOTAL OXIDANTS

SECTION VI

ENGINE PRELIMINARY DESIGN

1. ENGINE SIZING

The sizing of the three candidate engine cycles of Section III was based upon consistent but, in several cases, optimistic component efficiencies. For preliminary design and performance estimation of the selected MDB cycle, the following component efficiencies were used:

Inlet Total Pressure Recovery (P_{T_2}/P_{T_0})	0.98
Revised UDMH Thermal Decomposition Combustion Properties	(See Section V)
Primary (Ejector) Nozzle Efficiency (η_P)	0.96
Diffuser Efficiency (η_D)	0.90
Mixing Efficiency (η_M)	0.985
Combustion Efficiency (η_C)	
$\phi \leq 1.0$	0.93
$\phi = 1.25$	0.91
$\phi = 1.5$	0.83
Exit Nozzle Efficiency (η_N)	0.96

The largest change in component efficiency was that assigned to the diffuser. This parameter relates the total pressure loss across the diffuser as a function of the flow Mach number at the beginning of the diffuser. For this engine, the use of a diffuser efficiency of 90% is equivalent to the total pressure loss of a conical diffuser of about 13° total divergence angle based upon Reference 4.

The MDB engine was reoptimized at the Mach 0.75 @ 20000 feet design point by using the above revised component efficiencies. Table VI summarizes design point performance. A comparison of the design point engine performance and sizing for the revised design and the original optimization is presented in Table VII. In comparison to the preliminary results, the thrust coefficient was decreased 9.7% while the SFC was increased 16.7% by the use of the revised component efficiencies/UDMH properties.

TABLE VI. UDMH - FUEL EJECTOR RAMJET DESIGN CONDITION PERFORMANCE

$M_0 = 0.75$ @ 20,000 FT/S = 1.0

	** STATION DATA **								ENG. AREA RATIOS
	0	2	P	3	3P	4	5	6	
MACH NO.	0.750	0.351	2.763	0.508	0.146	0.360	0.360	0.796	(A2+AP)/A3
VELOCITY	778.3	379.1	5492.9	757.4	222.9	1124.5	1124.5	2398.2	1.0000
PRES.STATIC	6.737	8.810	8.659	9.148	10.539	9.279	9.279	6.737	A2/A4 A5/A4
H STATIC	107.14	116.37	797.33	253.46	243.93	1262.42	1262.42	1172.79	0.3149 0.5909
PRES. TOTAL	9.788	9.592	316.880	10.887	10.695	10.090	10.090	10.090	A3/A3P
H TOTAL	119.2	119.2	1400.0	244.9	244.9	1287.7	1287.7	1287.7	0.3245
FLOW	7.165	7.165	0.780	7.944	7.944	7.944	7.944	7.944	AD/MIN(A5,A6)
AREA	0.22669	0.38650	0.01171	0.39821	1.22720	1.22720	1.22720	0.73624	0.3079
GAMA	1.4015	1.4015	1.1980	1.3800	1.3800	1.3094	1.3094	1.3094	

********** EFFICIENCIES **********

ETA KE	PRI COMB	PRI NOZ	MIXING	MIX COMB	SEC COMB	DIFF.	A/B COMB	A/B NOZ
0.9486	0.0000	0.9600	0.9850	0.0000	0.0000	0.9000	0.9300	0.9800

********** ENGINE PERFORMANCE **********

THRUST	IMPULSE	SFC	CF A4	WS/WP	PT2/PTO	ENG DRAG	ENG CD	AREF CD	FFACTOR	PHI TOT.
419.6	538.3	6.688	0.8945	9.191	0.9800	0.0	0.0	0.0	1.000	1.0000

********** PROGRAM CONTROL PARAMETERS YES=1.0 NO=0.0 **********

ENG MODE	R/J	ERJ	FANR/J	FANERJ	RAMLACE	** **	VD	AO	M2	M3 **	TRACE
	0.0	1.0	0.0	0.0	0.0		0.0	0.0	1.0	0.0	0.0

ENG PARA	GAMA(2	P	3	4	5/6)	PT2O	A6FIX	A6MAX	PRI FUEL	OFF DES.	BI PROP	A/B BUR.
	0.0	1.0	1.0	1.0	1.0	1.0	0.0	0.0	1.0	1.0	0.0	

	PRIMARY OX	PRIMARY FUEL	SECONDARY FUEL	AFTERBURNER FUEL
FLOW	0.0000	0.7795	0.0	0.7795
TANK H *	0.	1400.	0.	470.
DEL H *	0.	0.	0.	0.

INPUT PARA. FOR FAN AND GAS GEN.	FLOW	PRES RATIO	FLOW	PHI
	0.0	1.0000	0.0	0.0

HEAT OF REC	12939.	12939.	12939.
PHI AND ST	1.000/0.000	0.0 /0.109	1.000/0.109

* TANK COND. 25 DEG C 1 ATM.

** UNITS **
FLOW-LBS/SEC AREA-FTSQ ENTHALPY-BTU/LB PRES-PSIA

TABLE VII. MDB ENGINE PERFORMANCE DESIGN POINT COMPARISON

M_0 = 0.75 at 20,000 ft

A_6/A_4 = 0.6 (fixed convergent exit nozzle)

ϕ = 1.0

A_4 = 1.227 ft^2 (D_4 = 15 in.)

Primary Total Pressure = 300 psia

Fuel = UDMH (decomposed)

Engine parameter	Initial component efficiencies	Revised component efficiencies
$C_{F_{A4}}$	0.991	0.895
SFC	5.730	6.688
M_2	0.350	0.351
A_2 (ft^2)	0.359	0.387
A_3 (ft^2)	0.372	0.398
W_S/W_P	9.191	9.191

2. PRELIMINARY PERFORMANCE ESTIMATES

Performance of the MDB fueled ejector ramjet engine of Table VI has been generated for the Mach number-altitude range of interest and for a range of fuel flows corresponding to ϕ of 0.5 to 1.5. Typical net jet thrust coefficient and specific fuel consumption are shown in Figures 9 through 11. Figures 9, 10, and 11 present preliminary performance at Mach numbers 0.7, 0.9, and 1.2, respectively.

Engine airflow, fuel flow, mixer inlet Mach number (M_2), and ejector mixer total pressure ratio (P_{T_3}/P_{T_2}) are tabulated in Tables VIII, IX, X, and XI. In addition, mixer inlet total pressure and temperature are presented in Figures 12 and 13. These data were used to design the hypermixing ejector test item and plan the experimental program.

SECTION VII

FLIGHT ENGINE HYPERMIXING EJECTOR DESIGN

The design of the hypermixing ejector subsystem for the flight engine was established at the engine design point of $M_0 = 0.75$ at 20,000 feet/$\phi = 1.0$. Ejector design point conditions were established during the engine performance optimization study:

W_P = 0.78 lb/sec

P_{T_P} = 300 lb/in^2

T_{T_P} = 1800°R

A_P = 1.68 in^2

$P_P = P_2$ = 8.81 lb/in^2

For these ejector design conditions $M_P = 2.73$ and $A_P/A^* = 5.8$.

The required total ejector nozzle throat flow area was computed to be 0.29 in^2 As will be seen, the nozzle throat height is approximately 0.020 inch. Therefore, a relatively low nozzle throat discharge coefficient of 0.90 was assumed. This estimate was based on Marquardt experience with small rocket engines and annular air film cooling tests. The required nozzle throat area was then computed to be 0.322 in^2.

TABLE VIII. ENGINE AIRFLOW - PPS

M_o	ϕ	Altitude - 1000 ft, S.L.	10	20	30
1.2	.5	32.08	22.04	14.99	9.82
	.75	28.72	19.66	13.33	8.70
	1.0	26.57	18.16	12.29	8.01
	1.25	27.80	19.00	12.87	8.39
	1.5	29.84	20.42	13.85	9.05
1.05	.5	26.87	18.44	12.54	8.21
	.75	23.89	16.35	11.08	7.24
	1.0	22.08	15.08	10.21	6.65
	1.25	23.10	15.79	10.69	6.97
	1.5	24.84	16.99	11.52	7.52
.9	.5	22.22	15.24	10.36	6.78
	.75	19.99	13.67	9.26	6.05
	1.0	18.58	12.69	8.58	5.59
	1.25	19.48	13.31	9.01	5.87
	1.5	20.94	14.32	9.70	6.33
.8	.5	19.49	13.37	9.08	5.94
	.75	17.65	12.07	8.18	5.34
	1.0	16.50	11.27	7.63	4.97
	1.25	17.44	11.92	8.06	5.26
	1.50	18.87	12.91	8.74	5.70
.75	.5	18.18	12.46	8.46	5.54
	.75	16.52	11.30	7.65	4.97
	1.0	15.51	10.59	7.17	4.67
	1.25	16.47	11.25	7.61	4.97
	1.5	17.90	12.16	8.29	5.41
.70	.5	16.89	11.75	7.86	5.14
	.75	15.42	10.54	7.14	4.66
	1.0	14.53	9.93	6.72	4.38
	1.25	15.52	10.60	7.17	4.68
	1.50	16.96	11.59	7.85	5.12

TABLE IX. ENGINE FUEL FLOW - PPS

M_o	ϕ	Altitude - 1000 ft S.L.	10	20	30
1.2	.5	1.745	1.199	.815	.534
	.75	2.344	1.604	1.088	.710
	1.0	2.890	1.976	1.337	.872
	1.25	3.780	2.584	1.750	1.142
	1.50	4.870	3.333	2.260	1.476
1.05	.5	1.462	1.003	.682	.447
	.75	1.950	1.334	.904	.590
	1.0	2.402	1.641	1.110	.724
	1.25	3.142	2.148	1.454	.948
	1.50	4.053	2.773	1.880	1.227
.9	.5	1.209	.829	.563	.369
	.75	1.631	1.116	.756	.493
	1.0	2.021	1.380	.934	.609
	1.25	2.650	1.810	1.225	.799
	1.5	3.418	2.337	1.583	1.033
.8	.5	1.060	.727	.494	.323
	.75	1.440	.985	.667	.435
	1.0	1.796	1.226	.830	.541
	1.25	2.372	1.620	1.097	.715
	1.50	3.080	2.106	1.427	.931
.75	.5	.989	.678	.460	.301
	.75	1.348	.922	.624	.406
	1.0	1.687	1.152	.780	.508
	1.25	2.239	1.530	1.035	.675
	1.50	2.921	1.984	1.343	.883
.70	.5	.919	.639	.428	.280
	.75	1.258	.860	.583	.380
	1.0	1.581	1.080	.731	.476
	1.25	2.110	1.441	.975	.636
	1.5	2.768	1.892	1.282	.836

TABLE X. EJECTOR/MIXER INLET MACH NUMBER (M_2)

M_o	ϕ	W_S/W_P	Altitude - 1000 ft S. L.	10	20	30
1.2	.5	18.38	.553	.533	.511	.489
	.75	12.25	.472	.454	.436	.418
	1.0	9.19	.426	.411	.394	.377
	1.25	7.35	.452	.435	.417	.399
	1.5	6.13	.497	.478	.459	.439
1.05	.5		.540	.520	.500	.478
	.75		.459	.442	.424	.406
	1.00		.414	.399	.383	.367
	1.25		.439	.422	.405	.388
	1.50		.483	.464	.446	.426
.9	.5		.508	.490	.471	.451
	.75		.441	.425	.408	.391
	1.0		.402	.387	.372	.356
	1.25		.427	.410	.394	.377
	1.50		.469	.451	.432	.413
.8	.5		.480	.463	.445	.427
	.75		.421	.406	.390	.374
	1.0		.388	.374	.359	.344
	1.25		.415	.400	.384	.367
	1.5		.460	.442	.424	.406
.75	.5		.462	.446	.429	.412
	.75		.409	.394	.379	.362
	1.0		.378	.365	.351	.336
	1.25		.407	.392	.377	.361
	1.50		.453	.432	.418	.400
.7	.5		.442	.435	.411	.395
	.75		.394	.380	.366	.351
	1.0		.367	.354	.340	.326
	1.25		.397	.383	.368	.352
	1.5		.444	.428	.411	.393

TABLE XI. EJECTOR/MIXER TOTAL PRESSURE RATIO (P_{T_3}/P_{T_2})

M_o	ϕ	W_S/W_P	Altitude - 1000 ft S.L.	10	20	30
1.2	.50	18.382	1.0417	1.0432	1.0446	1.0459
	.75	12.255	1.0919	1.0929	1.0938	1.0947
	1.00	9.191	1.1353	1.1361	1.1368	1.1375
	1.25	7.353	1.1873	1.1882	1.1892	1.1900
	1.50	6.127	1.2463	1.2477	1.2489	1.2501
1.05	.50		1.0427	1.0440	1.0453	1.0464
	.75		1.0927	1.0936	1.0944	1.0952
	1.00		1.1359	1.1366	1.1372	1.1379
	1.25		1.1880	1.1889	1.1897	1.1905
	1.50		1.2474	1.2486	1.2497	1.2508
.9	.50		1.0444	1.0455	1.0465	1.0474
	.75		1.0929	1.0937	1.0944	1.0951
	1.00		1.1361	1.1367	1.1373	1.1379
	1.25		1.1885	1.1892	1.1900	1.1907
	1.50		1.2481	1.2491	1.2501	1.2509
.8	.50		1.0453	1.0463	1.0471	1.0477
	.75		1.0922	1.0930	1.0937	1.0941
	1.00		1.1350	1.1357	1.1363	1.1366
	1.25		1.1880	1.1888	1.1895	1.1900
	1.50		1.2484	1.2494	1.2503	1.2510
.75	.50		1.0454	1.0462	1.0471	1.0479
	.75		1.0915	1.0921	1.0928	1.0931
	1.00		1.1339	1.1345	1.1350	1.1355
	1.25		1.1872	1.1879	1.1887	1.1892
	1.50		1.2482	1.2486	1.2500	1.2508
.70	.50		1.0453	1.0463	1.0468	1.0474
	.75		1.0903	1.0910	1.0916	1.0920
	1.00		1.1322	1.1328	1.1334	1.1337
	1.25		1.1859	1.1866	1.1872	1.1876
	1.50		1.2476	1.2486	1.2493	1.2500

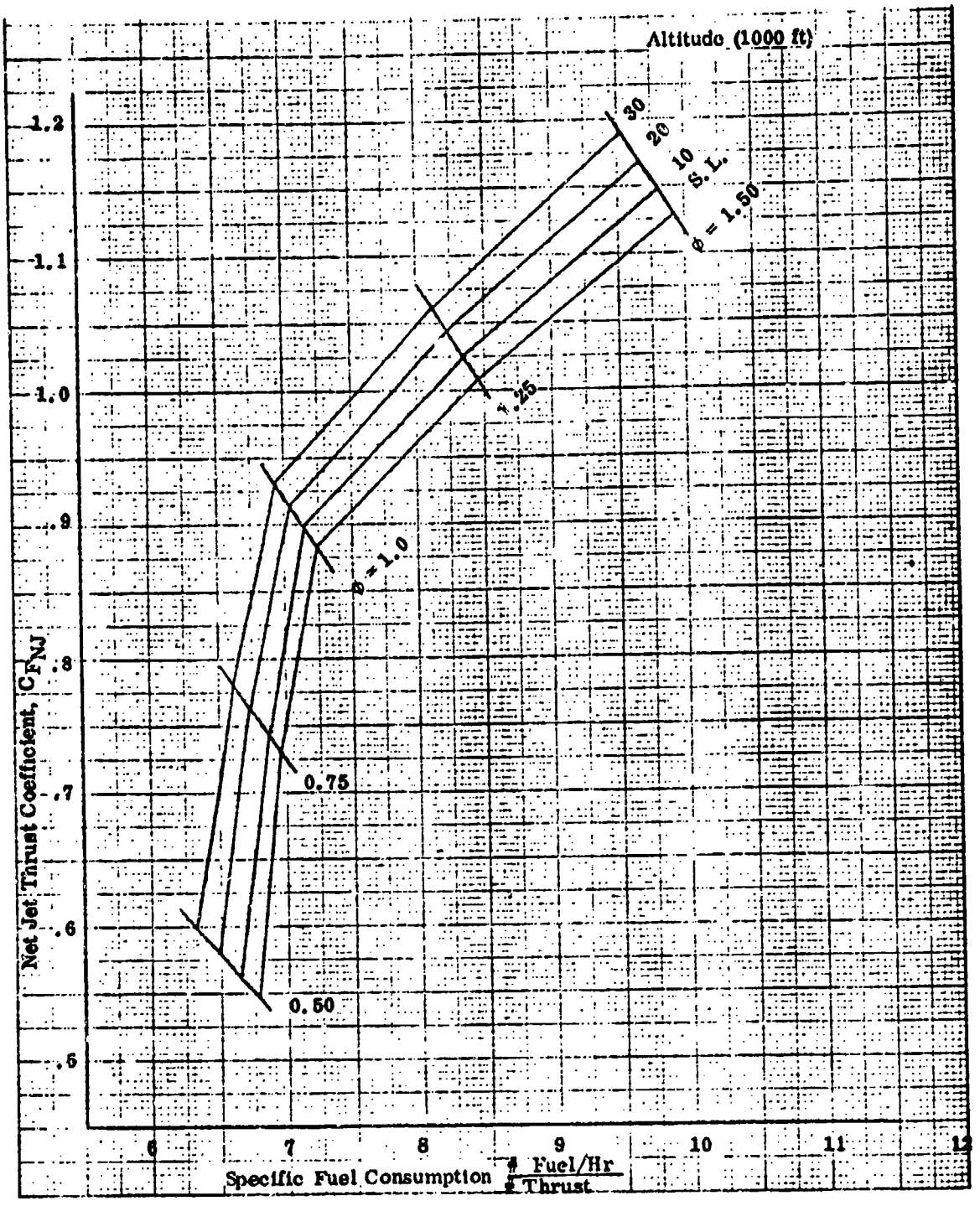

Figure 9. UDMH-Fueled Ejector Ramjet Engine Performance
$M_0 = 0.70$

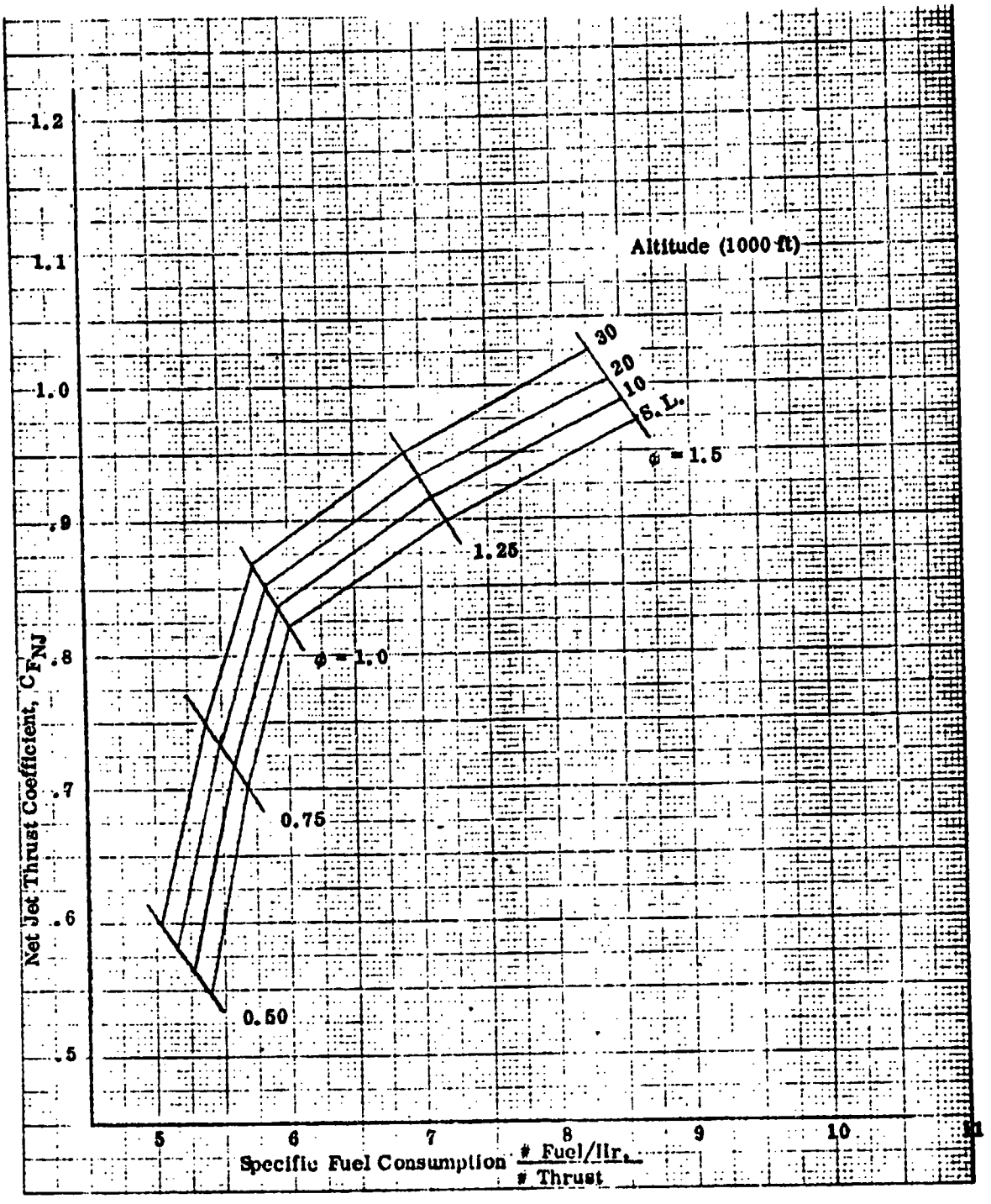

Figure 10. UDMH-Fueled Ejector Ramjet Engine Performance
$M_0 = 0.90$

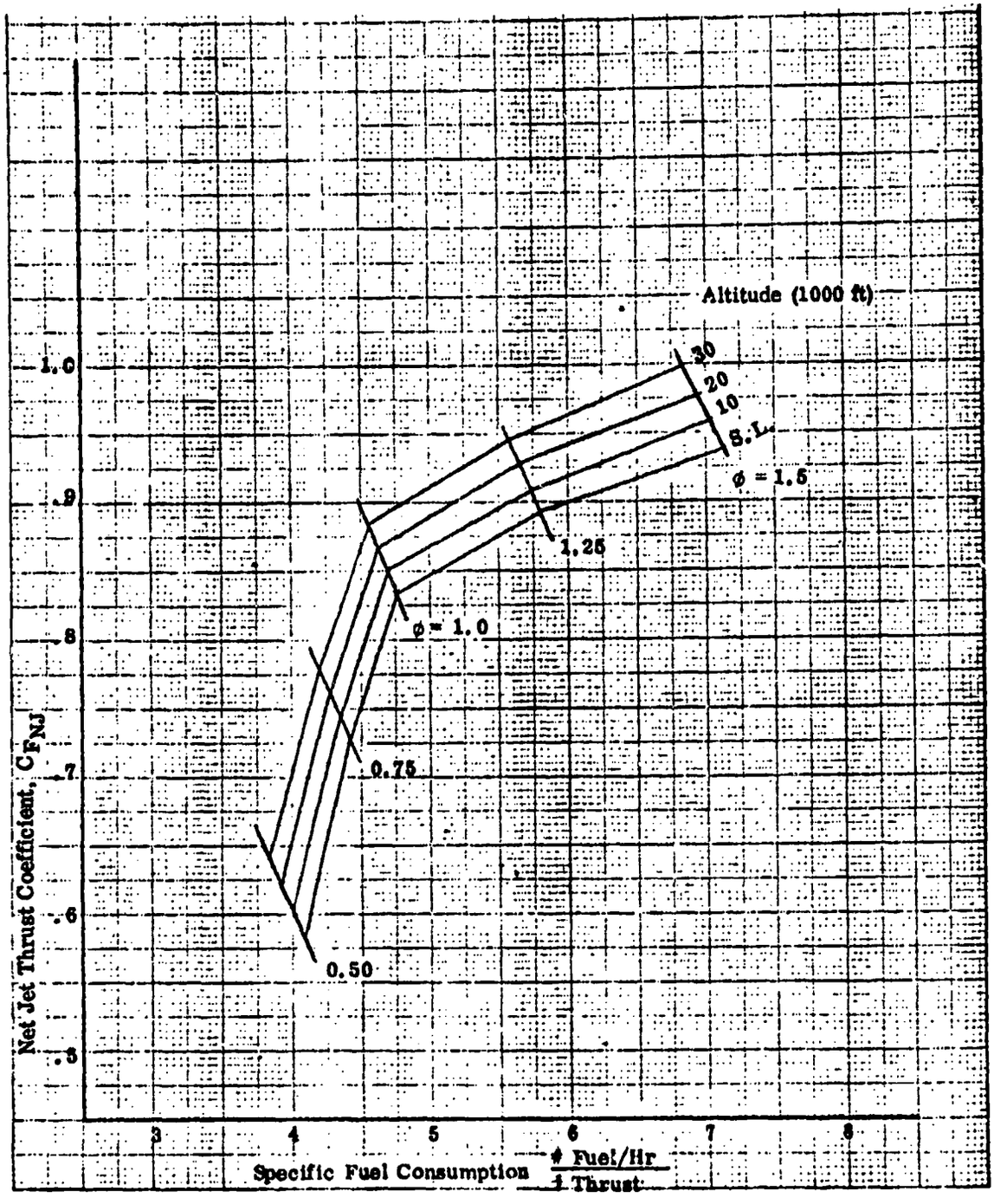

Figure 11. UDMH-Fueled Ejector Ramjet Engine Performance M_0=1.2

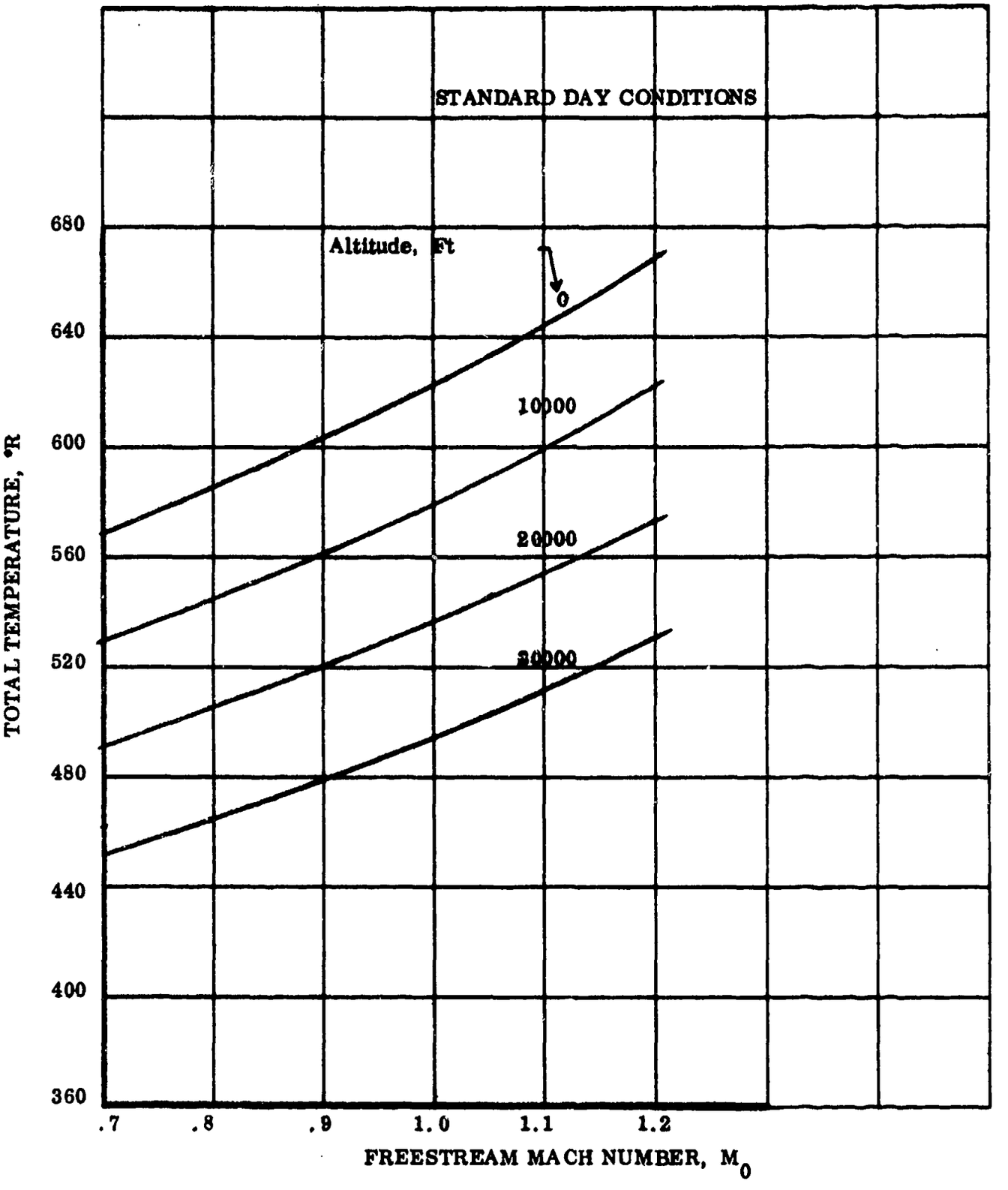

Figure 12. Freestream Total Temperature

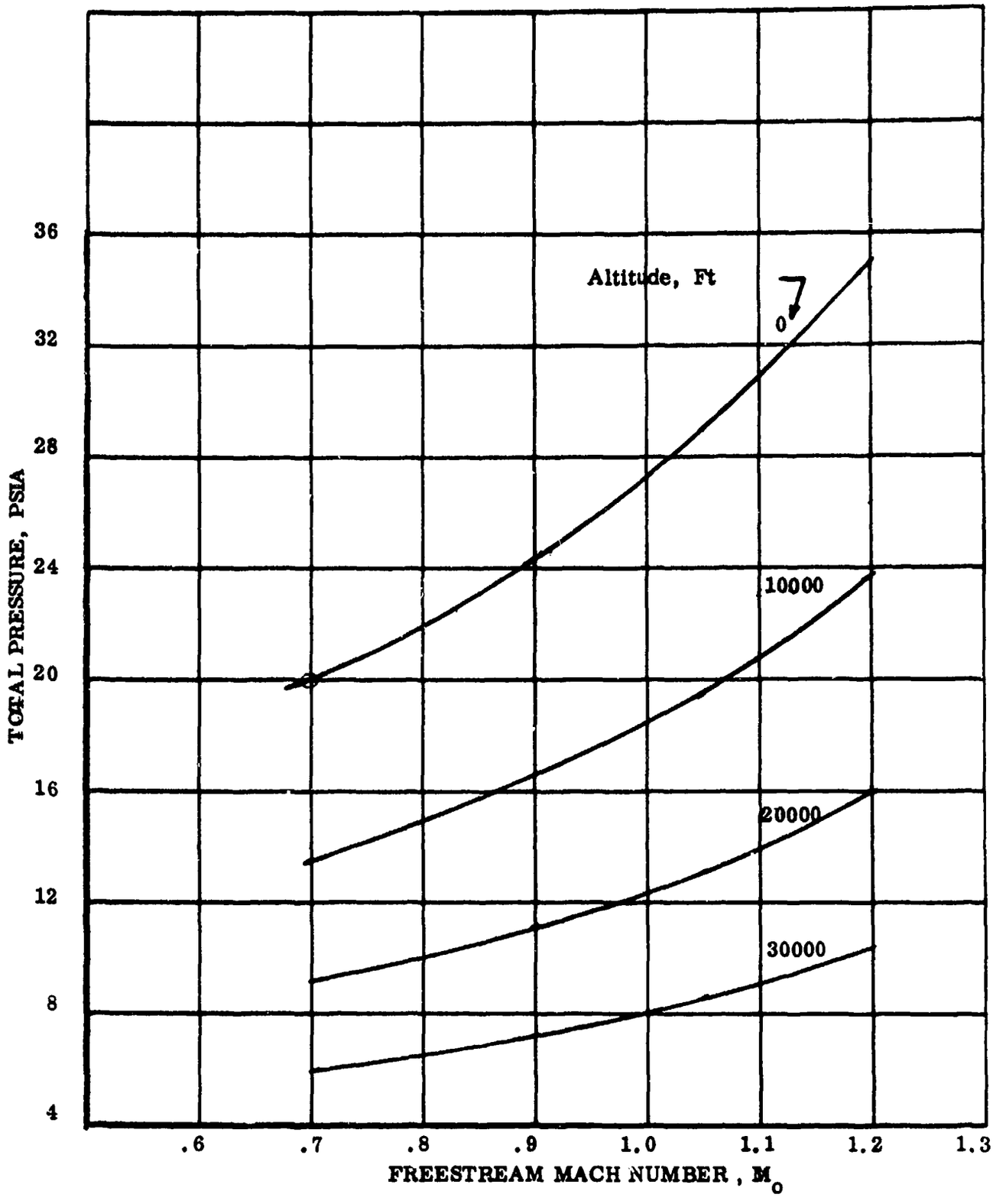

Figure 13. Mixer Inlet Total Pressure

Ejector nozzle geometry was sized with nozzle perimeter as the primary variable. The following relationships were used in this analysis:

$$\text{Nozzle Perimeter} = \frac{(2)\ (\text{Nozzle Exit Flow Area})}{\text{Nozzle Exit Height}}$$

$$\text{Nozzle Segment Aspect Ratio} = \frac{\text{Segment Length}}{\text{Exit Height}}$$

$$= 8 \text{ based on previous hypermixing ejector nozzle test data (Reference 5)}$$

$$\text{Number of Nozzle Segments} = \frac{\text{Nozzle Perimeter}}{(2)\ (\text{Segment Aspect Ratio})\ (\text{Exit Height})}$$

$$= \frac{\text{Nozzle Perimeter}}{(16)\ (\text{Exit Height})}$$

The results of this parametric design study are presented in Figures 14 and 15.

A manufacturing review of the proposed ejector nozzle assembly concluded that cost considerations clearly indicated a preference for a true annular nozzle rather than a large number of separately fabricated and assembled nozzle segments. Therefore, the annular nozzle was established as the baseline design concept.

The remaining question was: Where should the annular nozzle be located relative to the mixer diameter? Several approaches were taken in order to define this location.

Ejector primary/secondary air mixing basically is accomplished by shearing action and turbulence between the two streams. Therefore, a reasonable design approach is to locate the annular ejector nozzle so that the inner and outer duct flow areas are equal.

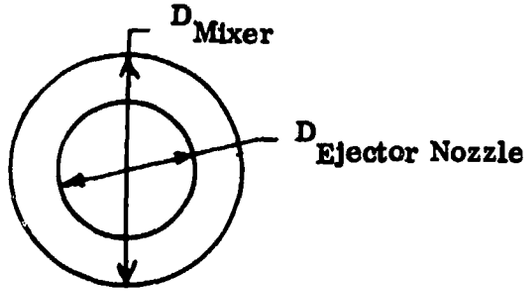

Therefore the ejector would be located where

$$\frac{D_{Ejector\ Nozzle}}{D_{Mixer}} = \sqrt{\frac{A_{Ejector\ Nozzle}}{A_{Mixer}}} = \sqrt{\frac{1}{2}} = 0.707$$

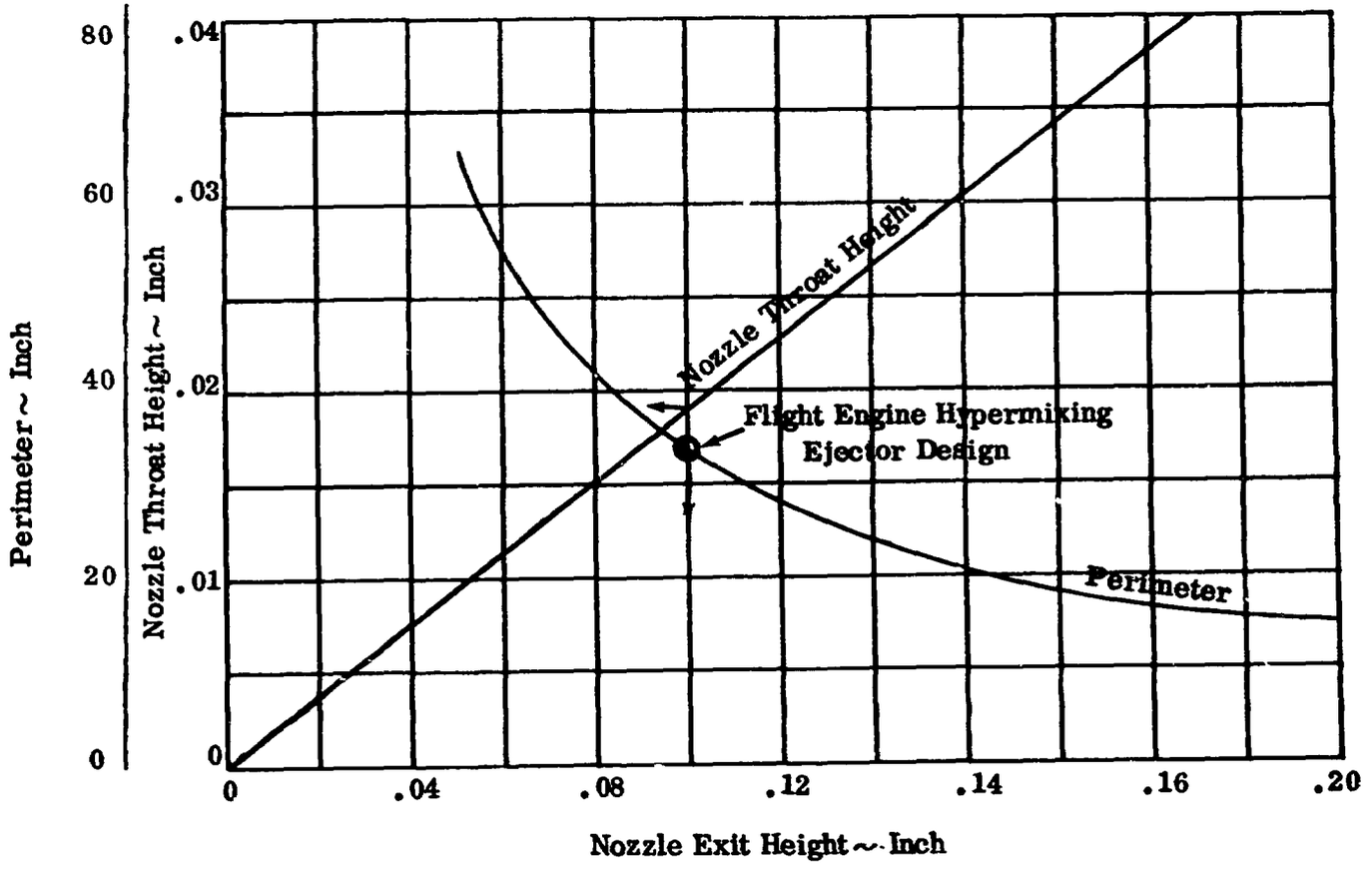

Figure 14. Hypermixing Ejector Geometry - Part 1

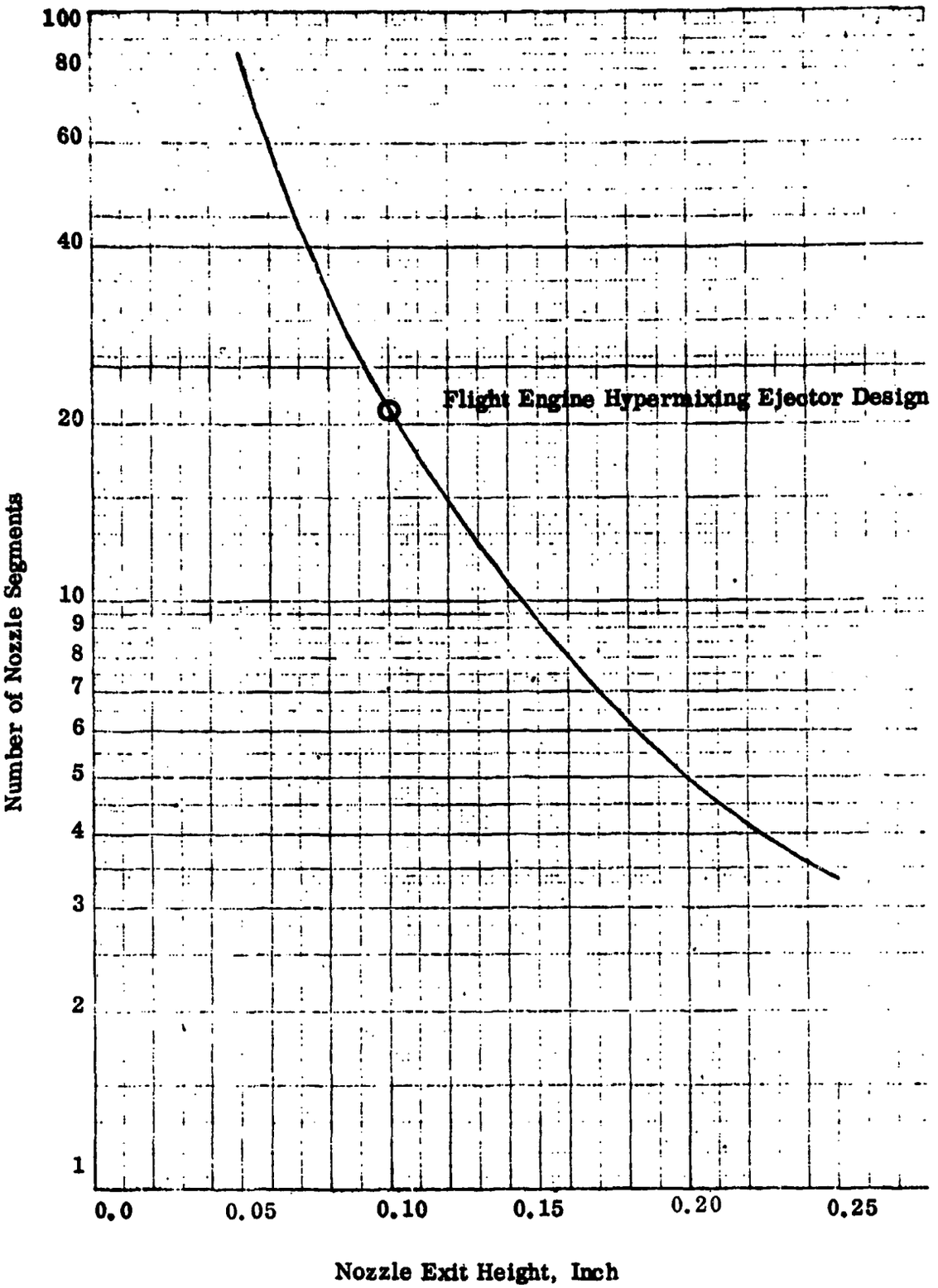

Figure 15. Hypermixing Ejector Geometry - Part 2

A mixing process spreading angle approach was the second technique used to locate the ejector nozzle.

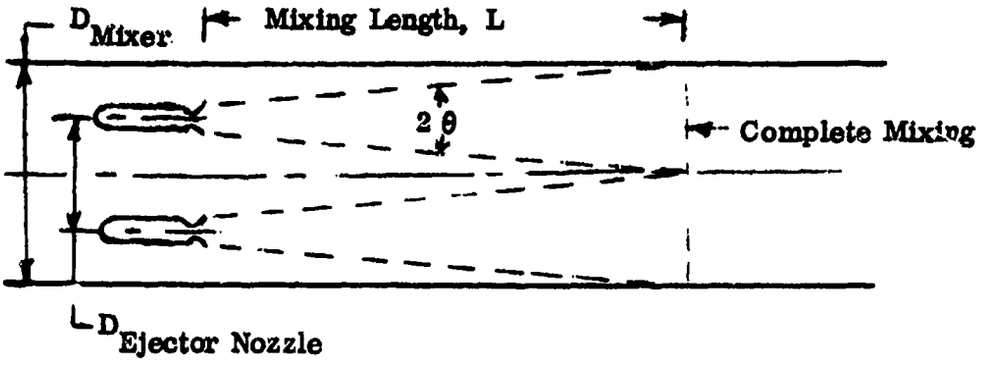

Obviously, this approach locates the ejector nozzle where

$$\frac{D_{Ejector\ Nozzle}}{D_{Mixer}} = 0.50$$

Mixing lengths were roughly estimated from this approach. Reference 5 data show that the spreading angle for the hypermixing ejector nozzle is ~ 12 degrees. Conventional mixing corresponds to a spreading angle of about 6 degrees. For the geometry under consideration, the following mixing lengths were computed:

Conventional mixing ($\theta = 6$ degrees) $L \cong 20$ inches

Hypermixing ($\theta = 12$ degrees) $L \cong 10$ inches.

These computed mixing lengths are obviously estimates but do indicate the potential of the hypermixing concept.

It is highly probable that, due to three dimensional pipe flow effects, neither of these approaches is correct. However, it is reasonable to assume that the actual flow process lies between these two limits. Therefore

$$0.50 < \frac{D_{Ejector\ Nozzle}}{D_{Mixer}} < 0.707.$$

An objective of this program is to compare hypermixing ejector with "conventional" ejector nozzle performance. Marquardt under Contract AF33(657) 12146 evaluated a "conventional" annular nozzle. In this test program

$$\frac{D_{Ejector\ Nozzle}}{D_{Mixer}} = 0.63.$$

This nozzle location meets our criteria and should be a valuable source of comparison. Therefore, this location was selected for the design of the flight engine hypermixing ejector.

Previous hypermixing ejector nozzle tests operated with subsonic flow discharge conditions (Reference 5). For the same scarf angle, it was reasoned that a supersonic ejector nozzle would promote more rapid mixing than a subsonic nozzle. It, therefore, follows, for the same mixing intensity, the supersonic nozzle scarf angle can be reduced. Previous subsonic nozzle tests evaluated this nozzle:

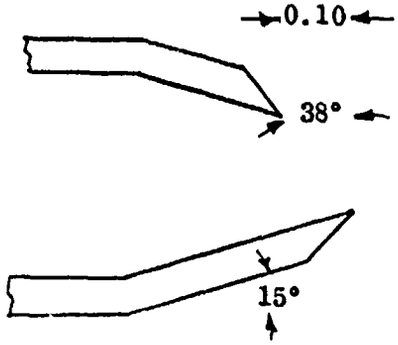

Somewhat arbitrarily, alternating supersonic nozzle segments of the flight engine hypermixing ejector subsystem were scarfed 30 degrees. The design characteristics of the flight engine hypermixing ejector subsystem are summarized below:

$\frac{D_{\text{Ejector Nozzle}}}{D_{\text{Mixer}}}$	0.63
D_{Mixer}	8.54 in.
$D_{\text{Ejector Nozzle}}$	5.38 in.
Nozzle Perimeter	33.8 in.
Number of Nozzle Segments	22
Nozzle Throat Height	0.017 in.
Nozzle Exit Height	0.100 in.
Nozzle Segment Aspect Ratio	7.68
Scarf Angle	30 degrees

Design details of the ejector subsystem are presented in Figure 16. Figure 17 shows the ejector subsystem integrated into the flight engine design. The flight engine mixer length/diameter ratio was specified as 1.24.

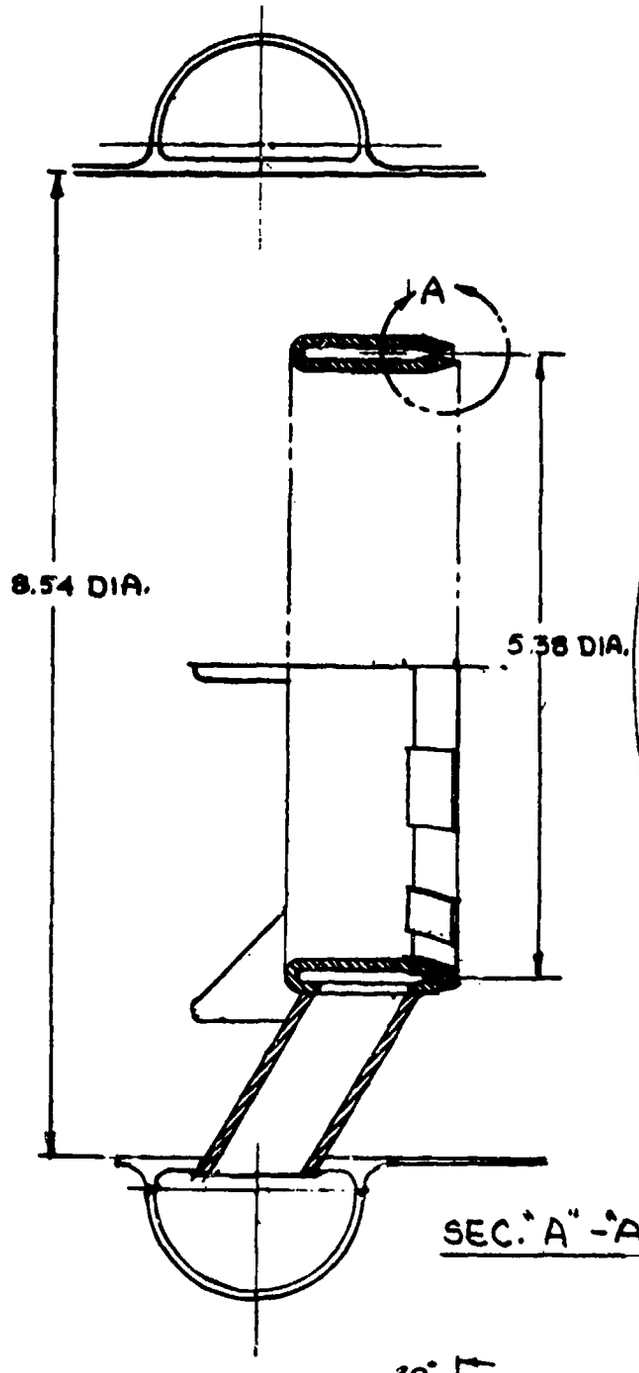

SEC. "A" - "A"

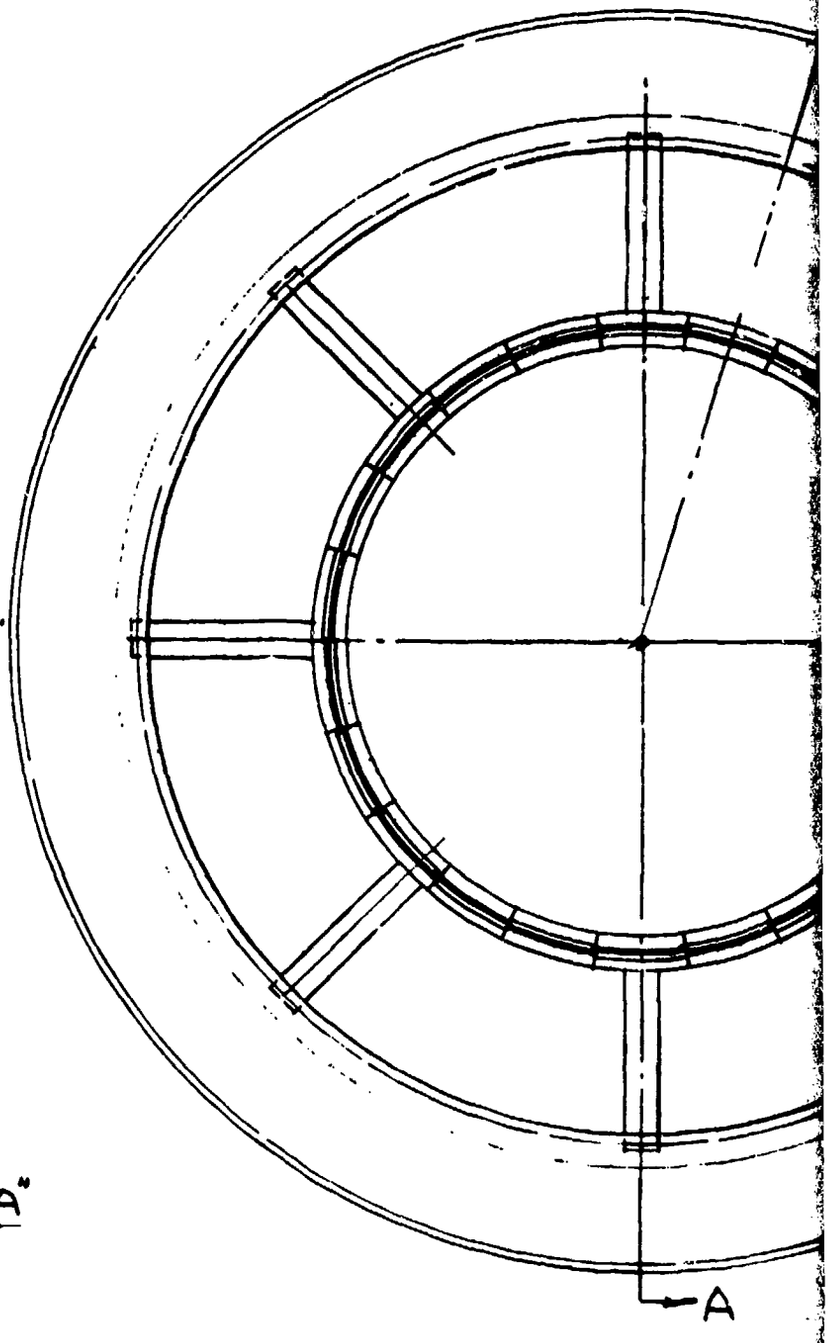

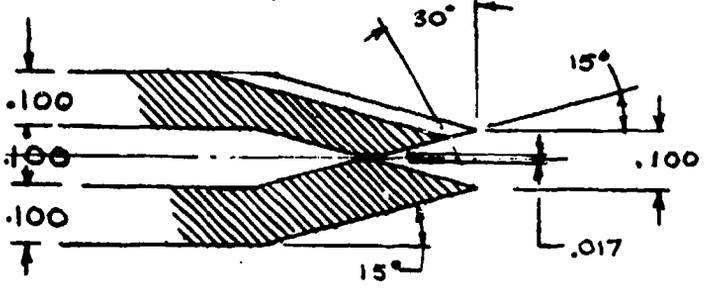

DETAIL "A"
SCALE: 5/1

A

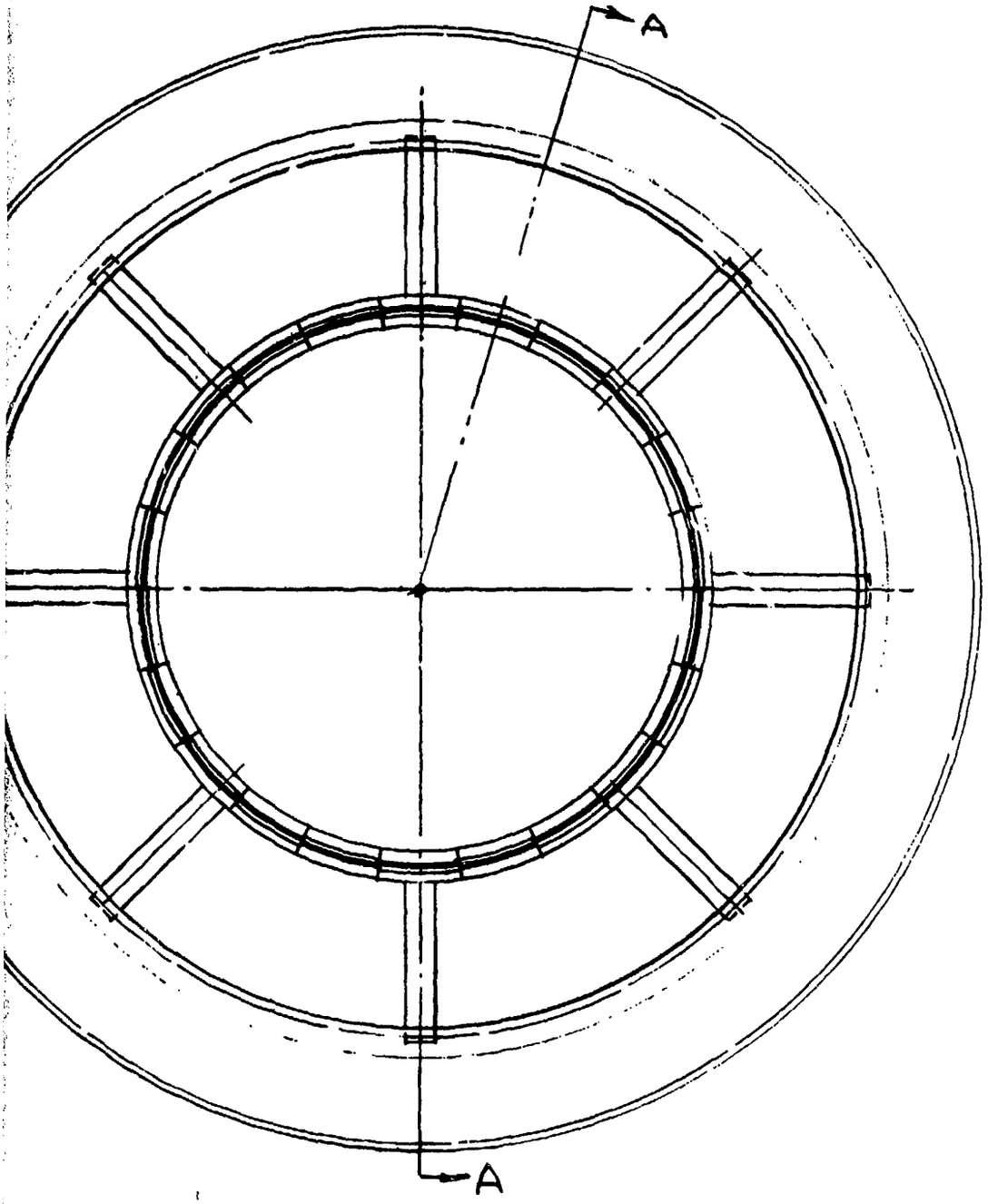

Figure 16. Hypermixing Ejector Nozzle Assembly

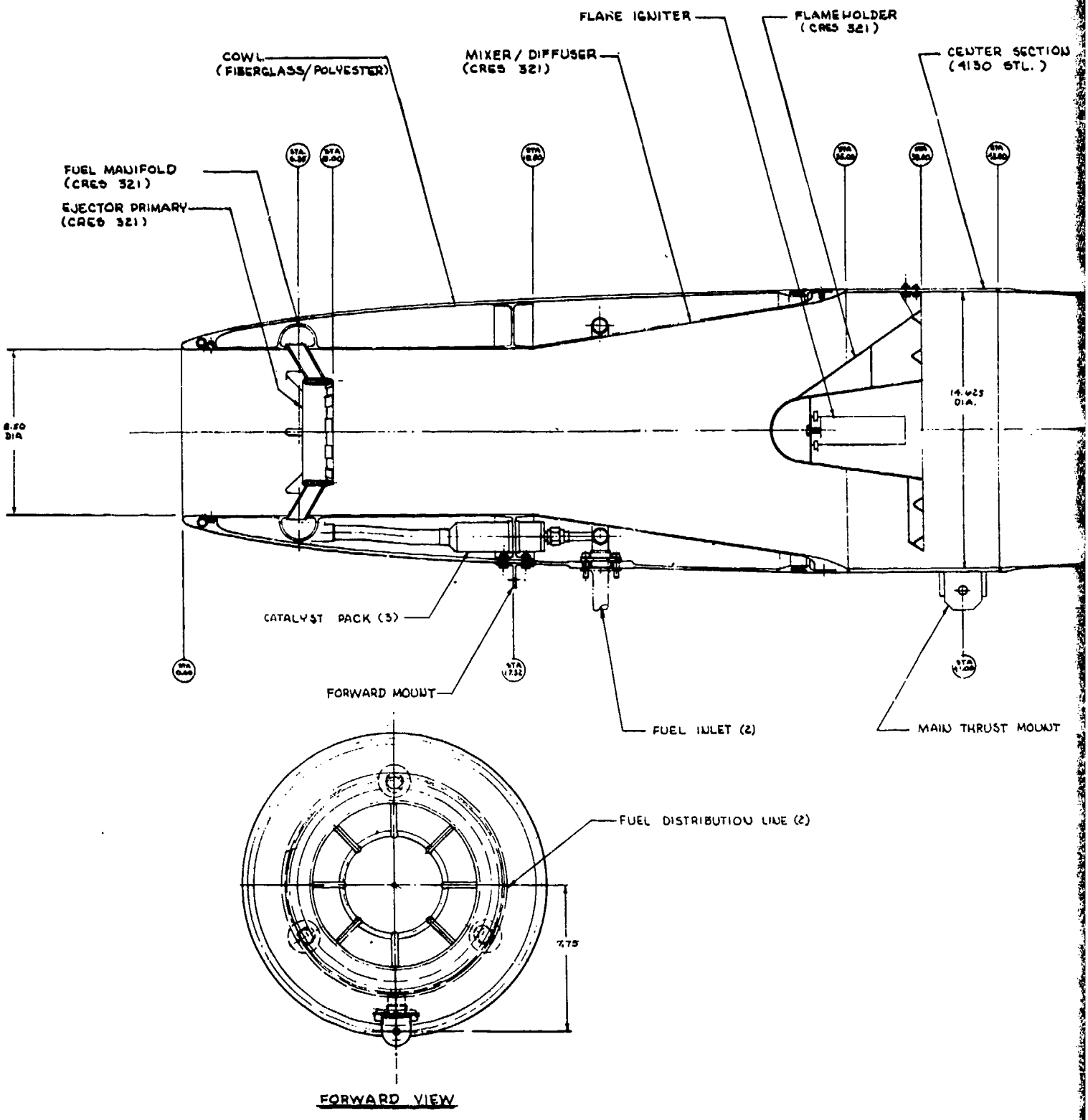
FLAME IGNITER
FLAMEHOLDER
(CRES 321)
COWL
(FIBERGLASS/POLYESTER)
MIXER/DIFFUSER
(CRES 321)
CENTER SECTION
(4130 STL.)
FUEL MANIFOLD
(CRES 321)
EJECTOR PRIMARY
(CRES 321)
8.50
DIA
14.625
DIA.
CATALYST PACK (3)
FORWARD MOUNT
FUEL INLET (2)
MAIN THRUST MOUNT
FUEL DISTRIBUTION LINE (2)
7.75
FORWARD VIEW

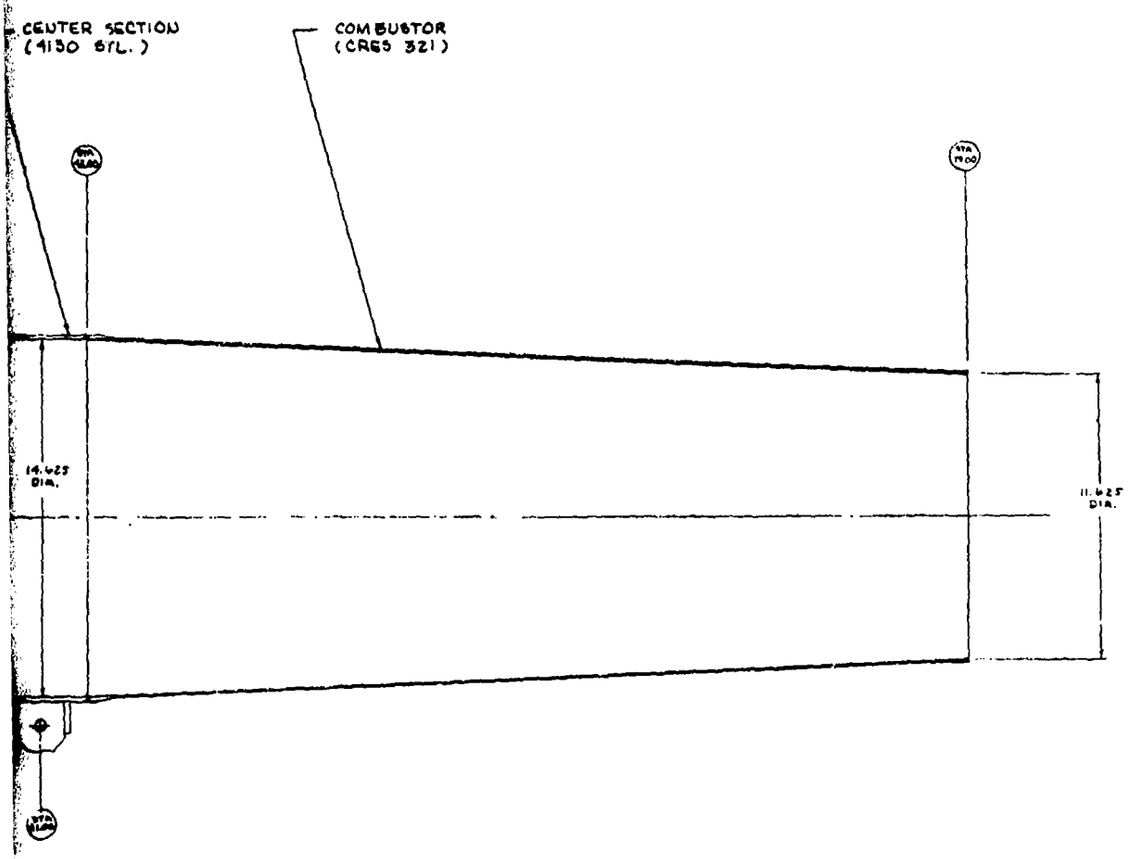

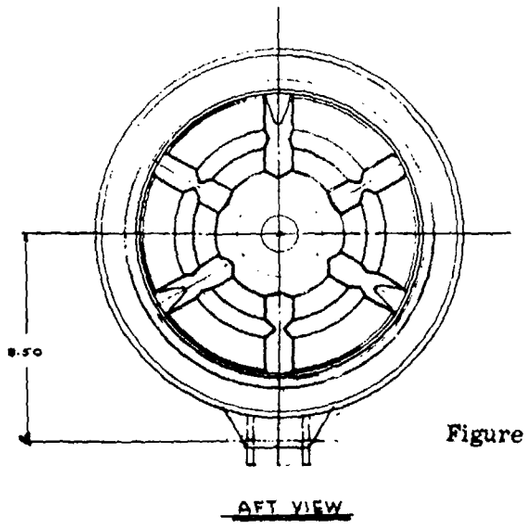

Figure 17. Low Cost Ejector Ramjet Engine Hypermixing Ejector Design.

SECTION VIII

HYPERMIXING EJECTOR TEST ITEM DESIGN

To minimize test cost, the hypermixing ejector test program was conducted at sea level conditions. By this is meant that the test item nozzle was exhausted to atmospheric conditions (~ 14.2 psia). Exhauster operation, which is costly, is required to reduce nozzle back pressure necessary for altitude simulation.

The test item was designed for the following conditions/specifications:

Simulated Flight Condition	$M_0 = 0.7$ at Sea Level at $\phi = 1$
Ejector Working Fluid	Heated Air
Secondary Fluid	Ambient Temperature Air
P_{T_P} =	300 psia
T_{T_P} =	1160°R
$P_P = P_2$ =	18.4 psia
M_2 =	0.35
A_2 =	22.5 in^2 (5.35 in. diameter duct)

For these test conditions, the secondary airflow rate is 5.70 lb/sec. With UDMH, $\phi = 1.0$ is equivalent to $\frac{W_S}{W_P} = 9.19$. Therefore, the hypermixing ejector nozzle test item was sized for a flow rate of 0.62 lb/sec.

To reduce test costs, the primary working fluid was air. Heated air was specified for the following reasons:

1) Increasing the total temperature of the primary increases the ejector discharge velocity, resulting in increased jet compression $\left(\frac{P_{T_3}}{P_{T_2}}\right)$.

2) Freon*, in small concentrations, was to be added to the primary fluid for gas sampling. A high primary total temperature avoids Freon condensation problems.

Test hardware design, fabrication, and operation costs are significantly reduced when non-water cooled hardware is specified. The desire for a high primary temperature was strongly tempered by this requirement. As a compromise the test hardware was designed for a primary total temperature of 1160°R (700°F).

*In the experimental program, carbon dioxide rather than Freon was used as the tracer gas.

The design conditions specified above defined a total nozzle throat area requirement of 0.147 in^2. The design nozzle pressure ratio

$$\left(\frac{P_{T_P}}{P_P}\right) = 16.3$$

corresponds to a nozzle exit Mach number of 2.47 and A_p/A^* ratio of 2.56. The resultant nozzle exit flow area is 0.376 in^2.

For the reasons presented in the flight engine ejector nozzle design discussion, an annular ring nozzle located where

$$\frac{D_{\text{Ejector Nozzle}}}{D_{\text{Mixer}}} = 0.63$$

was specified. Geometry constraints would not permit the ejector test item and the flight engine ejector to have both the same number of nozzle segments and segment aspect ratio. A decision was made to match the number of nozzle segments and let the segment aspect ratio fall out. The resultant aspect ratio was 11.5. Nozzle segments were alternately scarfed 30 degrees as was specified for the flight engine design.

The design characteristics of the hypermixing ejector test item are presented below:

$\frac{D_{\text{Ejector Nozzle}}}{D_{\text{Mixer}}}$	0.63
Ejector Nozzle Diameter	3.37 in.
Mixer Diameter	5.35 in.
Nozzle Perimeter	21.17 in.
Number of Nozzle Segments	22
Nozzle Throat Height	.0140 in.
Nozzle Exit Height	.031 in.
Nozzle Segment Aspect Ratio	11.5
Nozzle Scarf Angle	30 degrees

Figures 18 and 19 present the design details for the ejector test item.

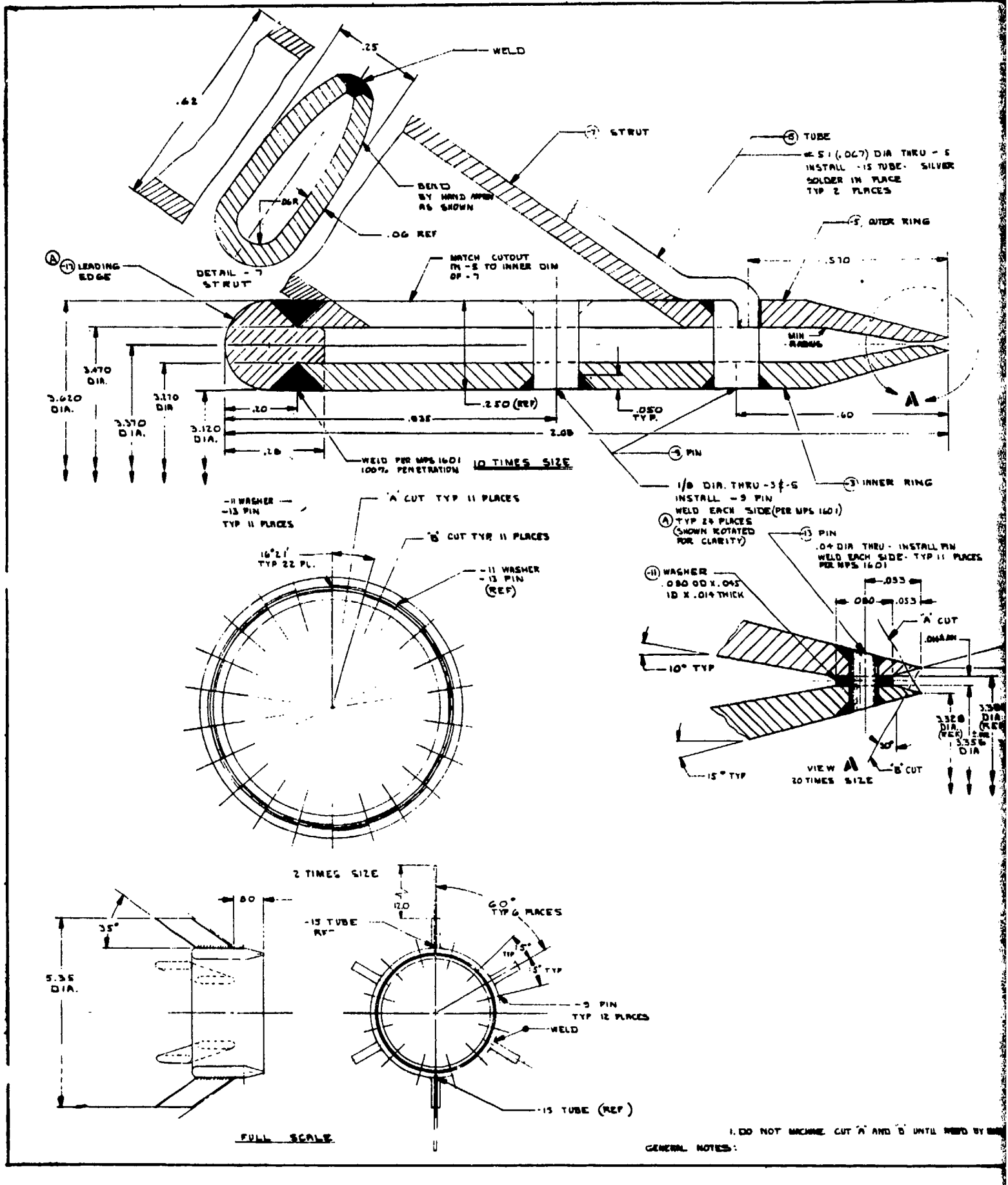

GENERAL NOTES:

1. DO NOT MACHINE CUT 'A' AND 'B' UNTIL [illegible]

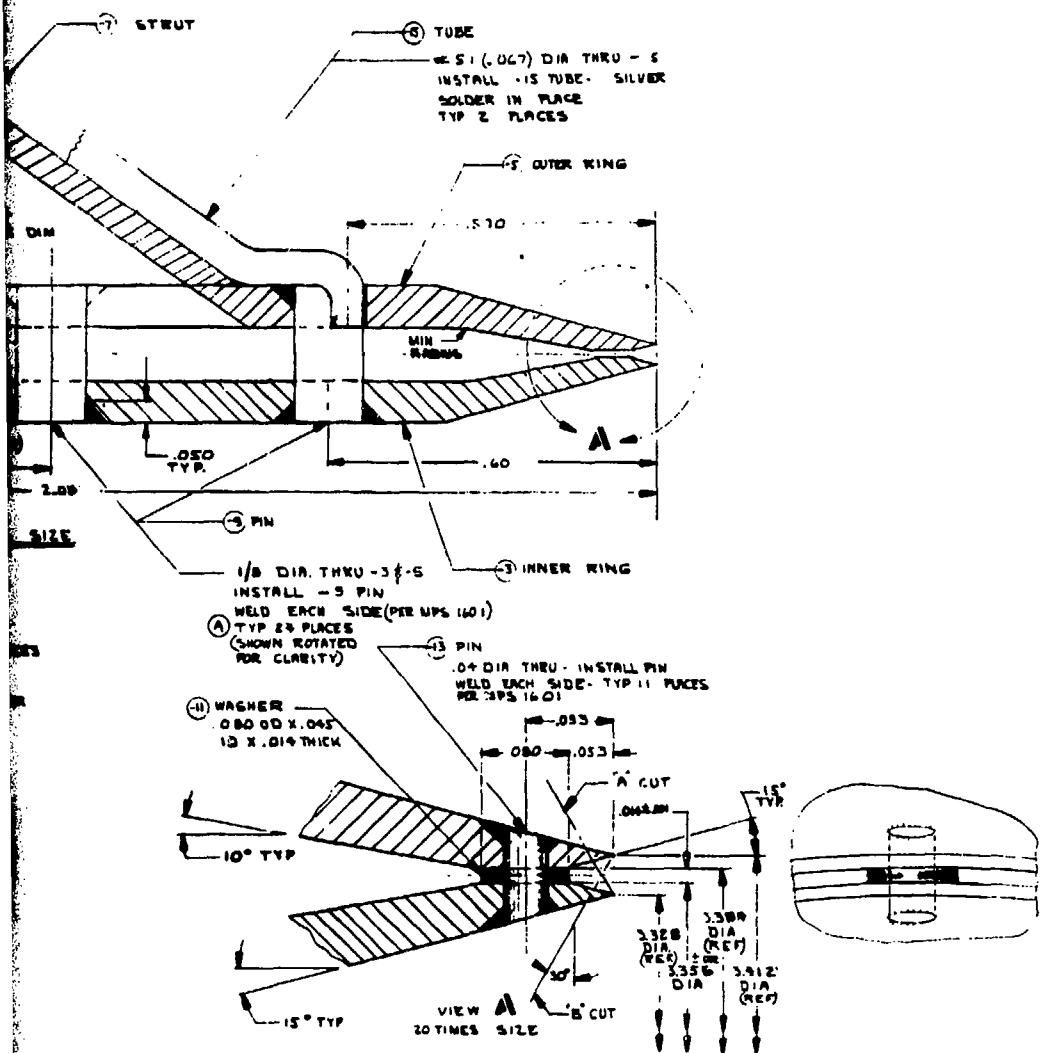

A	1	-17	LEADING EDGE	COML STAINLESS 321	.312 X .5 3/4 X 3 3/4		
	2	-15	TUBE	COML STAINLESS	1/16 ODX.012 WALL X 14.00 LG		
	13	-13	PIN	COML STAINLESS	.040 DIA X .375 LONG		
	11	-11	WASHER	COML STAINLESS	.014 SAME STOCK		
	24	-9	PIN	COML STAINLESS	.080 DIA X 1/8 LONG		
	6	-7	STRUT	COML STAINLESS 321	1/16 X 12 X 6.0 SHEET		PR MPS 1601
	1	-5	OUTER RING	COML STAINLESS 321	3.15 OD X .375 WALL TUBING		PR MPS
	1	-3	INNER RING	COML STAINLESS 321	3.5 OD X .250 WALL TUBING		PR MPS

LIST OF MATERIALS OR PARTS LIST

Figure 18. Hypermixing Ejector Nozzle Test Item

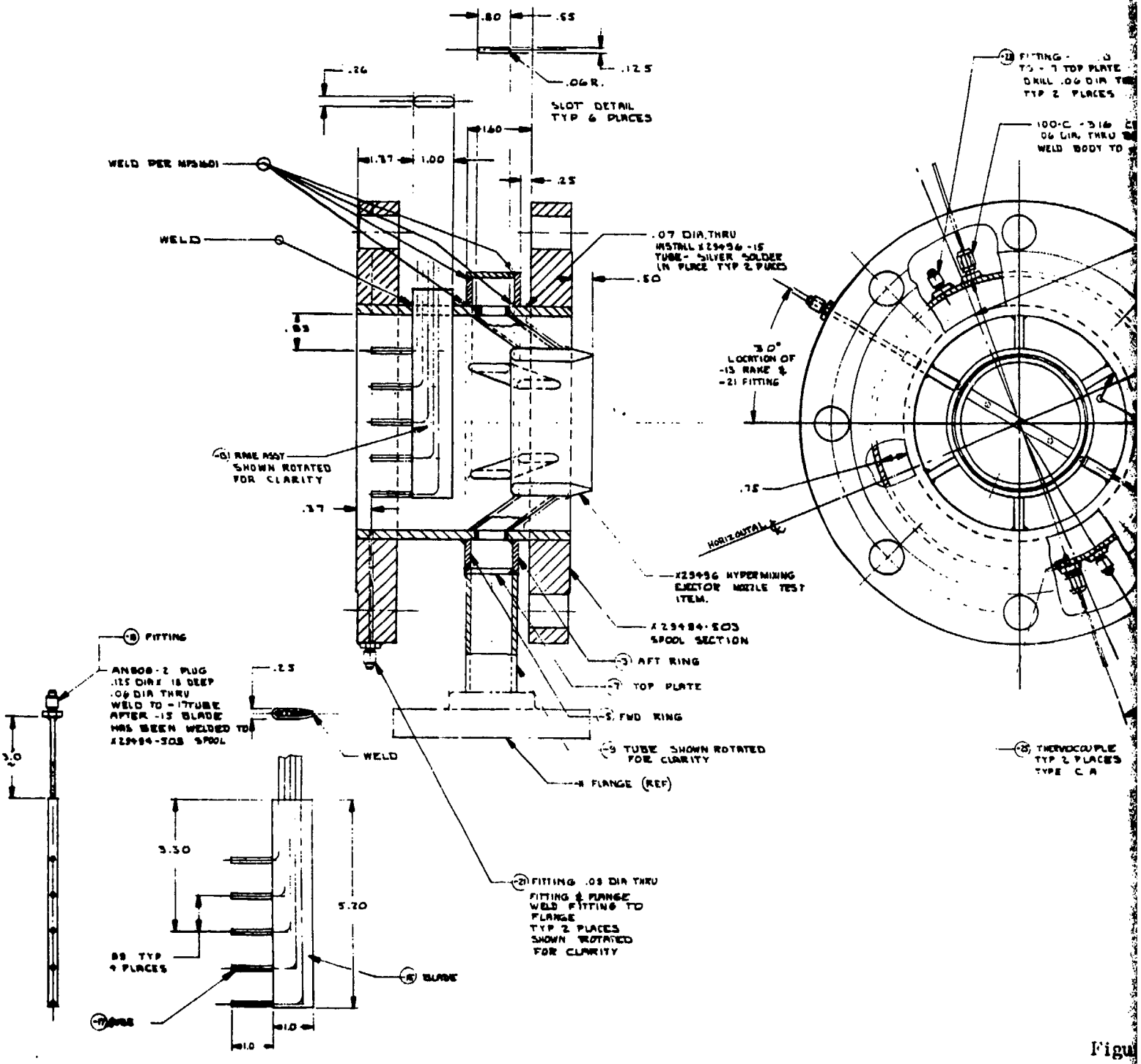

DETAIL -13 RAKE ASSY

Figu

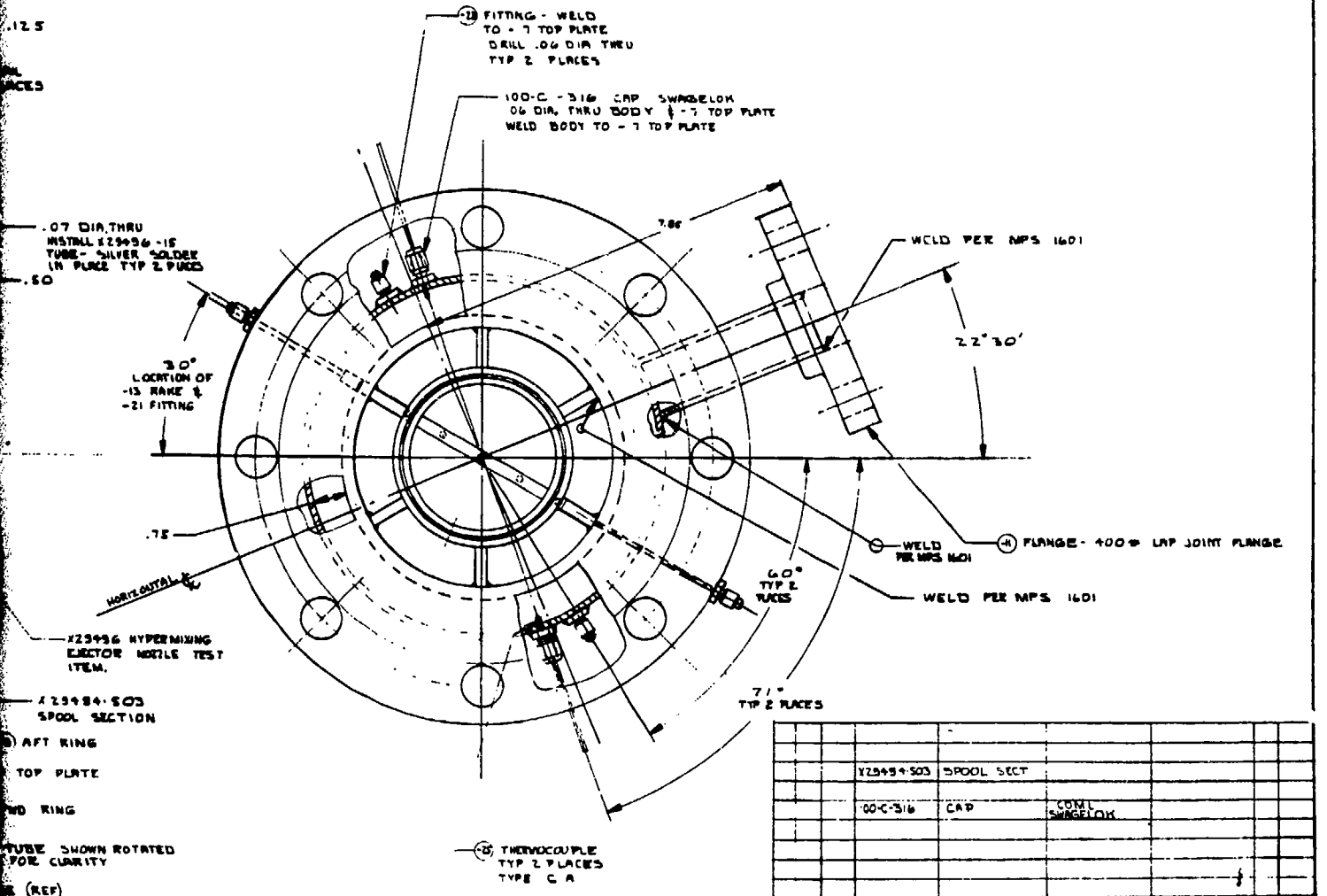

			X29494-503	SPOOL SECT				
			100-C-316	CAP	COML SWAGELOK			
			-23	FITTING	COML	AN806-8		
			-21	FITTING	COML	AN806-2		
			-13	FITTING	COML	AN806-2		
			-17	TUBE	COML 321 STAINLESS	1/8 OD X .049 WALL X 12.0 LG		
			-15	BLADE	COML 321 STAINLESS	.032 X 2 1/2 X 6.0		
			-13	RAKE ASSY				
			-11	FLANGE	COML-STEEL	400# LAP JOINT		
			-9	TUBE	COML 1015 MILD STEEL	1 (NOM) .120 WALL 9.0		
			-7	TOP PLATE	COML MILD STEEL	1/8 X 1 1/4 X 26.0		
			-5	FWD RING	COML MILD STEEL	1/8 X 8.0 X 8.0		
			-3	AFT RING	COML MILD STEEL	1/8 X 8.0 X 8.0		
QTY REQD	ITEM SYMBOL	PART OR IDENTIFYING NO.	DESCRIPTION OF MATERIAL OR PART	SPECIFICATION	MATERIAL OR SIZE	REMARKS	PART OR STOCK NO.	

LIST OF MATERIALS OR PARTS LIST

Figure 19. Hypermixing Ejector Nozzle Test Item Assembly

SECTION IX

EXPERIMENTAL PROGRAM

1. HARDWARE FABRICATION

The Hypermixing Ejector Test Item was fabricated in Marquardt's experimental shop. Photographs of the completed assembly are presented in Figures 20 through 23. For proper orientation, the reader is reminded that the ejector nozzle throat height and nozzle exit height are 0.014 inches and 0.031 inches, respectfully.

Three total pressure/gas sampling rakes were also fabricated and are shown in Figure 24. In addition, three mixer spool sections were fabricated in support of this program.

2. TEST SETUP

The test setup originally proposed is presented in Figure 25. The mixer was made up of varying length, constant internal diameter spools, joined at their flanges. By interchanging or removing the constant diameter mixer spools, the length of the mixer could be changed, and total and static pressure instrumentation could be relocated to determine mixer performance best. Downstream of the mixer was a diffuser, a plenum section, and exit nozzle to simulate components of the ejector ramjet engine. Engine airflow was simulated by bringing in airflow from pressurized storage tanks through suitable metering equipment. A flow straightening screen and setting section length was provided ahead of the ejector spool section to provide a near uniform flow profile to the test item. The ejector air supply was passed through a Sudden Expansion (SUE) burner and Freon was envisioned as a tracer gas to be monitored in the mixer to aid in determination of the rate of mixing of the secondary air and primary flow systems.

Figure 26 is a schematic of the actual test setup utilized in Cell 7 of Marquardt's test facility. This system was designed to provide a wide range of primary and secondary flow rates as well as interchangeability of mixer components. The secondary airflow system, the ejector test item, the interchangeable mixing section spools, diffuser, etc. are largely unchanged from those initially proposed. The principle variations from the original plan were associated with the primary airflow system and involved the use of a large SUE burner and the substitution of carbon dioxide (CO_2) for Freon as the tracer gas as discussed in the following paragraphs.

In Figure 26, the straightening spool, the ejector test item, the first mixer spool (L/D=2), and second mixer spool (L/D=1) are new hardware. The remainder of this hardware was available from previous Marquardt test programs. Note that two exit nozzle sizes and two secondary airflow metering venturis were used. For the smaller values of secondary airflow (25 and 50% of design), it was desired that the venturi remain choked for accurate metering purposes. The smaller venturi meter provided this capability. The smaller exit nozzle was used to maintain a higher backpressure

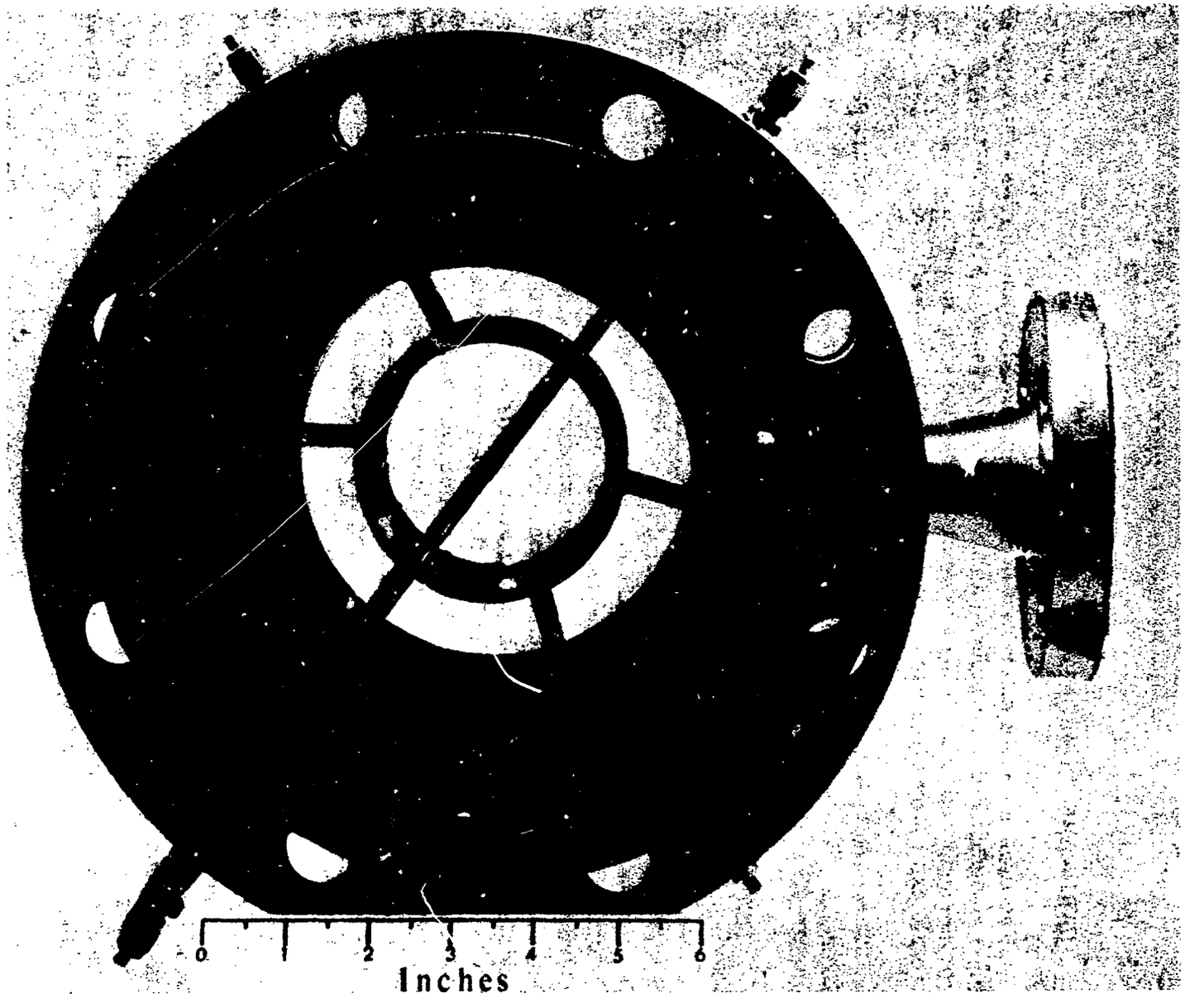

Figure 20. Hypermixing Ejector Nozzle Test Item Assembly, Front View

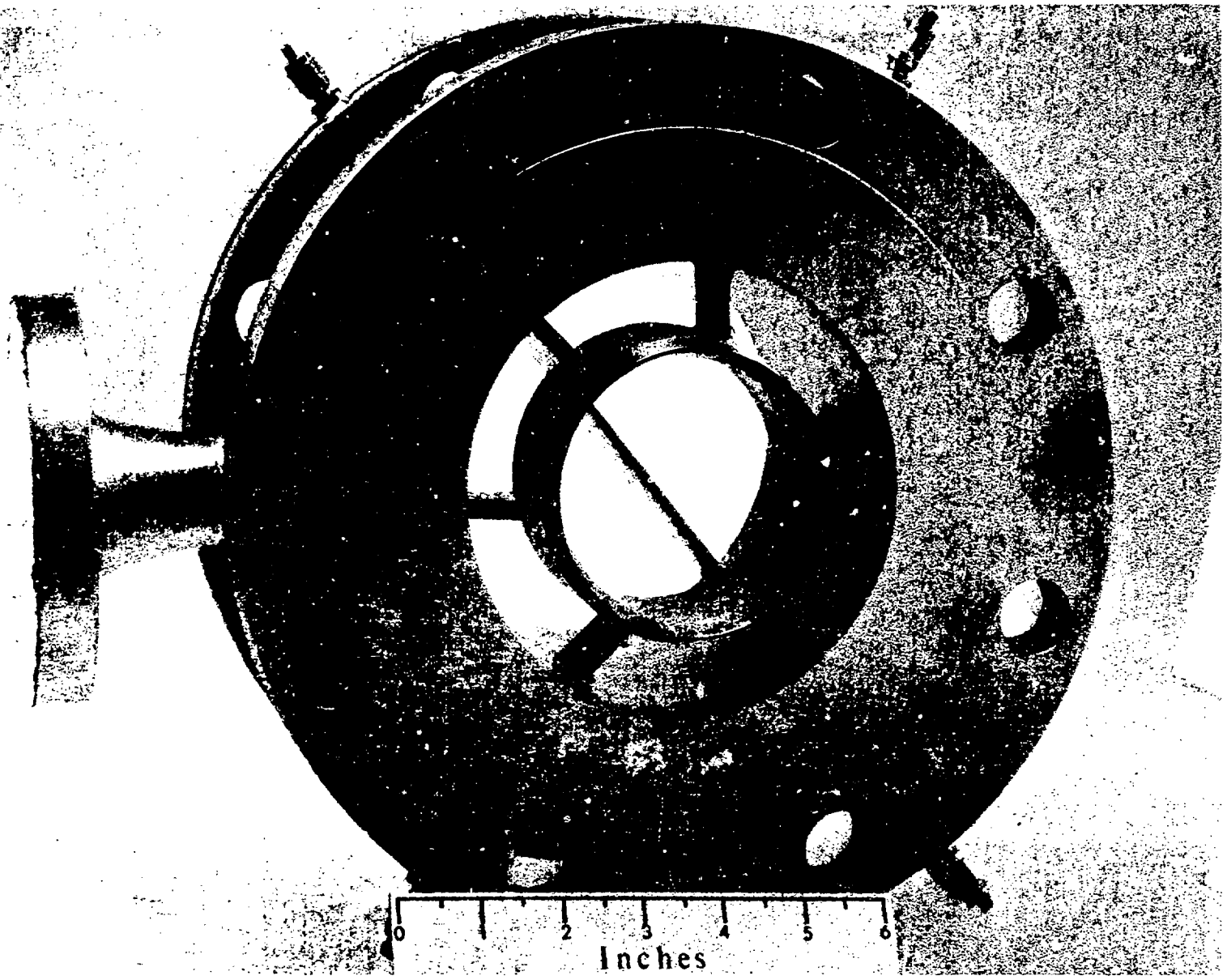

Figure 21. Hypermixing Ejector Nozzle Test Item Assembly, 3/4 Rear View

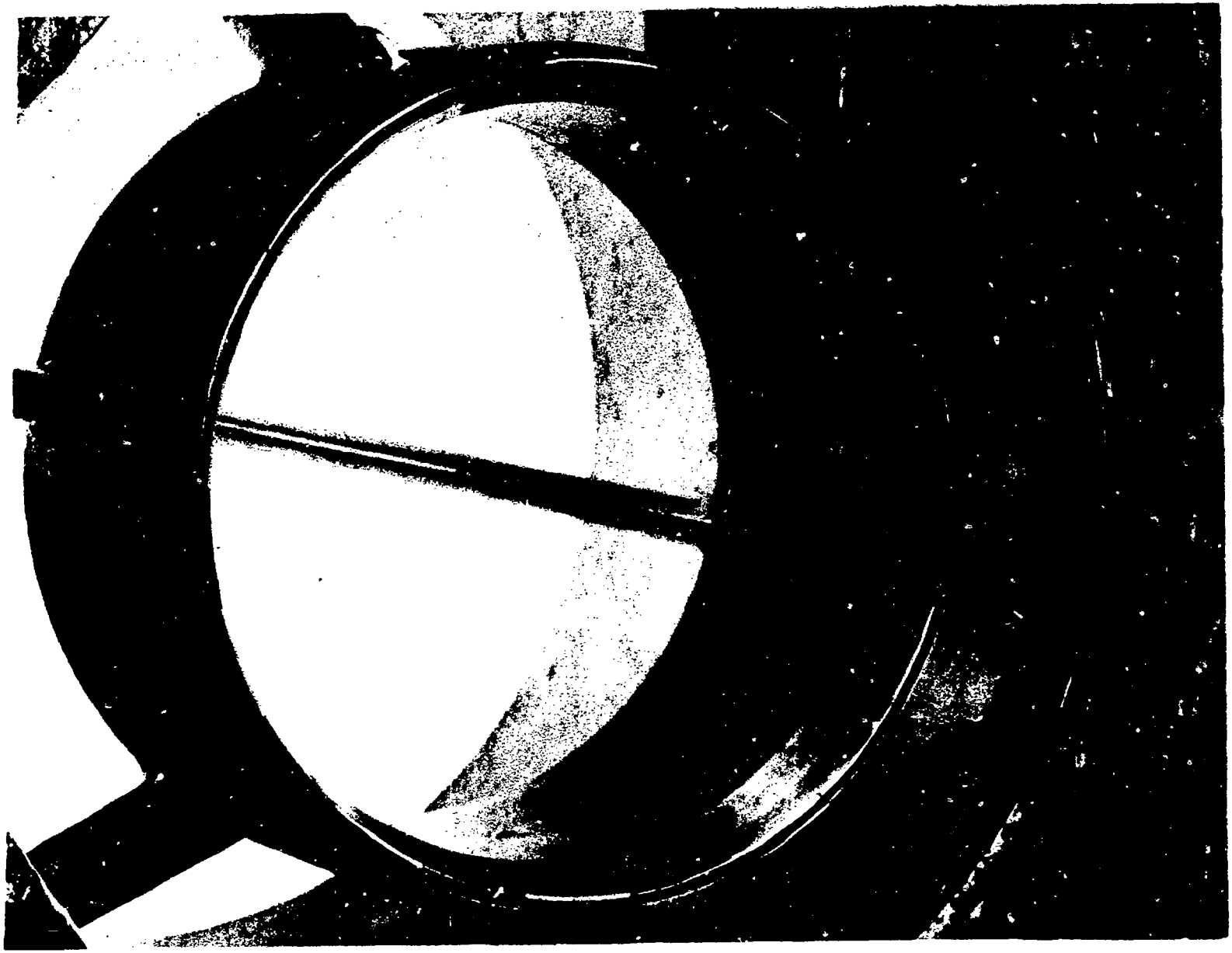

Figure 22. Hypermixing Ejector Nozzle Test Item, Close Up - 3/4 Rear View

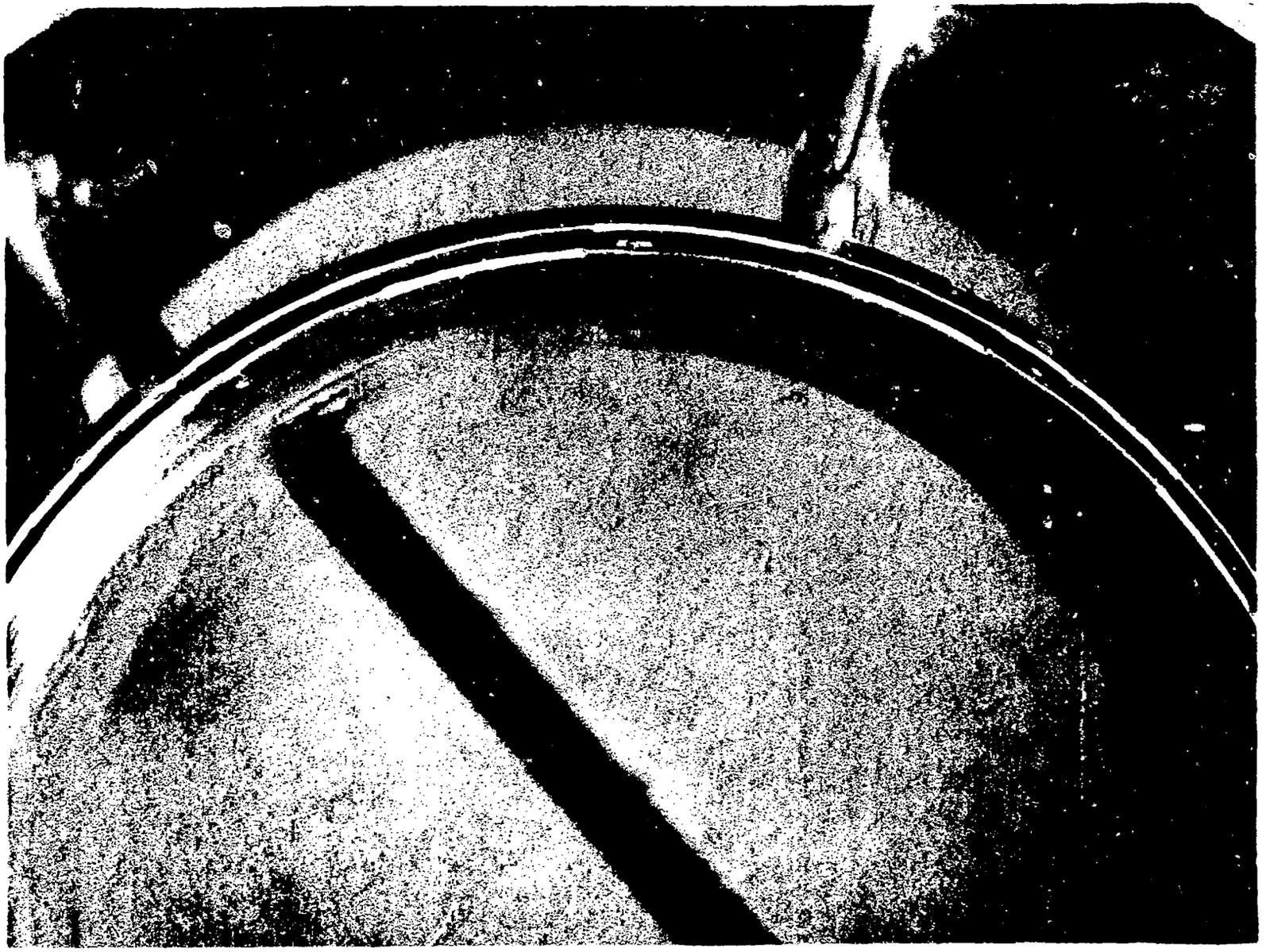

Figure 23. Hypermixing Ejector Nozzle Test Item, Extreme Close Up-Rear View

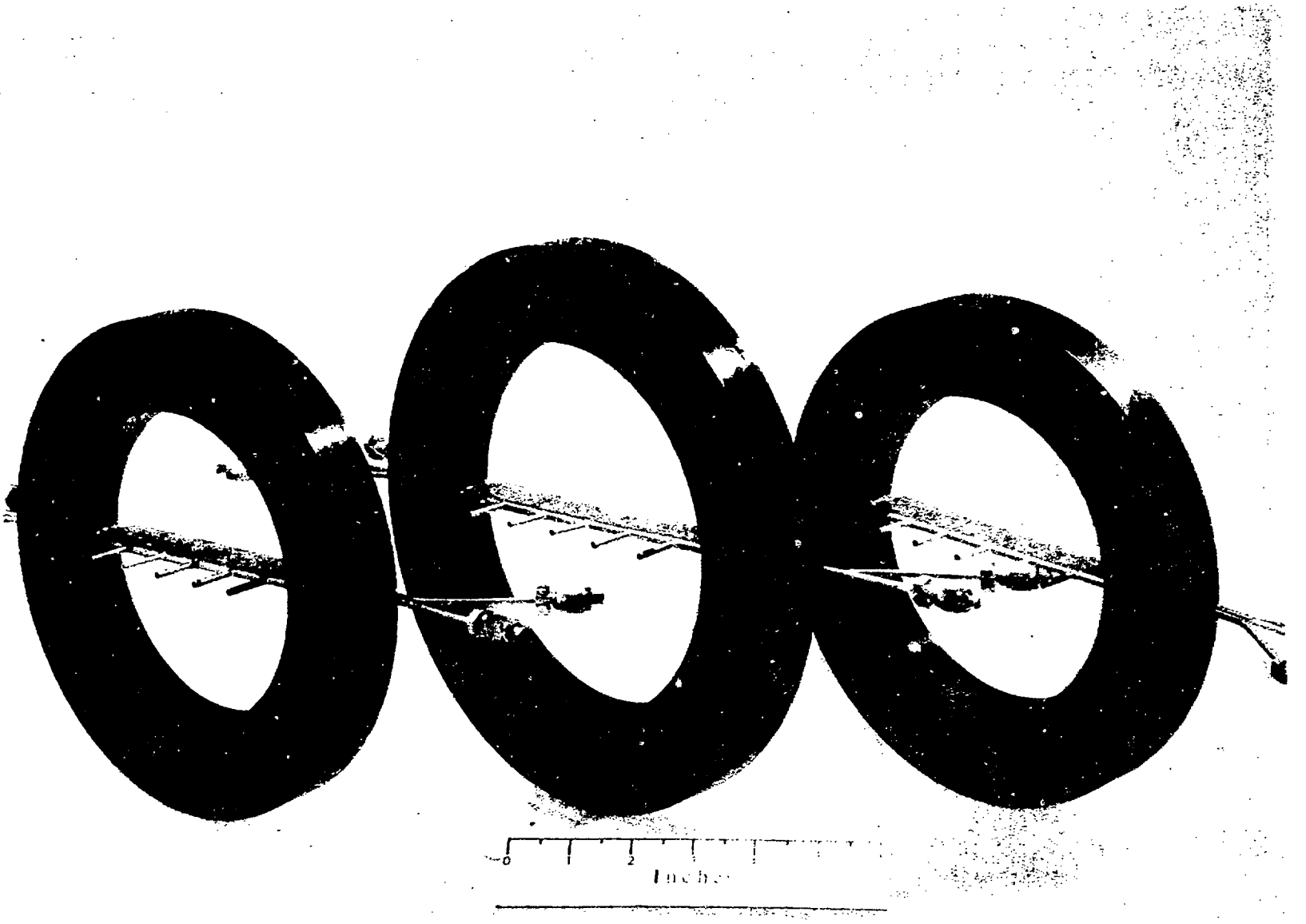

Figure 24. Total Pressure/Gas Sampling Rake Assemblies

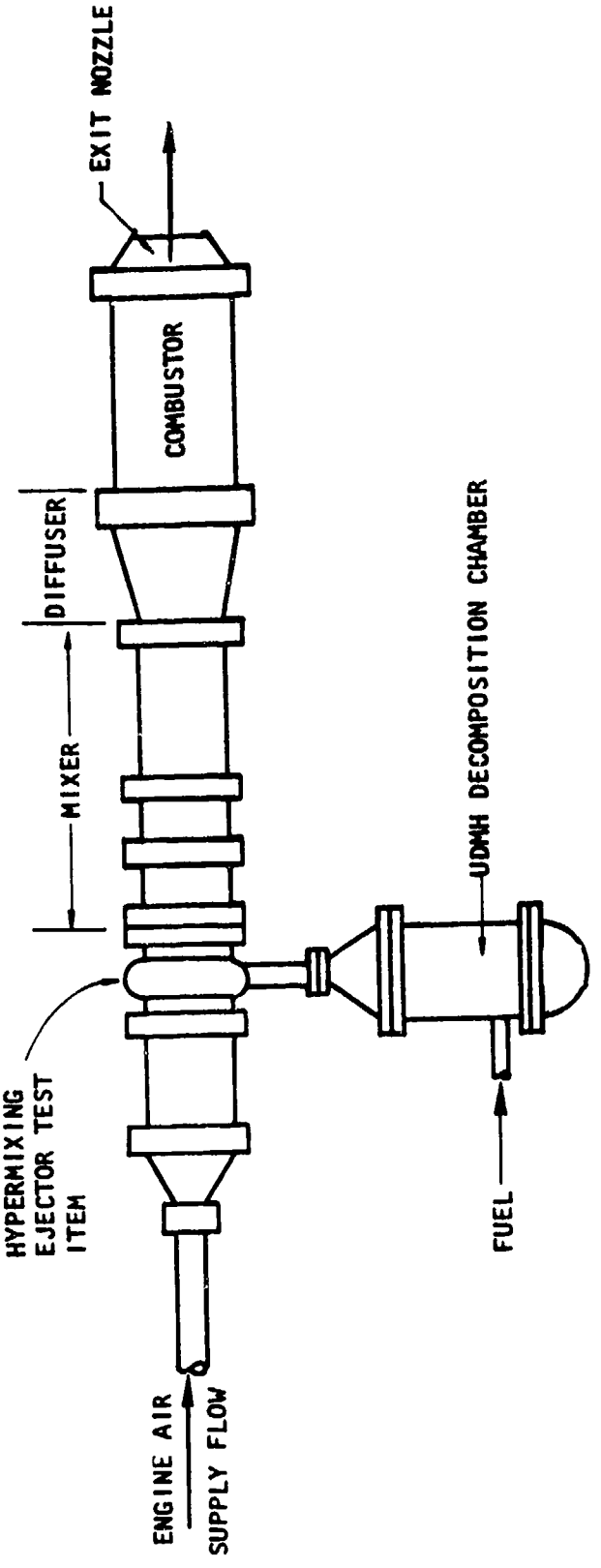

Figure 25. Hypermixing Ejector Test Program-Proposed Test Setup

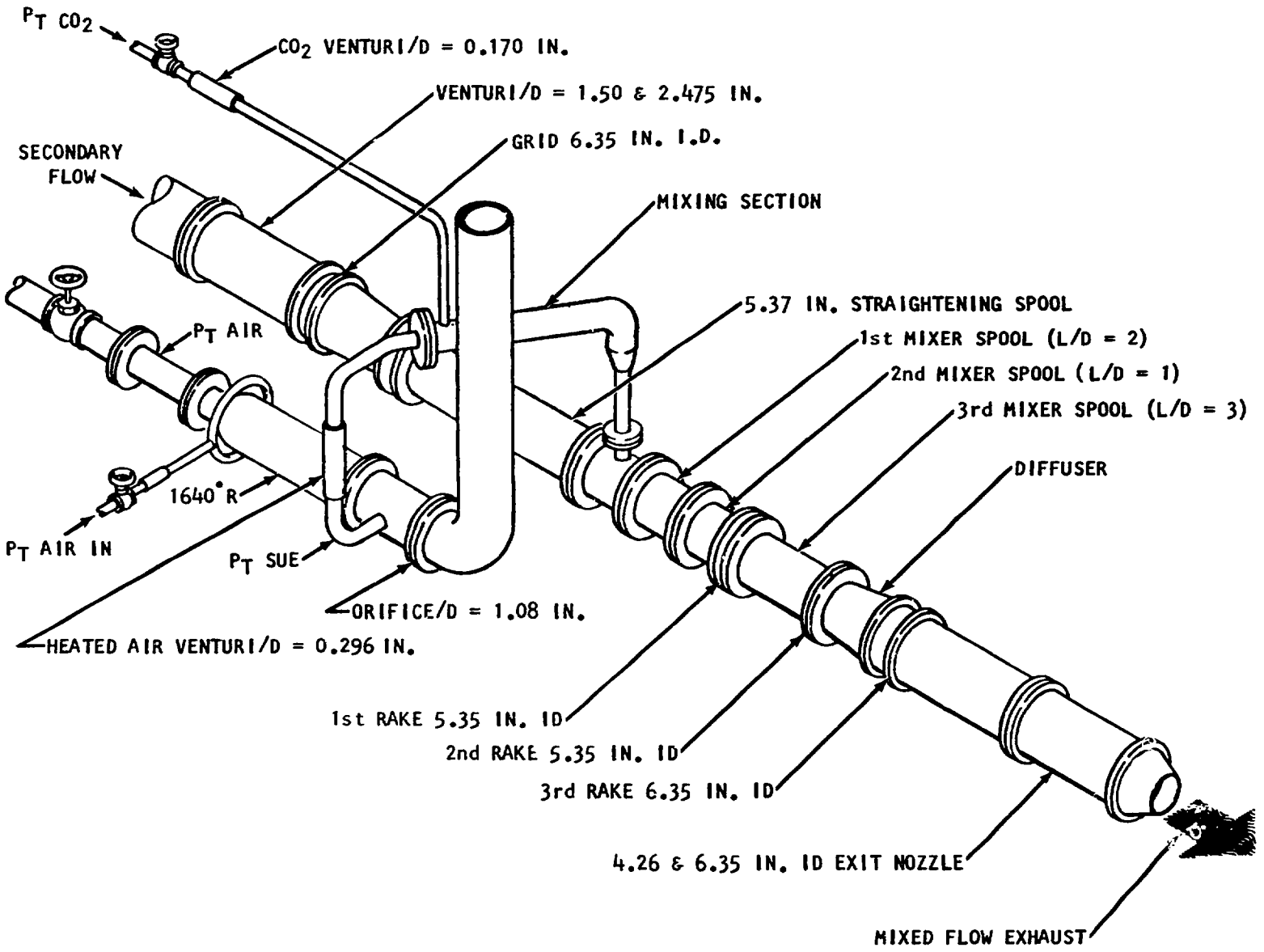

Figure 26. Hypermixing Ejector Test Setup

on the system at these low flow rates than would have been provided with the larger nozzle. In addition, the use of this small convergent/divergent nozzle resulted in the nozzle throat choking at total pressure levels (i.e., airflow) significantly lower than those with a convergent nozzle.

The small SUE burner originally planned for the primary subsystem was not available. A 3 x 6 inch facility burner was available but was judged to be unstable for the low flow rate (design ejector flow rate = 0.62 lb/sec), pressure and temperature conditions desired for the primary. The approach taken was to use the 3 x 6 inch facility burner with a bypass duct plumbing arrangement as shown in Figure 26. Stable operation of the burner was achieved by bypassing almost 90% of the total flow to the atmosphere through a standard ASME orifice. The quantities of heated air and CO_2 delivered to the primary system were measured with separate venturi meters. A venturi meter was also used to measure the secondary airflow, which was unheated.

The reasons for substituting CO_2 as a tracer gas rather than the originally planned Freon were as follows:

a. In reviewing the instrumentation requirements, it was concluded that the minimum mixed (i.e., primary and secondary airflows) tracer gas concentration should be approximately 5% by weight. With the design W_S/W_P value of 9.19, the tracer gas concentration in the primary fluid is about 50% by weight. It then follows that the thermodynamic properties of the tracer gas can significantly influence the ejector discharge velocity and, therefore, the ejector pumping total pressure ratio. Freon 12 has a high molecular weight and low specific heat ratio. Both of these properties significantly reduce the ejector discharge velocity, as shown in Table XII. Gaseous CO_2 has thermodynamic properties similar to those of air, is low in cost, and is readily available. As shown in Table XII, the performance of CO_2 is quite good.

b. It is a fact that Freon, when exposed to an open flame, can result in the generation of phosgene, a poison gas. In this test program, Freon would have been injected downstream of the SUE burner where the air temperature is approximately 1640°R. Granted that Freon would not be brought in contact with an open flame, the question remained: Could this combustion process/high temperature air cause phosgene to be generated? A limited library search and technical consultation were inconclusive.

c. The gas sampling instrument (Beckman Infrared Dispersion Model) is sensitive to CO_2 in less concentrated mixtures than Freon, and in fact was originally designed for CO_2.

Thus, consideration of test safety, ejector performance, tracer gas cost, and availability led to the decision to use gaseous carbon dioxide as the tracer element in the test program.

TABLE XII. GAS SAMPLING TRACER GAS COMPARISON

Tracer gas	Molecular weight	Specific heat ratio	Ejector working fluid $T_{T_P = 1160^{\circ}}$	Ejector chamber pressure* P_{T_P}, lb/in.^{2}	Ejector discharge velocity** ft/sec	Toxic	Cost $/lb	Availability
None	28.9 (air)	1.37 @ 1160°R	100% Air	300	2705	-	-	-
Freon 12	120.9	1.14 @ 86°F	46% Freon*** 54% Air	197	1759	?	0.63	Readily available
Carbon Dioxide	44.0	1.21 @ 1160°R	50% CO_2; 50% Air	267	2450	No	0.19	Readily available

* Total pressure required to discharge 0.62 lb/sec with the ejector test item design

** Primary nozzle expanded to $P_P = P_2 = 18.4$ lb/in.^{2}; nozzle velocity coefficient = 0.98

*** Concentration by weight

Photographs of the test setup are shown in Figures 27 and 28. In Figure 27, the main elements of the test item, including ejector section, mixer, diffuser, plenum, and exit nozzle as well as the upright primary heater bypass system and duct to transfer the heated air/CO_2 mixture to the ejector section can be seen. On the left of the photograph is the array of CO_2 gas sampling bottles. Figure 28 presents a view of these same items (less gas sample rack) looking in the downstream direction. Figure 29 presents a better view of the gas sampling setup.

3. INSTRUMENTATION

Test instrumentation is schematically indicated in Figure 30. The secondary airflow instrumentation system consisted of a venturi, measurement of the total pressure for airflow calculation, and a throat static pressure to insure that the venturi was choked. Downstream of the flow profile straightening screen and stilling section, the total pressure (P_{T_1}) was measured with a five tube rake just ahead of the ejector system. Static pressure was also measured at this station. A total of 13 static pressure taps were located in the mixer, diffuser, plenum, and nozzle section. To identify these static pressures with the various mixer spools, refer to Figure 31. This figure identifies the total pressure rake locations as well as static pressure taps. The circled numbers indicate total pressure rake stations; i.e., 1 identifies the total pressure rake just ahead of the mixer, and the average total pressure at this station is $\bar{P}_{T_1}$. There were four total pressure rakes, three in the 5.35 inch diameter mixer duct and one in the 6.35 inch diameter plenum duct at the exit of the diffuser. The rakes utilized equal tube spacings in single spokes, as opposed to equal area tube locations. The center tube of each rake was located on the duct centerline. The tube spacing was 0.89 inches for the three rakes located in the 5.35 inch diameter section and 1.06 inches for the single rake located in the 6.35 inch diameter section. All pressures were measured on direct reading gauges, and photographs of the pressure gauge panels were taken for each test point for later data reduction.

Note in Figure 30 that each of the mixer and diffuser total pressure rakes were teed to the gas sampling bottles as well as to the rect reading pressure gauges. Figure 32 illustrates the approach used in acquiring an individual gas sample. A probe inserted in the stream was used for both total pressure measurement and gas sampling. This probe was connected to a gas sample bottle through a series of valves, and the bottle was connected to a vacuum. When the solenoid operated valves were opened, the sampling fluid was drawn through the bottle. After an appropriate time span (10-15 seconds) the lower solenoid valve was closed, and then the upper solenoid valve was closed, capturing a gas sample within the bottle. The bottles were then removed from the rack by closing the hand valves and disconnecting the hoses at the coupling.

The analyses of the CO_2-air mixtures from the sampling systems were performed at Marquardt by using a Beckman Model 315A nondispersive infrared gas analyzer. Three of these instruments exist at Marquardt, and two were designed to sense specific pollutants, i.e., carbon monoxide, CO, and nitric oxide, NO. The third instrument was originally calibrated for CO_2, and was recalibrated for these tests.

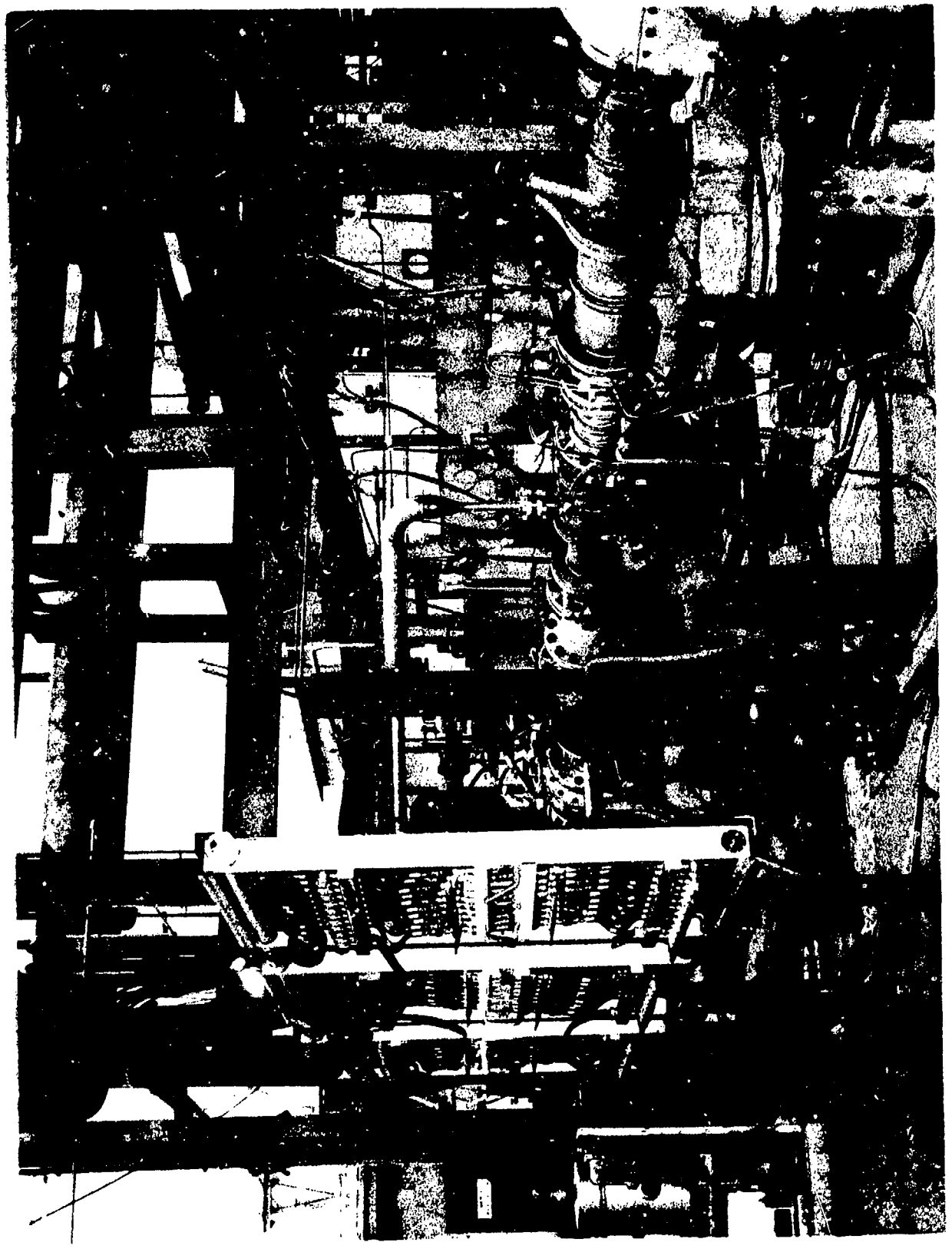

Figure 27. Hypermixing Ejector Test Setup-Rear View

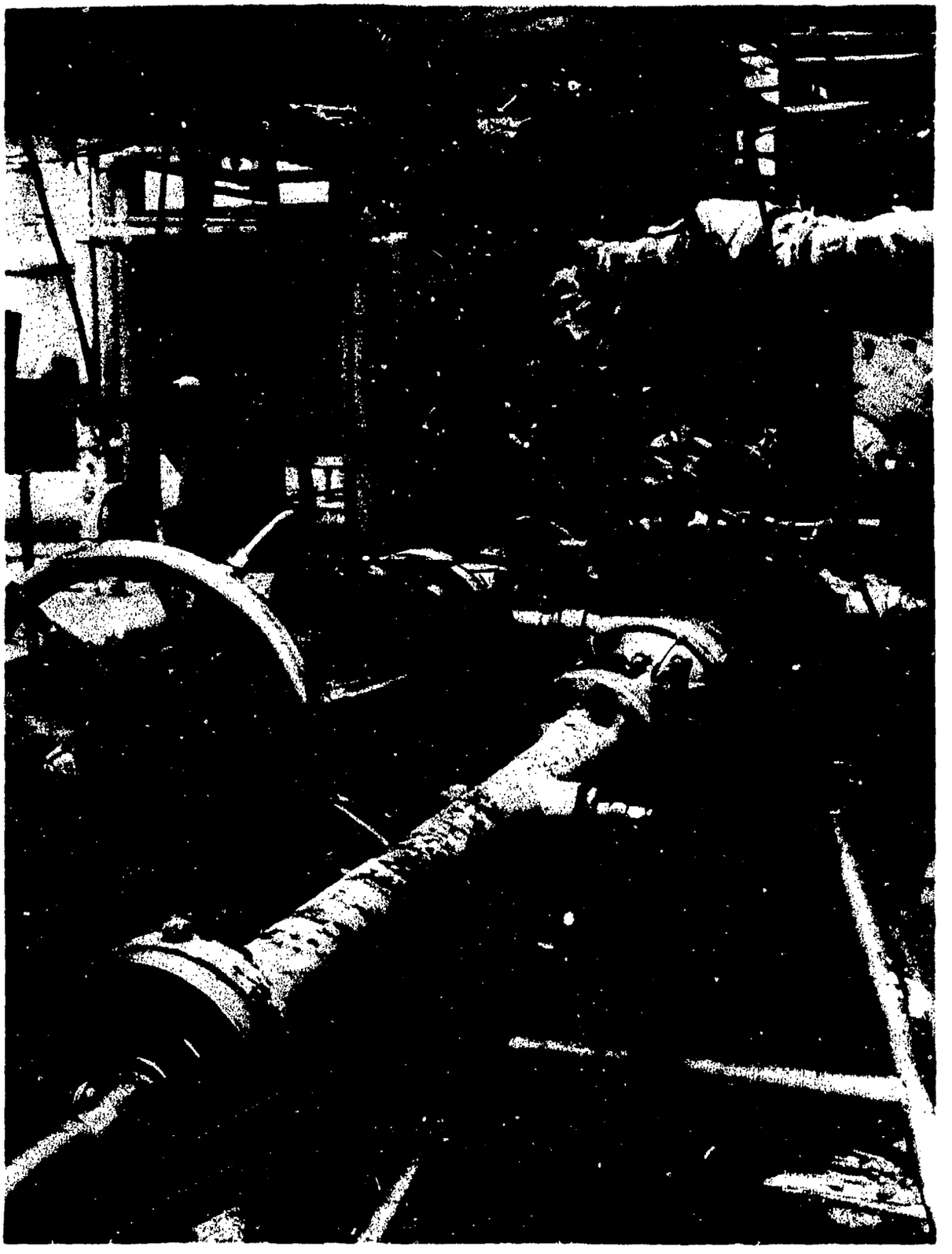

Figure 28. Hypermixing Ejector Test Setup-Front View

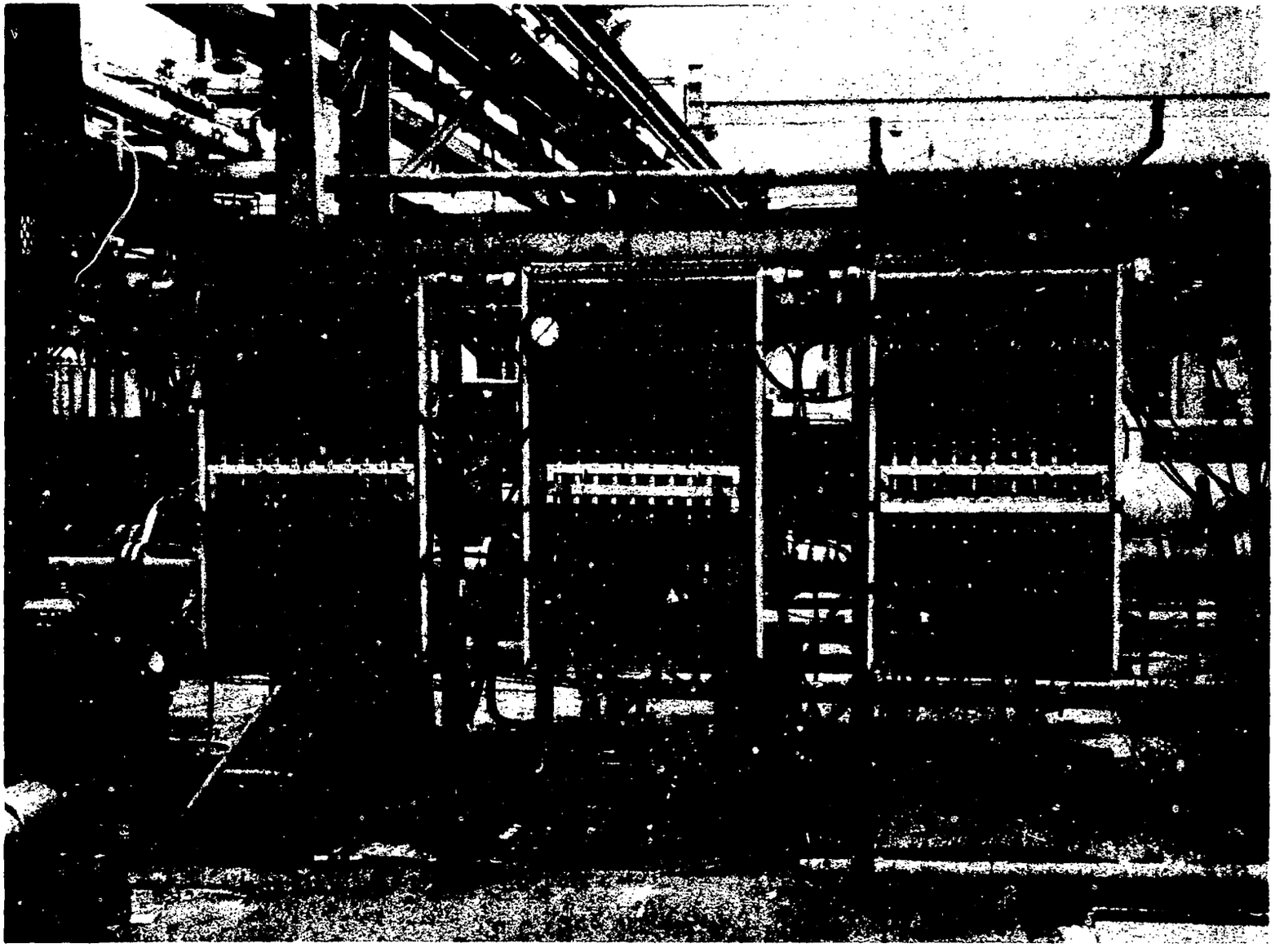

Figure 29. Gas Sample Setup

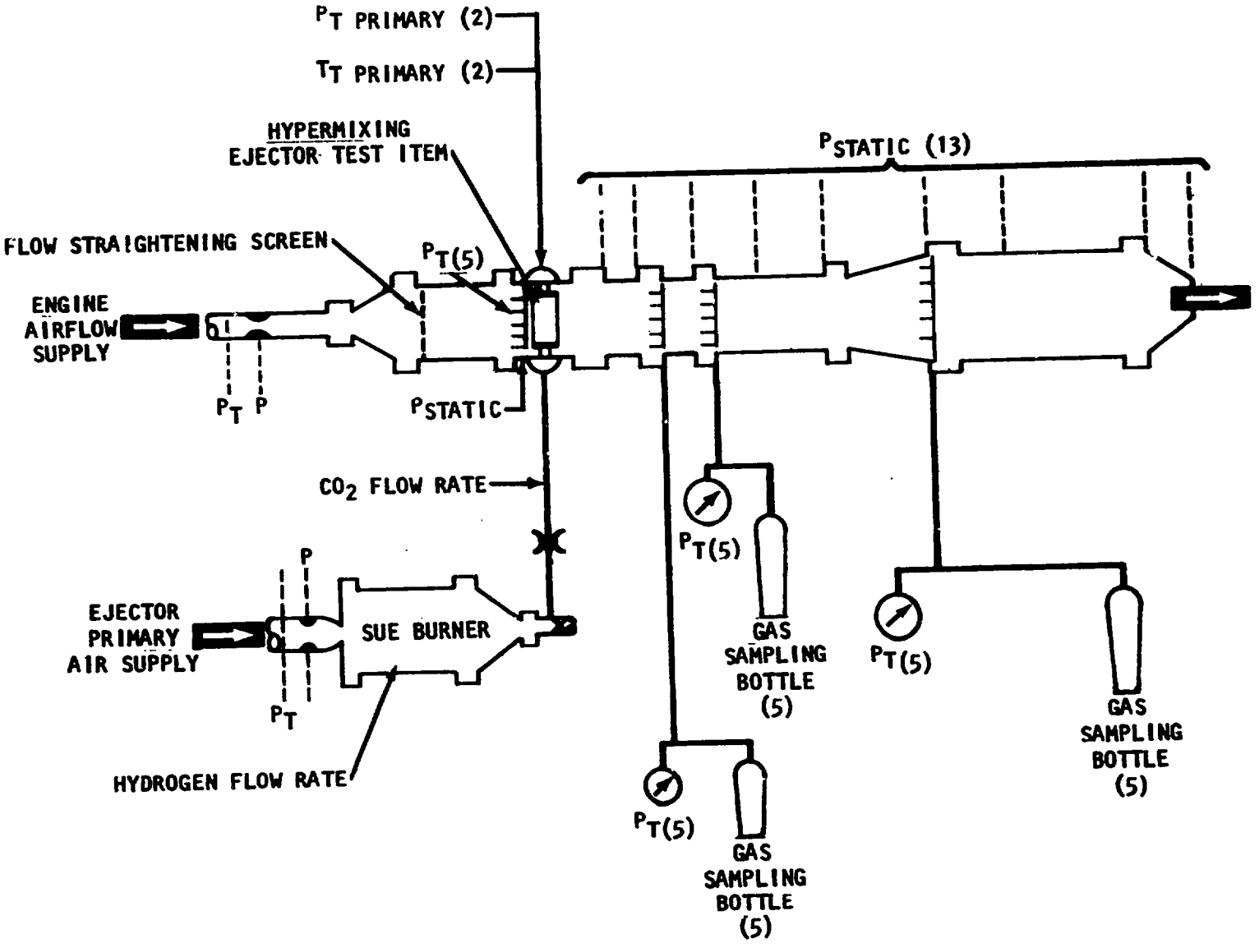

Figure 30. Hypermixing Ejector Test Program-Test Instrumentation

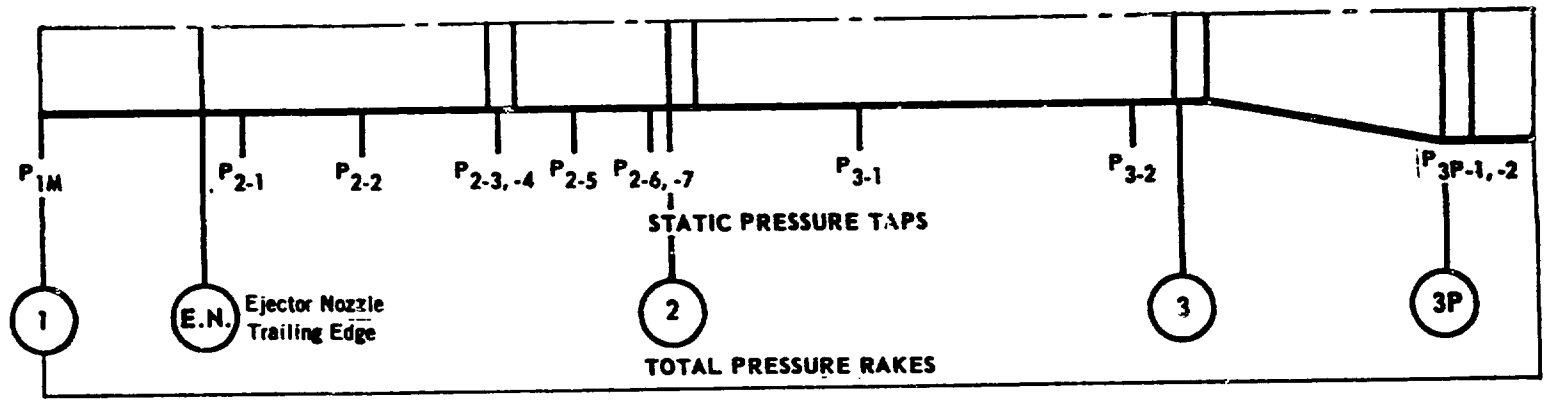

Figure 31. Mixer Spool Arrangement/Pressure Instrumentation

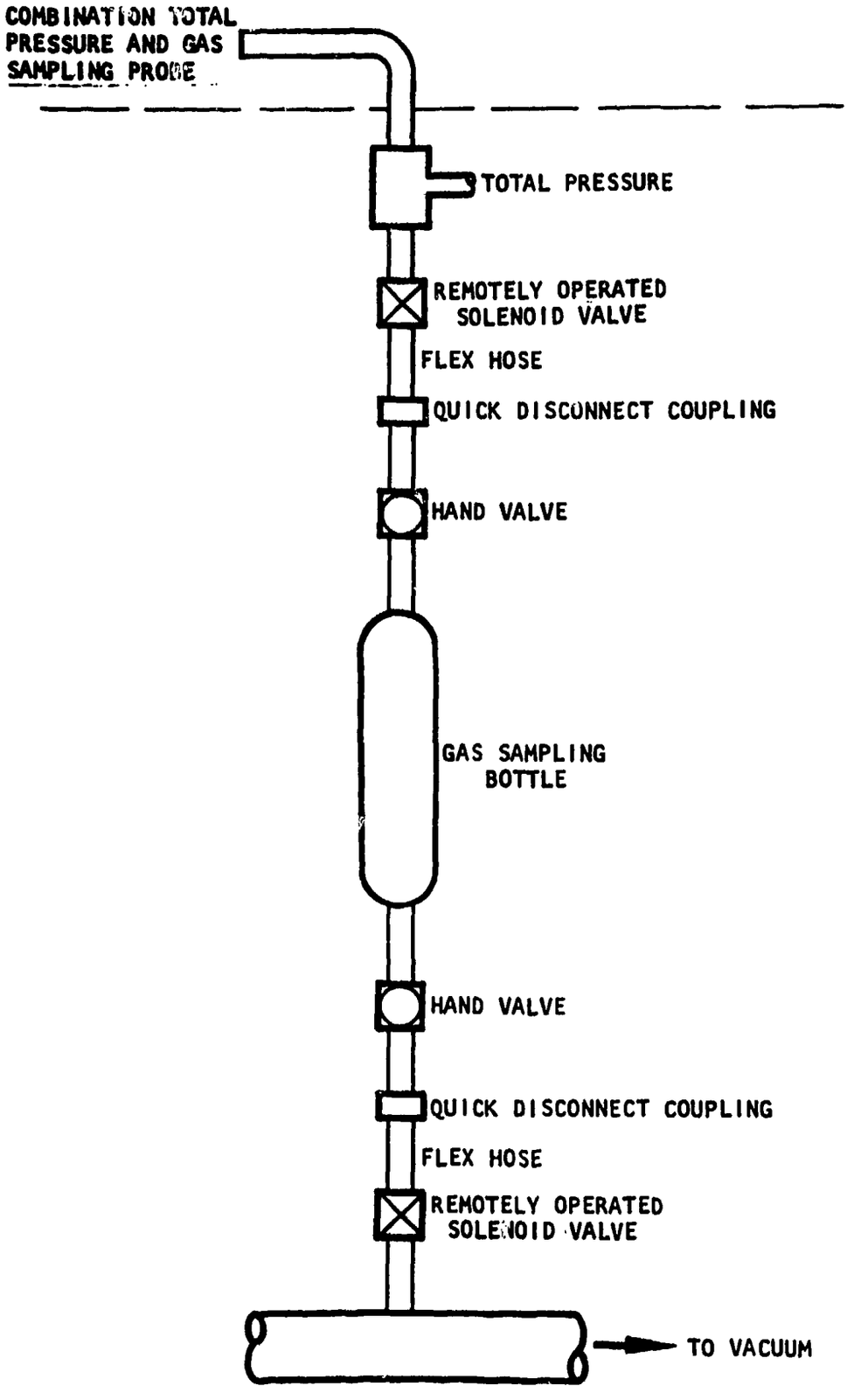

Figure 32. Gas Sampling Technique

Operation of the Beckman instrument, which is shown schematically in Figure 33, is based upon the differential absorption of infrared radiation energy of a specific wavelength in a reference and sample chamber. The gas in the reference cell does not absorb this specific radiation, and the light beam will pass through this chamber to the detector without depletion of energy. The equal light beam passing through the sample chamber loses a portion of its energy, dependent upon the concentration of the particular gas species in the sample. These parallel light beams are then passed through both sides of the detector, which contains gas of equal concentrations of the particular species. The detector gases absorb radiant energy at the specific wavelength, raising the temperature levels of the confined gas. Since the reference chamber absorbs no energy, this side of the detector becomes hotter than the sample gas side. The temperature differential produces a pressure differential which deflects the diaphragm separating the two detector chambers. This causes the detector to become a variable capacitor which produces a signal in response to the species concentration in the sample gas. This signal is electronically conditioned to produce a meter reading.

These instruments are equipped with two external calibration adjustments normally used to compensate for component performance variations with time (for example, lamp filament output variations over a period of years). The first adjustment is the zero adjust. A sample known to be free of species which will absorb radiation at the same wavelength as the detector is passed through the sample chamber and the instrument zeroed. The second adjustment is used to set the instrument gain. A gas sample, containing a known amount of a species which will absorb radiant energy at the specific detector wavelength, is passed through the sample chamber, and the meter reading is adjusted (with the attenuator) to produce a preselected reading. Calibration of the instrument response for the range of concentration of the species of interest is accomplished by using a number of known gas samples of different concentrations and recording meter readings with the zero adjust and attenuation adjust fixed. Once such a characteristic calibration curve is obtained, the instrument can be set (zeroed and gain adjusted) for each day's operation by use of a single reference sample.

A sample pretest and post test calibration is presented in Figure 34. The calibration shown is meter reading versus percent CO_2 by volume in air. This curve is then converted to percent CO_2 by weight in air by the appropriate molecular weight relationships.

4. TEST PROGRAM

As discussed in a previous section of this report, the ejector test item design flow rates were:

$$\text{Secondary Airflow Rate, } W_S = 5.70 \text{ lb/sec}$$
$$\text{Primary Flow Rate, } W_P = 0.62 \text{ lb/sec.}$$

The design flow ratio W_S/W_P was then 9.19 and corresponds to the air to UDMH fuel ratio at stoichiometric conditions. Test conditions which varied the secondary flow rate over the range of 25% to 125% of the design value were developed. Similarly, the primary flow rate was varied over the range of 50% to 125% of its design value. The resulting W_S/W_P variation was from 1.8 to 18.4. The developed test conditions are shown in Table XIII.

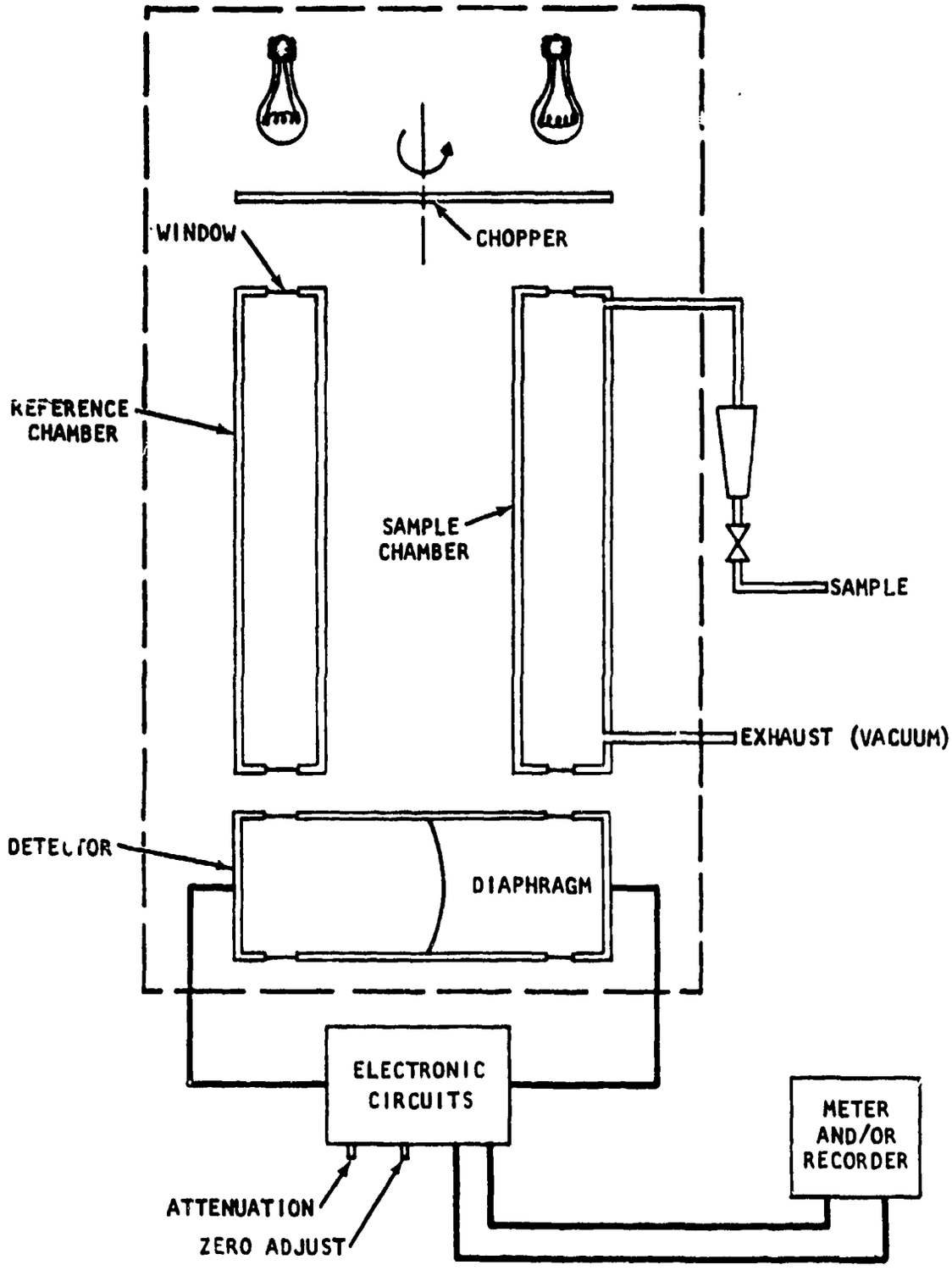

Figure 33. Beckman Model 315A Gas Analyzer

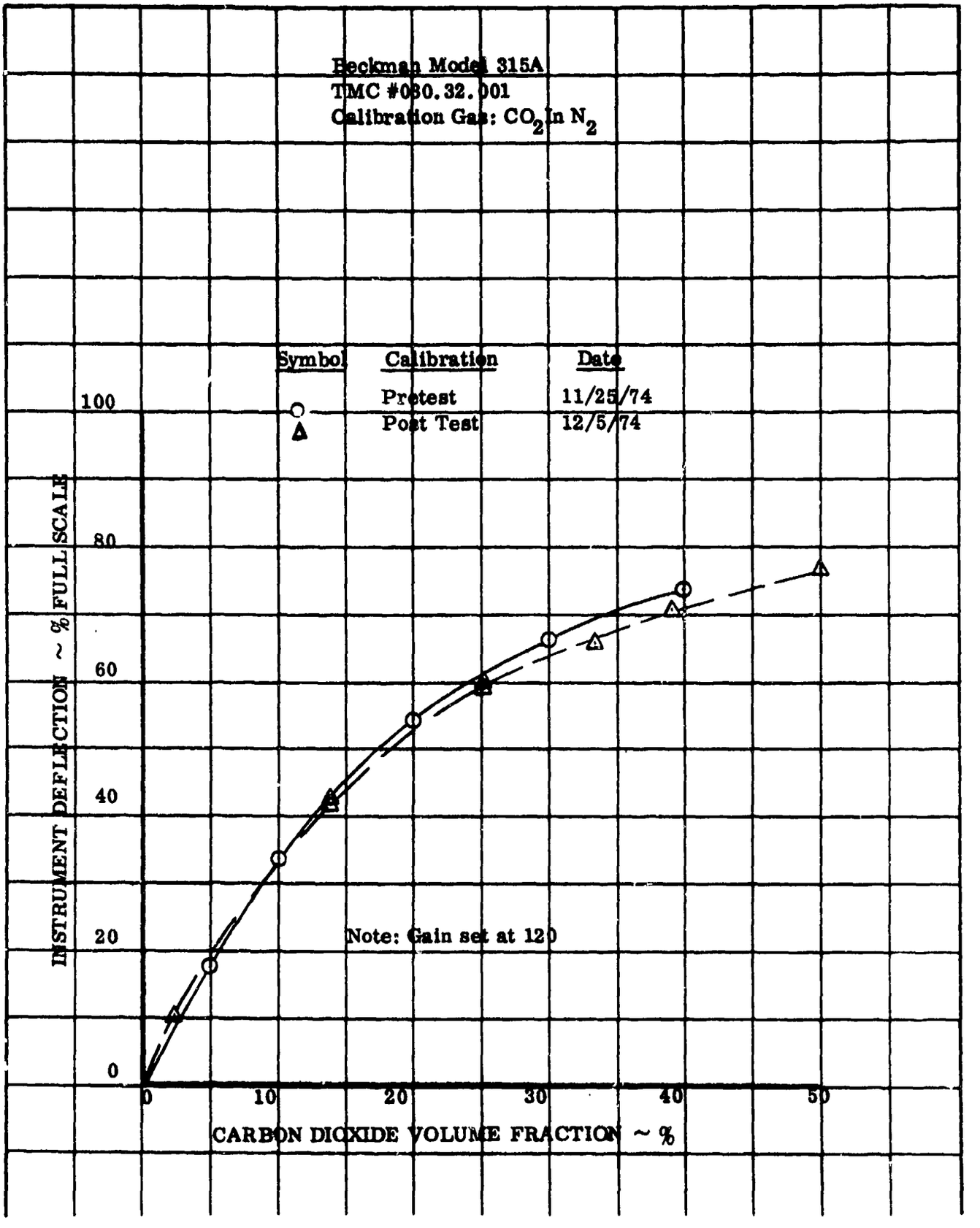

Figure 34. Carbon Dioxide Analyzer Calibration

TABLE XIII. HYPERMIXING EJECTOR TEST CONDITIONS

$\frac{W_S}{W_{S_D}}$ %	$\frac{W_P}{W_{P_D}}$ %	$\frac{W_S}{W_P}$	ø	W_S lb/sec	W_P lb/sec	P_{T_P} psia	W_{AIR_P} at 1640°R lb/sec	$W_{CO_2\ P}$ at 520°R lb/sec	$\frac{W_{CO_2}}{W_S + W_{AIR\ P}}$ %
125	125	9.19	1.00	7.13	0.775	334	0.388	0.388	5.16
125	100	11.49	0.80	7.13	0.620	267	0.310	0.310	4.17
100	125	7.35	1.25	5.70	0.775	334	0.388	0.388	6.37
↓	100	9.19	1.0	↓	0.620	267	0.310	0.310	5.16
	75	12.25	0.75		0.465	200	0.233	0.233	3.93
	50	18.38	0.50		0.310	134	0.155	0.155	2.65
75	125	5.51	1.667	4.27	0.775	334	0.388	0.388	8.33
↓	100	6.89	1.333	↓	0.620	267	0.310	0.310	6.77
	75	9.19	1.000		0.465	200	0.233	0.233	5.17
	50	13.78	0.667		0.310	134	0.155	0.155	3.50
50	125	3.68	2.50	2.85	0.775	334	0.388	0.388	11.98
↓	100	4.59	2.00	↓	0.620	267	0.310	0.310	9.81
	75	6.12	1.50		0.465	200	0.233	0.233	7.56
	50	9.19	1.00		0.310	134	0.155	0.155	5.16
25	125	1.84	5.00	1.425	0.775	334	0.388	0.388	21.40
↓	199	2.30	4.00	↓	0.620	267	0.310	0.310	17.87

W_S = Secondary Flow W_{S_D} = Design Secondary Flow

W_P = Primary Flow W_{P_D} = Design Primary Flow

In order to evaluate the hypermixing ejector, the test item was first tested without scarfing the nozzle trailing edges, thus resulting in an annular nozzle which by definition does not incorporate hypermixing. These tests were conducted with design secondary airflow with the primary flow varied from 50% to 125%. The ejector nozzle trailing edge was then scarfed in accordance with Section VIII, and the tests were run over a range of secondary and primary flow rates. Table XIV summarizes these test runs together with those conducted for the annular nozzle. Note that the air metering venturi and exit nozzle sizes are indicated for each run. As stated earlier, smaller sizes for these components were utilized for the 25 and 50% airflow cases.

It should be noted that for Runs 1 through 9, inclusive, the various interchangeable mixing spools were left in a fixed position, namely, that shown earlier in Figure 26. All data for these tests will be shown for the instrumentation arrangement of Figure 31.

5. TEST RESULTS

Typical axial static pressure distributions at 100% secondary airflow and for a range of primary flows are shown in Figures 35 and 36, for the annular and hypermixing configurations, respectively. Station notation is indicated at the top of each figure, together with the ejector nozzle trailing edge station. In each figure, the local static pressure is divided by the average total pressure at station 1. It will be noted that there appears to be little difference in static pressure rise mixing length between the two configurations. The maximum pressure rise occurs at station 2, which corresponds to a mixer L/D of 2.83.

Figures 37, 38, and 39 present total pressure profiles at stations 1, 2,and 3 as identified in Figures 31, 35,and 36. Comparisons between the annular and hypermixing ejector nozzles are again made at 100% secondary airflow for differing amounts of primary flow rate in succeeding figures. At station 1 in each case, the flow was quite uniform, showing the effects of the flow straightening screen and section length ahead of the ejector test item. At station 2, the approximate point of maximum static pressure rise, the total pressure is somewhat distorted, with minimum pressure occurring at the center of the duct and maximum pressure near the walls. At station 3, corresponding to a mixer L/D of 5.82, the total pressure distortion has reduced considerably but is still present. In comparing the annular and hypermixing ejectors in these figures, one finds very little difference. This conclusion was supported by static pressure distributions of Figures 35 and 36,which also showed little difference between the annular and hypermixing configurations.

Figures 40 and 41 present CO_2 sampling data results at stations 2 and 3, respectively. In each figure, the secondary airflow was at its design value, while the primary flow rate was varied from 100 to 50%. Comparisons are again made between the annular and hypermixing configurations and again the results indicate very little difference between the shapes of the profiles.

TABLE XIV. HYPERMIXING EJECTOR TEST RUN SUMMARY

Run no.	Ejector/Test configuration	$\frac{W_s}{W_{s_{design}}}$	$\frac{W_p}{W_{p_{design}}}$	Remarks
1	Annular only - Facility metering nozzle diameter (D_{MN}) = 2.475" Test Item Exit Nozzle diameter (D_6) = 4.26"	50 to 125 100%	0 50%	Secondary duct calibration Checkout primary heating system
2	" " "	100%	50%, 75% 100%, 125%	Losing CO_2 pressure for 125% W_p
3	Hypermixing D_{MN} = 2.475", D_6 = 4.26"	100%	50%, 75% 100%	Run stopped by low air pressure
4	" " "	125%	125%	H_2 control valve failure
5	" " "	125% 75%	100%, 75% 50% 50%	Good data run
6	" " "	100% 75%	125% 125% 100%, 75%	Good data run
7	Hypermixing D_{MN} = 1.50" D_6 = 2.45"	50%	125%, 100% 75%, 50%	Good data run
8	" "	25%	125%, 100% 75%, 50%	Good data run
9	Hypermixing D_{MN} = 2.475" D_6 = 4.26"	100%	100% 125% 100%	Good data run

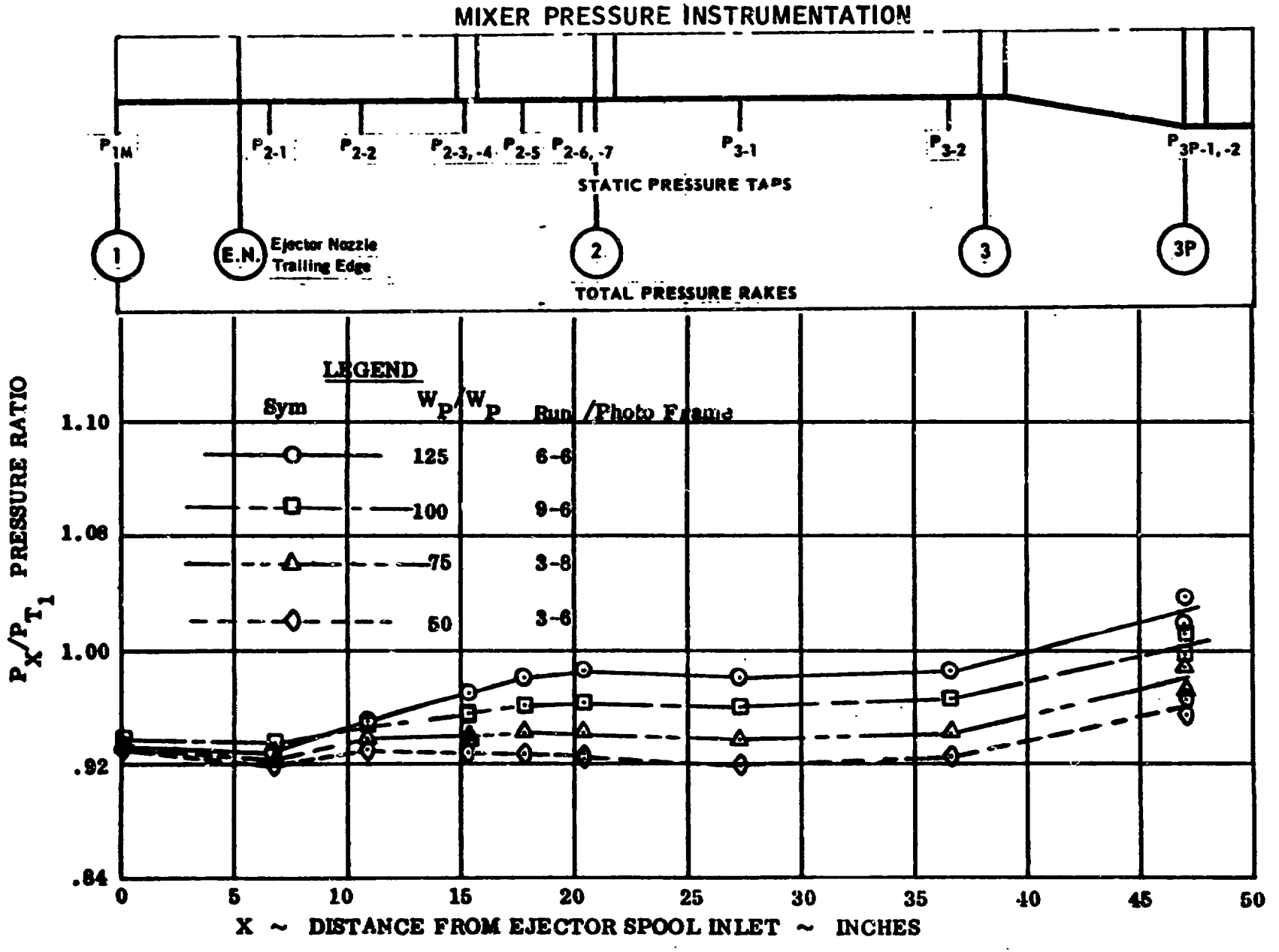

Figure 35. Axial Pressure Distribution W_S/W_{3_D} = 100%/Annular Ejector

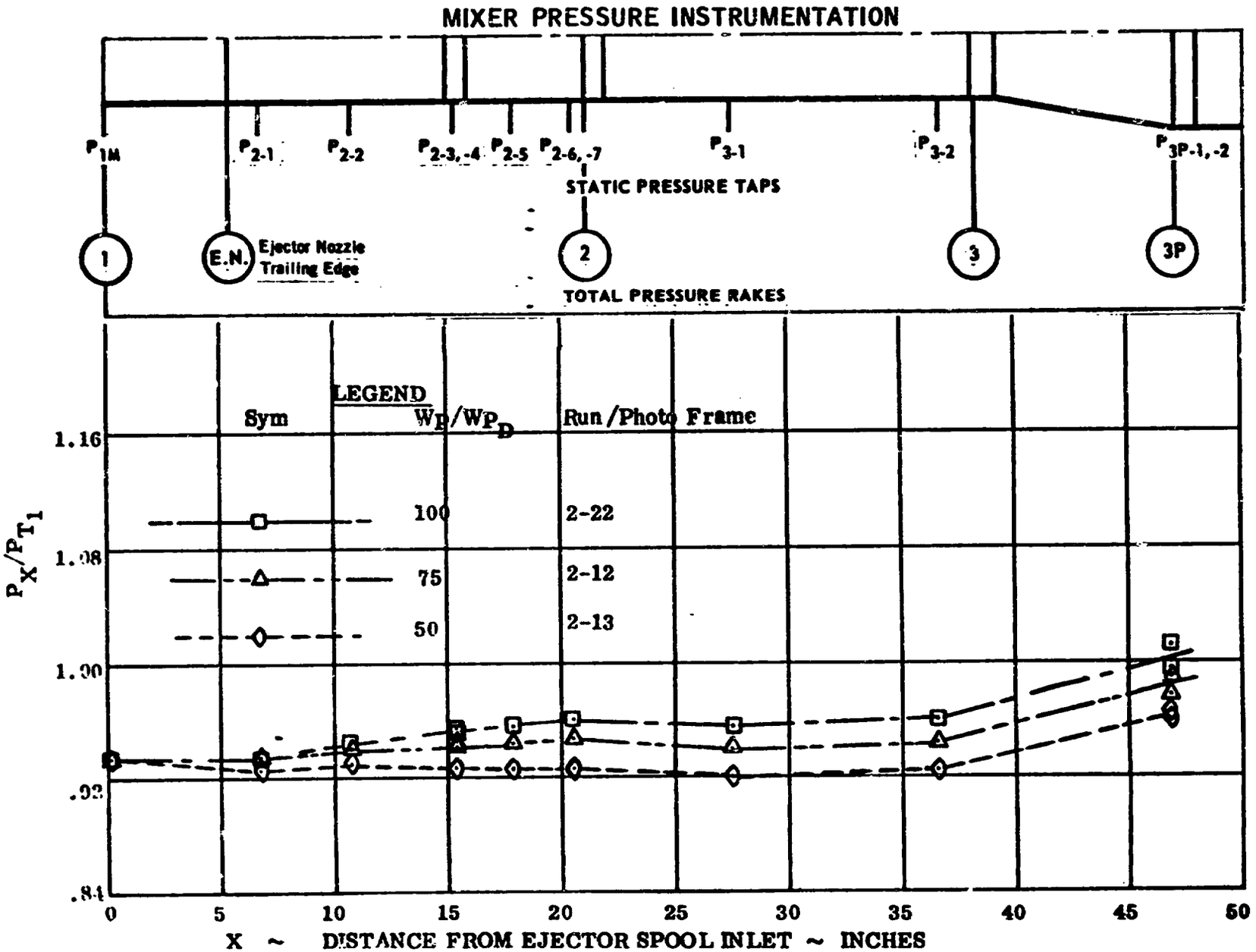

Figure 36. Axial Pressure Distributions, W_S/W_{S_D} = 100%/Hypermixing Ejector

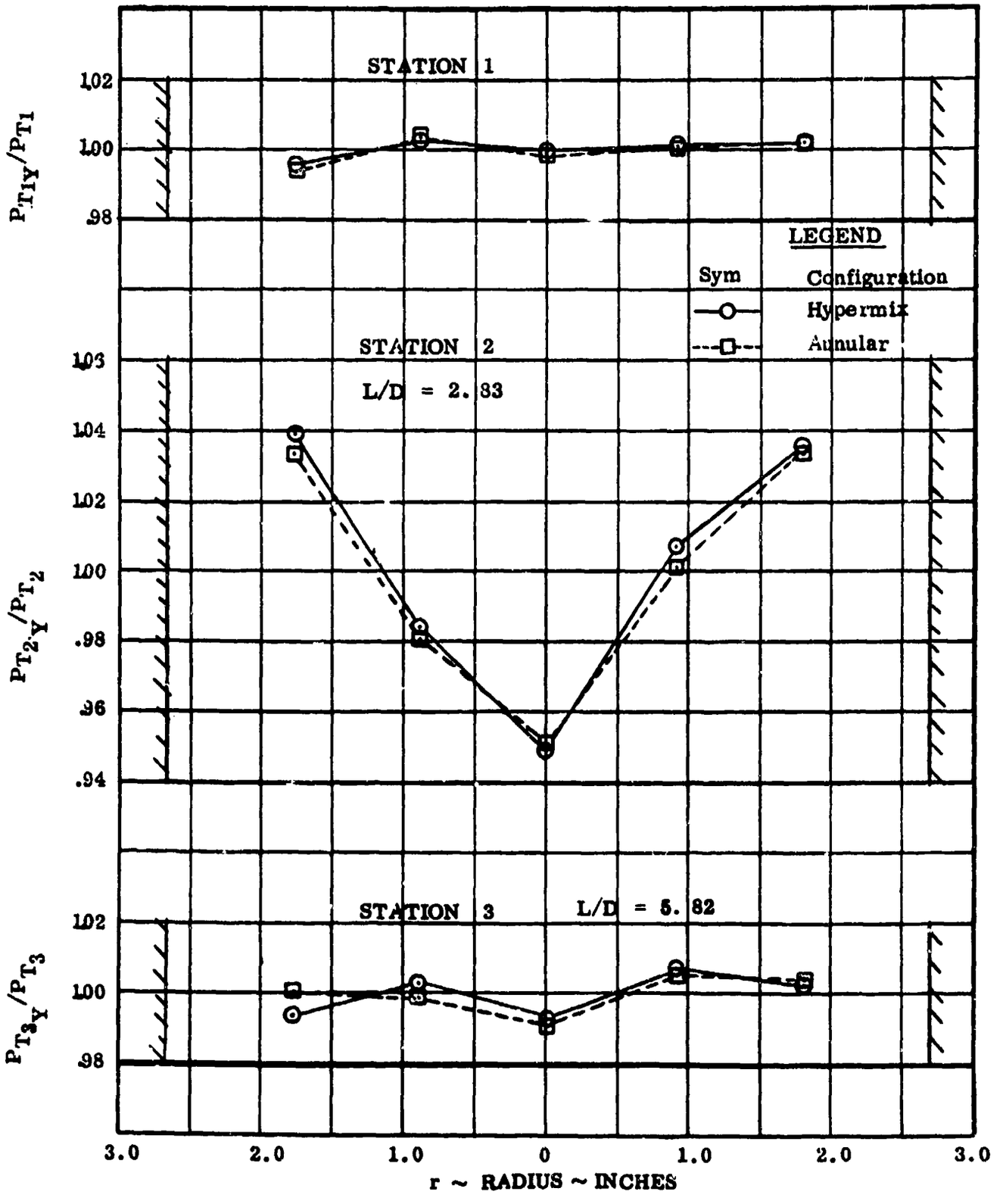

Figure 37. Comparison of Total Pressure Profiles - $\frac{W_S}{W_{S_D}} = 100\%$, $\frac{W_P}{W_{P_D}} = 100\%$

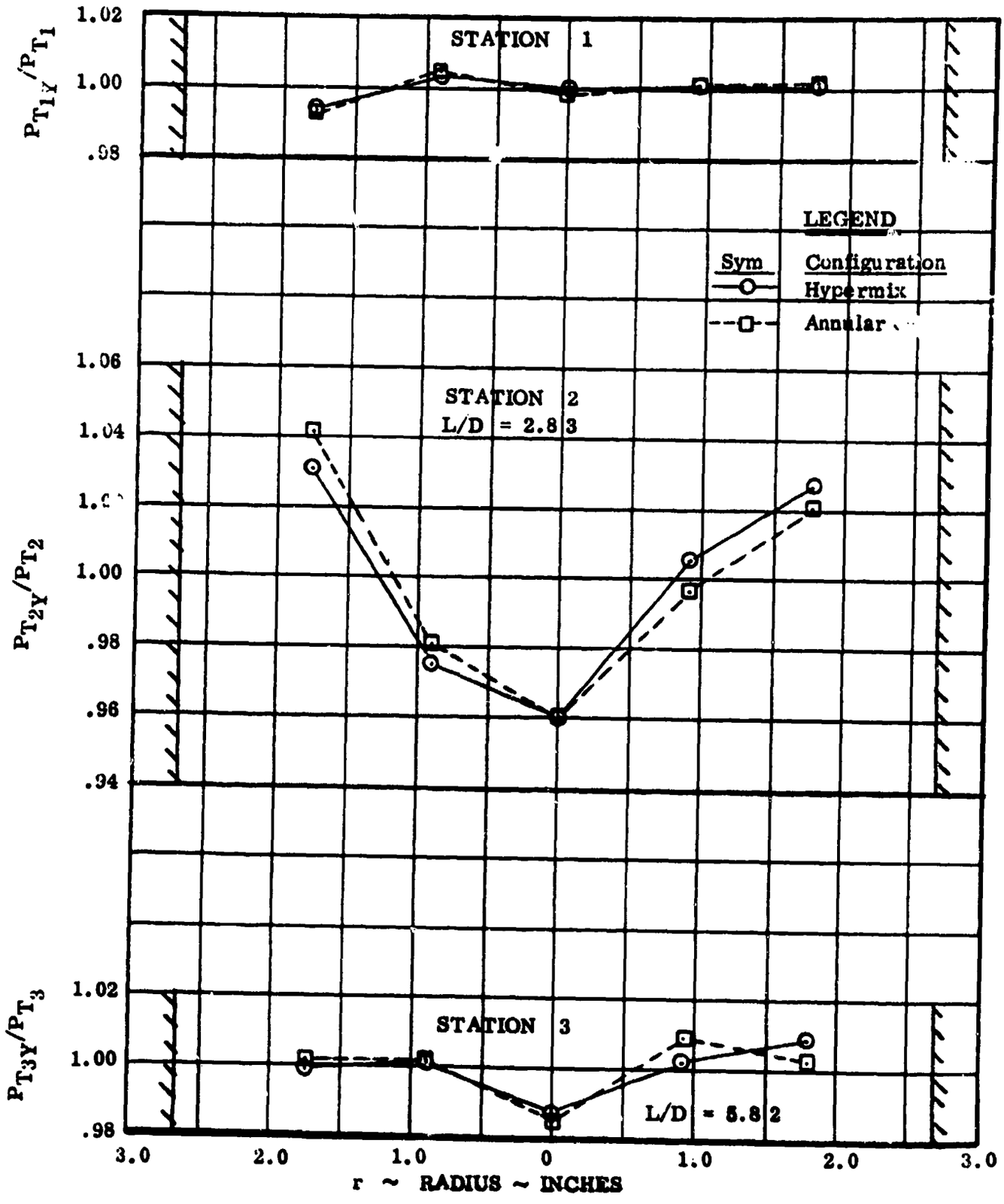

Figure 38. Comparison of Total Pressure Profiles, $W_S = 100\%$, $W_P = 75\%$
$\overline{W_{S_D}}$ $\overline{W_{P_D}}$

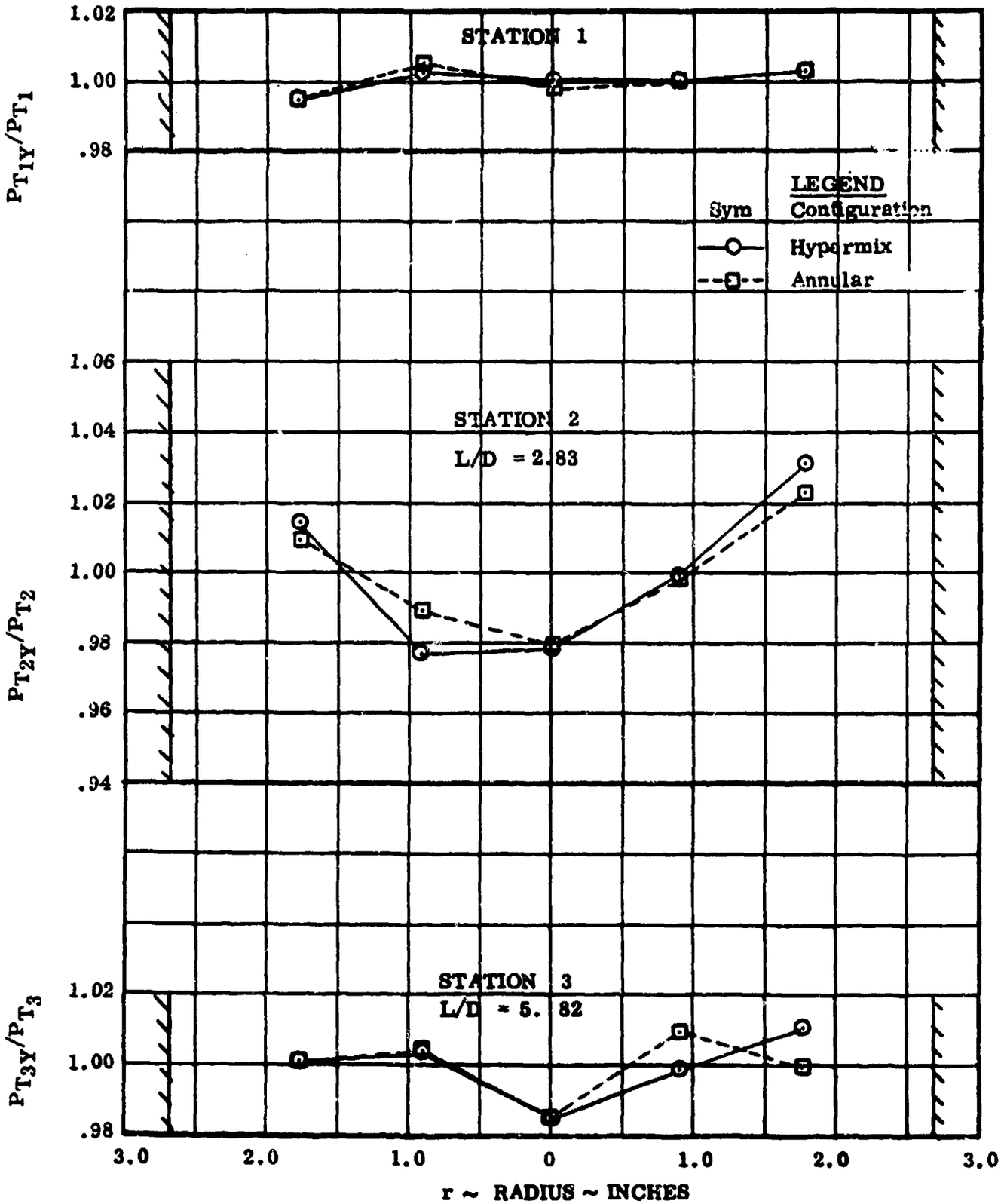

Figure 39. Comparison of Total Pressure Profiles, $\frac{W_S}{W_{S_D}}$ = 100%, $\frac{W_P}{W_{P_D}}$ = 50%

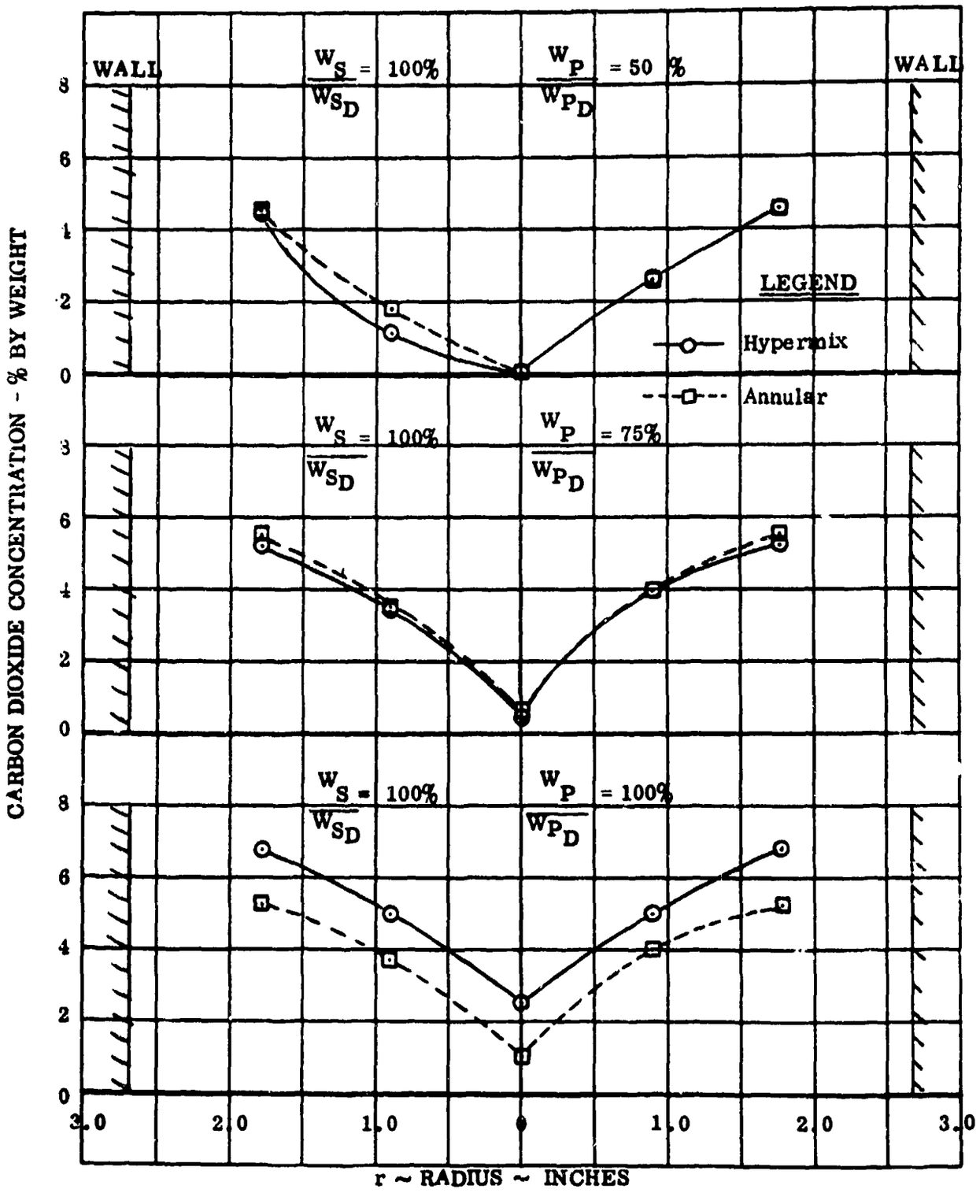

Figure 40. Comparison of Station 2 -CO_2 Distribution with and without Hypermixing

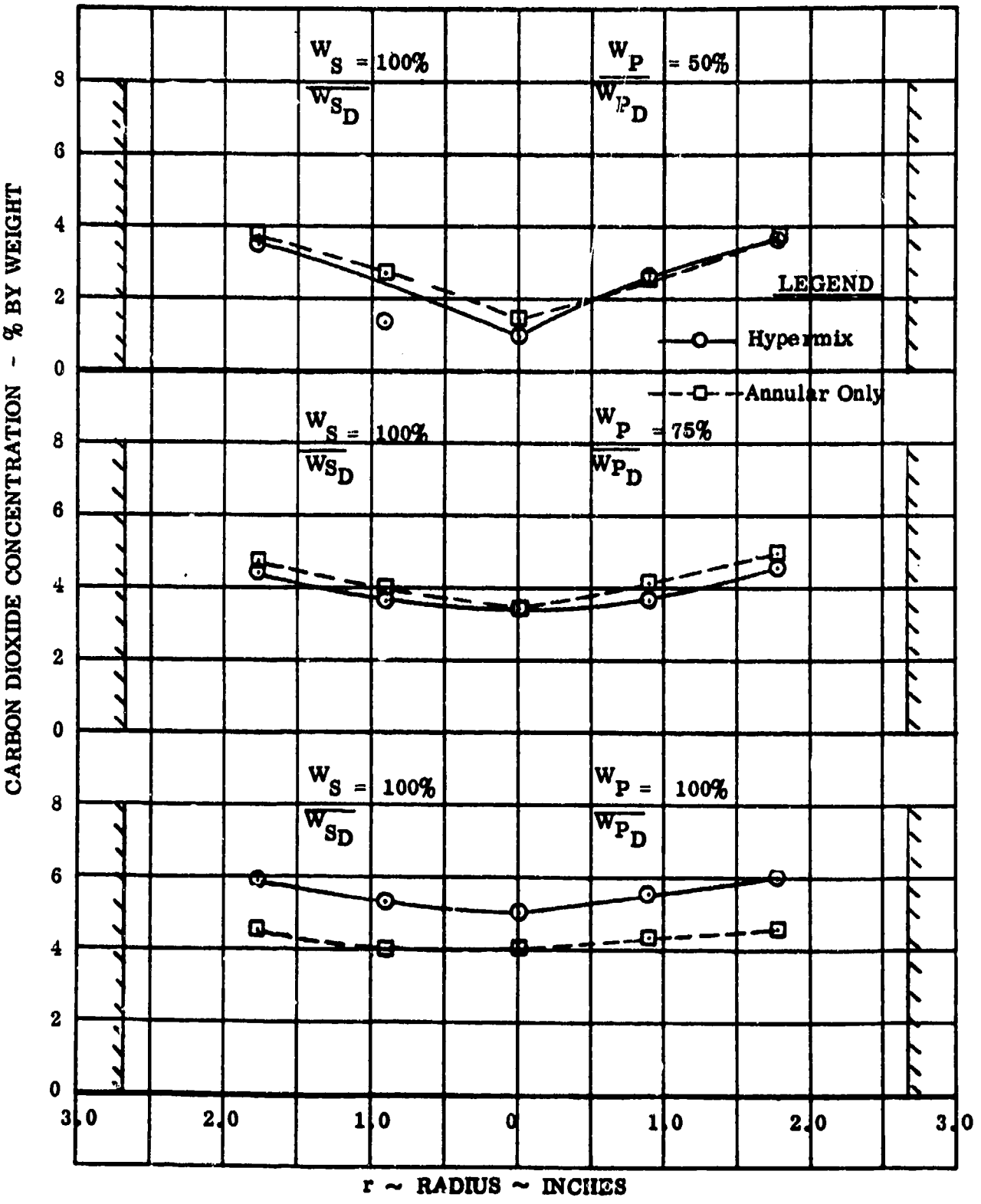

Figure 41. Comparison of Station 3-CO_2 Distributions with and without Hypermixing

Comparison of all annular and hypermixing nozzle data led to the conclusion that there was virtually no difference in mixing rate between these two ejector configurations. Shadowgraphs of the hypermixing configuration exhausting directly into ambient air were taken over a range of pressure ratios*. These shadowgraphs are presented in Figures 42 through 46. It may be seen that there is very little spreading of the nozzle exit wake, and in fact it appears that, as the nozzle pressure ratio is increased, the wake tends to move toward the centerline rather than spread outward.

Based upon the foregoing results, it was reasoned that the selected design for the hypermixing nozzle did not provide a sufficiently large radial flow component to be effective and therefore did not introduce the desired vorticity into the flow. A proposal was submitted to the Aerospace Research Laboratories to modify the hypermixing nozzle and run additional tests. This proposal was accepted by ARL. The following sections of this report describe this ejector modification and its experimental evaluation.

The foregoing has presented only a brief review** of these initial test results, sufficient to draw the conclusion that the original hypermixing nozzle design offered little, if any, performance improvement over the simple annular nozzle. In discussing test results for the modified hypermixing ejector, additional test data for the annular and hypermixing ejector (Runs 1-9) will be presented for comparison.

* Ejector design pressure ratio is 19.3

**Additional test data is presented in Appendix B of this report.

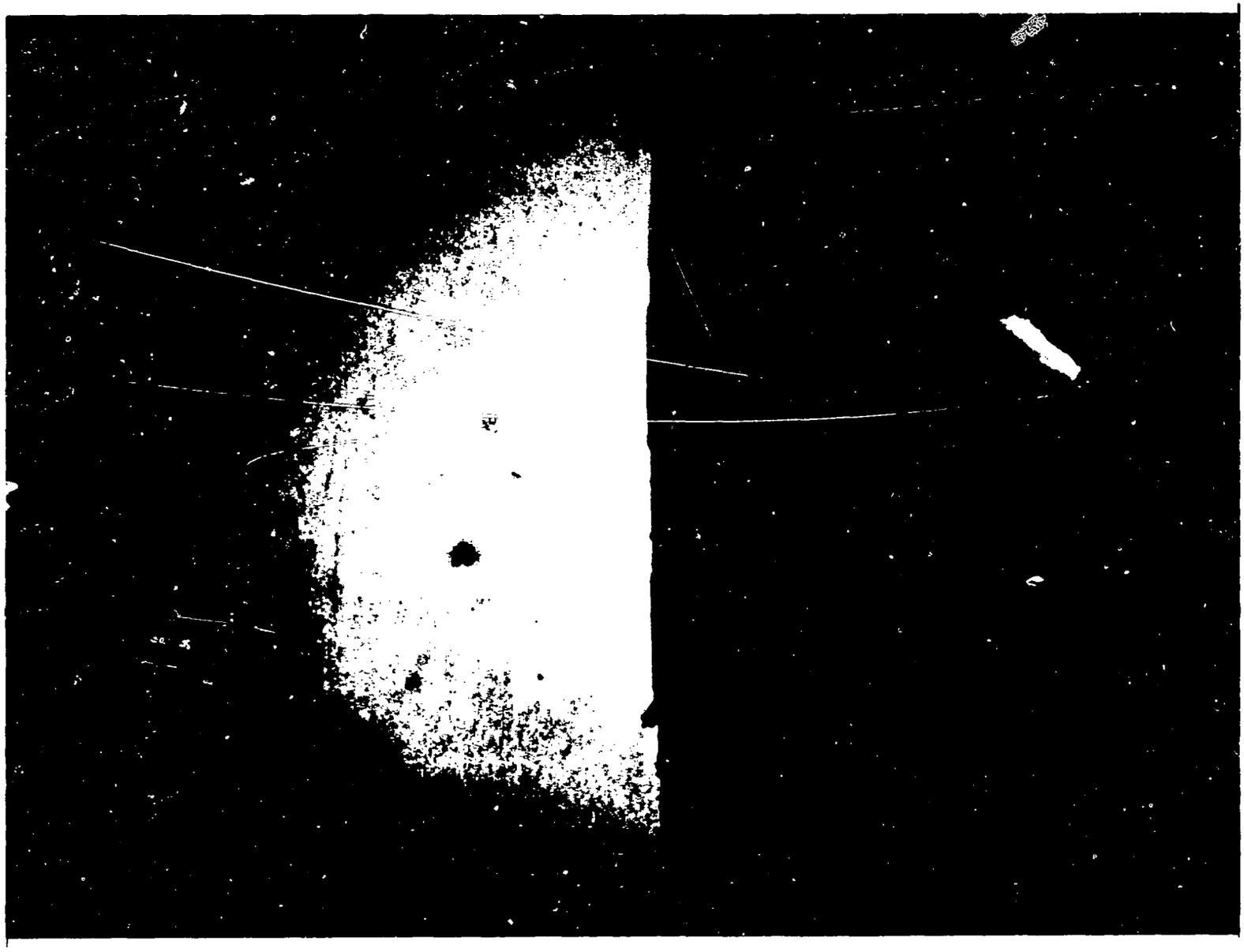

Figure 42. Initial Hypermixing Ejector Test Shadowgraph
Ejector Pressure Ratio = 2.6

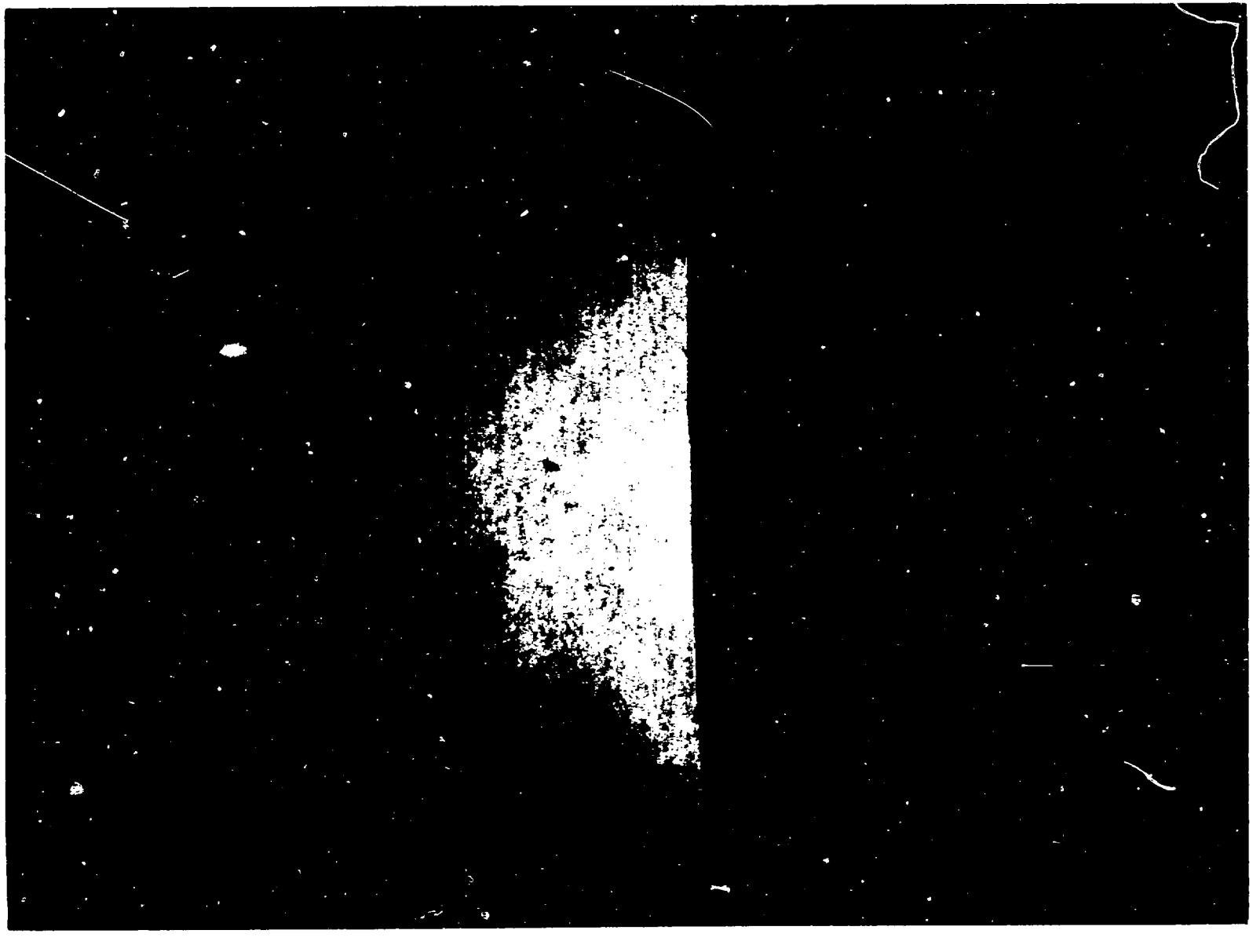

Figure 43. Initial Hypermixing Ejector Test Shadowgraph
Ejector Pressure Ratio = 4.9

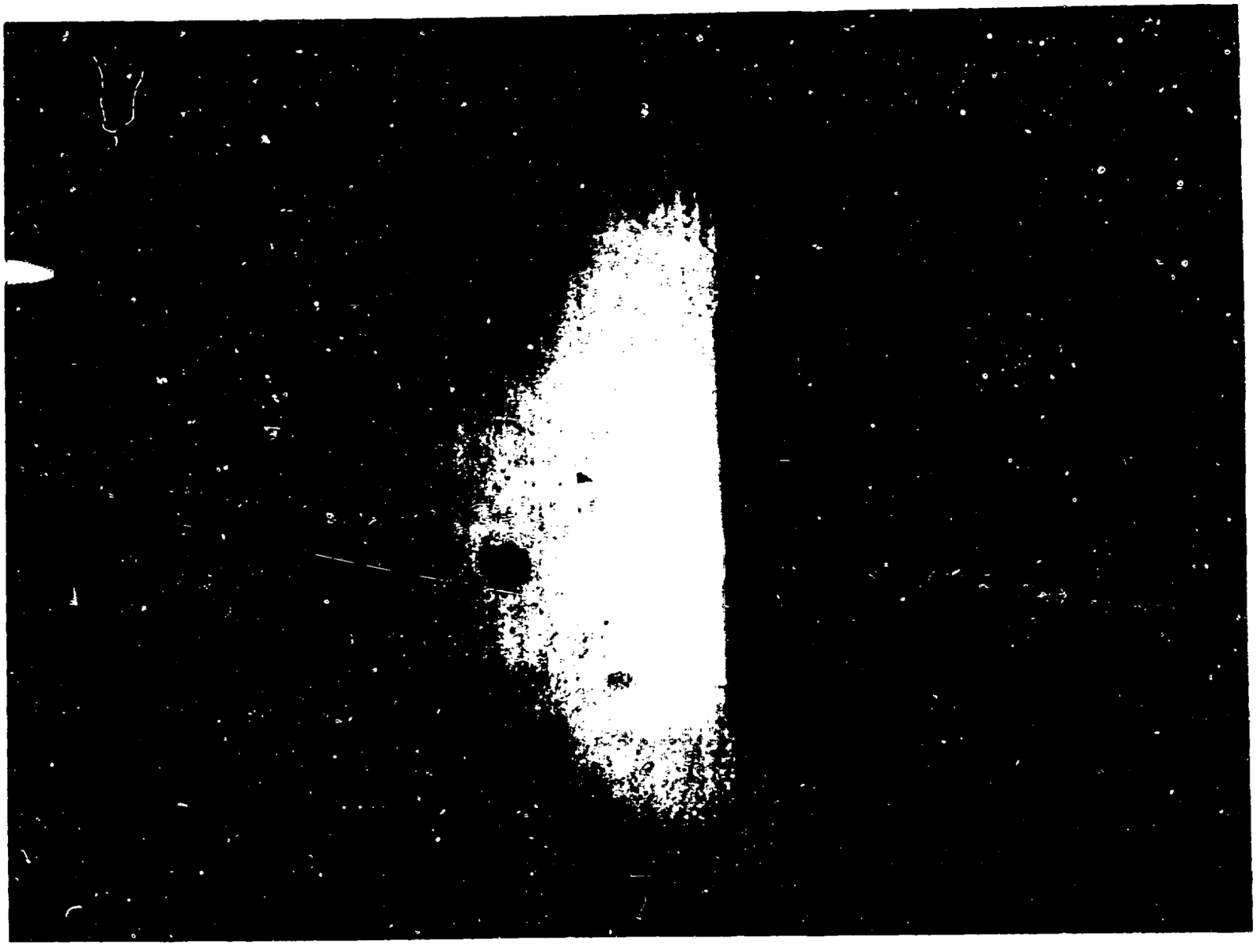

Figure 44. Initial Hypermixing Ejector Test Shadowgraph
Ejector Pressure Ratio = 7.3

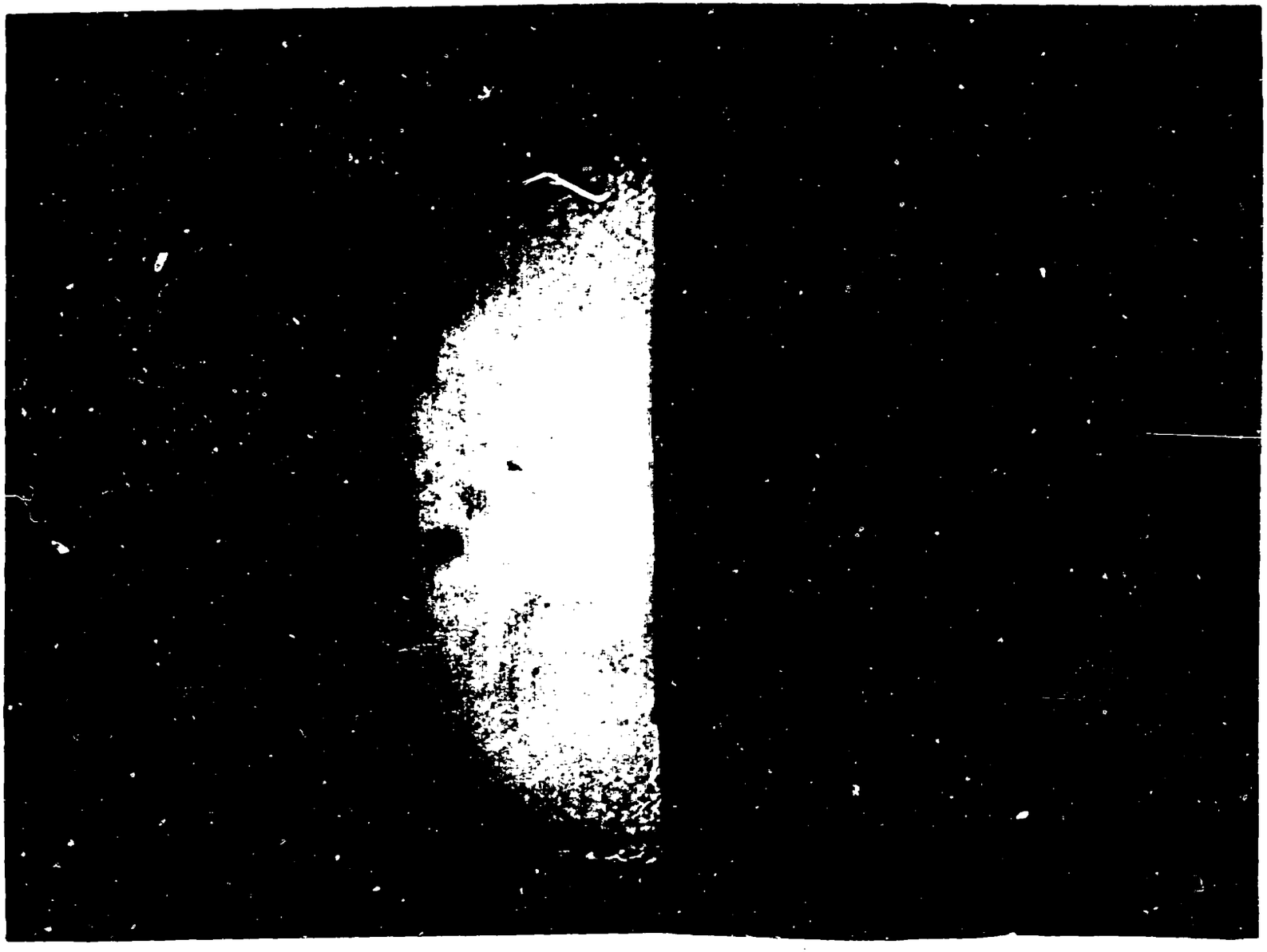

Figure 45. Initial Hypermixing Ejector Test Shadowgraph
Ejector Pressure Ratio = 9.7

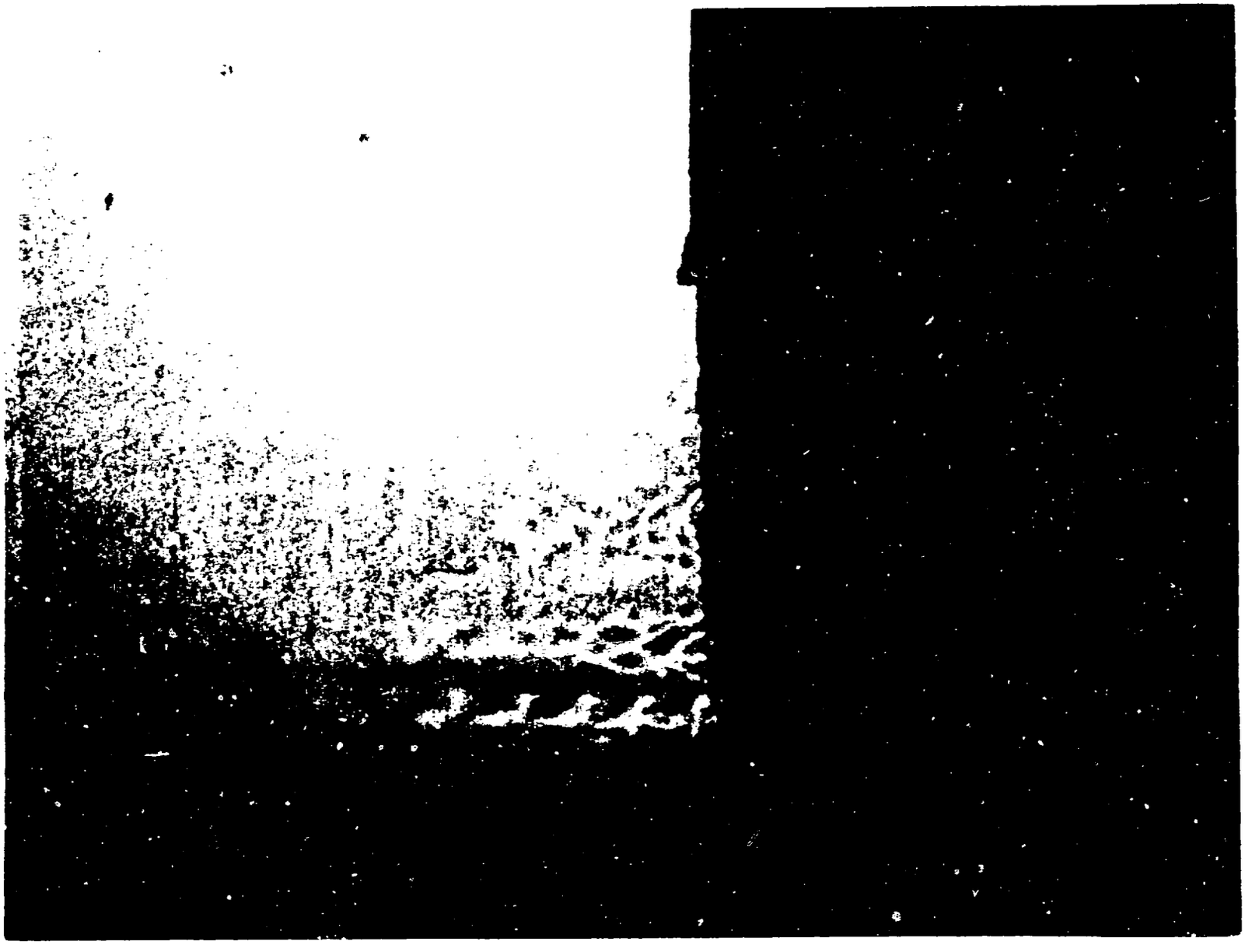

Figure 46. Initial Hypermixing Ejector Test Shadowgraph
Ejector Pressure Ratio = 9.7 (Enlargement of Figure 45)

SECTION X

MODIFIED HYPERMIXING EJECTOR DESIGN

The hypermixing ejector concept with two-dimensional subsonic flow exit nozzles has been convincingly demonstrated by ARL in past test programs (Reference 5). With the ejector ramjet engine concept developed in this program, the ejector subsystem is annular, and the primary exit flow is supersonic. The annular ejector creates an axisymmetric flow pattern but locally approximates a two-dimensional nozzle flow field. Therefore, the supersonic exit is the fundamental difference between the ramjet ejector and previous ARL tests.

With the hypermixing ejector design developed in this program (See Section VII of this report) the radial or vertical flow component results from the nozzle exit plane static pressure differential. With this ejector configuration, the nozzle throat is horizontal. The resulting flow pattern is shown below:

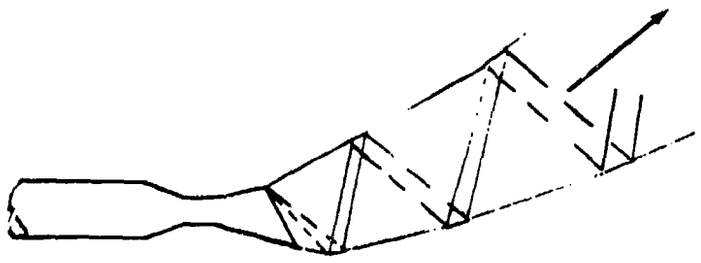

As discussed in the preceding report section, this ejector nozzle configuration resulted in little, if any, increase in local mixing intensity.

The ARL exit nozzle geometry was again reviewed. The baseline configuration is shown below:

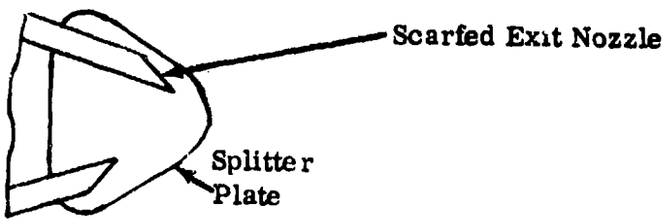

In particular, it should be noted that the nozzle throat centerline is inclined to the horizontal axis. Marquardt/ARL discussions led to the conclusion that the nozzle throat of the supersonic ejector nozzle should also be inclined. Several ejector nozzle configurations, which inclined the nozzle flow axis to the horizontal axis, were developed. Figure 47 describes the selected configuration. The nozzle flow centerline axis is inclined 15 degrees to the horizontal; therefore, a large radial or vertical velocity component will result. Furthermore, adjoining nozzle segments will create large vertical velocity differentials, resulting in zones of intense interaction. ARL's test experience indicates that these intense local flow interactions (i.e., stream vortices) are basic to the hypermixing concept. It should also be noted in Figure 47 that this configuration provides for flow splitting at the juncture of adjoining nozzle segments. In addition, this configuration results in a smooth exterior geometry.

The resulting ejector nozzle configuration is mechanically more complex than the initial design but can be machined by using conventional techniques. The small nozzle size is more of a constraint than nozzle geometry.

In the ejector design presented in Figure 47, the existing ejector was modified to incorporate this design approach. The nozzle section of the initial ejector design was cut away, and the new nozzle section was welded to the existing hardware. It should be noted that the ejector radial location, number of nozzle segments, nozzle throat area, and nozzle segment aspect ratio did not change from the initial design.

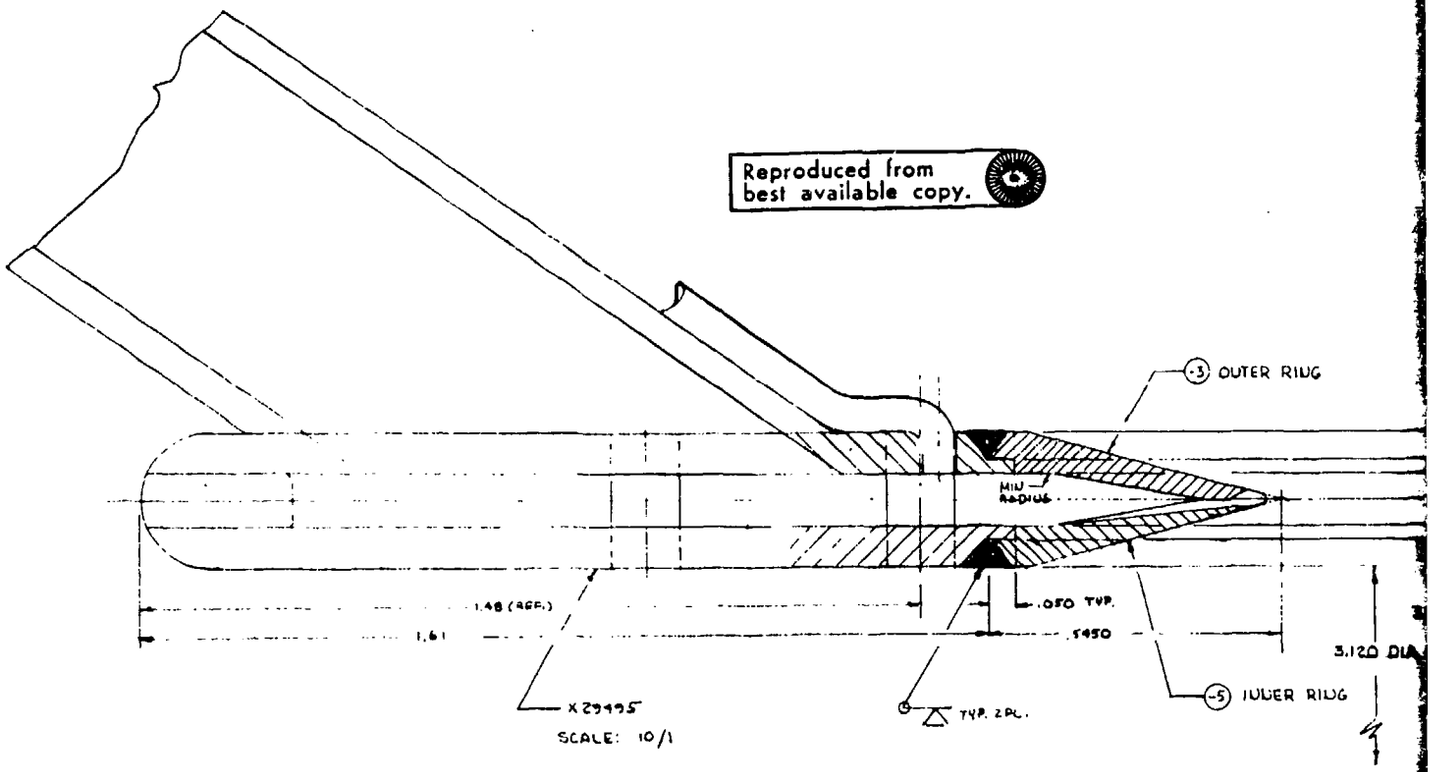

SCALE: 10/1

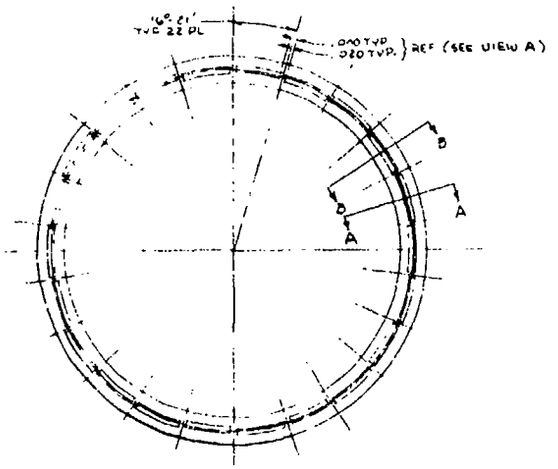

SCALE: 2/1

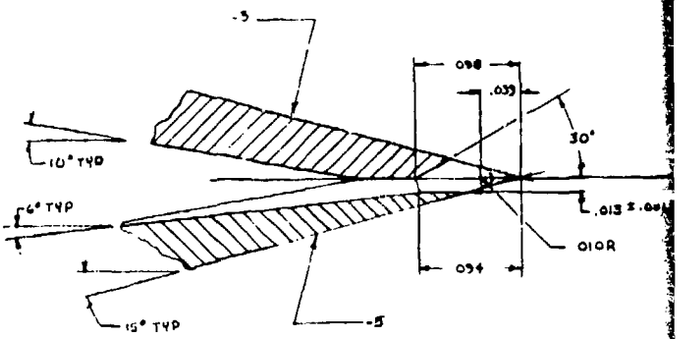

SEC. "A"-"A"
SCALE: 20/1

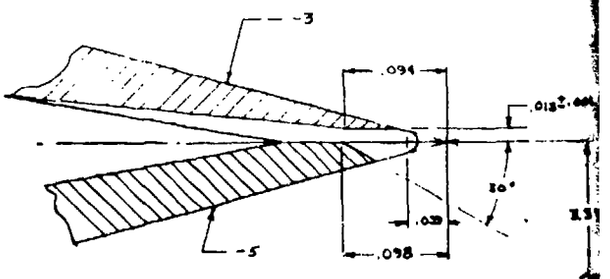

SEC. "B"-"B"
SCALE: 20/1

A

Notes:
1. ALL WELDS PER MPS 1601

Figure 17.

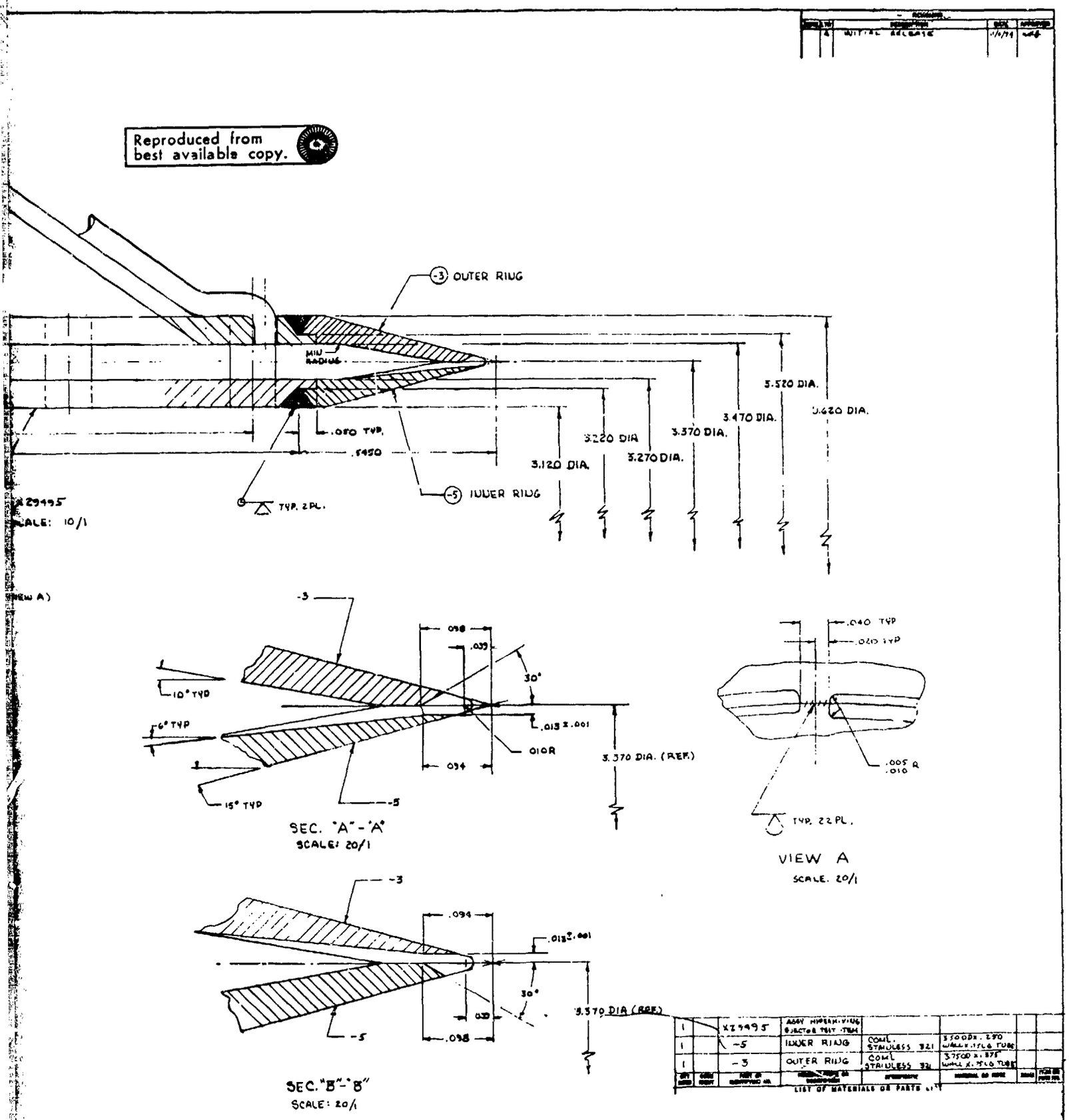

1		X2995	ASSY HYPERMIXING EJECTOR TEST ITEM			
1		-5	INNER RING	COMP. STAINLESS 321	3.500 O.D. x .250 WALL x 17.6 TUBE	
1		-3	OUTER RING	COMP. STAINLESS 321	3.750 O.D. x .375 WALL x 17.6 TUBE	

LIST OF MATERIALS OR PARTS

Notes:
1. ALL WELDS PER MPS 1601

Figure 17. Modified Hypermixing Ejector Test Item

SECTION XI

MODIFIED HYPERMIXING EJECTOR EXPERIMENTAL PROGRAM

1. HARDWARE FABRICATION

The Modified Hypermixing Ejector Test Item was fabricated in Marquardt's experimental shop. Completed assembly photographs are presented in Figure 48 and Figure 49. No additional hardware was required.

2. TEST SETUP

The test setup used to evaluate the initial hypermixing ejector design was also used to evaluate the Modified Hypermixing Ejector. This setup is fully described in Section IX of this report. Figures 50 and 51 are photographs of the Modified Hypermixing Ejector Test Item installed in Marquardt test cell 7.

3. INSTRUMENTATION

The test instrumentation system used to measure the performance of the initial hypermixing ejector design was also used to evaluate the Modified Hypermixing Ejector. This test instrumentation system is described in Section IX of this report.

4. TEST PROGRAM

The Modified Hypermixing Ejector was evaluated over the range of 50% to 125% of the primary design flow rate. The secondary flow rate was maintained at its design value. Nominal test conditions are summarized in Table XV. A test run summary is presented in Table XVI. As discussed in Section IX of this report, three mixer spools and two mixer total pressure rakes could be arranged in several different test configurations. The mixer spool configuration for each test run is presented in Table XVI. The location of the total pressure rakes and static pressure taps for each test run is presented in the following subsection of this report.

5. TEST RESULTS

Axial static pressure distributions for the Modified Hypermixing Ejector nozzle configuration are shown in Figures 52 through 54. As shown at the top of these figures, the constant diameter mixer spools and the two forward total pressure rakes were arranged in several test configurations. Note that total pressure rake 3 for the initial ejector nozzle configuration (Figure 26) has been moved forward and renumbered 1.5. In comparing these static pressure distributions with those for the annular and initial hypermixing nozzle configurations presented earlier, it is noted that the maximum static pressure rise is achieved in a much shorter distance with the modified hypermixing ejector design. The test configuration shown in Figure 53 is believed to offer the best test instrumentation location to determine this pressure rise, and it may be seen that the peak static pressure rise occurred at about station 13* rather than at station 21*

*$W_P/W_{P_D} = 100\%$

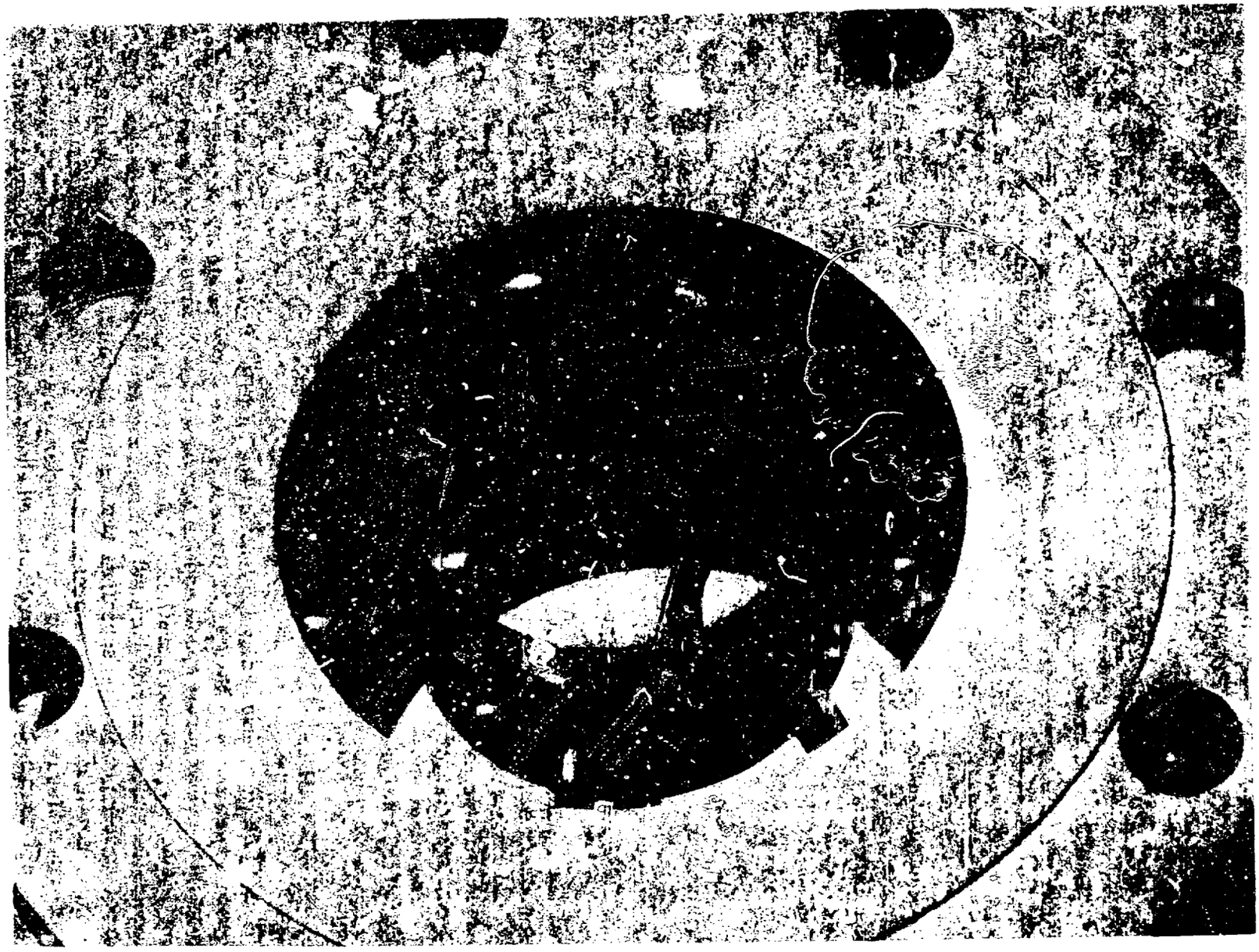

Figure 48. Modified Hypermixing Ejector Test Item-Close Up View

Figure 49. Modified Hypermixing Ejector Test Item

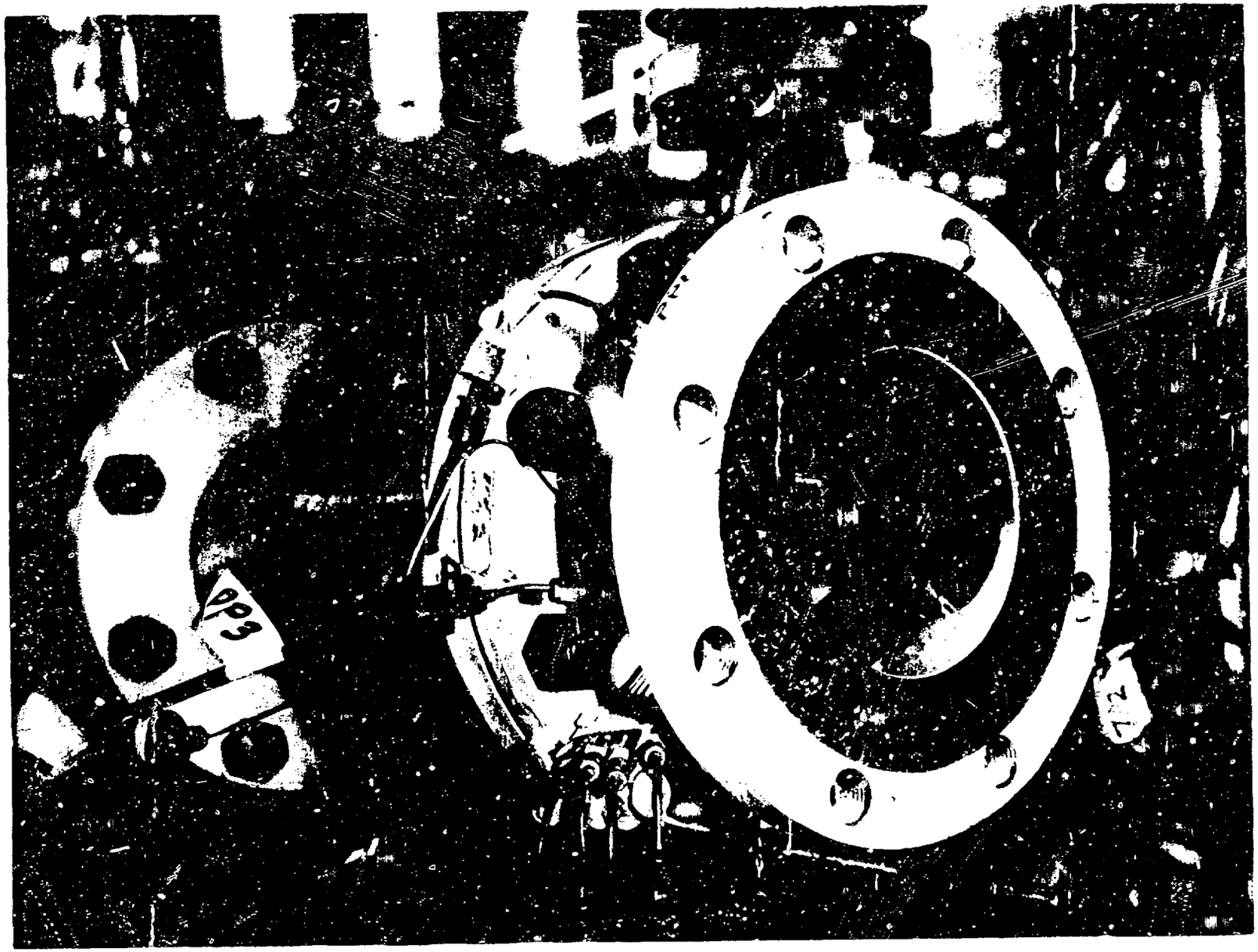

Figure 50. Modified Hypermixing Ejector Test Assembly

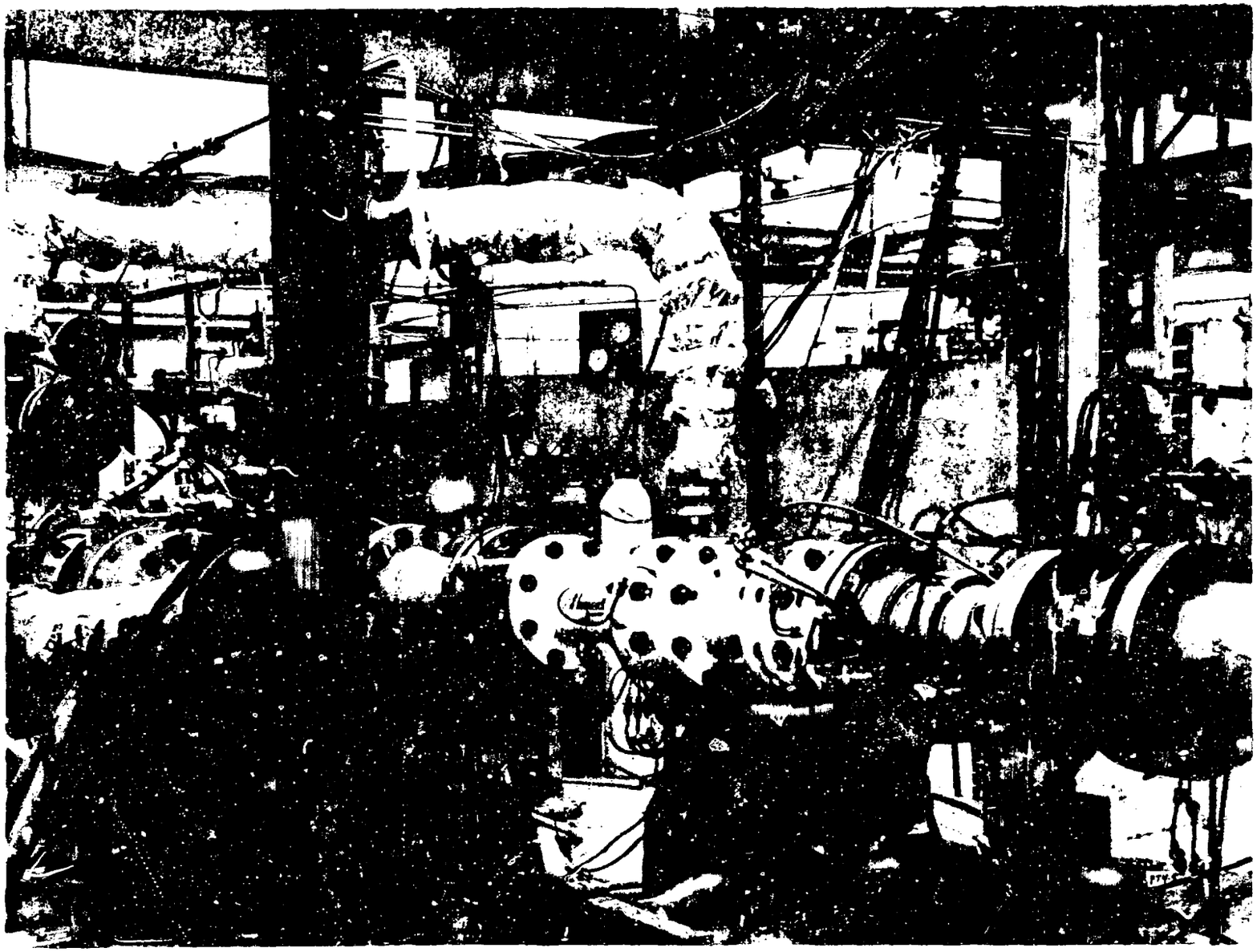

Figure 51. Modified Hypermixing Ejector Test Setup

TABLE XV. MODIFIED HYPERMIXING EJECTOR TEST CONDITIONS

$\frac{W_S}{W_{S_D}}$ %	$\frac{W_P}{W_{P_D}}$ %	$\frac{W_S}{W_P}$	ϕ	W_S lb/sec	W_P lb/sec	P_{T_P} psia	W_{AIR_P} at 1640°R lb/sec	W_{CO_2} P at 520°R lb/sec	$\frac{W_{CO_2}}{W_S + W_{AIR\ P}}$ %
100	125	7.35	1.25	5.70	0.775	334	0.388	0.388	6.37
↓	100	9.19	1.0	↓	0.620	267	0.310	0.310	5.16
	75	12.25	0.75		0.46	200	0.233	0.233	3.93
	50	18.38	0.50		0.310	134	0.155	0.155	2.65

W_S = Secondary Flow

W_P = Primary Flow

W_{S_D} = Design Secondary Flow

W_{P_D} = Design Primary Flow

TABLE XVI. MODIFIED HYPERMIXING EJECTOR TEST RUN SUMMARY

Run no.	Test Configuration	$\frac{W_S}{W_{S_{design}}}$	$\frac{W_P}{W_{P_{design}}}$	Remarks
10	First mixer spool, L/D = 2 Second mixer spool, L/D=1 Third mixer spool, L/D=3	100%	125%, 100%, 75%, 50%	Good data run
11	First mixer spool, L/D=1 Second mixer spool, L/D=2 Third mixer spool, L/D=3	100%	125%, 100%, 75%, 50%	Gas samples not obtained for $\frac{W_P}{W_{P_D}}$ = 100% and 75%
11R	Same as run 11	100%	100% and 75%	Good data run
12	First mixer spool, L/D=2 Second mixer spool, none Third mixer spool, none	100	125%, 100% 75%, 50%	Good data run

Secondary (air) metering nozzle diameter = 2.475 in.
Test item exit nozzle diameter = 4.26 in.

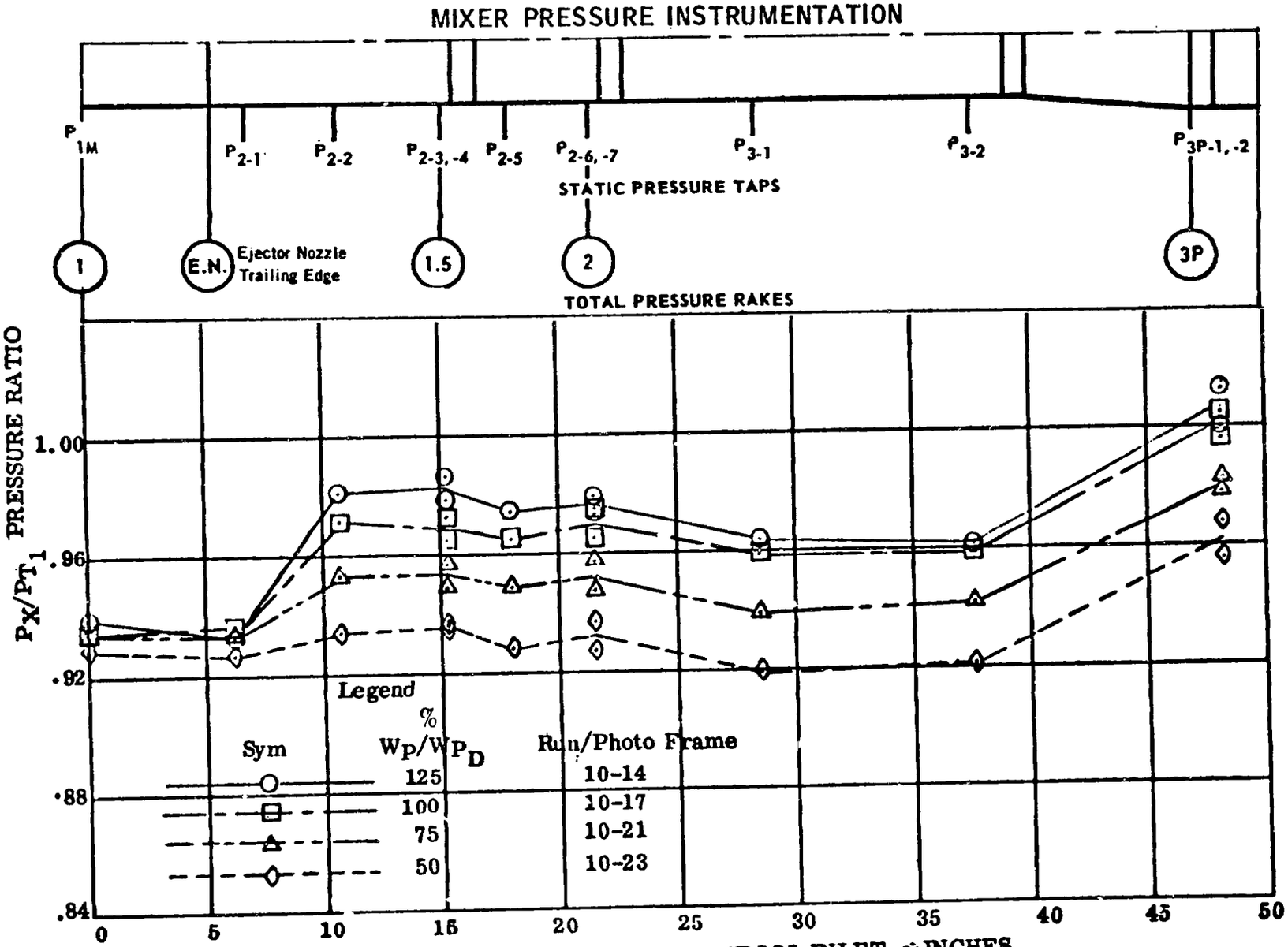

Figure 52. Axial Pressure Distributions, $W_S/W_{S_D} = 100\%$

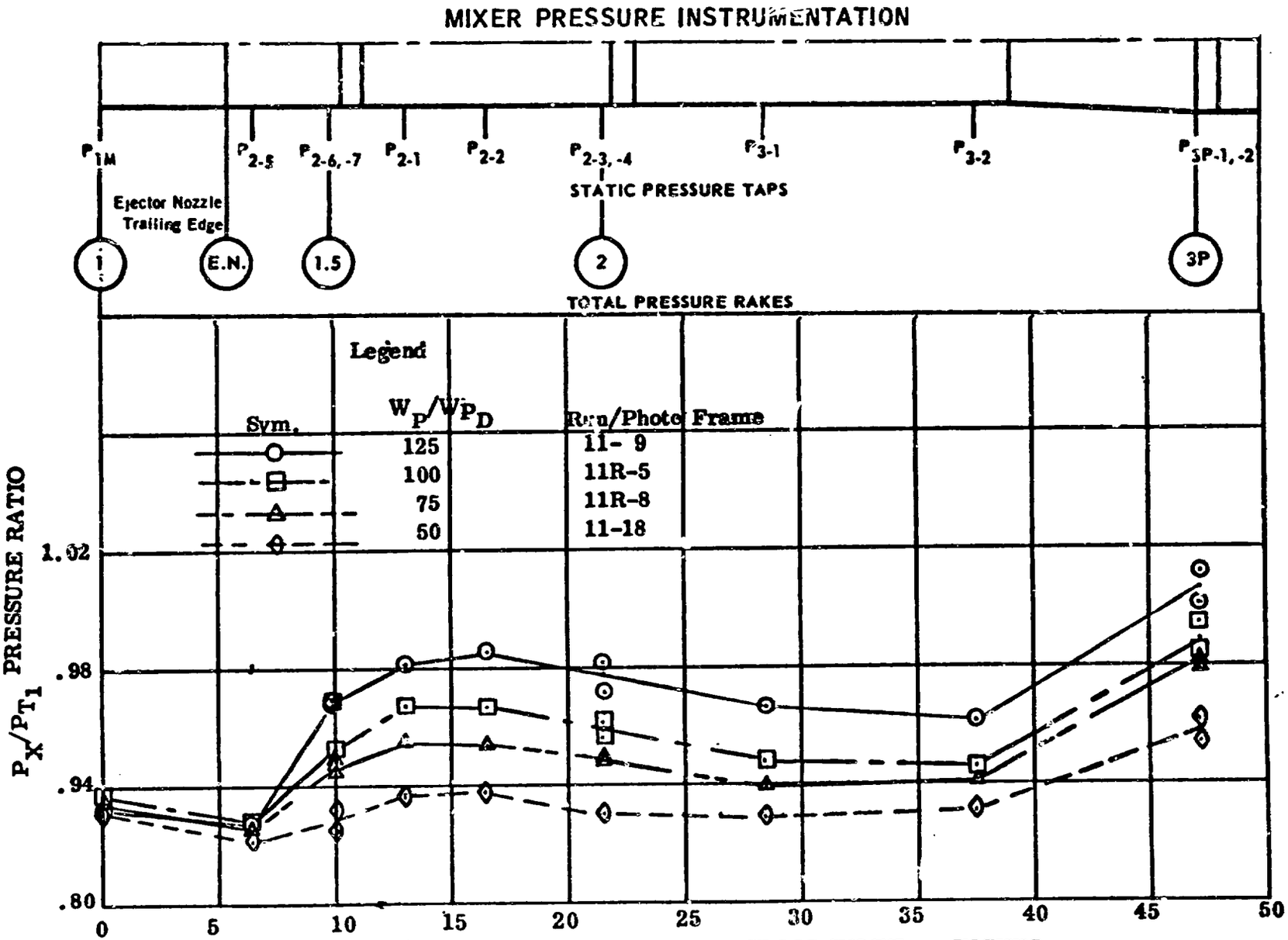

Figure 53. Axial Pressure Distributions, W_S/W_{S_D} = 100%

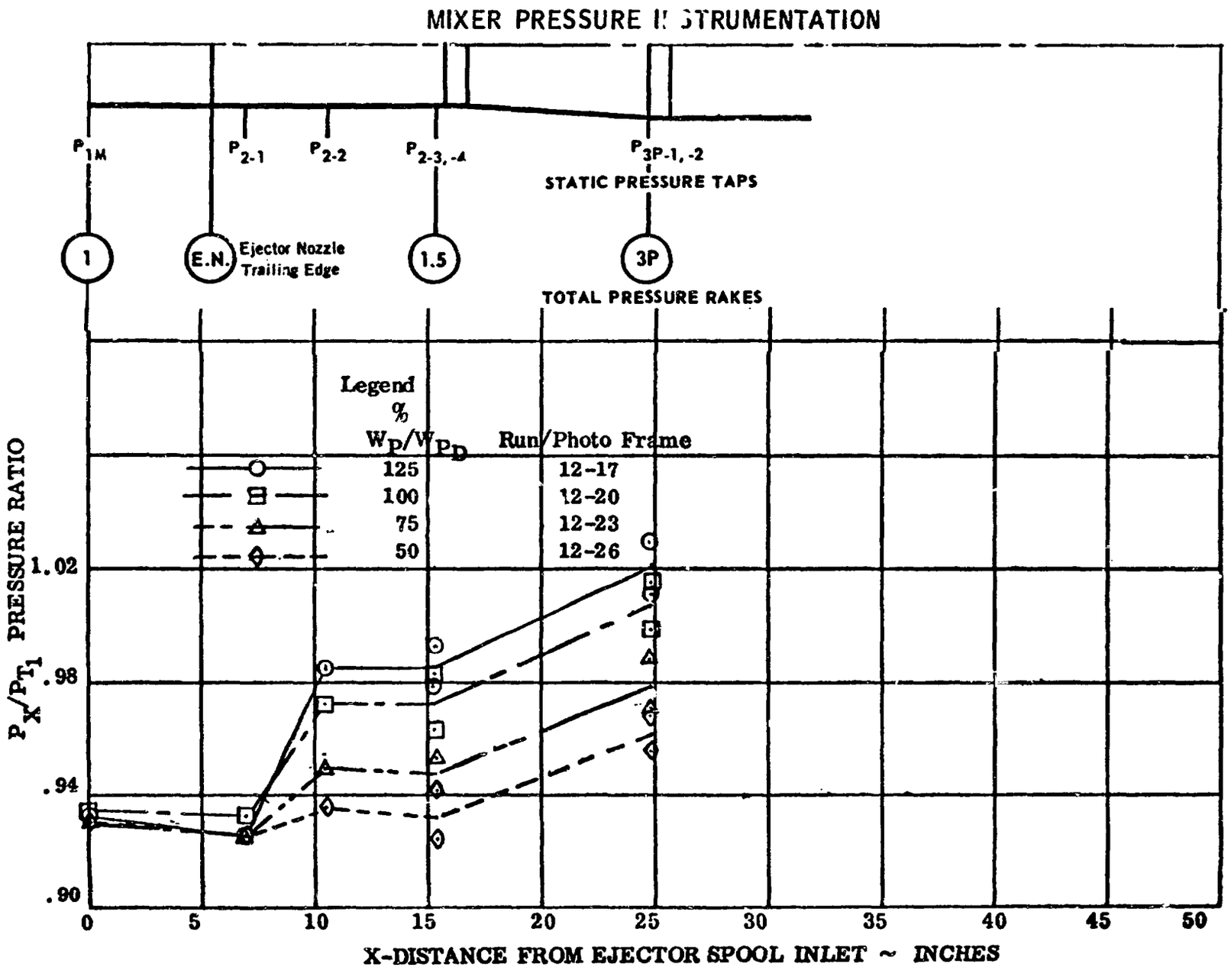

Figure 54. Axial Pressure Distributions, W_g/W_{S_D} = 100%

for the initial hypermix and annular nozzles. Also, it is noted in Figures 52 and 53 that the static pressure decreases beyond about station 17.5, indicating that for these configurations the mixer is too long and that viscous losses are beginning to build up. Figure 54 with the shortened mixer length does not show this characteristic and indicates a higher static pressure ratio at the end of the diffuser, which is the result of eliminating these viscous losses.

Figure 55 presents a comparison of the axial distribution of total pressure in the mixer for the annular ejector nozzle, the initial hypermixing ejector design, and the modified hypermixing ejector design. This comparison is based upon nominal design conditions for both the primary flow rate and secondary flow rate. In addition to presenting the averaged rake total pressure data in the mixer and diffuser, shown as open symbols, total pressures computed from measured static pressures and continuity relations are shown as solid symbols. Conclusions that were drawn from these results include:

1) The maximum total pressure recovery in the mixer is essentially identical for the annular and initial hypermixing nozzle configurations, thus supporting previous observations.

2) The maximum total pressure for the annular and initial hypermixing nozzle configuration occurs approximately at station 21 (15.5 inches downstream of ejector nozzle trailing edge).

3) The maximum total pressure for the modified hypermixing ejector configuration occurs at station 13, indicating the reduction in mixing length achieved with the modified design.

4) The absolute value of maximum total pressure achieved between the initial and modified hypermixing designs cannot be compared directly inasmuch as this parameter is strongly affected by actual test conditions. It should be noted that the notation $W_P/WP_D = 100\%$ or $W_S/WS_D = 100\%$ represent nominal values, and the actual values may vary ± 5%. Comparison of total pressure pumping ratio and mixing efficiency between ejector configurations is presented in this report section.

In discussing Figure 55, the question might be asked about fairing the data curves through the static pressure-continuity values rather than the total pressure rake data. In addition to there being more static pressure data, the averaged total pressure rake data tend to give erroneous values when the flow is not uniform. In the initial sections of the mixer, an arithmetic average tends to underestimate the total pressure since the lowest reading tubes represent a small percent of the total flow area or mass flow. On the other hand, with long mixing lengths, a turbulent flow profile characteristic is developed, and an arithmetic average tends to overestimate the total pressure by not accounting for the large percent of area and flow developed near the walls.

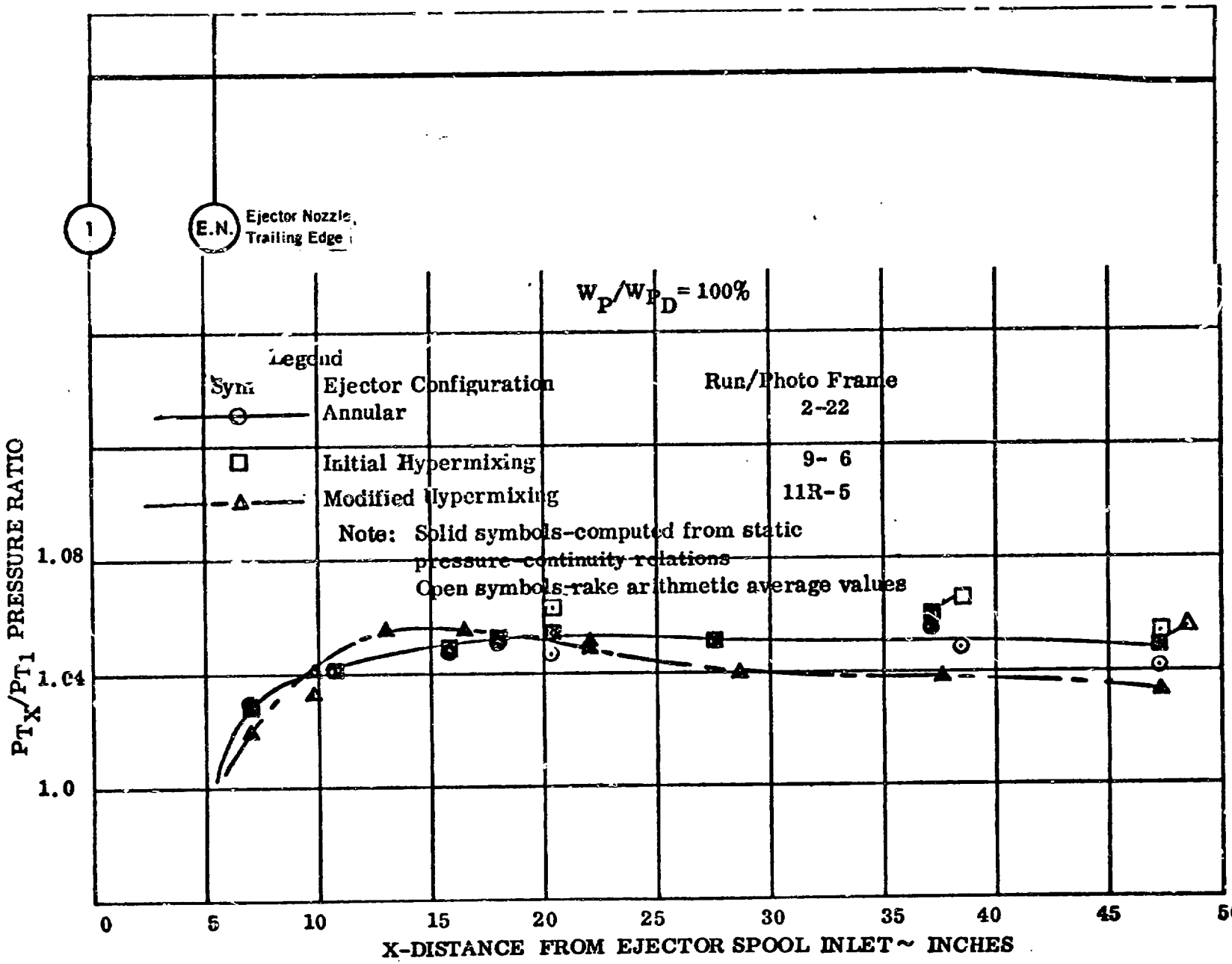

Figure 55. Axial Total Pressure Distribution Comparison, WS/WS_D = 100%

Similar axial total pressure distributions are shown in Figures 56 and 57 for the annular and initial hypermixing ejectors, respectively, over a range of primary flow rates. It will be noted that the required mixing lengths for both configurations are similar, supporting the earlier conclusion that the original hypermixing ejector offered no advantage over the annular ejector. Note that at the low primary flow rate both ejectors achieved the maximum total pressure at about station 11, whereas for the higher primary flow rates this maximum was delayed to approximately station 21. With respect to maximum total pressure level achieved, it should be noted that these levels ($P_{T_{max}}/\bar{P}_{T_1}$), as a function of secondary to primary flow rate (W_S/W_P), are essentially the same between the annular ejector and the initial hypermixing configuration except for W_P/W_{P_D} = 125%. Nominal test conditions were not achieved with the annular ejector (Runs 2-23) in that only about one half of the desired CO_2 was delivered to the primary. Had nominal test conditions been achieved, it is believed that the pressure rise for the annular ejector would have increased to that achieved for the initial hypermixing design.

Figure 58 presents similar data for the modified hypermixing ejector for a range of primary flow rates. As noted earlier, the maximum total pressure was achieved with shorter lengths, and, unlike the results presented in Figures 56 and 57 for the annular and initial hypermixing design, the mixer length for maximum total pressure rise did not change appreciably with primary flow rate over the range of W_S/W_P tested.

The effect of varying secondary airflow at constant primary flow could only be determined for the initial hypermixing ejector configuration. (See test conditions in Table XIV). These data are presented in Figure 59. Over the range of W_S/W_P covered, the length required to reach maximum total pressure varied little. It will be noted that the maximum total pressure ratio generally decreased as the value of W_S/W_P increased. An apparent exception to this rule is observed, however, inasmuch as the pumping ratio for W_S/W_P = 6.63 exceeds that for W_S/W_P of 4.76. However, a larger exit nozzle was used for values of $W_S/W_P \geq 6.63$. The Mach number into the mixer has correspondingly been increased, which increases jet pumping. Increased jet pumping with increase in M_1 is shown in Figure 60, where the maximum total pressure achieved in the mixer is plotted versus a correlation parameter involving M_1 and W_S/W_P. As may be seen, this correlation applies with good accuracy to the annular ejector, initial hypermixing ejector nozzle, and modified hypermixing ejector.

Figures 55 through 58 provided the necessary information to define the mixer lengths required to achieve full mixing. The mixer lengths required to develop maximum mixer total pressure and to develop 95% of this pressure rise were determined. Figure 61 compares required mixer length data (in terms of mixer length/diameter ratio) for the annular, initial, and modified hypermixing ejectors. It clearly shows the major reduction in required mixing length discussed above. At the ejector design point, the required mixer length was reduced approximately fifty percent. In addition, the data of Figure 61 supports the general conclusion that there was little difference between the annular and initial hypermixing ejector designs.

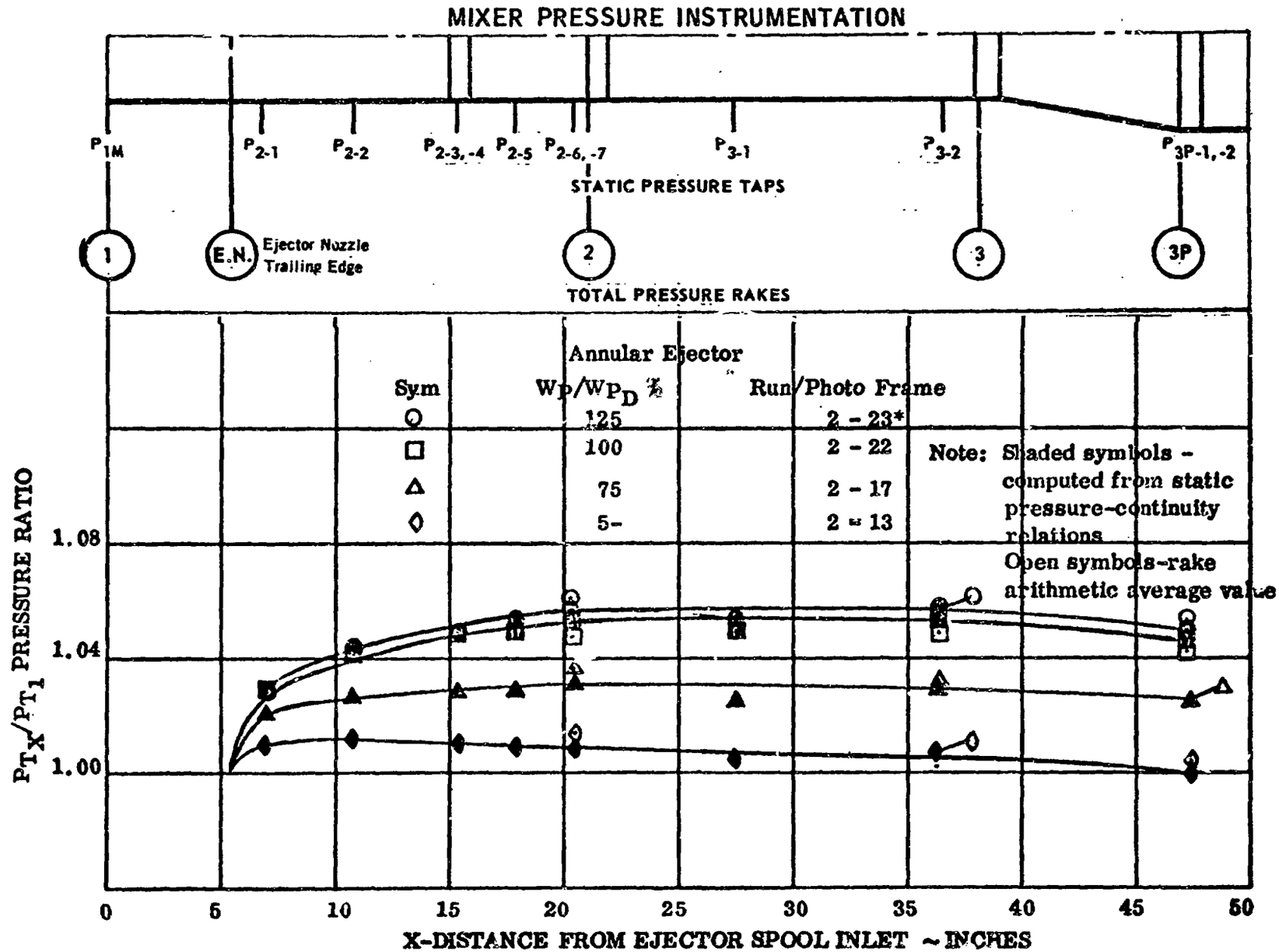

Figure 56. Annular Ejector Axial Total Pressure Distribution $W_P/W_{S_D} = 100\%$

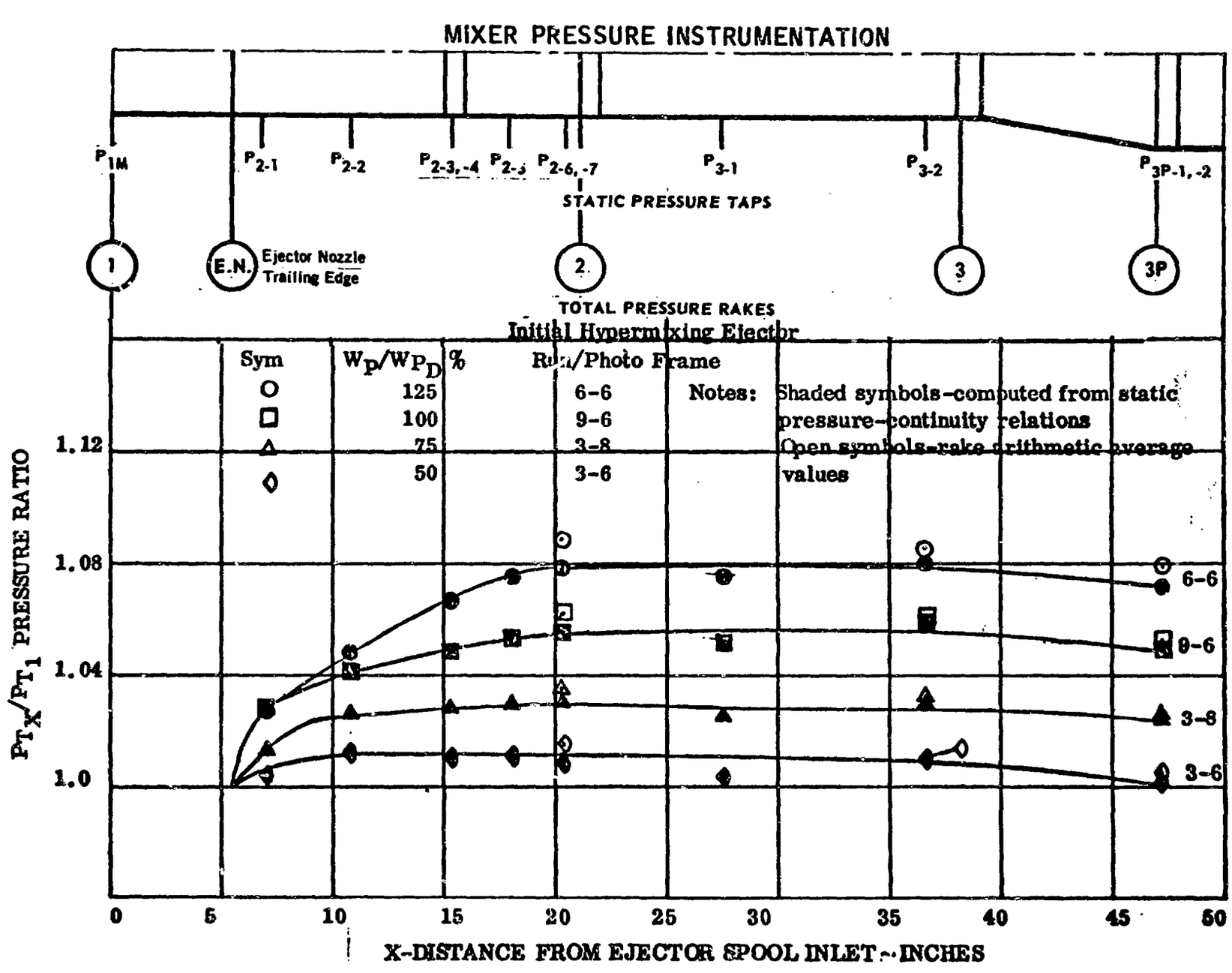

Figure 57. Initial Hypermixing Ejector Axial Total Pressure Distributions, W_S/W_D= 100%

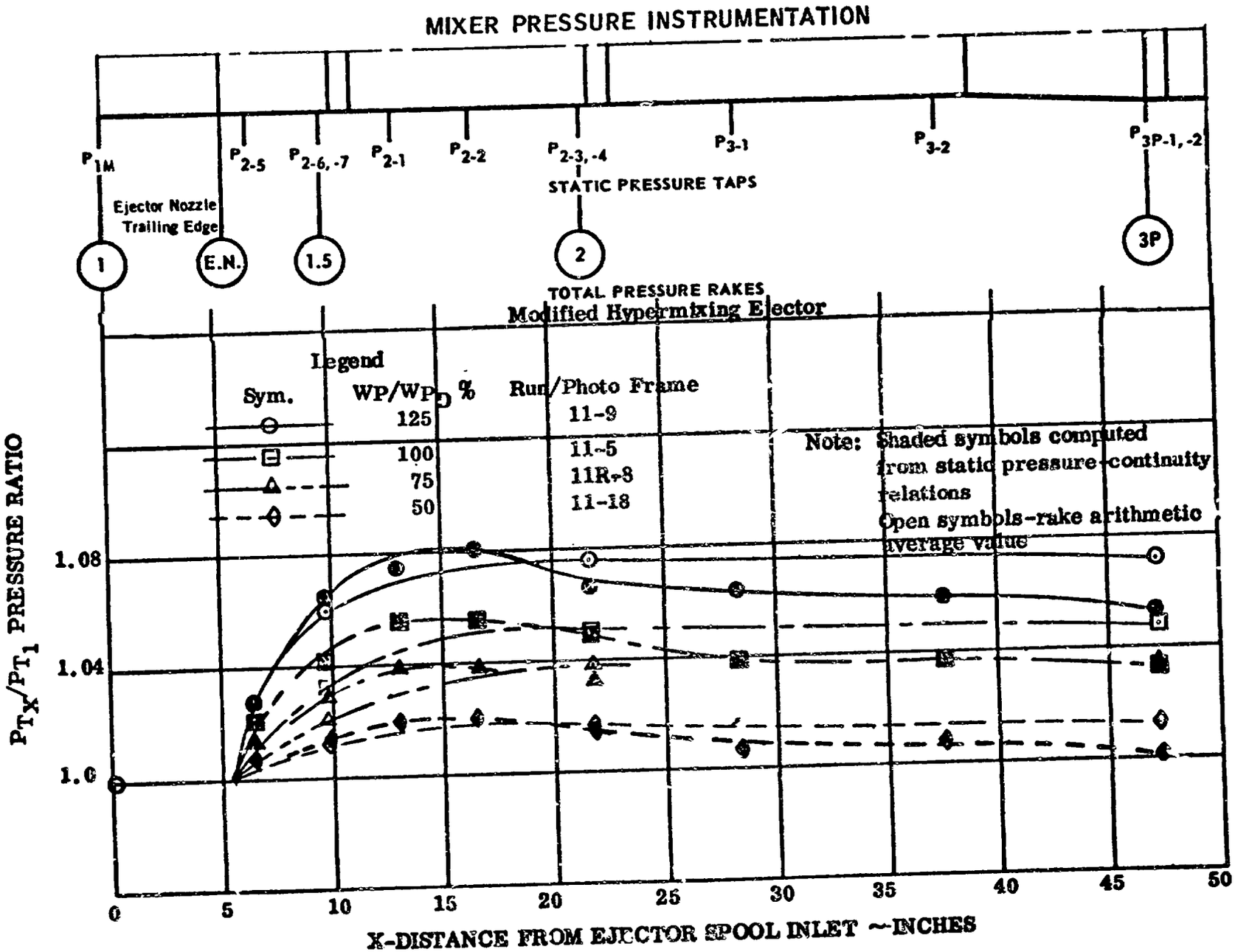

Figure 58. Axial Total Pressure Distributions, W_S/W_{S_D} = 100%

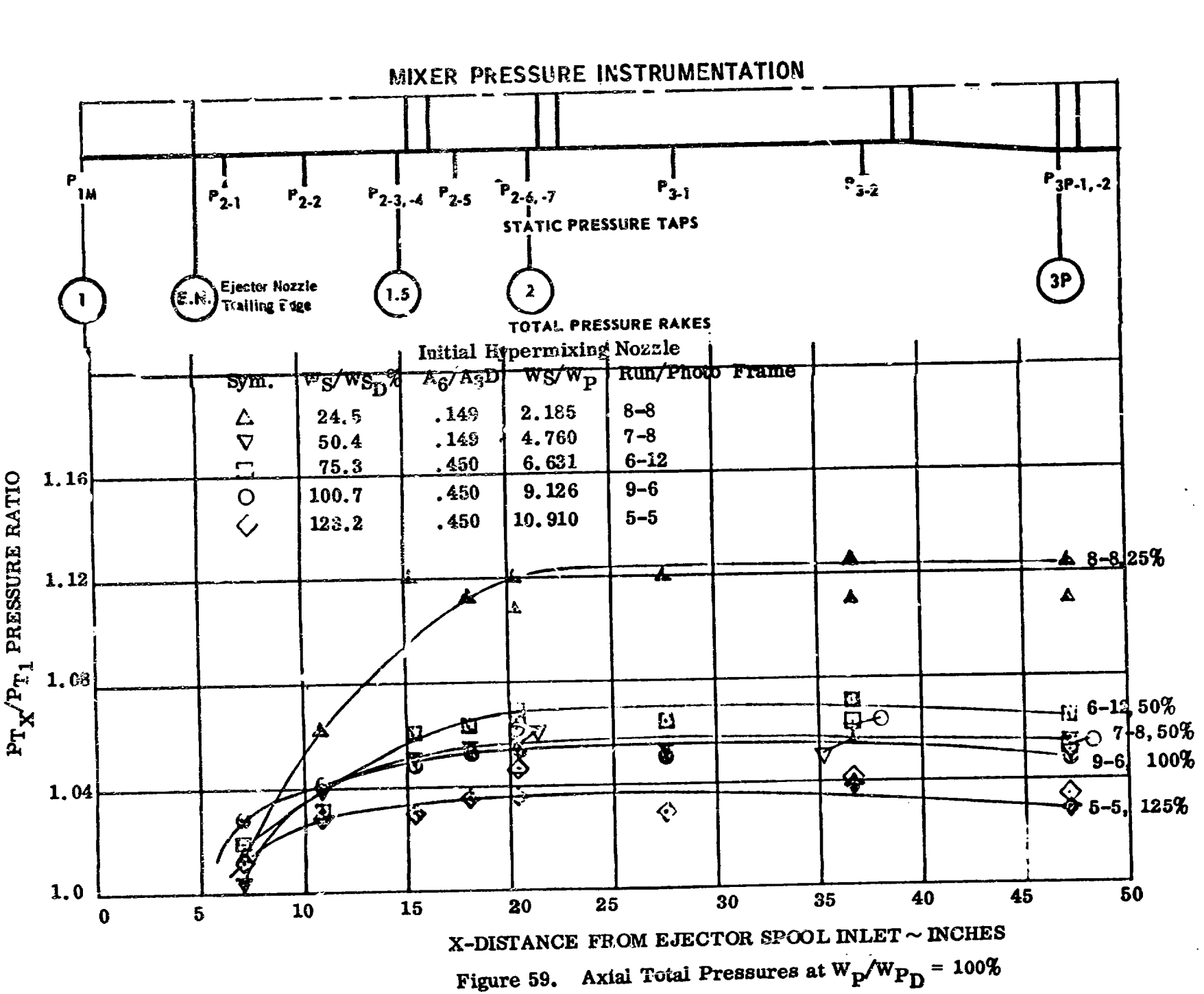

Figure 59. Axial Total Pressures at W_P/W_{P_D} = 100%

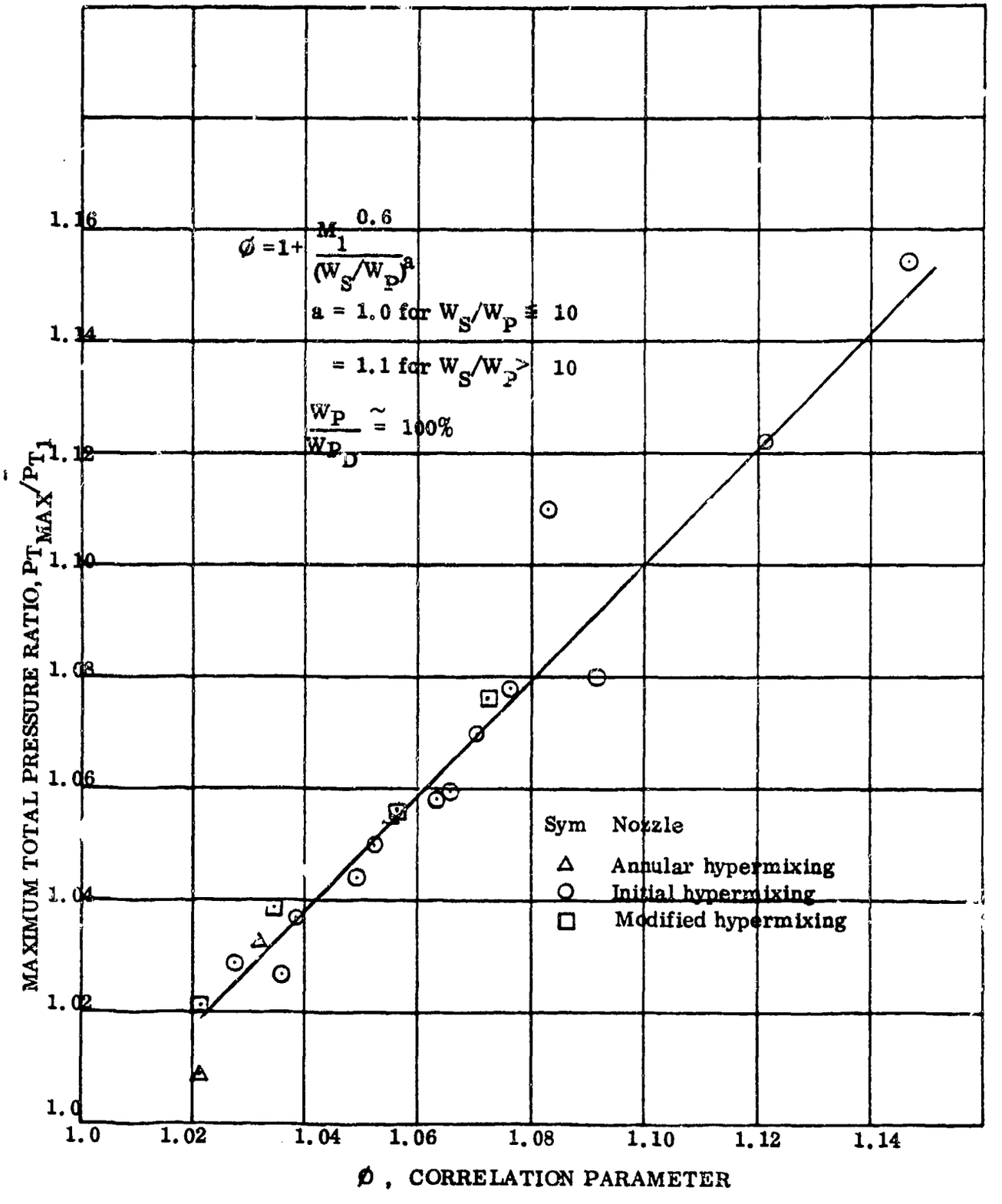

Figure 60. Maximum Mixer Total Pressure Ratio Correlation

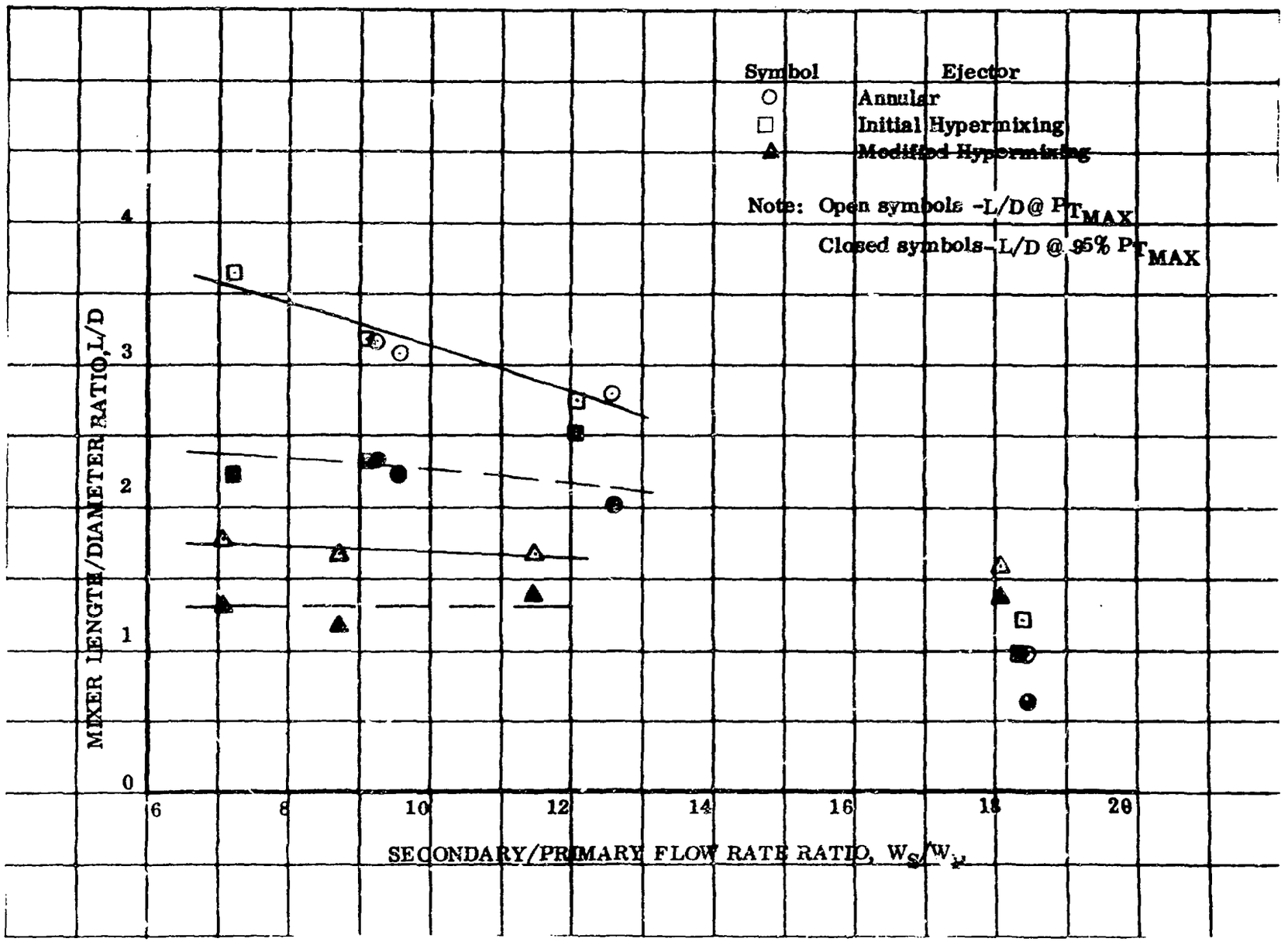

Figure 61. Required Mixer Length-Annular, Initial and Modified Hypermixing Ejectors

Marquardt had previously conducted several ejector/jet compression test programs under U. S. Air Force sponsorship. As a result of this work, required mixer length was correlated as a function of the number of primary nozzles, the primary exit Mach number, the secondary/primary flow rate ratio (W_S/W_P), primary/secondary total temperature ratio, and mixer/ejector geometry. Figure 62 compares this experimentally derived mixer length correlation with the mixing length data obtained in this program. With the exception of the W_P/W_{P_D}=50% data (i.e. large correlation parameter) the data obtained in this program compare well with the previously developed correlation. At the W_P/W_{P_D} = 50% test conditions, the ejector nozzles may have experienced flow separation. Test instrumentation did not permit resolution of this question.

As a summary presentation, Figure 63 contains the following:

- The modified hypermixing ejector mixing length data obtained in this program.
- Marquardt's previously derived mixer length correlation.
- Mixer length data from several previous Marquardt test programs. Data are shown for one, four, eight, and thirty-six primary nozzle ejectors. In addition, data for the annular ejector* tested under Contract AF33(657)-12146 are presented.

Mixer efficiency is a measure of total pressure and momentum losses in the ejector nozzle/mixer. In order to determine the mixing efficiencies achieved in these tests, actual test conditions were used as Marquardt ejector ramjet performance computer program input, and mixer efficiency was parametrically varied until a a pumping total pressure rise that matched the experimental data was achieved. Typical results for the annular nozzle are illustrated in Figure 64. These data indicate an achieved mixing efficiency value between 98.5 and 99%. These values are consistent with previous experimental data and verify the 98.5% assumption used to predict ejector ramjet performance.

Similar mixer efficiency data for the initial hypermixing configuration are shown in Figure 65. The data again fall between 98.5 and 99%. Finally, data for the modified hypermixing ejector design are presented in Figure 66. Although some difference in shape of this curve with the two previous curves exists, the general result is that the mixing efficiency is about 99%. The conclusion then is that use of the hypermixing nozzle to shorten the length required for complete mixing does not introduce additional pressure losses into the system. It is probable that the reduced length results in reduced friction losses in the mixer, thus offsetting the mixing/shock losses incurred with the hypermixing ejector design.

* $\frac{D_{\text{ejector nozzle}}}{D_{\text{mixer}}} = 0.63$ (See Section VII of this report.)

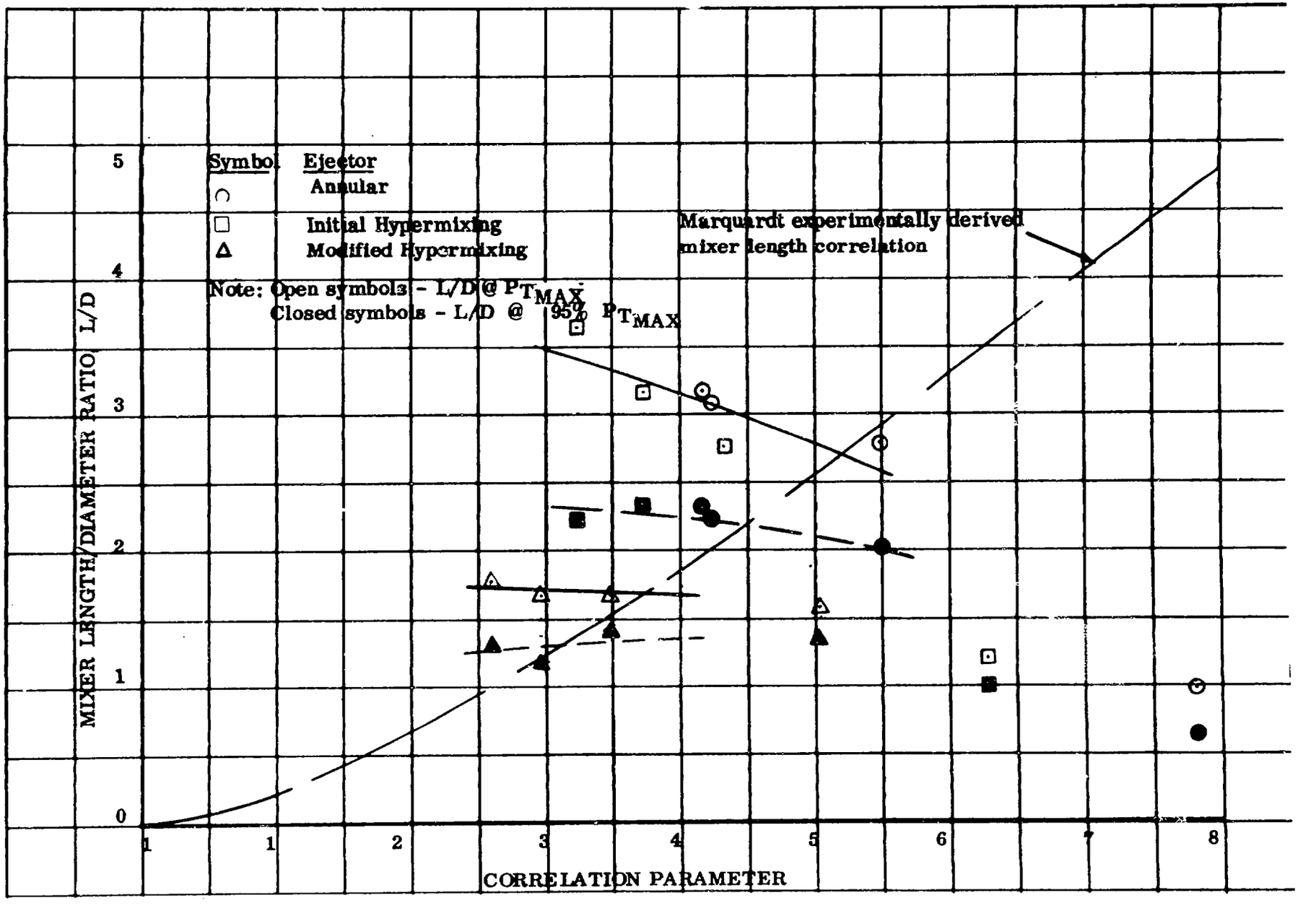

Figure 62. Mixer Length Comparison

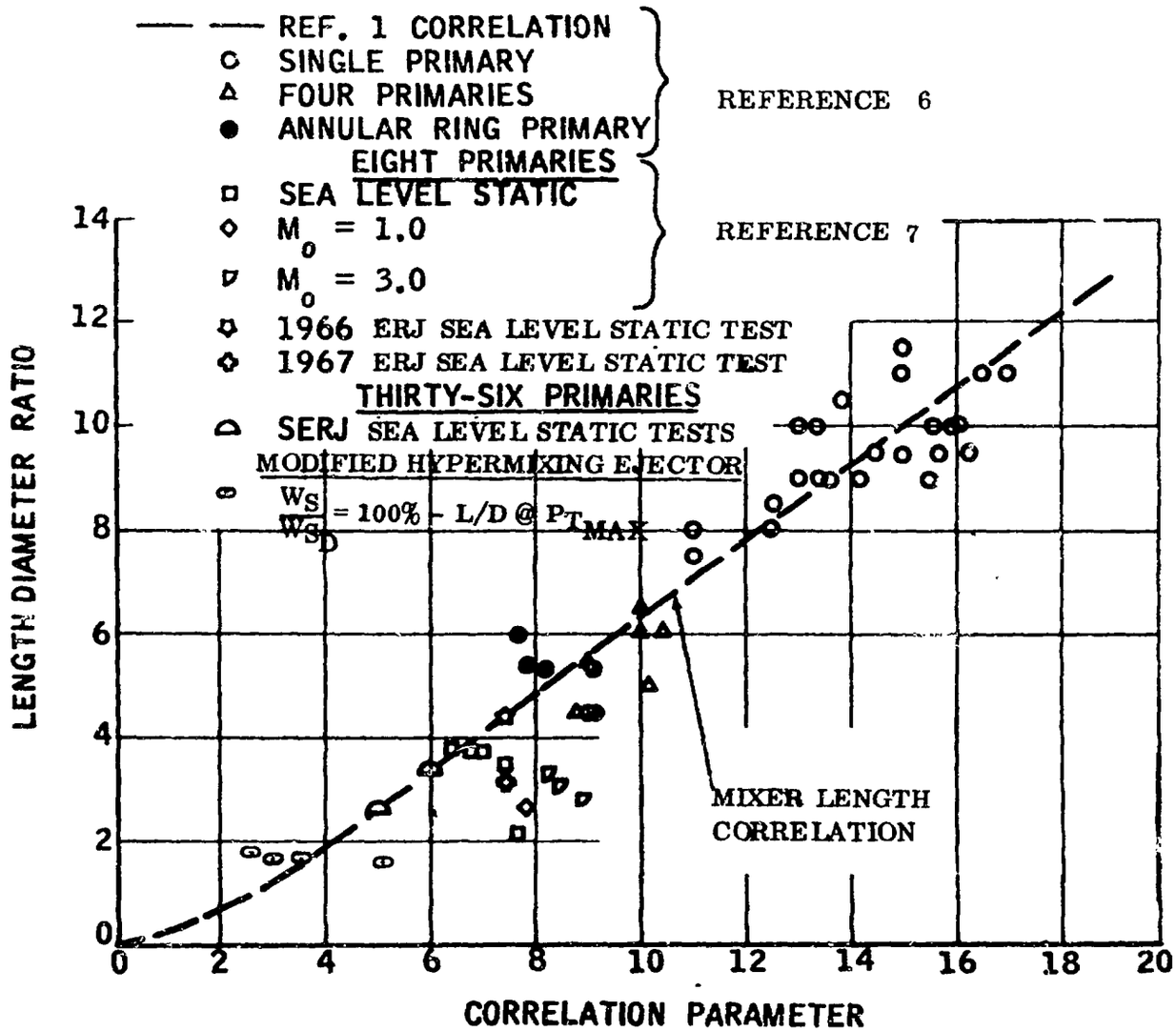

Figure 63. Required Mixer Length Data Compilation and Correlation

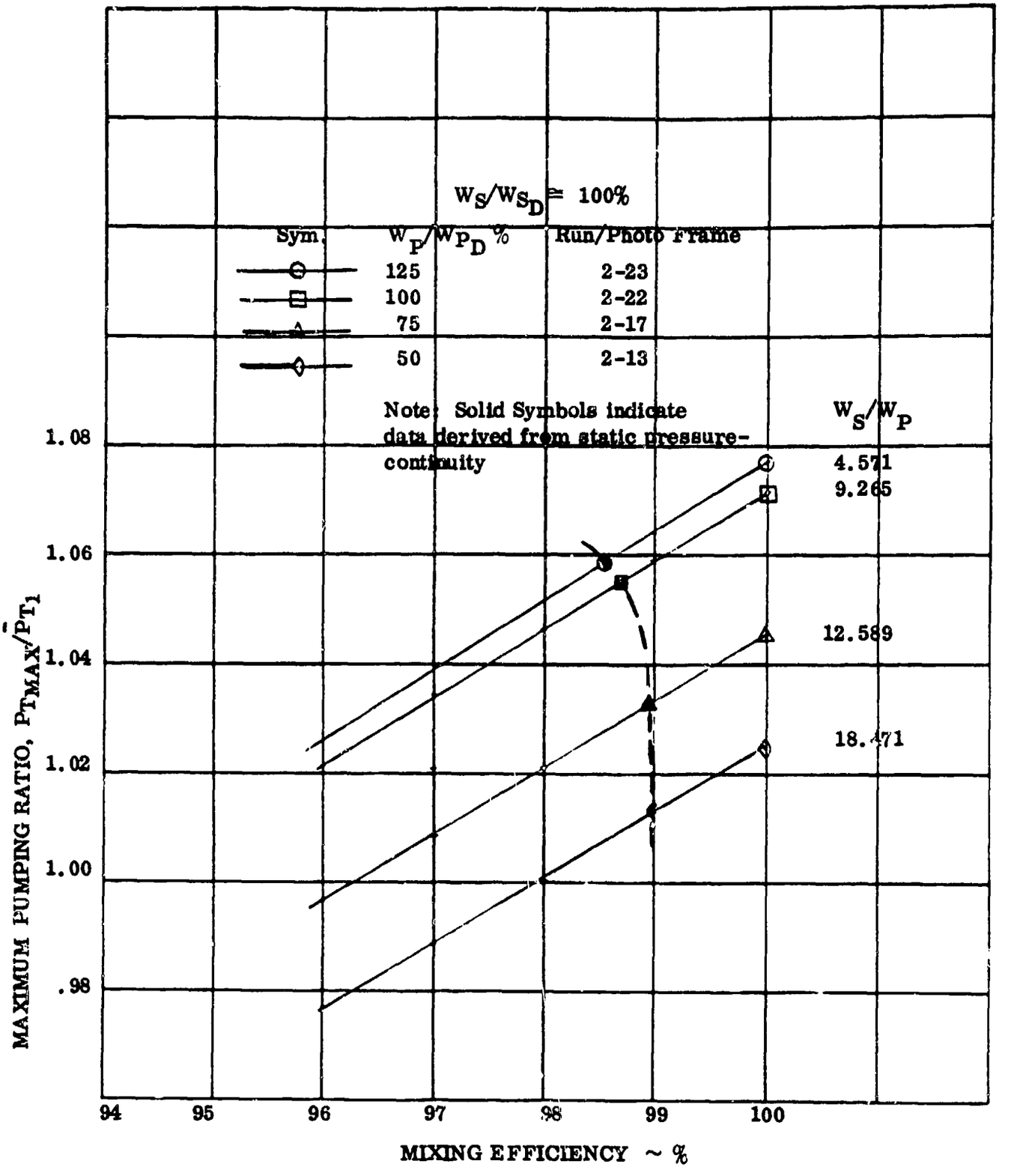

Figure 64. Mixing Efficiency-Annular Ejector

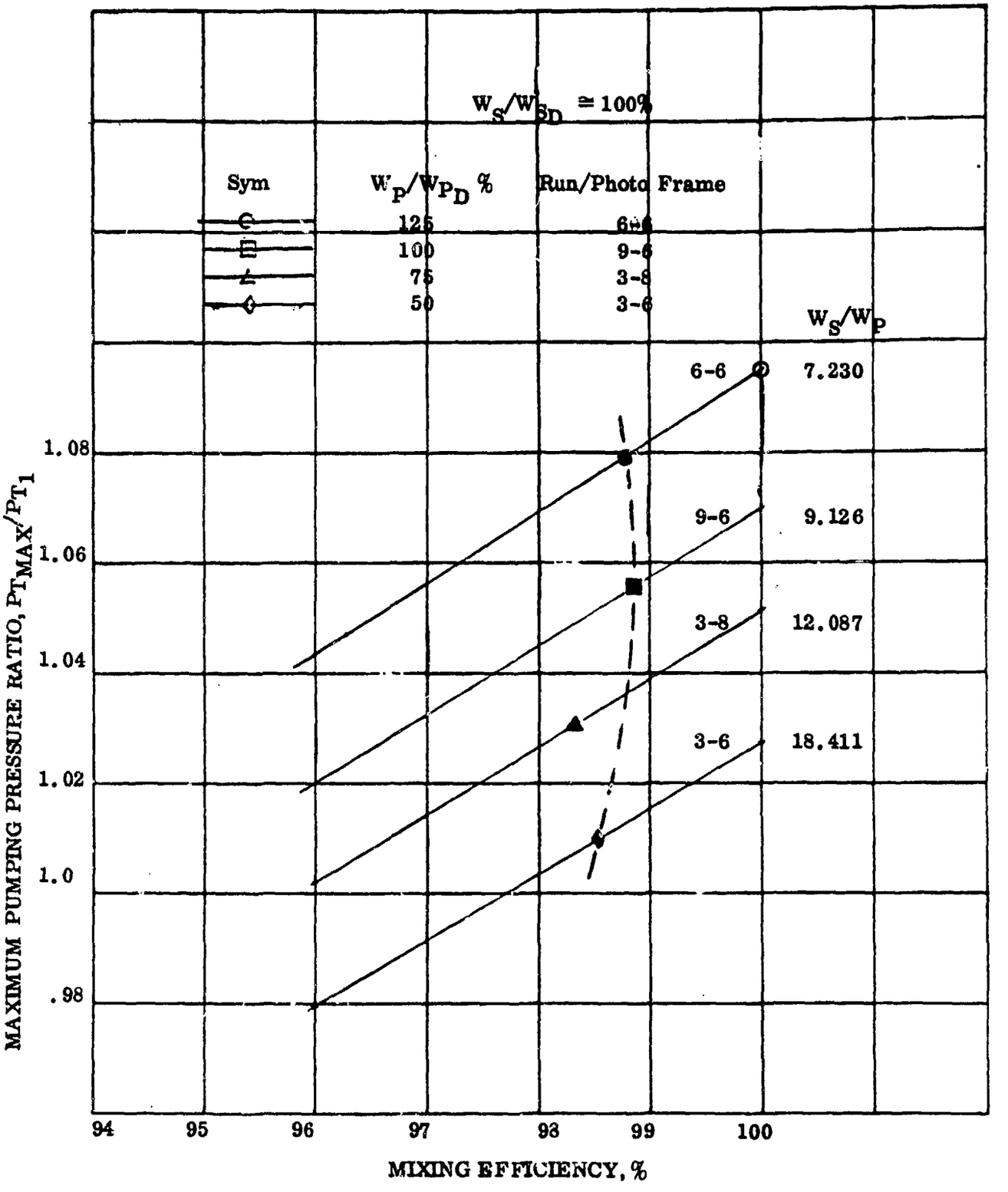

Figure 65. Mixing Efficiency-Initial Hypermixing Ejector

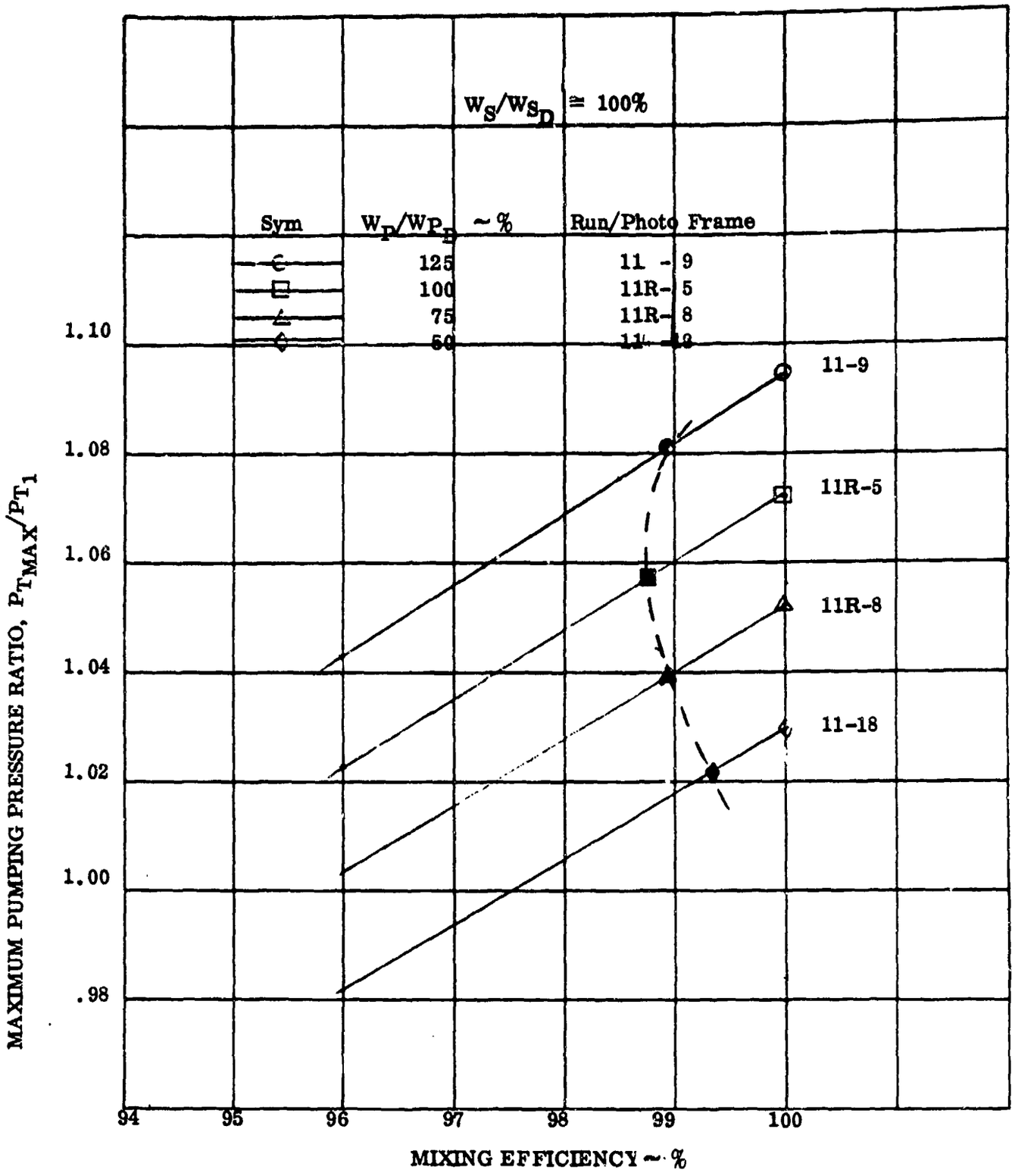

Figure 66. Mixing Efficiency-Modified Hypermixing Ejector

Finally, Figure 67 indicates the mixing efficiency for a large range of secondary flow rates with constant primary flow for the initial hypermixing configuration. Two distinct curves are seen, where one produces the familiar 98.5-99% mixing efficiency value, while the second provides mixing efficiencies of greater than 99.5%. This second curve applies to the low mixer inlet Mach number data discussed previously, resulting from use of a small exit area nozzle. This result indicates that mixer inlet Mach number, M_1, should be low for high mixing efficiency, while previous data (Figure 60) indicate a lower pumping pressure ratio as M_1 is decreased.

Total pressure profiles for the annular, initial, and modified hypermixing ejector are compared in Figures 68, 69, and 70. In these curves, the primary and secondary flow rates were nominal design values. The conclusions drawn from study of these curves support the previously presented test analyses and, therefore, are not reported here.

Appendix C of this report presents additional total pressure profile data. In addition, this appendix also presents carbon dioxide profile data. The CO_2 profile data support the test analyses/conclusions reported above and therefore are not presented in the main body of this report.

It has been established from the achievement of maximum static and total pressure rise in the mixer that the required mixing length for the modified hypermixing ejector occurs between axial stations 13 and 15. At these stations, the flow is not uniform. This is illustrated in Figures 71 and 72. In Figure 71, the CO_2 distortion factor f' is plotted versus mixer axial station, where "f" is defined by

$$f' = \frac{f_{max} - f_{min}}{\bar{f}}$$

A given quantity of CO_2 was injected through the primary nozzle. If the flow were completely mixed, the weight percentage of CO_2 would be constant at a value

$$\bar{f} \equiv \frac{W_{CO_2}}{W_P + W_S}$$

and f' would be equal to zero. Values of f' greater than zero then are a measure of nonuniformity of the injected CO_2 across the mixer. In Figure 71, f' starts out at a high value at the ejector nozzle exit, indicating nonmixed flow, and then decreases almost asymtotically with mixer length.

Figure 72 presents similar total pressure distortion data as a function of mixer length. Here the distortion factor was defined as

$$\frac{P_{T_{max}} - P_{T_{min}}}{P_{T_{ave}}}$$

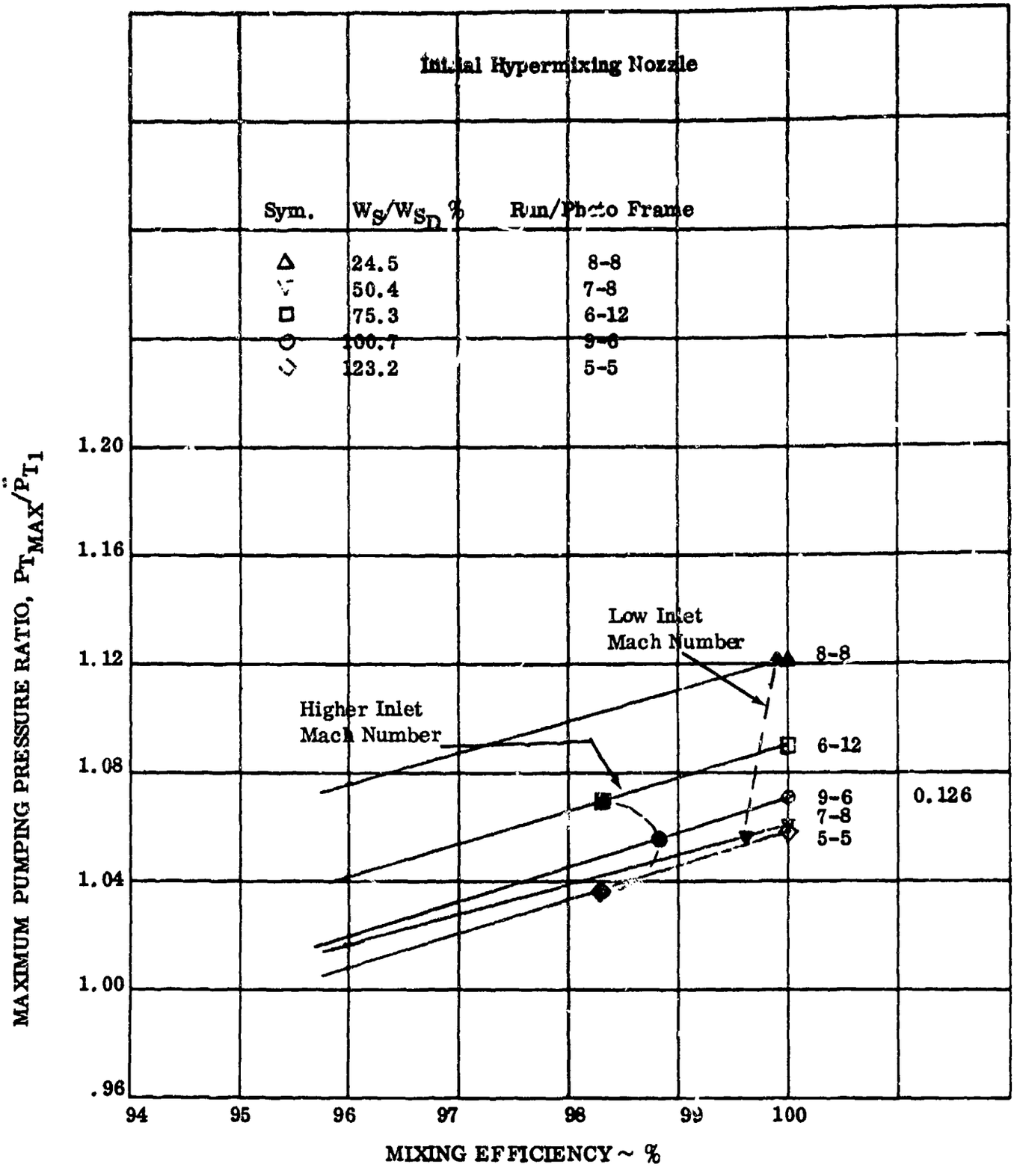

Figure 67. Mixing Efficiency, W_P/W_{P_D} = 100%

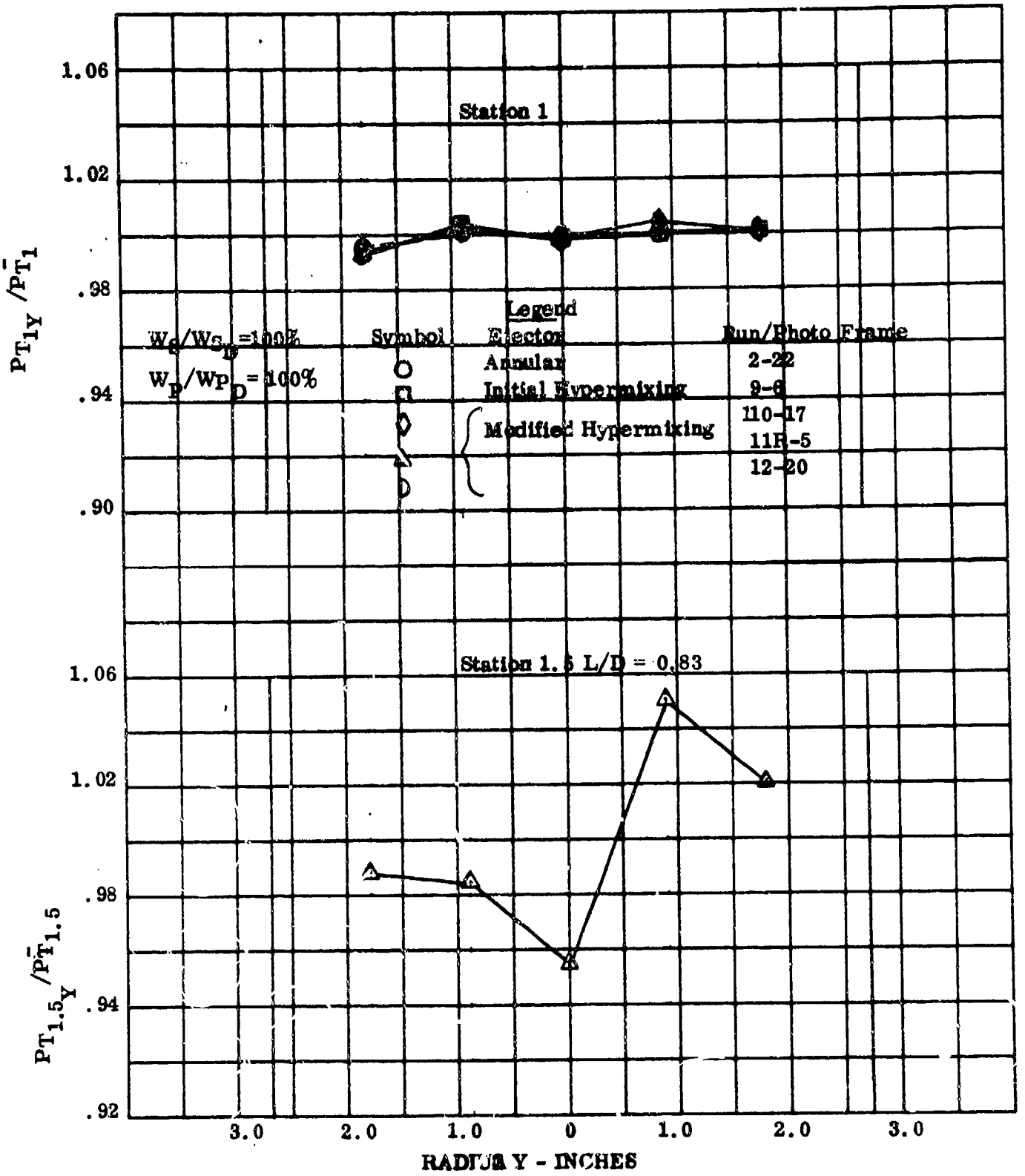

Figure 68. Comparison of Total Pressure Profiles Mixer Station 1 and 1.5

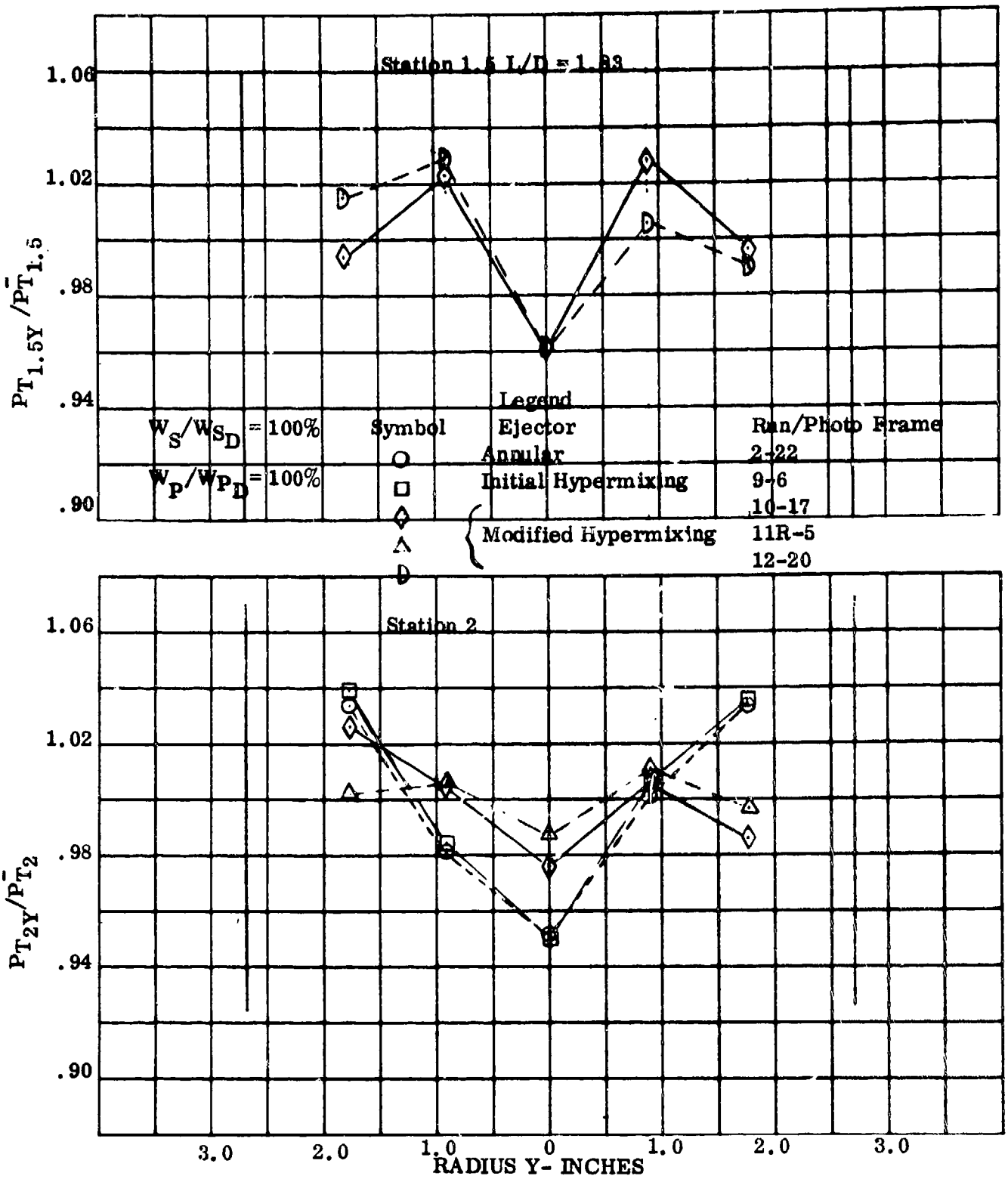

Figure 69. Comparison of Total Pressure Profiles Mixer Station 1.5 and 2

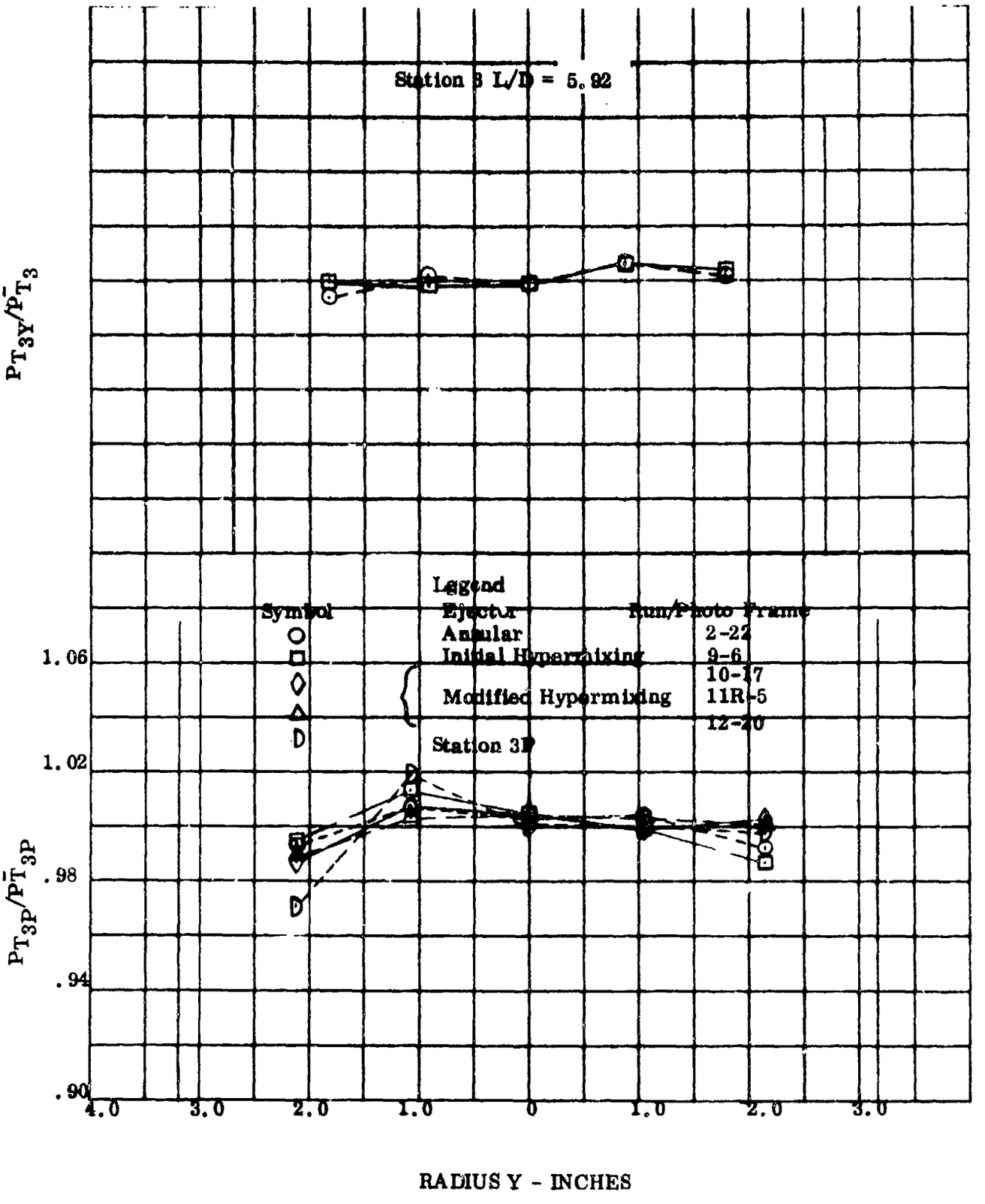

Figure 70. Comparison of Total Pressure Profiles Mixer Station 3 and 3P

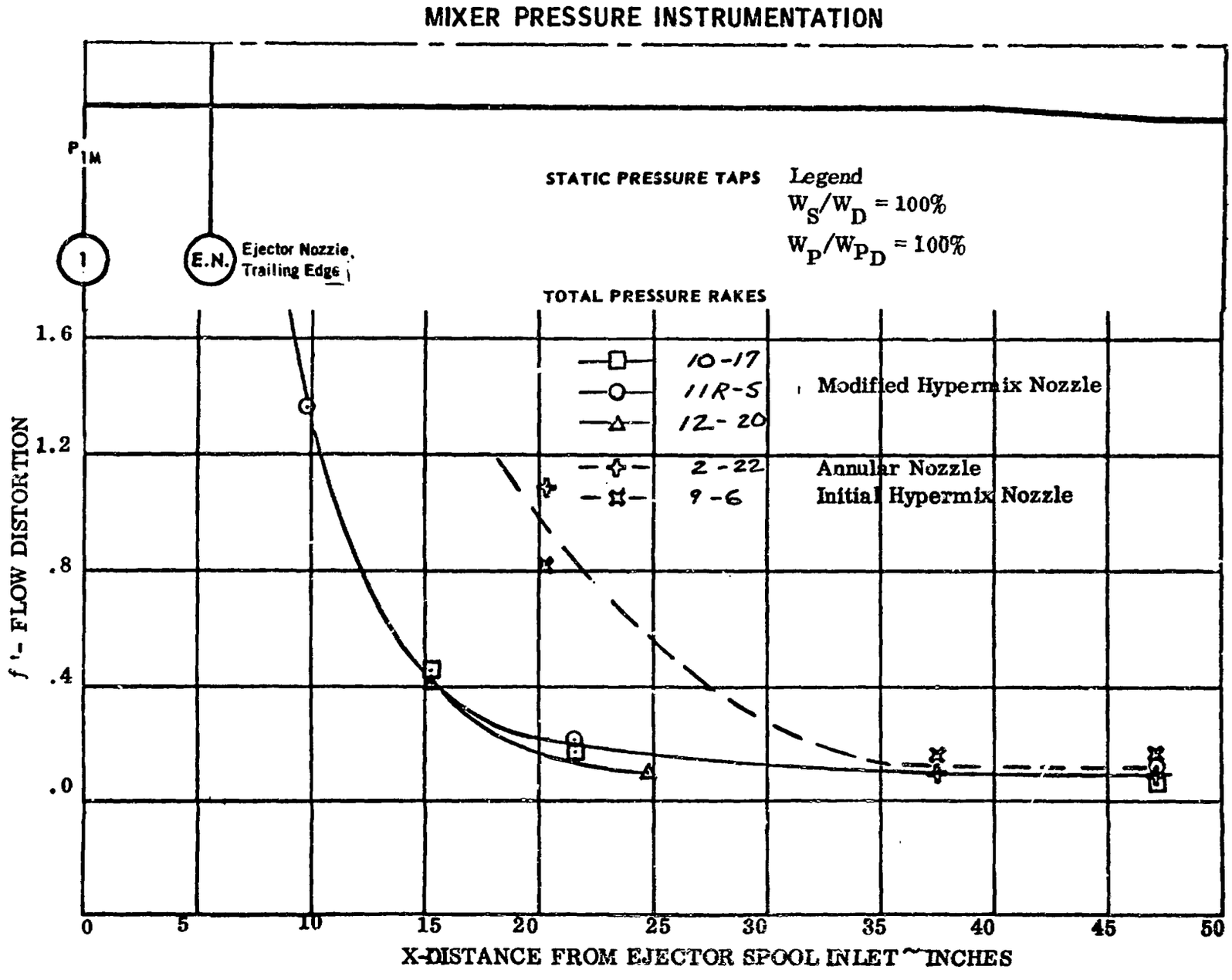

Figure 71. Axial Distribution of Carbon Dioxide Concentration

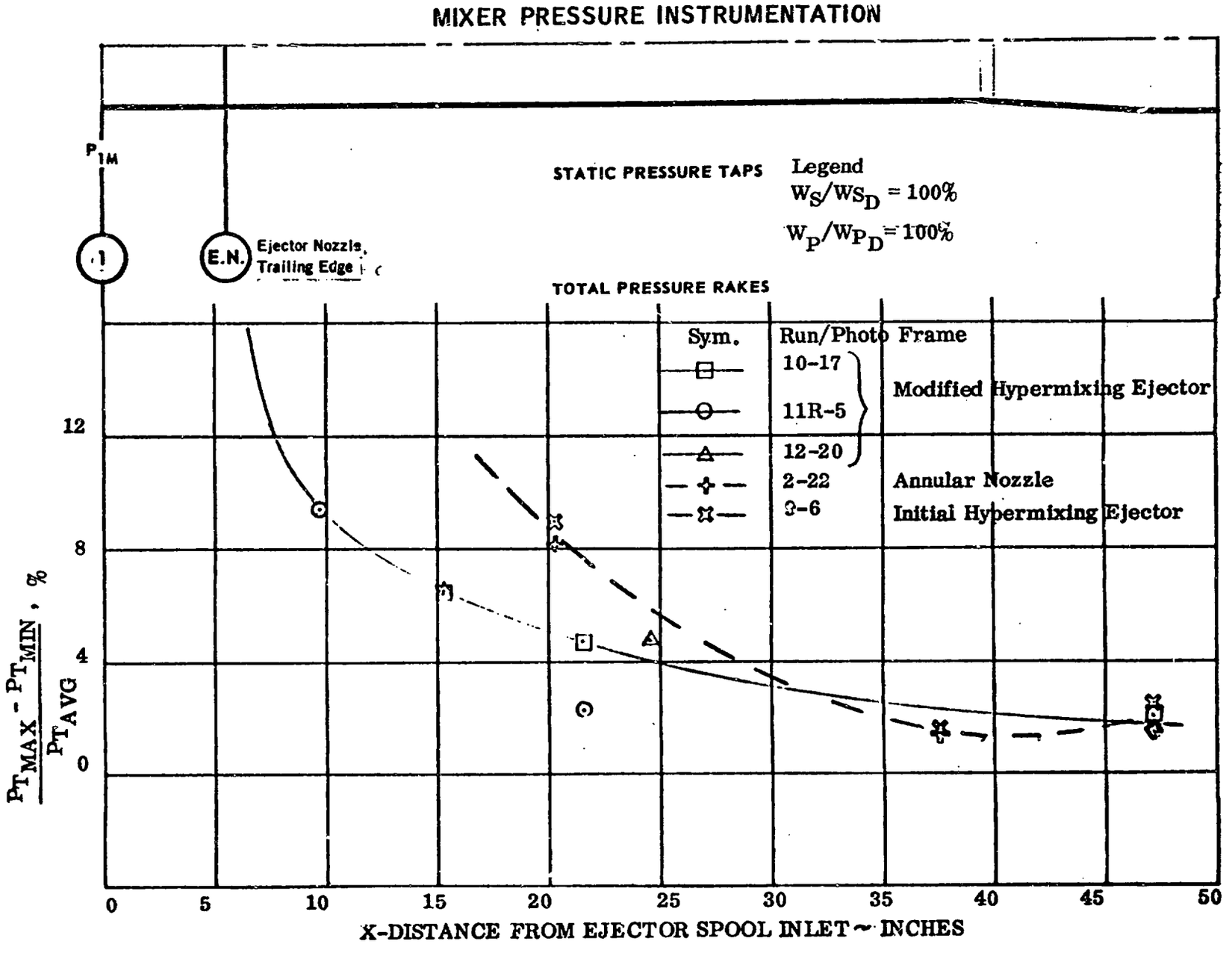

Figure 72. Axial Distribution of Total Pressure Distortion

The shape of this curve is similar to that of f', and serves to illustrate that the length required for complete mixing is a function of the parameter chosen, i.e., static pressure, total pressure, total pressure distortion, etc. For the purpose of ejector ramjet engine design, the length required for maximum total pressure rise is the most meaningful parameter, inasmuch as engine performance and efficiency increase with pressure while not being particularly sensitive to flow distortion. The length provided by the diffuser will provide additional mixing, thus reducing total pressure distortion and f', and at the same time increasing combustor static pressure.

A sample indication of diffuser performance is given in Figure 73. Ideal and measured total and static pressures across the test diffuser are shown for design airflow and primary flow values. The total pressure recovery across the diffuser was 0.991 compared to the ideal 1.00. For a diffuser entrance Mach number of 0.361, the diffuser efficiency is 89%. This efficiency was established by using the results of Figure 74. A diffuser efficiency of 90% was used to estimate ejector ramjet performance. Based upon this limited analysis, the 90% diffuser efficiency value appears to be warranted.

The foregoing results indicate significantly improved mixing with the modified hypermixing ejector design. Shadowgraphs were taken of the flow at the exit of the modified ejector nozzle dumping into ambient air over a range of pressure ratios. These shadowgraphs are presented in Figures 75 through 80. In comparison to the shadowgraphs for the initial hypermixing ejector design (Figures 42 through 46), the modified design provided distinct radial flow patterns which by alternating the direction in and out provided the necessary vorticity to increase rapidly the rate of mixing.

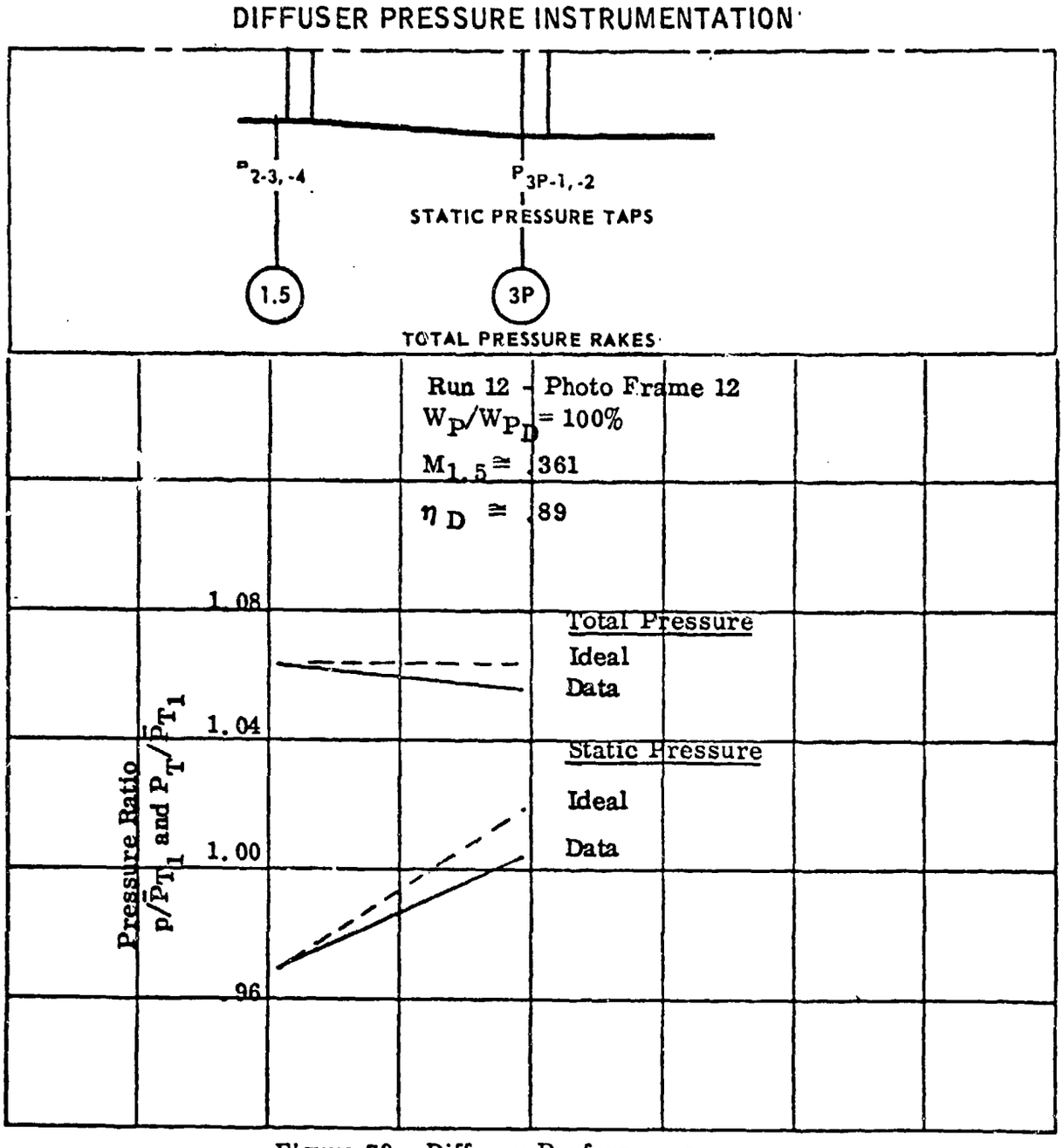

Figure 73. Diffuser Performance
W_S/W_{S_D} = 100%

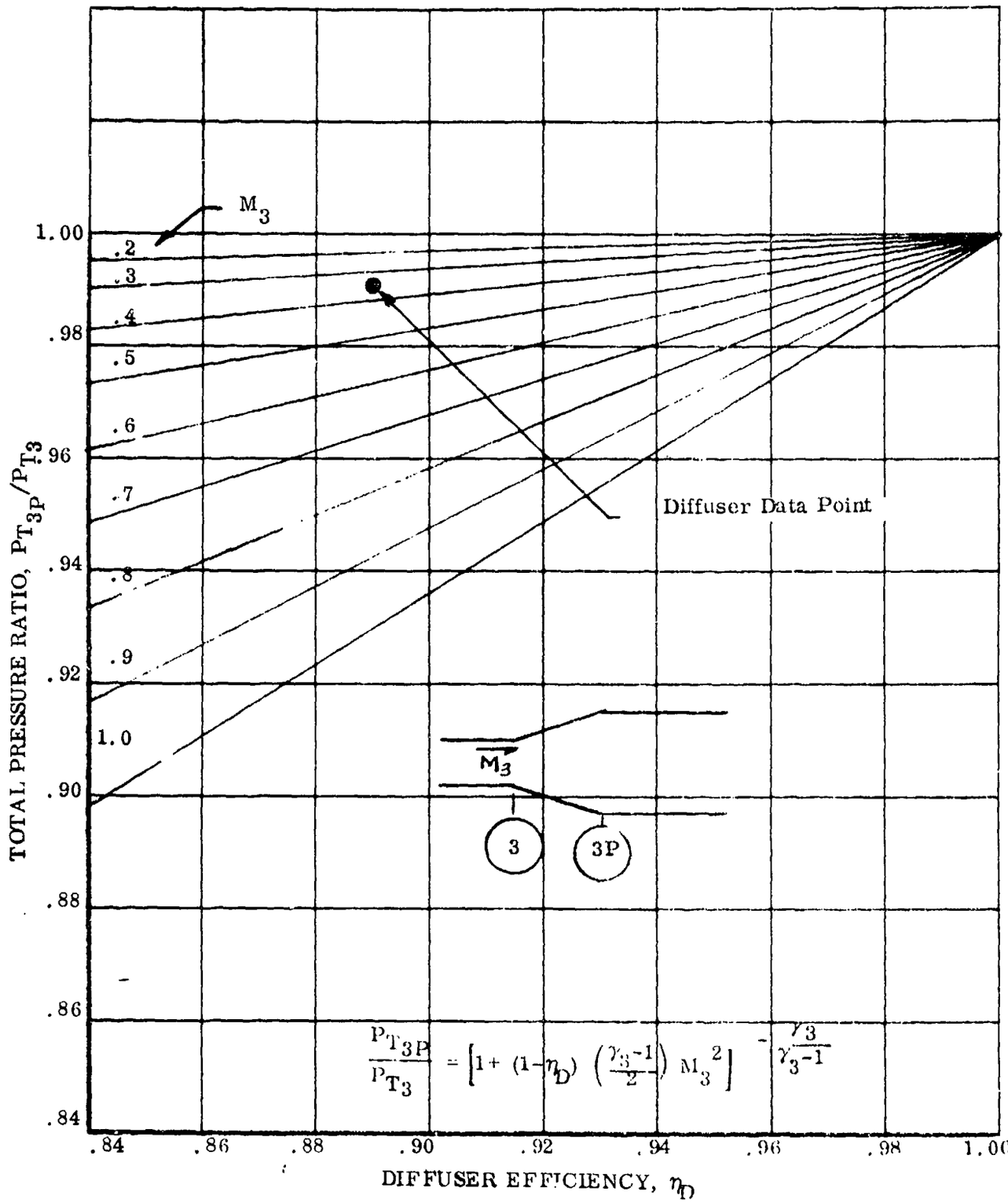

Figure 74. Diffuser Efficiency Definition

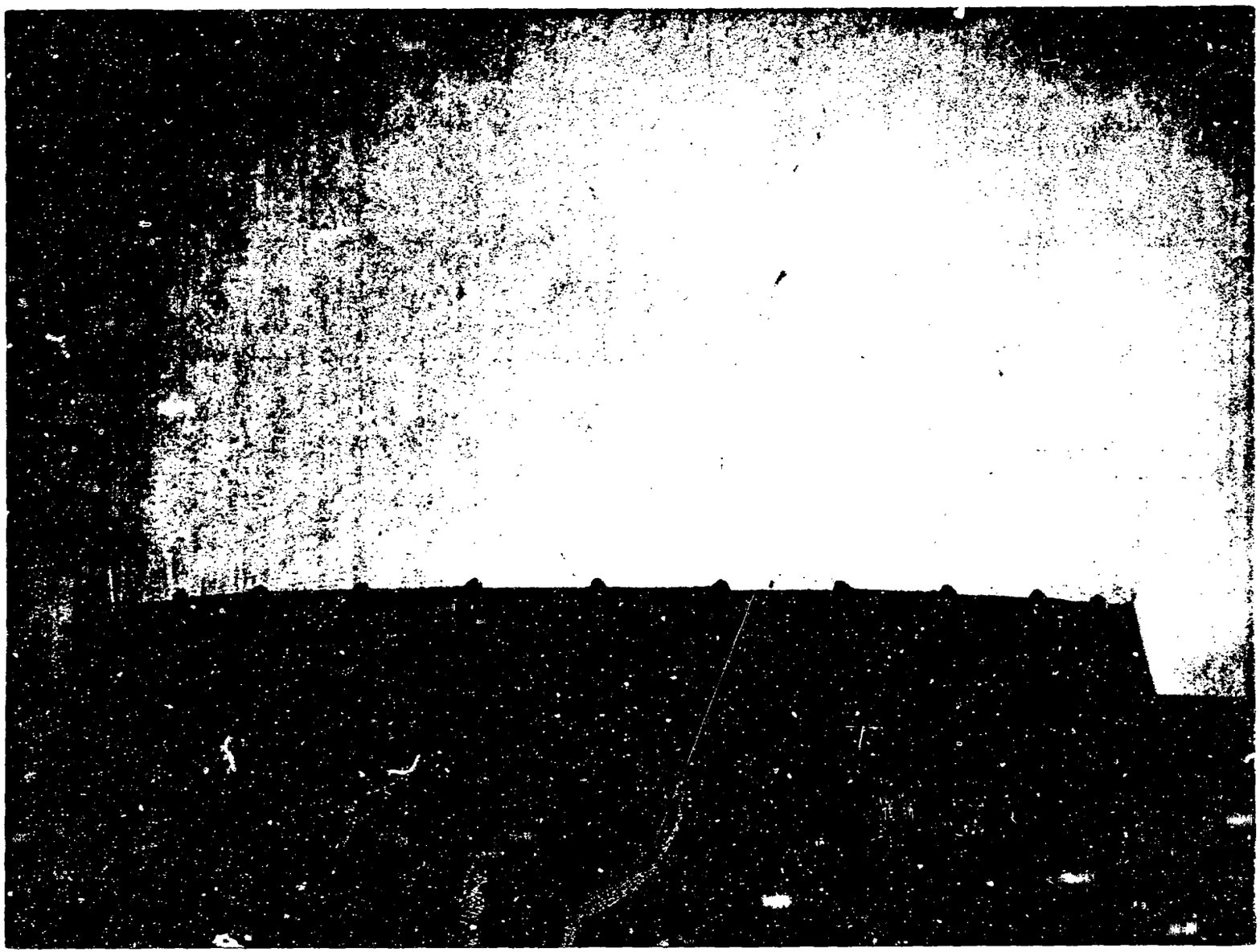

Figure 75. Modified Hypermixing Ejector Test Shadowgraph
Ejector Pressure Ratio = 2.6

Figure 76. Modified Hypermixing Ejector Test Shadowgraph
Ejector Pressure Ratio = 5.2

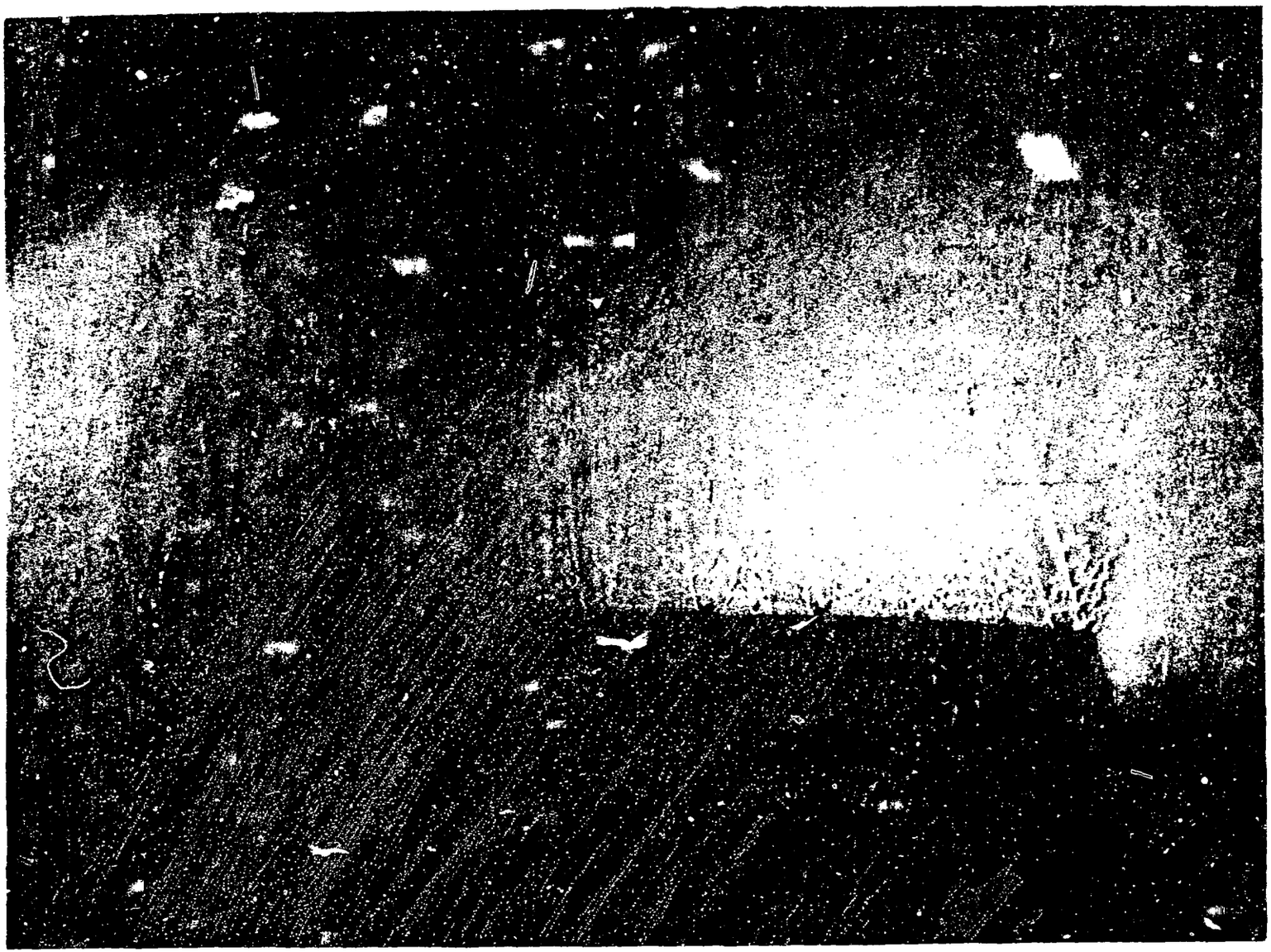

Figure 77. Modified Hypermixing Ejector Test Shadowgraph
Ejector Pressure Ratio = 7.3

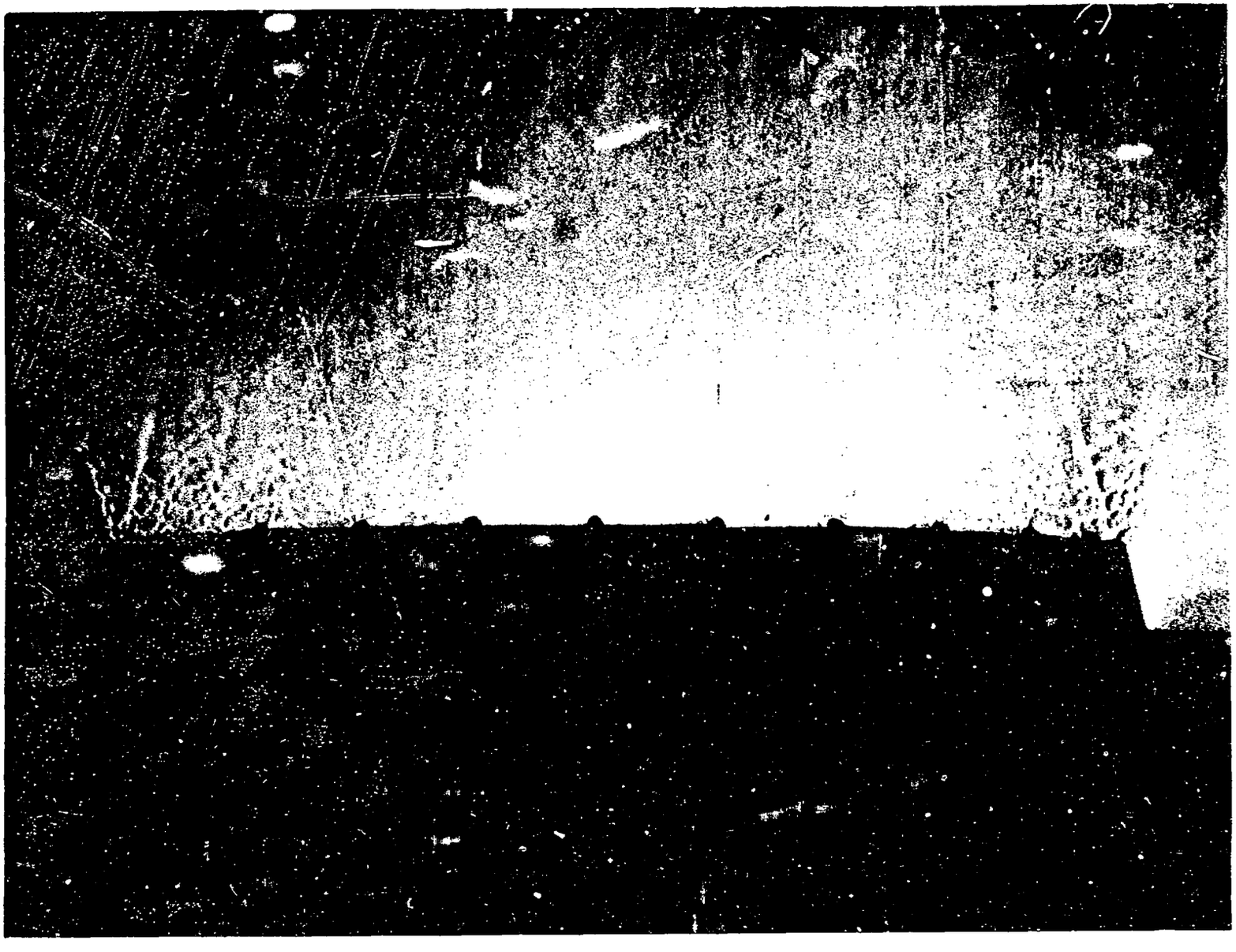

Figure 78. Modified Hypermixing Ejector Test Shadowgraph
Ejector Pressure Ratio = 9.7

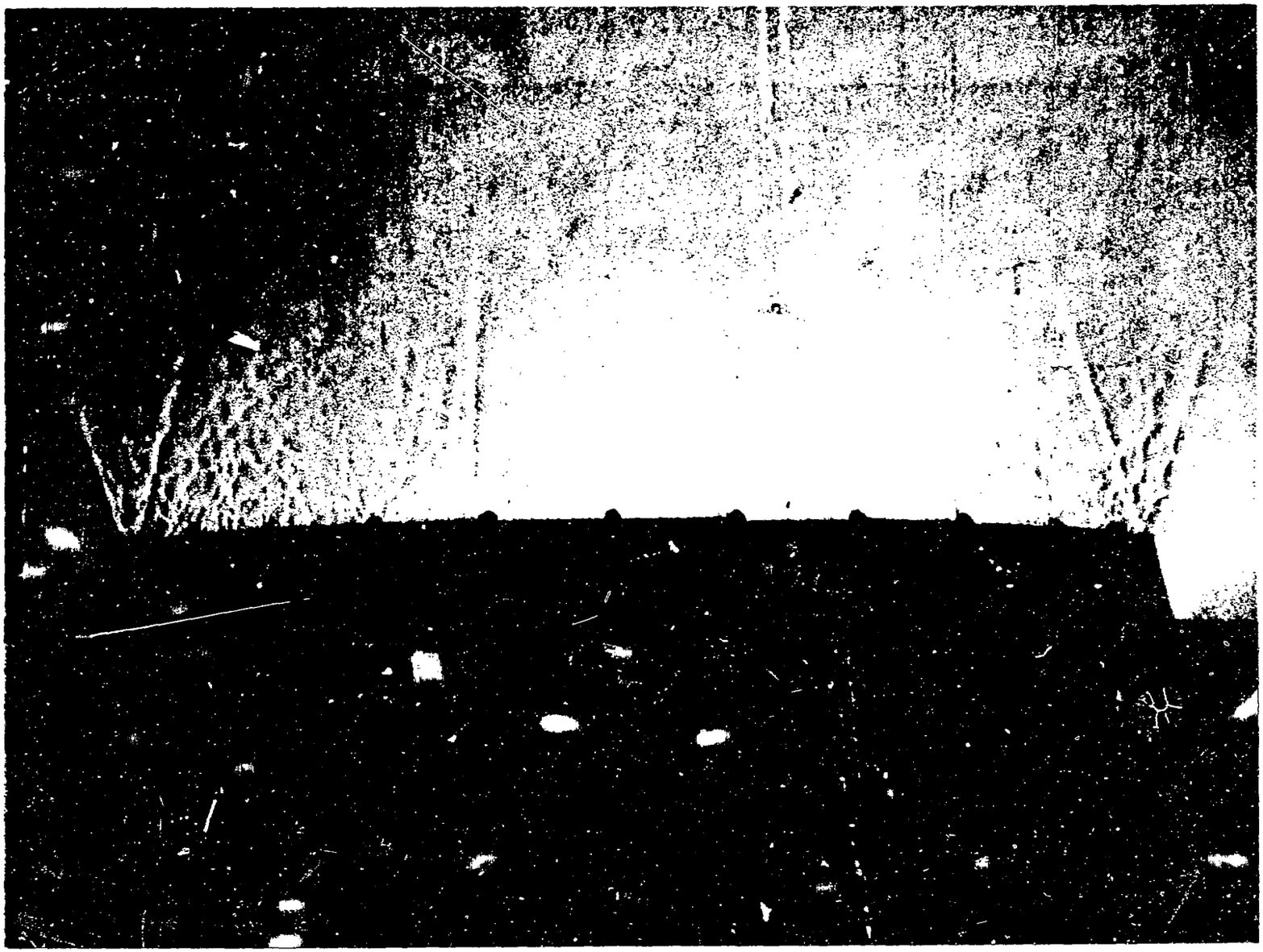

Figure 79. Modified Hypermixing Ejector Test Shadowgraph
Ejector Pressure Ratio = 12.0

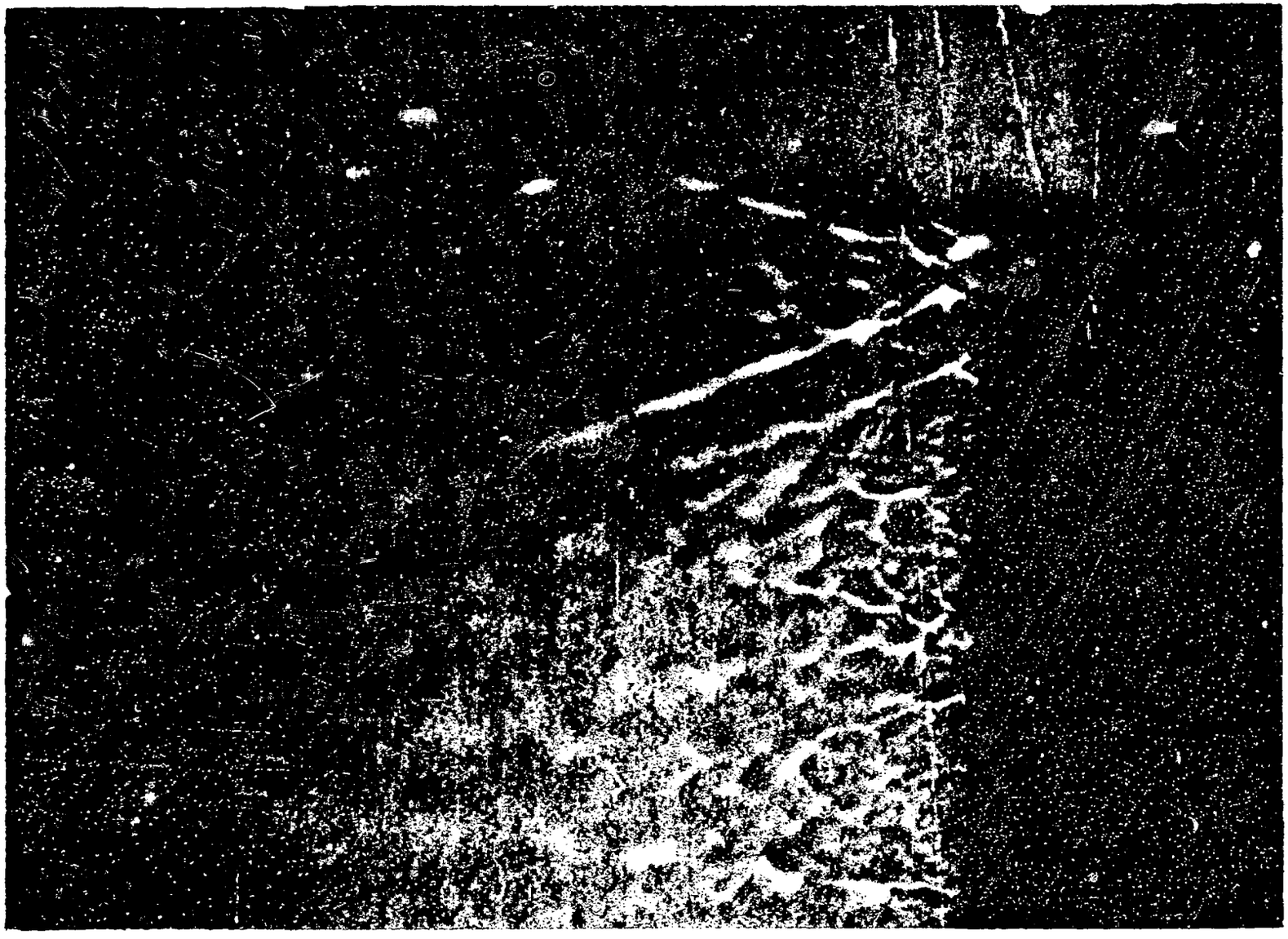

Figure 80. Modified Hypermixing Ejector Test Shadowgraph
Ejector Pressure Ratio = 12.0 (Enlargement of Figure 79)

SECTION XII

CONCLUSIONS & RECOMMENDATIONS

Six fundamental conclusions were drawn during conduct of this program. These conclusions are presented below.

1. The specified engine operating envelope was Mach 0.70 to 0.90 from sea level to 30000 feet altitude. The engine design point was taken as Mach 0.75 @ 20000 feet altitude. Three ejector ramjet engine cycle variations were evaluated at the design point : 1) Fuel addition - mix/diffuse/burn; 2) Fuel addition - simultaneous/mix burn and 3) Oxidizer addition. The fuel addition-mix/duffuse/burn cycle was clearly shown to be superior. The selected fuel was unsymmetrical dimethylhydrazine (UDMH).

2. A preliminary design of the fuel addition-mix/diffuse/burn engine was established by using realistic component efficiencies and UDMH thermo chemical properties. Engine performance was estimated. At the engine design point, the ejector ramjet produced about twice the thrust of a conventional hydrocarbon fueled ramjet with a small penalty in specific fuel consumption. It is believed this engine can be developed with a suitable program.

3. The initial hypermixing ejector design developed in this program was annular in planform, the ejector nozzle centerline was parallel to the mixer centerline and the supersonic exit nozzle was scarfed in alternating nozzle segments to create the desired vorticity. Tests of an annular ejector and the hypermixing ejector showed little, if any,difference in performance. Performance was measured in terms of mixing length required for full mixing and mixing efficiency. Mixing efficiency is a strong indicator of the ejector nozzle thrust coefficient (i.e., nozzle efficiency).

4. The initial hypermixing ejector configuration was modified to incline the ejector nozzle centerline 15° to the horizontal mixer centerline. All other ejector design characteristics were unchanged. The mixing performance of this ejector was outstanding. The length to mix fully was approximately 50% that of the annular and initial hypermixing designs. At the ejector design point, full mixing (maximum mixer total pressure) was achieved in 1.7 duct diameters. To achieve 95% of the maximum mixer total pressure required 1.3 duct diameters. The mixing efficiency of this ejector configuration was equal to that of the annular and initial hypermixing designs, i.e., 98.5 to 99%.

5. The required mixing length for the modified ejector design correlated well with previous Marquardt ejector/ejector ramjet test data. As pointed out above, at the ejector design point, full mixing was achieved in 1.7 duct diameters.

It is interesting to note that, while maintaining ejector geometry/test conditions, approximately sixty individual planar nozzles is required to achieve the same mixing length. This relationship was developed from prior Marquardt test experience.

6. The use of hypermixing ejector technology has demonstrated a short, light weight, and relatively simple ejector/mixer which meets the requirements of an attractive ejector ramjet engine.

Two recommendations are made for future work.

1. The modified hypermixing ejector performed quite well, but this design was not optimized. Further experimental work should be undertaken to refine/optimize this ejector design concept for supersonic primary exit conditions.

2. Additional applications of this ejector technology should be considered. Two specific examples are: 1) Ducted Rocket solid fuel gas generator primary nozzle(s) and 2) Boundary layer energized large angle subsonic diffusers.

REFERENCES

1. Kit, Boris and Evered, Douglas, S., Rocket Propellant Handbook, The Mac Millan Company, 1960

2. Propellant Performance Data, Callery Chemical Company, 1961.

3. Pardee', Robert P., "A Preliminary Study of Unsymmetrical Dimethylhydrazine as a Monopropellant," Jet Propulsion Laboratory, Progress Report No. 30-11, 23 February 1959.

4. Henry, John R., "Design of Power Plant Installations-Pressure Loss Characteristics of Duct Components," NACA, ARR No. 24F26, 1944.

5. Eastlake, Charles N., Jr., "The Macroscopic Characteristics of Some Subsonic Nozzles and the Three-Dimensional Turbulent Jets They Produce," Air Force Systems Command/Aerospace Research Laboratories, Report ARL71-0058, AD728676, March 1971.

6. Totten, J.K. and Campbell, J.R., Final Summary Technical Report on the Calendar Year 1963 Ramjet Technology Program, Volume 2, Jet Compressors and Ejector Ramjet Investigations, Marquardt Report 25, 116, April 1964.

7. Flornes, B.J., Stroup, K.E.,"1964 Advanced Ramjet Concepts Program, Volume I, Advanced Jet Compression Engine Concepts, AFAPL-TR-65-32, May 1965.

~~UNCLASSIFIED~~

~~CONFIDENTIAL~~

APPENDIX A

PROGRESS REPORT NO. 30-1

A PRELIMINARY STUDY OF UNSYMMETRICAL DIMETHYLHYDRAZINE AS A MONOPROPELLANT

ROBERT P. PARDEE

JET PROPULSION LABORATORY
CALIFORNIA INSTITUTE OF TECHNOLOGY
PASADENA, CALIFORNIA
FEBRUARY 23, 1959

~~CONFIDENTIAL~~

National Aeronautics and Space Administration
Contract No. NASw-6

PROGRESS REPORT No. 30-1

A PRELIMINARY STUDY OF UNSYMMETRICAL DIMETHYLHYDRAZINE AS A MONOPROPELLANT

Robert P. Pardee

Donald R. Bartz, *Chief*
Power Plant Research Section

Copy No._____

JET PROPULSION LABORATORY
California Institute of Technology
Pasadena, California
February 23, 1959

PREFACE

Portions of the following report were originated under studies conducted for the Department of Army Ordnance Corps under Contract No. DA-04-495-Ord 18. Such studies are now conducted for the National Aeronautics and Space Administration under Contract No. NASw-6.

CONFIDENTIAL

This document contains information affecting the national defense of the United States, within the meaning of the Espionage Laws, Title 18, U.S.C., Sections 793 and 794, the transmission or revelation of which in any manner to an unauthorized person is prohibited by law.

CONTENTS

TABLES

FIGURES

ABSTRACT

A summary is presented of the results of an experimental investigation to determine the operating characteristics of unsymmetrical dimethylhydrazine (UDMH) as a monopropellant. Smooth, reliable, thermal decomposition was obtained with a chamber having a characteristic length (L^*) of 5000 in. At this L^*, tests were made over a chamber-pressure range of 50 to 600 psia. The characteristic velocity (c^*) at 300-psia chamber pressure was found to be approximately 3200 ft/sec. Also investigated were: (1) the catalytic decomposition of mixtures of UDMH and hydrazine, (2) the thermal decomposition of UDMH at L^* values of 2115 to 8000 in., (3) the thermal decomposition of UDMH utilizing regeneratively preheated fuel, and (4) the thermal decomposition of UDMH utilizing supplementally preheated fuel. Testing under this latter condition permitted operation at L^* values as low as 386 in.

Exhaust gases were analyzed, and an attempt was made to determine quantitatively the carbon content of the exhaust products.

I. INTRODUCTION[1]

Interest in unsymmetrical dimethylhydrazine as a rocket fuel has increased quite rapidly since it was first produced in reasonable quantities a few years ago. Undoubtedly, the greatest incentive for detailed evaluation of this compound has been the rise to national importance of storable liquid-propellant systems. One of the most interesting aspects in the utilization of UDMH is that, in addition to possessing reasonably good theoretical bipropellant performance (Ref. 1), it is thermochemically unstable, which should permit its use as a monopropellant.

The freezing point of UDMH is −71 F (compared with 34.5 F for anhydrous hydrazine), and it was principally this freezing-point advantage which led to several previous investigations of the desirability of UDMH as a monopropellant. The thermal stability of UDMH

[1] The experimental program described in this Report was completed in July 1957. Until the present time, however, publication of the results was restricted to internal use.

was tested at the Metalectro Corporation (Ref. 1) by exposing its vapor to a heated wire: there was no audible or visible reaction even at white heat. Hydrazine vapors under similar conditions ignited rather violently. The Naval Ordnance Test Station (Ref. 2) found that, after a duration of one second, UDMH vapor at 10 $^{-3}$ mol liter in nitrogen was partially decomposed at 450 C and completely decomposed at 500°C.

Aerojet-General Corporation (Ref. 3) states that UDMH heated slowly in a stainless-steel bomb does not decompose explosively below 675°F (357°C).

Griffin (Ref. 4) of Olin Mathieson Chemical Corporation reported on an attempt to operate UDMH as a monofuel gas-generant in a small-volume, large-L' reaction chamber. This attempt was unsuccessful, and it was concluded that use of UDMH as a monopropellant was doubtful. Griffin also reported some calculated performance values for UDMH, assuming that it would operate as a monopropellant: I_s, 180 sec and T_c, 2257 F. This flame temperature is considerably higher than desirable for most monopropellant gas-generation applications. This potential shortcoming of UDMH gave Griffin further doubts as to its applicability as a monopropellant gas-generant.

In an experiment at the Jet Propulsion Laboratory, Grant (Ref. 1) reported on a typical monopropellant-hydrazine catalytic decomposition chamber operating on a mixture of UDMH with 10 wt % hydrazine for about 60 sec. The reaction was initiated by first operating the chamber on pure hydrazine; after 10 sec, the mixture was introduced. Approximately 30 attempts made to duplicate this experiment were without success.

II. EXPERIMENTAL PROGRAM

With the background described in Sec. I, an experimental program was initiated. The program had the following objectives: (1) Determine whether or not UDMH could be made to operate reliably as a monopropellant, and if so, (2) investigate the operating characteristics of UDMH under various conditions.

A. Monopropellant Tests with Hydrazine–UDMH Mixtures

In as much as the results of the previous investigators had indicated the potential difficulty of operating UDMH as a monopropellant, a series of experiments was carried out to determine the extent to which hydrazine could be diluted with UDMH and still support decomposition in a typical hydrazine-gas generator. Grant had already shown (Ref. 4) that, under conditions suitable for hydrazine, a mixture containing 90% (by wt) UDMH appeared to be beyond the limit of reproducible decomposition. A mixture containing a concentration of 93% UDMH is required in order to obtain a −40°F freezing point (Fig. 1).

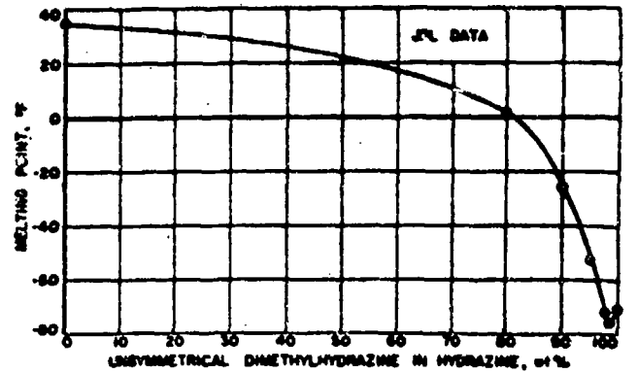

Fig. 1. Melting Points of the UDMH–Hydrazine System

The subject experiments utilized the gas generator shown in Fig. 2; the internal construction of the generator is shown in Fig. 3. The chamber (8 in. long × 1.6-in. ID with liner) was filled with hydrazine-decomposition catalyst,* H-A-3 or H-7, which was electrically preheated to from 1000 to 1600°F. The fuel mixture was sprayed on top of the catalyst bed by means of a hollow-cone spray injector. The L^* was 1038 in.; chamber-pressure and fuel flow-rate measurements provided data from which c^* values were calculated. Chamber pressure was maintained at approximately 300 psia. Experimental results under these conditions are shown in the left-hand portion of Fig. 4. As this series of tests progressed, it became apparent that carbon formation in the catalyst bed would limit the extent to which UDMH could be substituted for hydrazine in the feed mixture. The amount of carbon left in the bed after each test increased with increasing UDMH concentration until, at 40% UDMH, the decomposition reaction could not be maintained for the usual 4-min test duration.

By removing the catalyst, increasing the initial preheated chamber temperature to 1900°F, and increasing the L^* (smaller nozzle diameter), it was possible to continue monopropellant operation with increased UDMH concentration up to and including 100% UDMH. The resulting experimental performance is plotted in the right-hand portion of Fig. 4.

The experimental c^* and T_c for pure UDMH decomposition are compared with theoretical values calculated on the basis of chemical equilibrium and assuming final reaction products of H_2, N_2, CH_4, NH_3, HCN, and C (heat of formation (Q_f) for UDMH + 12.72 kcal/mol).

UDMH Decomposition (300 psia)

	Experimental	*Calculated*
c^*, ft/sec	3220	3690
T_c, °F	1262	1467

Under the same conditions of pressure and theoretical reaction temperature, the calculated c^* for hydrazine† is 4185 ft/sec. Thus, a 12% decrease in c^* based on theoretical calculations was to be expected upon going from hydrazine to UDMH gas-generator operation; whereas, a 22% decrease in c^* was experimentally observed.

*These catalysts consist of iron, nickel, and cobalt supported on alumina. In the case of H-A-3, the alumina is activated, in H-7, the alumina is fused (Ref. 5).

†The decomposition temperature of hydrazine can be controlled by varying the catalyst bed depth. Temperature of 1467°F corresponds to 74.5% ammonia dissociation (Ref. 5).

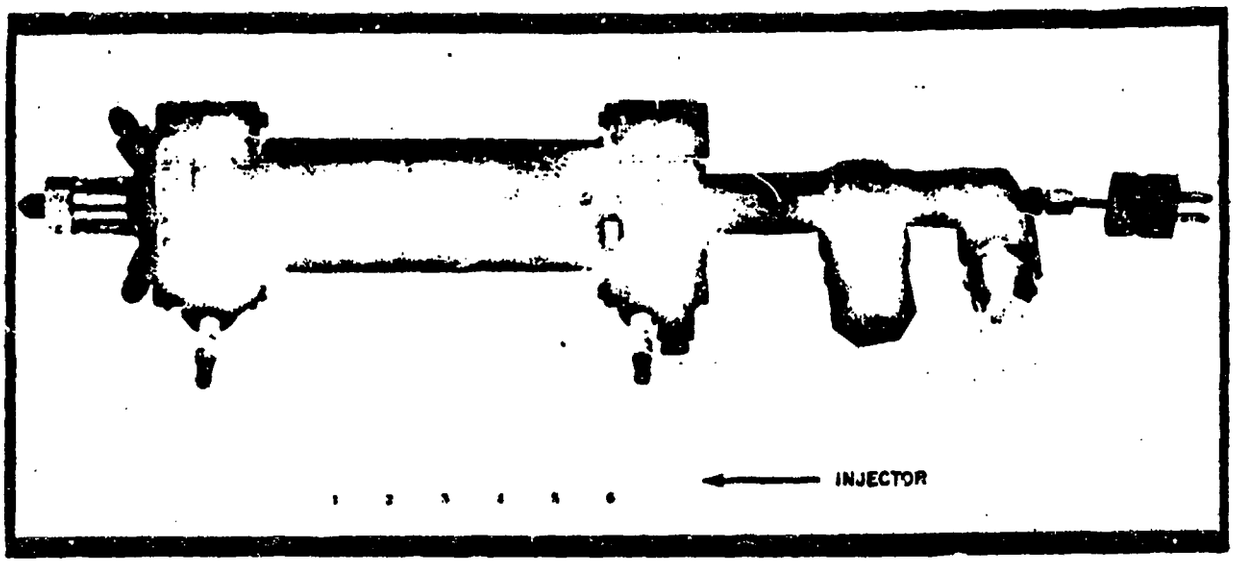

Fig. 2. UDMH Decomposition Chamber with Spray Injector

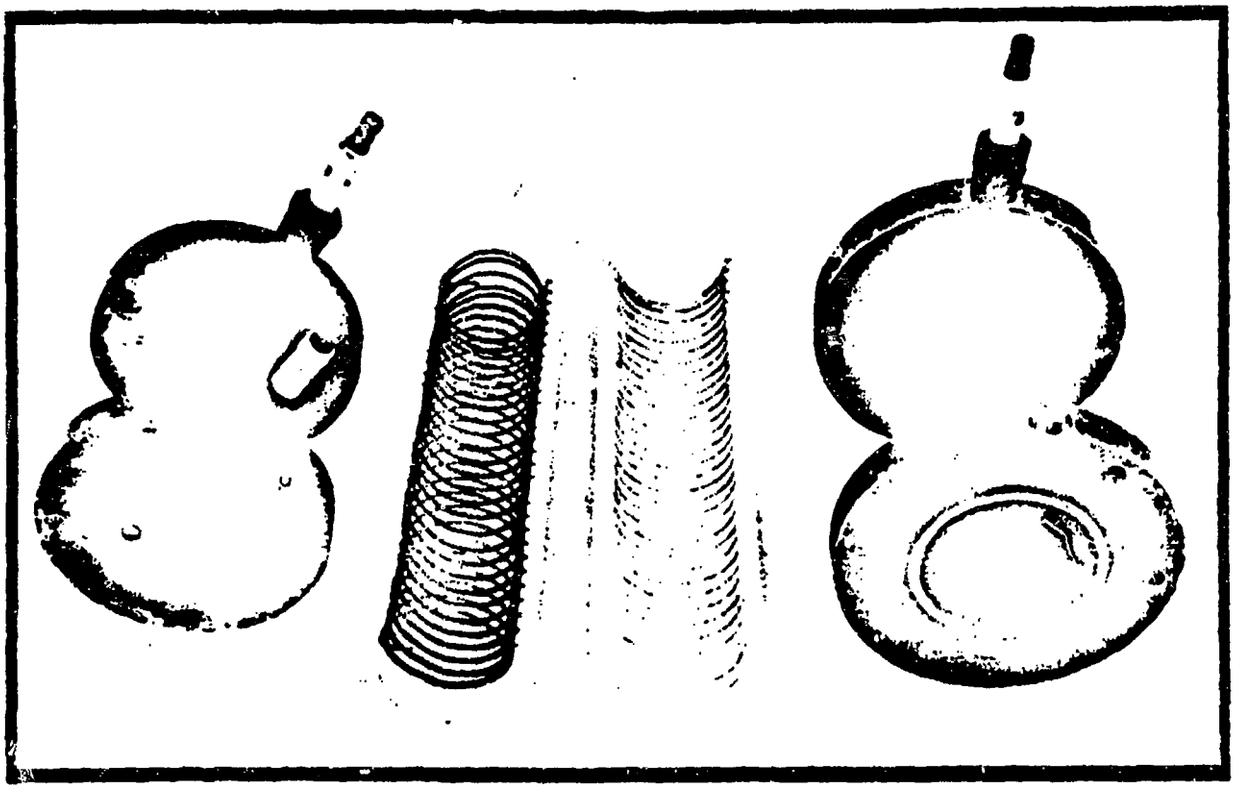

Fig. 3. UDMH Decomposition Chamber with Lava Liner and Nichrome Coil

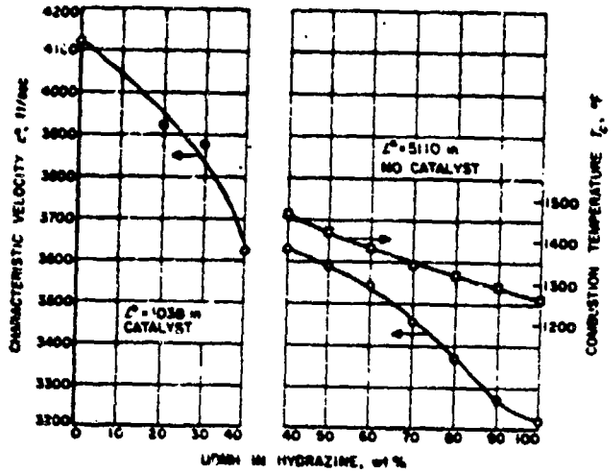

Fig. 4. Performance of UDMH–Hydrazine Mixtures

B. Monopropellant Tests with UDMH

Having found that UDMH would perform as a monopropellant under certain conditions, it remained to study the effect which variations in these conditions would have on its performance. The effects of changes in chamber pressure, L^*, and fuel-injection state; i.e., liquid or vapor, were determined.

1. Unheated fuel

a. Effect of chamber pressure on performance. A number of monopropellant tests were made with UDMH at chamber pressures from 50 to 600 psia. The resulting chamber temperature and c^* values (average of 4 to 22 tests at 4540 to 5090-in. L^*) are given in Figs. 5 and 6 and Tables 1 and 2. For purposes of comparison, the theoretical values calculated on the basis of thermochemical equilibrium at 75, 300, and 600 psia are included in Figs. 5 and 6 and tabulated in Table 3.

Table 1. Experimentally Determined Values of Characteristic Velocity for Monopropellant UDMH

Chamber Pressure psia (± 5%)	Characteristic Velocity ft/sec				
	L^* 7870-8000 in.	L^* 4540-5090 in.	L^* 3660 in.	L^* 2870 in.	L^* 2115 in.
100	3236 (4)	3156 (9)	3255 (2)		
200	3125 (6)	3168 (10)	3065 (4)	3160 (1)	3290 (2)
300	3236 (5)	3196 (22)	3064 (5)	3210 (2)	3110 (2)
400	3299 (5)	3177 (5)	3058 (2)		3080 (2)
500	3266 (7)	3187 (5)	3214 (4)		
600	3215 (4)	3276 (4)	3322 (2)		3090 (2)

Note: Encircled numbers indicate number of individual test results which were averaged to obtain tabulated number. Averages include all individual results to ± 50 psia of the nominal chamber pressure shown.

Table 2. Measured Values of Reaction Temperature for Monopropellant UDMH

Chamber Pressure psia (± 5%)	Reaction Temperature °F				
	L^* 7870-8000 in.	L^* 4540-5090 in.	L^* 3660 in.	L^* 2870 in.	L^* 2115 in.
100	1312 (4)	1246 (8)	1184 (2)		
200	1264 (6)	1256 (10)	1285 (4)	1230 (1)	1213 (1)
300	1252 (5)	1275 (22)	1244 (5)	1282 (2)	1271 (2)
400	1267 (5)	1254 (5)	1303 (2)		1273 (2)
500	1299 (7)	1321 (5)	1315 (4)		
600	1296 (4)	1322 (4)	1322 (2)		

Note: Encircled numbers indicate number of individual test results which were averaged to obtain tabulated number. Averages include all individual results to ± 50 psia of the nominal chamber pressure shown.

It is evident from these curves that thermochemical equilibrium is not attained. Theoretical chamber temperatures ranged over 300 F between 75 and 600 psia;

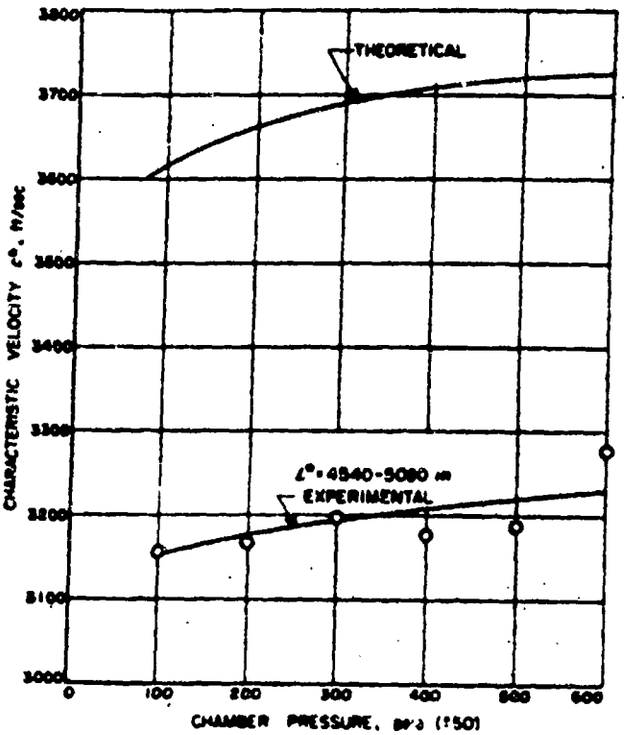

Fig. 5. UDMH Performance (Unheated Fuel Feed), c^* vs p

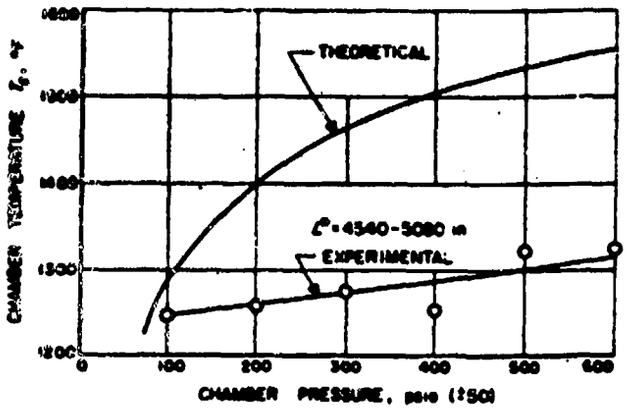

Fig. 6. UDMH Performance (Unheated Fuel Feed), T_c vs p_c

whereas, observed temperatures changed only about 75 F. Undoubtedly, errors of temperature measurement are involved also; the temperatures were measured by means of a bare chromel–alumel thermocouple located in the center of the chamber. The experimental and theoretical c^* curves show better agreement in shape or amount of change over the 100- to 600- psia range, but the measured values are about 500 ft sec lower than theoretical values.

On the basis of actual experimental results, it is evident that changes in chamber pressure over the range investigated have a small, but detectable, effect on performance of UDMH as a monopropellant.

b. Effect of L^* on performance. Although most of the UDMH testing was done at 4540- to 5080-in. L^*, tests were also made at 2115, 2870, 3660, and 7870 to 8000 in. Averaged results are included in Tables 1 and 2. No trend in chamber temperature or c^* values could be detected for the L^* range investigated. Monopropellant operation could not be extended below 2115-in. L^*. Even at 2115-in. L^*, chamber-pressure fluctuations made operation rough, and tests were limited to short duration. At 300-psia chamber pressure, average c^* values varied irregularly from 3064 to 3236 ft sec over the L^* range of 2115 to 8000 in., and chamber temperatures varied from 1244 to 1282°F.

Hence, within the limits of accuracy involved in the UDMH experiments, there was no detectable consistent effect of changes in characteristic chamber length (L^*) from 2115 to 8000 in. on c^* or chamber temperature. However, as L^* was decreased, chamber-pressure fluctuations increased.

Table 3. Calculated Performance of UDMH as a Monopropellant*

Parameter	Chamber Pressure, psia		
	75	300	600
$\bar{M}_{av}$	10.33	11.93	12.45
T_c, °F	1324	1467	1556
c^*, ft/sec	3400	3490	3735
I_{sp}, sec	123	139	172

*Based on: 1. Heat of formation Q_f = +17.72 kcal mol (2) Assuming that mechanical equilibrium and products are H_2, N_2, CH$_4$, NH$_3$, HCN, and C

2. *Heated fuel.* The possible effect of preheated UDMH on monopropellant performance was investigated using (1) heat from the decomposition reaction to heat the UDMH, and (2) heat from the decomposition reaction plus supplementary heat from an auxiliary source.

a. Operation with regeneratively heated liquid injection. A regenerative-heating system was fabricated by wrapping the decomposition chamber with stainless-steel tubing, as shown in Fig. 7. The UDMH passed through this coil from the bottom to the top of the chamber collecting heat transmitted to it from the decomposition zone. The heat had passed through a ¼-in. ceramic liner and two stainless-steel walls of 0.153-in. total thickness. The heated fuel then went directly to the hollow-cone spray injector; the injector pressure drop maintained a high enough pressure upstream of the injector to keep the UDMH in a liquid state. At flow rates of 0.005 to 0.015 lb sec, feed temperatures of 170 to 306°F were recorded for the heated liquid UDMH.

Initial (preheated) chamber temperatures were found to be quite critical in starting the gas generator when using the regenerative-fuel coil. Optimum starting temperature, as indicated by the bare chromel–alumel thermocouple, was determined by experience to be from 1100 to 1200 F. At higher temperatures, decomposition in the coil was likely to occur and could not be moved through the injector into the chamber by increasing UDMH tank pressure.

UDMH-performance data (c^* and T_c) under regenerative-heating conditions (liquid state) are listed in Table 4, and c^* values are plotted in Fig. 8. It can be seen in Fig. 8 that regenerative heating has a minor effect on c^*. At the two chamber pressures of comparison, 200 and 300 psia for liquid-state injection, regenerative

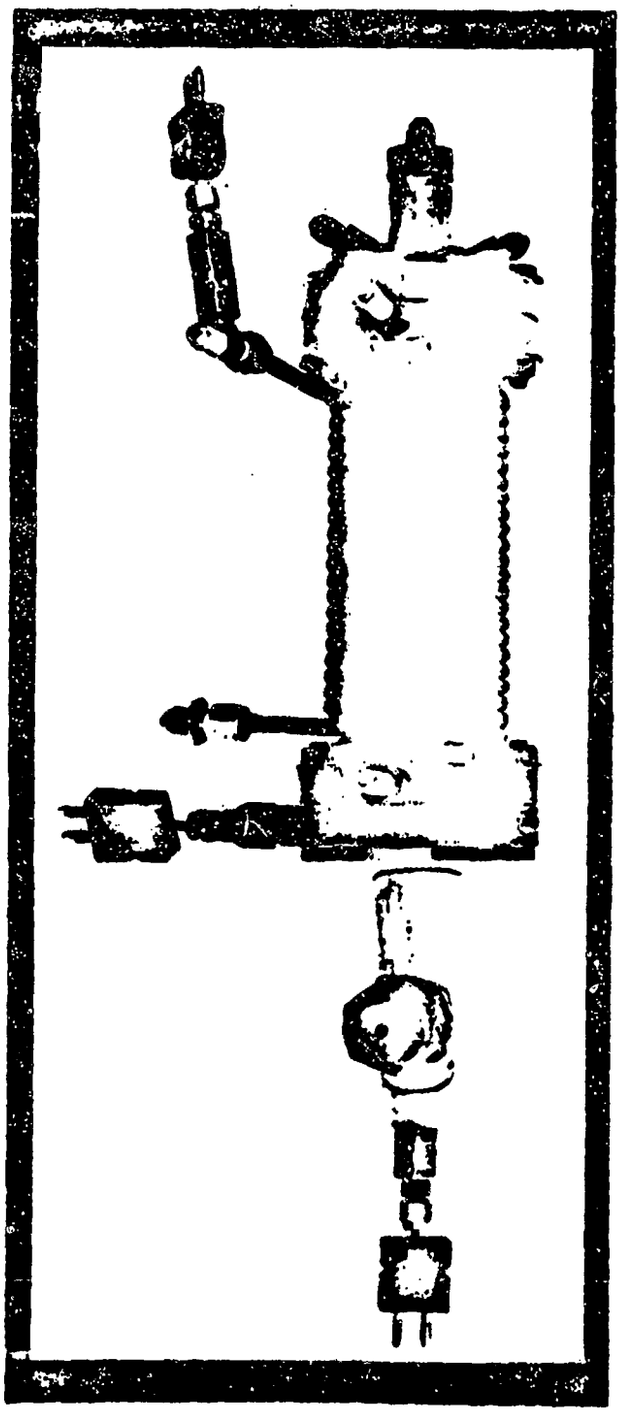

Fig. 7. UDMH-Decomposition Chamber with External Regenerative Fuel Heater

Table 4. Experimentally Determined Monopropellant-UDMH Performance Utilizing Regeneratively Heated Liquid Feed*

Chamber Pressure psia (±50)	Average c^* ft/sec	Average T_c °F	No. of Tests Averaged
280	3280	1246	10
300	3333	1268	6

*L^* = 4730-4750 in.
Note: Averages include all individual results to ±50 psia of the nominal chamber pressure shown.

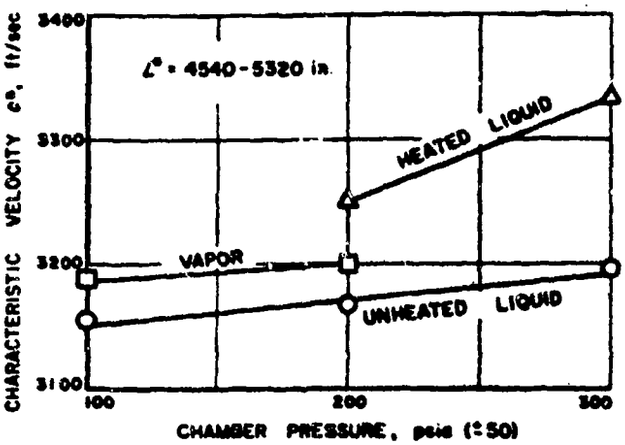

Fig. 8. Effect of Regenerative Fuel Heating on UDMH Performance

operation resulted in c^* increases over that for unheated liquid feed of approximately 100 ft/sec. It is postulated that this small c^* increase resulted from reduction of over-all system heat loss.

b. Operation with regeneratively heated vapor injection. In the course of operating a UDMH-gas generator under vaporized-injection conditions, four design modifications were made in order to provide for improved vaporization. First, the hollow-cone spray injector was removed and a restriction was placed in the fuel tubing immediately in front of the heating coil. This reduction in injection pressure to nominally that of the chamber pressure permitted vaporization to take place at temperatures reached in the heated-liquid-injection experiments.

Second, resistance to heat flow from decomposition zone to incoming UDMH was reduced by a redesign of the electrical heating system so as to eliminate the ceramic liner. Instead of the liner, a central ceramic core

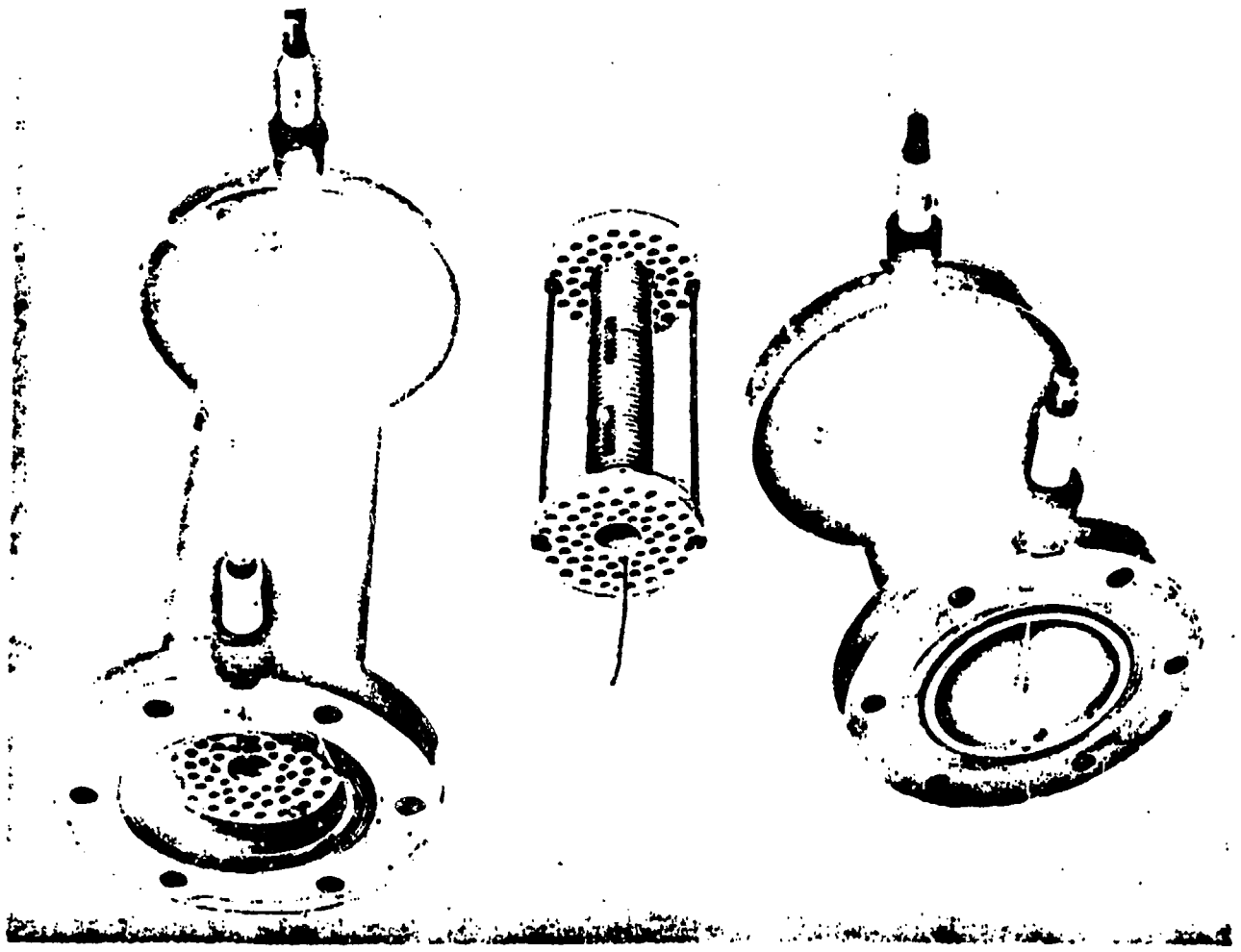

Fig. 9. UDMH-Decomposition Chamber, Nichrome Coil Supported on Lava Core

was supported in the chamber and heating wire was coiled around this, as shown in Fig. 9.

Third, improvement in heat transfer resulted from replacing the external regenerative coil with an internal coil. However, a chamber section made up in this manner (illustrated in Fig. 10) could not be used as the primary UDMH-decomposition zone since the more rapid extraction of heat quickly stopped the reaction.

The fourth modification was counter-flow injection as provided by the chamber section shown in Fig. 11. This modification, when combined with the three previous features, resulted in the decomposition chamber shown in Fig. 12. Elimination of the spray injector, keeping other things the same as for heated-liquid injection, made it possible to operate a 4740-in.-L^* gas generator with vapor feed at chamber pressures not over 50 psia, which corresponded to a fuel flow rate of about 0.0025 lb/sec. The additional modifications incorporated in the triple-section chamber of Fig. 12 made it possible to increase UDMH vaporization rate to 0.02 lb sec and chamber pressure to 206 psia at essentially the same L^* (4875 in.). Vapor temperatures of 242 to 541°F were recorded.

The effect of regenerative vaporization on UDMH c^* values can be judged from the plotted data in Fig. 8. Tabulated data, including T_c values and additional data at 42 to 49 psia, are shown in Table 5. For the two

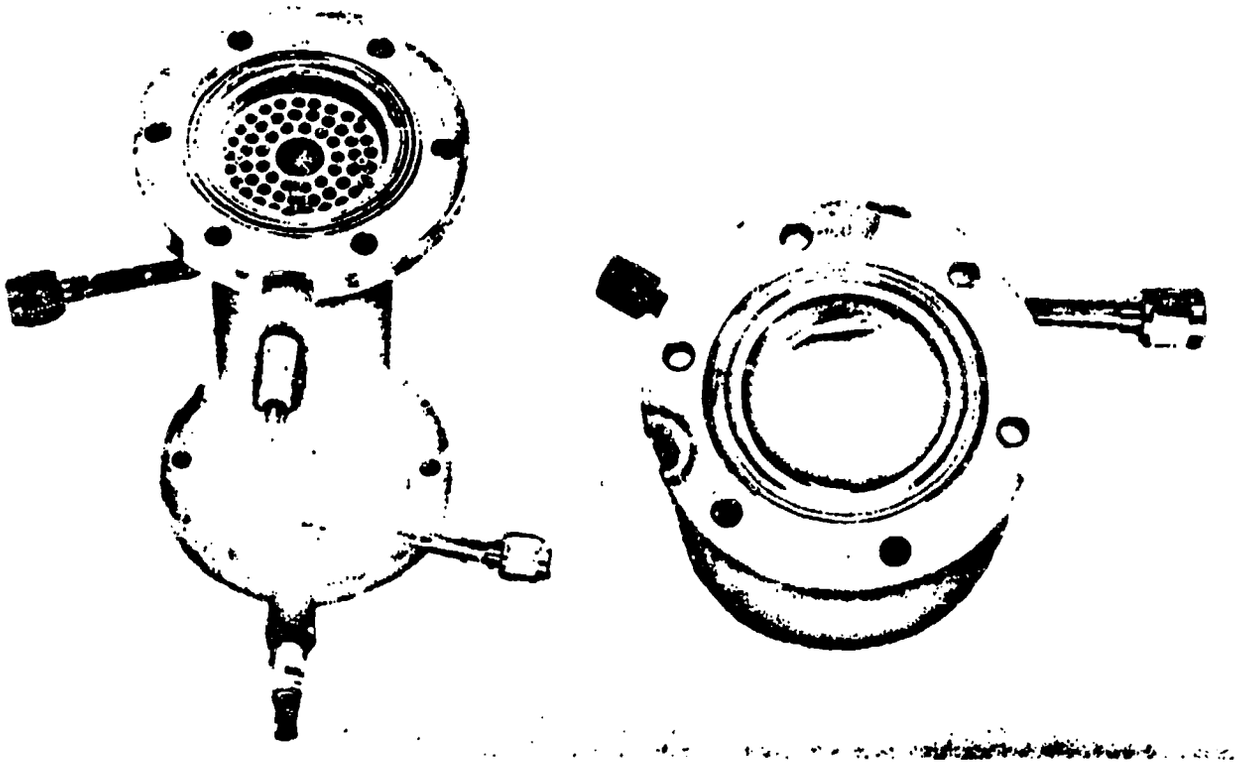

Fig. 10. UDMH-Decomposition Chamber with Internal Regenerative Fuel Heating

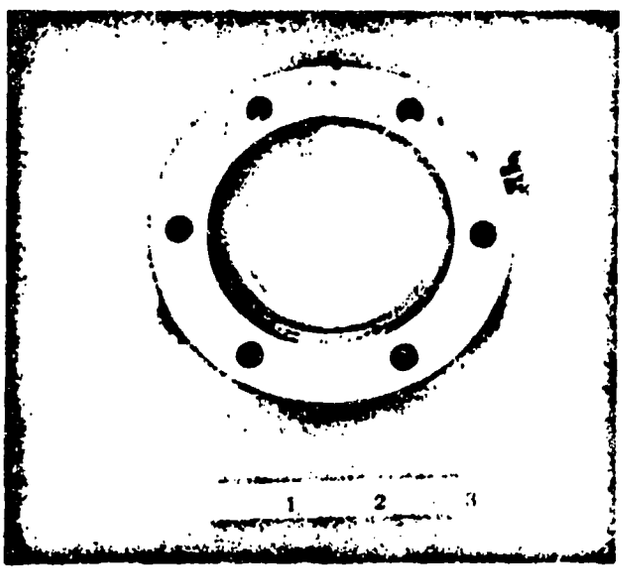

Fig. 11. Counter-Flow Vaporized UDMH Injection Section

chamber pressures where comparison can be made with unheated liquid injection, 100 and 200 psia, average c^* values are higher by about 40 ft/sec for vapor injection. As with heated-liquid injection, this slight but detectable increase in c^* is probably the result of decrease in system heat loss.

c. Operation with supplementally heated fuel. A series of UDMH experiments was conducted using vaporized-fuel injection for the purpose of determining if UDMH decomposition could be carried out in a much smaller (lower L^*) chamber than was found to be possible with unheated UDMH. For this purpose, a supplementary UDMH heating system was installed to increase the vaporization capacity beyond that provided by regenerative heating. The complete installation is shown in Fig. 13. Heating of the UDMH was accomplished by passing it through a 30-ft coil of stainless-steel ¼-in. tubing, shown in Fig. 14, which was immersed in molten cerrosafe metal. The cerrosafe was heated by a 5-kw electric immersion heater, the two elements of which extended

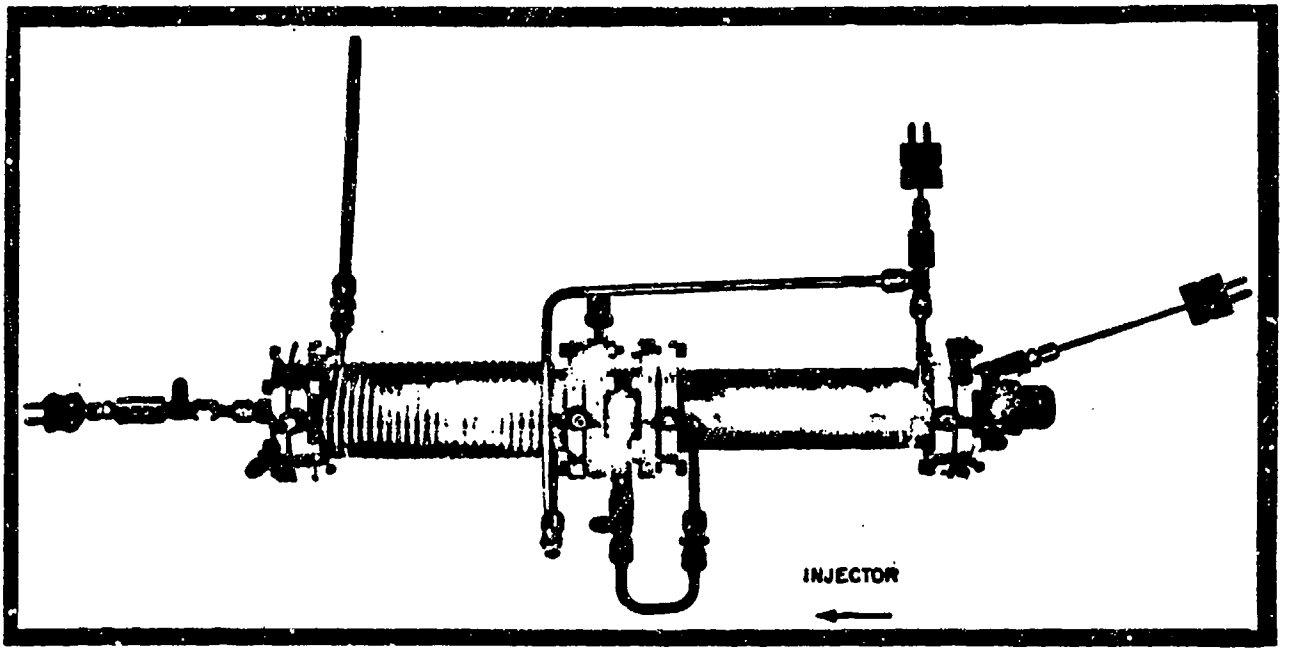

Fig. 12. Triple-Section UDMH-Decomposition Chamber with External and Internal Regenerative Fuel Heating

upward and inside the fuel coil. In the arrangement shown in Fig. 13, UDMH was first preheated regeneratively, passed through the supplemental metal-bath heater, and then led directly into the top of the decomposition chamber.

By this means, it was possible to extend UDMH gas-generator operation down to an L^* of 366 in.; no smaller chambers were tested. Since heat has been added to the system, comparisons of results with previously discussed data have little significance; c^* and T_c results from tests made with added heat would be expected to be somewhat higher, and this is shown by comparing the limited data in Table 6 with data from tests without added heat.

Table 5. Experimentally Determined Monopropellant-UDMH Performance Utilizing Regeneratively Heated Vapor Feed[a]

Chamber Pressure psia	Average c^* ft/sec	Average T_c °F	No. of Tests Averaged
42 to 49	2870	1196	4
100 ± 50	3188	1251	4
200 ± 50	3300	1246	4

[a] L^* 4740 to 5320 in.

However, it is worth noting that an appreciable decrease in both c^* and T_c occurred when the L^* was reduced to 366 in., as is evident in the following comparison:

UDMH Gas-Generator Operation with Vaporization

	Regenerative Coil	*Supplemental Heat*
L^*	4740	366
Chamber Pressure, p_c, psia	42-49	58
Avg. c^*, ft/sec	2870	2165
Avg. T_c, °F	1196	752
No. of Tests Averaged	4	2

Hence, even with added heat, it appears that the lower L^* is, nevertheless, too small to permit decomposition to proceed to the extent it does in larger chambers, and an appreciable amount of undecomposed UDMH was probably being discharged from the exhaust nozzle of the 366-in.-L^* chamber.

C. *Exhaust-Gas Analysis*

At a chamber pressure of 300 psia, calculations based on conditions of thermochemical equilibrium indicate

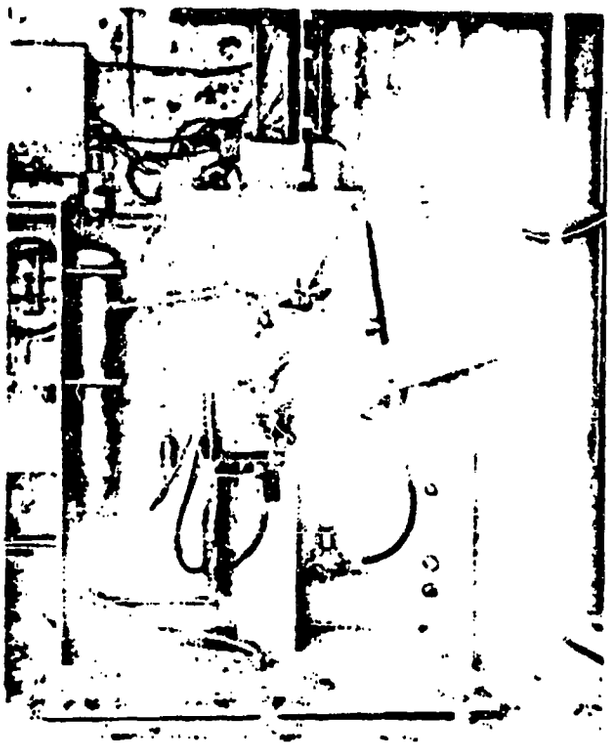

Fig. 13. UDMH-Gas Generator with Regenerative and Supplemental Metal-Bath Fuel Heating

that UDMH should decompose into principally H_2, N_2, CH_4, and C in the approximate mole percentages of 40-20-20-20. Calculated compositions at 75-, 300-, and 600-psia chamber pressure are listed in Table 7. However, the experimental UDMH monopropellant gas-generation operation would seem to indicate that these are not the actual exhaust compositions since discrepancies between theoretical and actual performance parameters have been noted.

The following two sections give results of experimental work which was done to determine UDMH-exhaust composition.

1. Determination of solid exhaust products. A cyclone separator, shown in Fig. 15, was installed on the exhaust nozzle of a UDMH-gas generator in an attempt to collect the solid carbon in the exhaust gases.

Figure 16 shows the separator installed on a gas generator of I_{sp} 280 in., and Fig. 17 shows the amount of carbon and liquid material (probably undecomposed

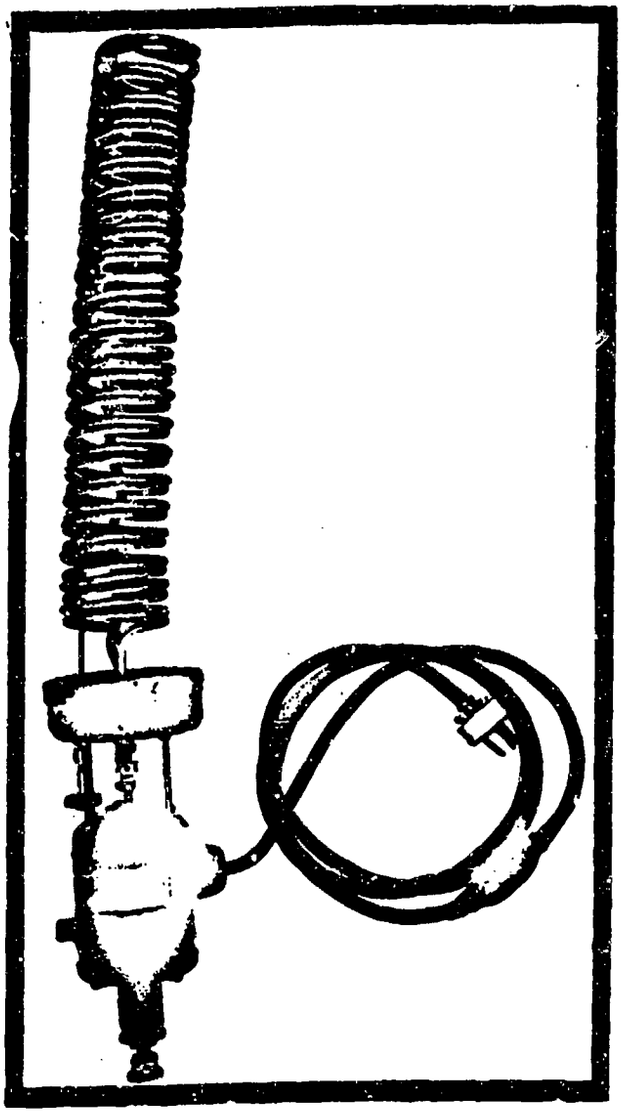

Fig. 14. Metal-Bath Supplemental Fuel-Heating Coil

UDMH) collected from a test in which 6 lb of UDMH were consumed. If about 20% carbon had been formed, as had been predicted on the basis of thermochemical calculations, over 1 lb of carbon should have been collected. Actually, although more carbon was in the separator than is shown in Fig. 17 (because of holdup on the separator walls), not more than a few grams of carbon could be accounted for. In addition, some of the carbon formed remained adhered to the chamber wall in the decomposition chamber (Fig. 18).

Hence, it appears that either the cyclone separator was not effective in collecting carbon or carbon formation is considerably less than thermochemical calculations predicted. Probably both of these explanations are partially correct.

2. Determination of gaseous exhaust products. Gas samples were taken by means of the apparatus shown in Fig. 19. After expansion through a nozzle, exhaust from the gas generator was cooled in a long, horizontal, air-cooled heat exchanger and then exhausted to the atmosphere. A constriction at the end of the heat exchanger forced a small part of the gas stream to be diverted through one or more traps in order to remove entrained solids and liquids prior to being collected in double-ended gas-sample bottles. A bubbler flow-indicator downstream of the sample bottles provided a visual check in order to insure sufficient gas flow during the test, and check valves automatically sealed off the sample bottles at the test termination. Tests were carried out with a gas generator having an L^* of 4330 in.; chamber pressure was maintained at 320 psig. Measured decomposition temperature under these conditions was 1275 to 1285°F.

A total of six gas-sampling tests was made; duplicate samples were taken in all but one test. Two methods of analysis were used to determine gas compositions: (1) mass spectrography and (2) infrared spectrography supplemented by Orsat analysis (Ref. 6). The second method was used also to obtain the hydrogen-nitrogen ratio. The experimentally obtained carbon-free exhaust-gas compositions determined by both methods of analysis are shown in Table 8, together with the calculated thermochemical equilibrium gas composition determined on a carbon-free basis (refer to Table 7). The mass-spectrograph

Table 6. Experimentally Determined Monopropellant-UDMH Performance Utilizing Supplementally Heated Vapor Feed

L^* in.	Chamber Pressure psia	Average c^* ft/sec	Average T_c °F	No. of Tests Averaged
4810	305 to 313	3327	1373	3
2145	143 and 149	3435	1378	2
1174	200 ± 50	3258	1364	6
1070	100 ± 50	2954	1362	6
881	71 and 78	2960	1355	2
366	58	2165	752	2

results[a], which consisted of three analyses, included compositions of duplicate samples determined one month apart. These samples were included in an attempt to reveal any effects of sample age on analytical results.

[a]Analyses made by Consolidated Electrodynamics Corporation, Pasadena, California.

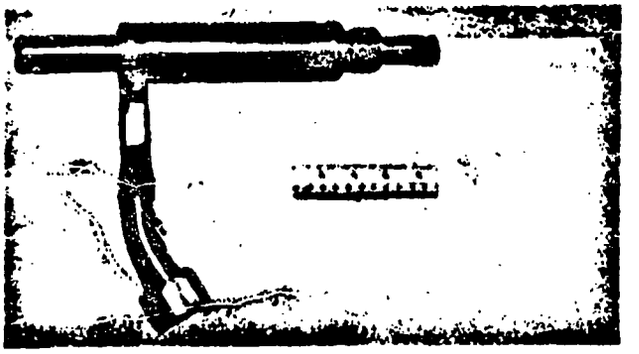

Fig. 15. Cyclone Separator for Quantative Carbon Determination

Table 7. Calculated Theoretical Exhaust-Gas Composition from UDMH Decomposition[a]

Exhaust Component	Chamber Pressure psia					
	75		300		600	
	Total	Excluding carbon	Total	Excluding carbon	Total	Excluding carbon
H_2	46.7	61.0	40.2	50.4	38.1	47.1
N_2	17.7	23.1	19.9	24.9	20.5	25.4
CH_4	12.1	15.8	19.7	24.6	22.1	27.3
NH_3	0.1	0.1	0.1	0.1	0.1	0.2
HCN	[b]	[b]	(11 ppm)	(14 ppm)	(20 ppm)	(25 ppm)
C	23.4	—	20.1	—	19.2	—
	100.0	100.0	100.0	100.0	100.0	100.0

[a]Basis: (1) Heat of formation O_2 + 12.72 kcal/mol, (2) Assuming thermochemical equilibrium (3) Values given in mol %
[b]Not calculated

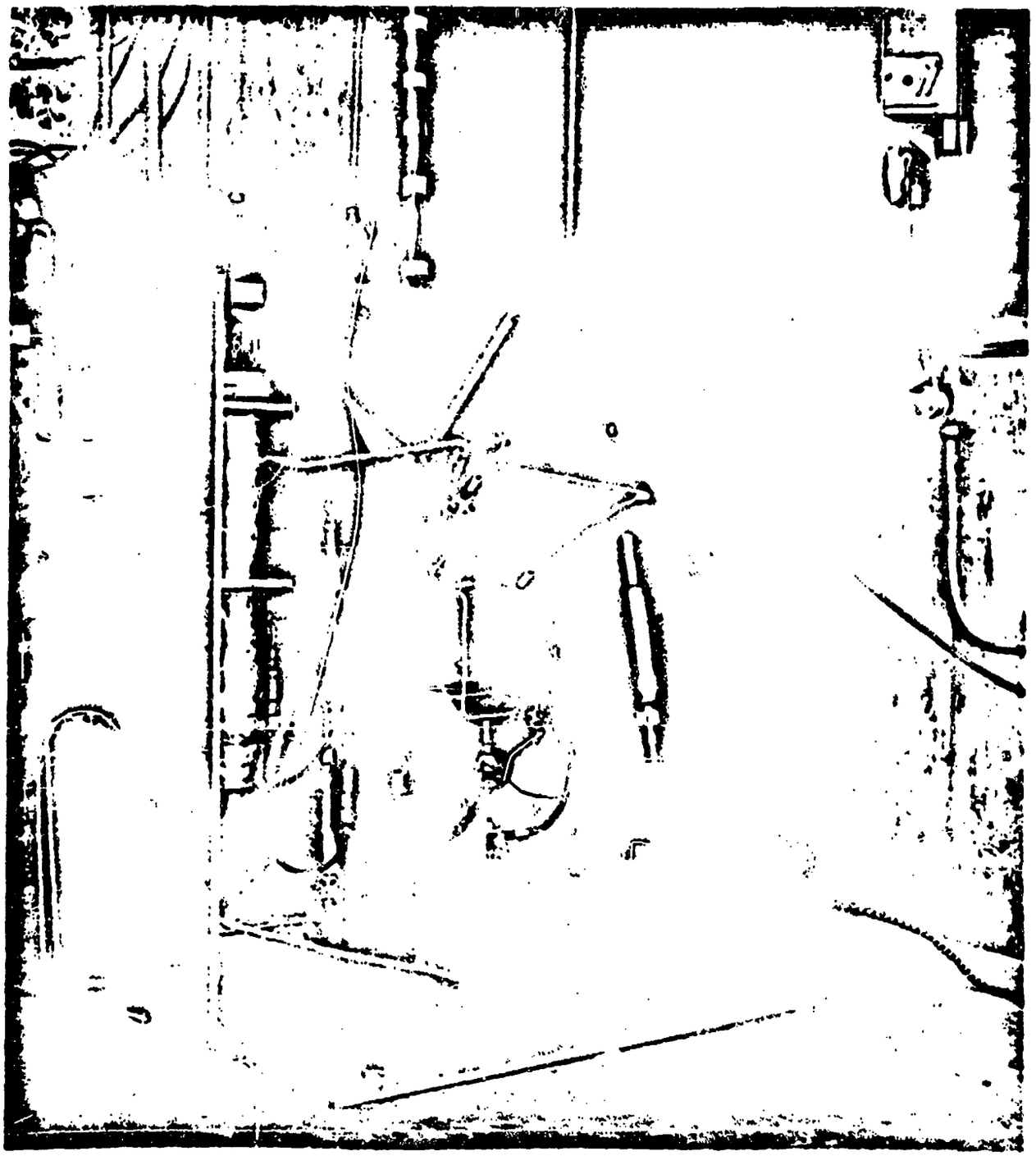

Fig. 16. UDMH-Gas Generator with Cyclone Separator

Significant differences were found: for example, HCN and NH_3 increased from 4.1 and 0.1 to 18.5 and 5.8 mol %, respectively; whereas, CH_4, H_2, and N_2 showed smaller decreases. However, in a similar comparison made using the infrared–Orsat method, no significant changes were found.

Another discrepancy between the two methods was noted in analyses of duplicate samples from one test. In this instance, the mass spectrograph showed HCN and NH_3 contents as 16.6 and 0.8 mol %, respectively; whereas, the infrared–Orsat method showed 6.5 and 16.4 mol %. This extremely large difference in NH_3 analyses led to a careful proof-testing of the infrared–Orsat method using a synthetic-gas mixture of known composition. The method was found to be quite accurate for NH_3 (±0.2 mol %) as well as other components. For this reason, no further samples were analyzed by the mass-spectrograph method.

An examination of the data in Table 9 reveals the following items of interest:*

1. Both analytical methods gave wide variations in the concentrations of some components. Most of this variation occurred between gas-generator tests and not between duplicate samples.
2. The amount of HCN and NH_3 actually found was considerably greater than that calculated on the basis of thermochemical equilibrium.
3. The actual range of CH_4 concentrations was somewhat higher and the range of hydrogen concentration lower than calculated values.
4. Average exhaust-gas composition based on infrared–Orsat results was as follows:

Component	*Mol %, Average*
CH_4	38.4
N_2	22.7
NH_3	17.9
H_2	11.9
HCN	6.9
C_2H_6	1.7
C_2H_4	0.3
C_2H_2	0.14

*Detailed analytical results of the exhaust-gas analysis are given in Tables 9 and 10.

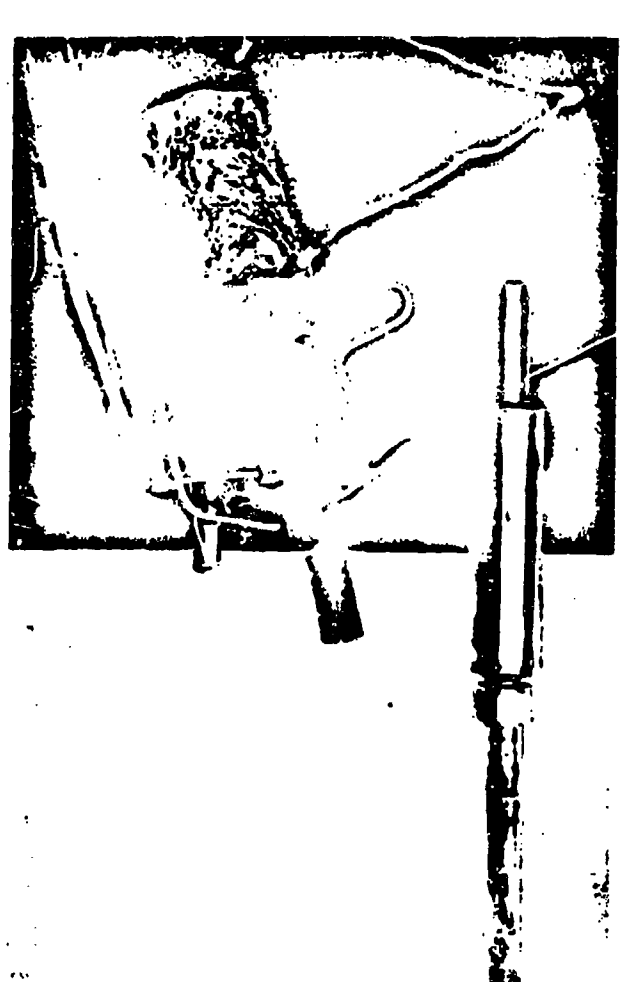

Fig. 17. Carbon Separated from Six Pounds of UDMH-Gas Generation

5. Atomic proportions for this composition correspond to $C_{1.68}H_{7.1}N_{3.0}$, which, for the theoretical carbon-free equilibrium composition is $C_{1.68}H_4N_3$. The formula for UDMH is $C_2H_8N_2$. This comparison indicates that, at least proportionally, all the nitrogen and most of the hydrogen are accounted for by exhaust-gas analysis, and that UDMH, when it decomposes, does not form solid carbon to the extent predicted by thermochemical equilibrium calculations. If the total exhaust contained 16 mol % carbon, all carbon would be accounted for.

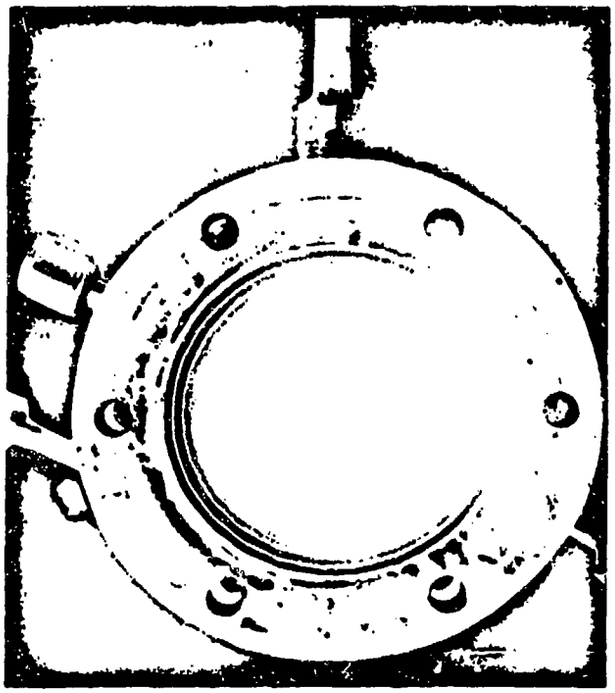

Fig. 18. Carbon Formation in Chamber after Vapor-Injection Gas-Generation Test Using UDMH as Monopropellant

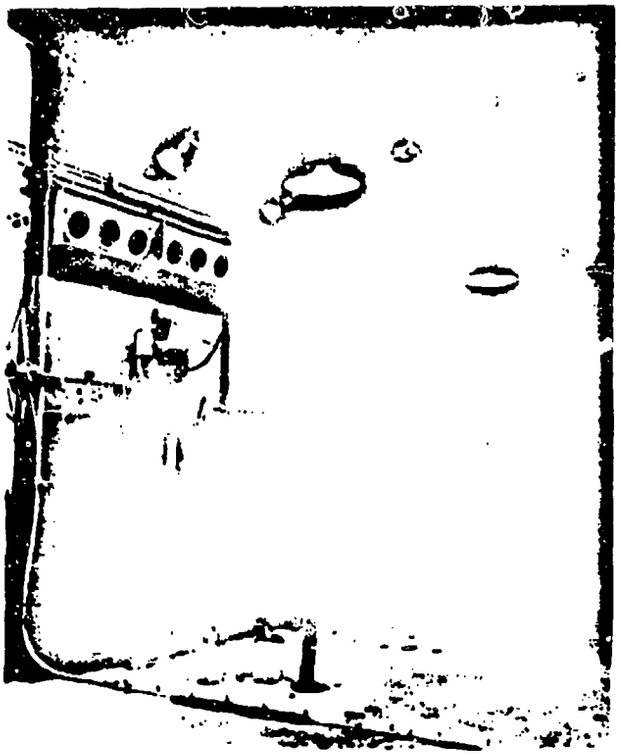

Fig. 19. UDMH Exhaust-Gas Sampling Apparatus

6. The c^* value calculated for the above-average composition at 1280 F is 2835 ft sec as compared with about 3200 ft sec actually observed. The difference between these two values probably resulted from inaccuracies in the temperature measurement and gas analysis.

Table 8. UDMH Exhaust-Gas Analysis with Chamber Pressure at 320 psig

Gas Component	Calculated Thermochemical Equilibrium Composition (300 psia) mol %	Infrared and Orsat Analysis (JPL) mol %	Mass Spectrograph* mol %
Methane	34.6	37.2 — 48.0	41.3 — 58.4
Nitrogen	34.9	12.3 — 34.5	16.9 — 22.6
Hydrogen	30.4	6.1 — 17.3	10.3 — 16.1
Hydrogen cyanide	14 ppm	5.5 — 10.4	4.1 — 18.5
Ethane	Nil	Nil — 1.9	2.9 — 3.9
Ethylene	Nil	Nil — 0.5	1.0 — 1.8
Propane	Nil	1.2 — 2.2	0.4 — 0.5
Ammonia	0.1	13.9 — 25.7	0.1 — 5.8
Other	Nil	Nil	1.1 — 2.0

*Consolidated Electrodynamics Corporation

Table 9. UDMH Exhaust-Gas Composition Determined by Infrared–Orsat Method

Component	Composition mol %								
	Test 272	Test 296		Test 303	Test 304		Test 305		Avg.
	2	1	2		1	2	1	2	
CH_4	48.0	36.0	36.0	45.0	27.3	34.5	42.0	38.5	38.4
N_2	15.3	24.4	20.0	12.3	34.5	27.2	23.1	24.8	22.7
H_2	10.2	12.2	10.0	6.1	17.3	15.1	11.5	12.4	11.9
HCN	6.5	5.2	6.4	10.4	5.5	5.7	5.9	6.9	6.9
C_2H_6	1.9	0.2	0.2	Nil	Nil	Nil	Nil	Nil	0.3
C_2H_4	0.48	Nil	Nil	Nil	0.12	0.14	0.17	0.18	0.14
C_2H_2	1.2	1.7	1.7	2.2	1.4	1.7	2.1	1.9	1.7
NH_3	16.4	17.3	25.7	23.8	13.9	15.7	15.1	15.3	17.9
Atomic proportions									
Carbon	1.73	1.36	1.32	1.70	0.84	1.20	1.62	1.44	1.46
Hydrogen	8.0	6.58	7.26	8.0	4.59	6.21	7.74	6.90	7.25
Nitrogen	1.47	2.0	2.0	1.61	2.0	2.0	2.0	2.0	2.0

Table 10. UDMH Exhaust-Gas Composition Determined by Mass Spectrograph

Component	Composition mol %		
	Test 258		Test 271
	1	2*	3
CH_4	50.4	41.3	44.7
N_2	22.6	16.9	19.1
H_2	16.1	10.3	11.8
HCN	4.1	18.5	16.6
C_2H_6	3.9	2.9	3.4
C_2H_4	1.0	1.8	1.7
C_2H_2	0.5	0.4	0.4
C_4H_2	0.2	0.1	0.2
NH_3	0.1	5.8	0.8
Other	1.1	2.0	1.3
Atomic proportions			
Carbon	2.0	2.0	2.0
Hydrogen	8.0	6.86	6.76
Nitrogen	1.46	1.58	1.49

*Sample No. 2 was taken at the same time as sample No. 1, but was analyzed one month later.

III. CONCLUSONS

Experimental investigation of UDMH as a monopropellant lead to the following conclusions:

1. Unsymmetrical dimethylhydrazine (UDMH) can be made to operate reliably as a monopropellant under suitable conditions of ignition, injection, and combustion volume.

2. Changes in chamber pressure between 100 and 600 psia indicate a small but detectable increase in c^* values.

3. Changes in L^* between 2100 in. and about 8000 in. have no consistent effect on c^* values. However, with unheated fuel, an L^* of 2100 in. is the approximate lower limit of monopropellant operation.

4. Regeneratively heating UDMH prior to its injection into the chamber in the form of either liquid or vapor slightly improved c^* values. It is postulated that this c^* increase results from reduction of overall system heat loss.

5. Employing supplementally preheated UDMH extends monopropellant operation to chambers of relatively low L^*.

6. Carbon formation in UDMH decomposition is less than predicted on the basis of thermochemical equilibrium calculations; whereas, ammonia and hydrogen cyanide are formed in considerably greater quantities than calculated.

NOMENCLATURE

c^* = characteristic velocity, ft/sec.

f_t = nozzle-throat area, in.^{2}

g = gravitational constant, ft/sec.^{2}

I_s = specific impulse, sec.

l^* = characteristic length, in.

p_c = chamber pressure, psia.

T_c = combustion temperature, °F.

V_c = combustion volume, in.^{3}

w = propellant flow rate, lb/sec.

REFERENCES

1. *Improved Liquid Propellants: Systems with Hydrazine-Hydrazine Derivatives*, Technical Report No. M-52-1-ONR. Metalectro Corporation, March 1, 1953 (Confidential).

2. *Research in Chemistry*, NAVORD Report 3462. United States Naval Ordnance Test Station, Dover, New Jersey, March 31, 1955 (Confidential).

3. *Data on Unsymmetrical-Dimethylhydrazine (DMH)*, Revision No. 3. Aerojet General Corporation, Azusa, California, June 7, 1954 (Confidential).

4. *Proceedings of 2nd Monopropellant Conference* (Sponsored by Navy Bureau of Aeronautics). Wyandotte Chemicals Corporation, Wyandotte, Michigan, October 4-5, 1955 (Confidential).

5. Grant, A. F., Jr., *Basic Factors Involved in the Design and Operation of Catalytic Monopropellant-Hydrazine Reaction Chambers*, Report No. 20-77. Jet Propulsion Laboratory, Pasadena, California, December 31, 1954 (Confidential).

6. *Combined Monthly Summary No. 58* (February 1 to April 1, 1957). Jet Propulsion Laboratory, Pasadena, California, April 15, 1957 (Confidential).

APPENDIX B

TEST DATA

INITIAL HYPERMIXING EJECTOR DESIGN

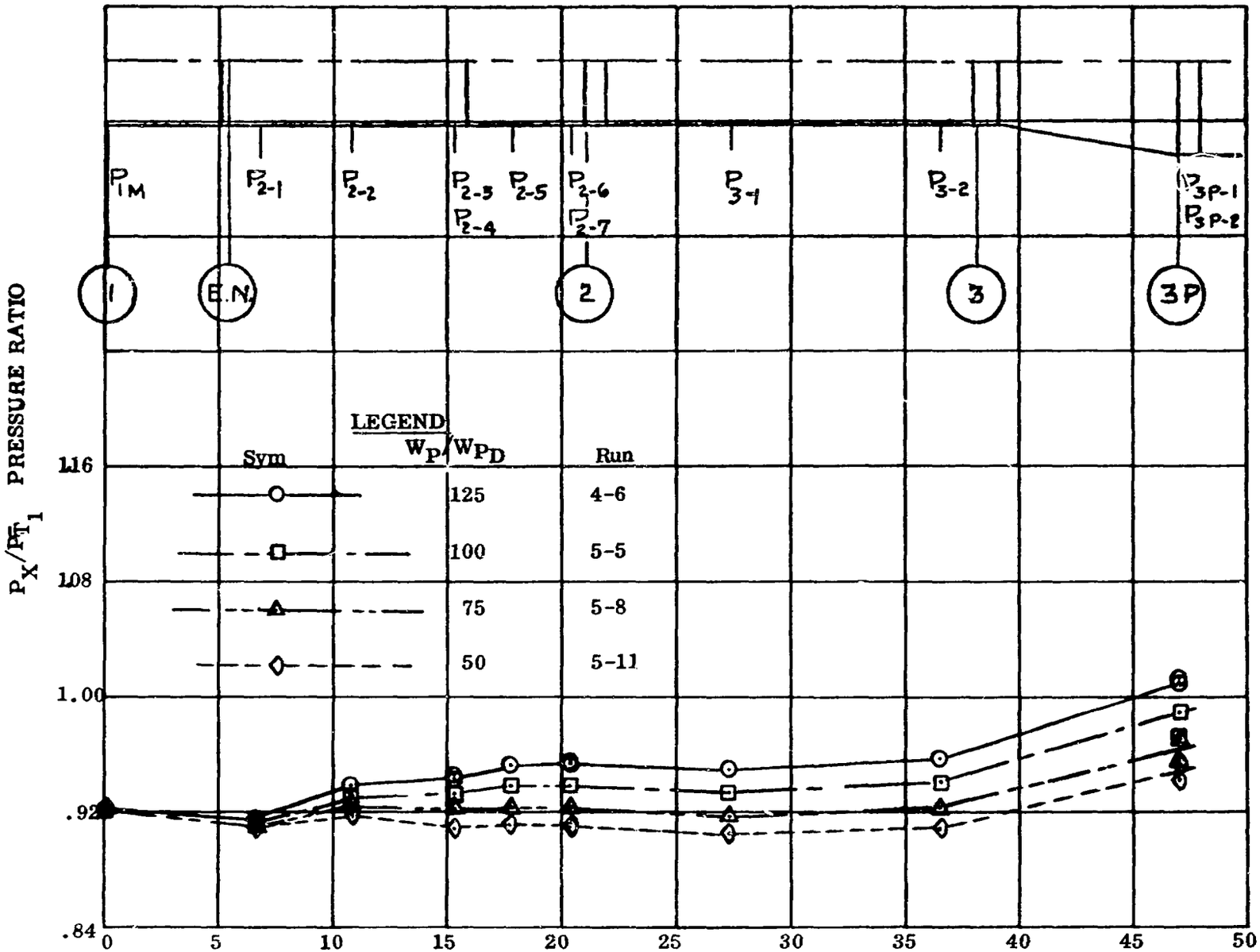

Figure 81. Axial Pressure Distribution, W_S/W_{S_D} = 125%

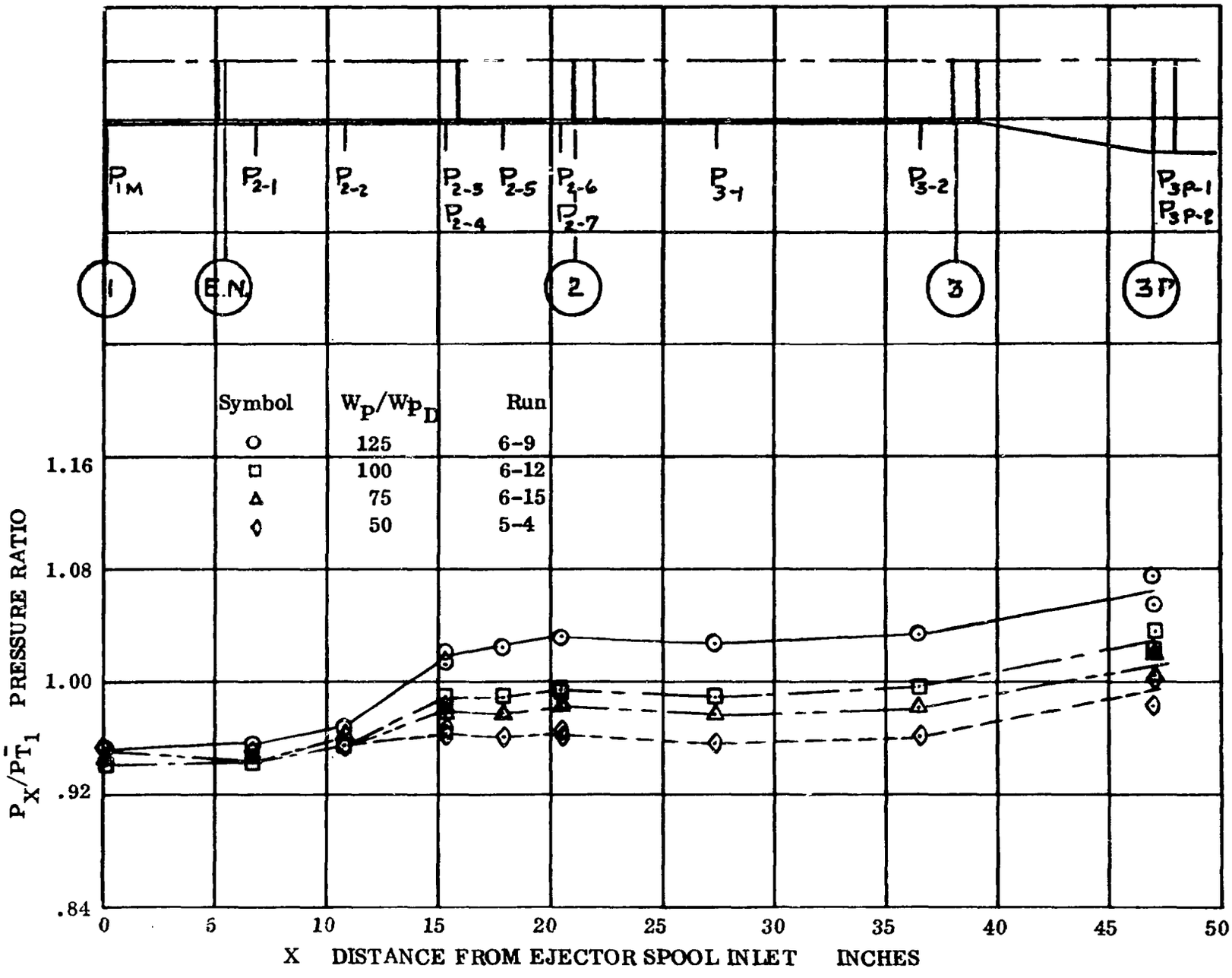

Figure 82. Axial Pressure Distribution, W_S/W_{S_D} = 75%

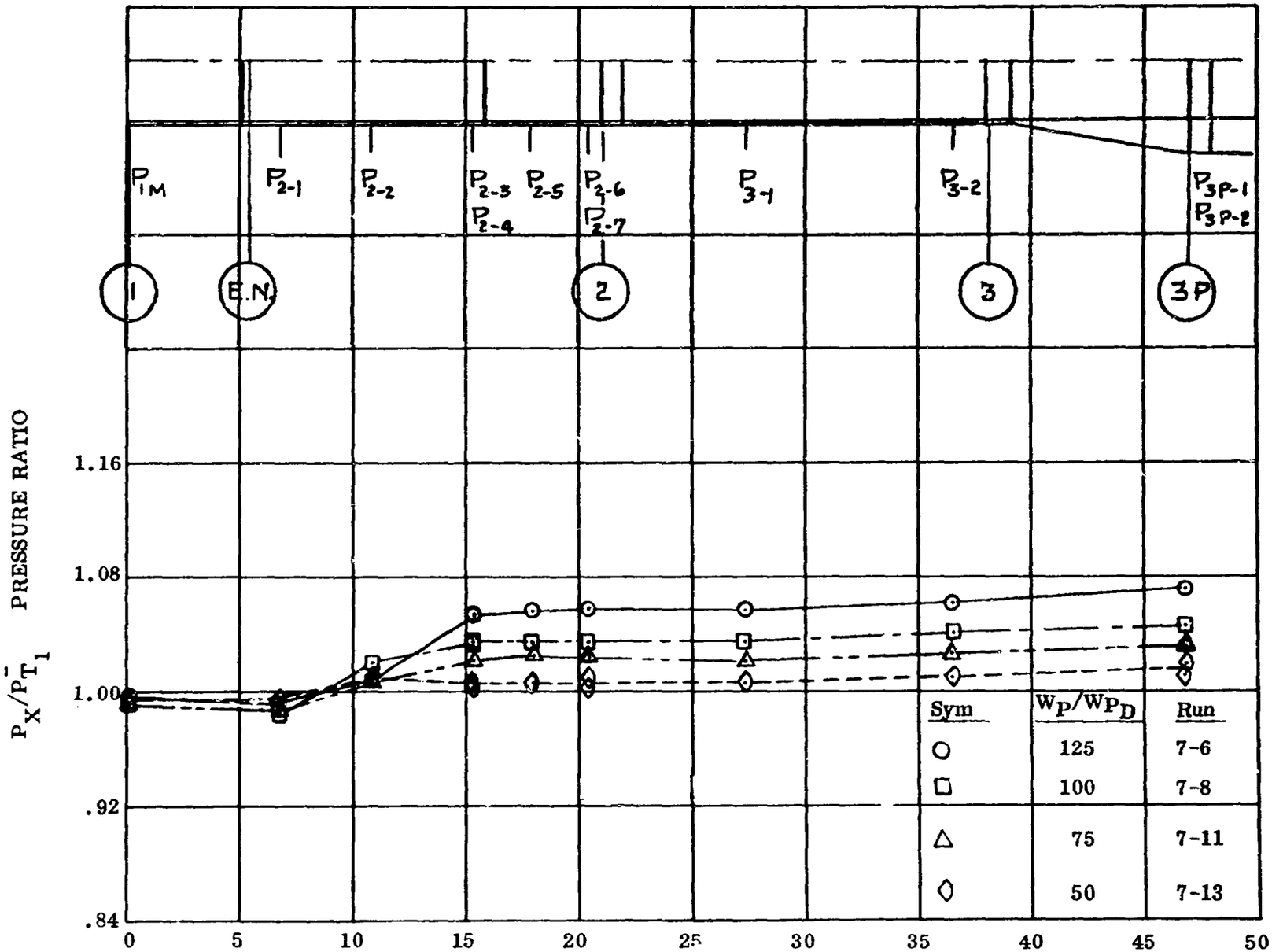

Figure 83. Axial Pressure Distribution, W_S/W_{S_D} = 50%

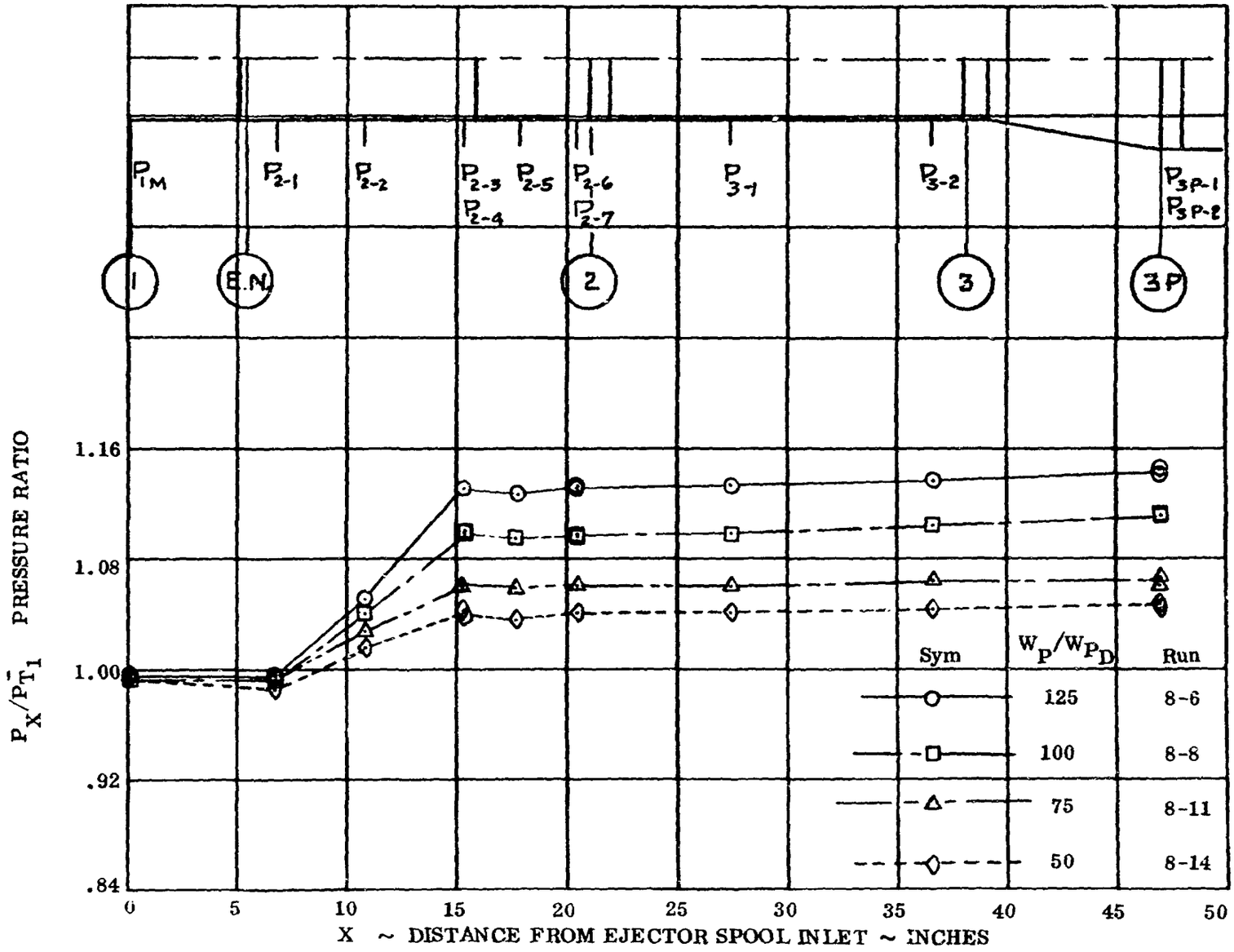

Figure 84. Axial Pressure Distribution, $W_S/W_{S_D} = 25\%$

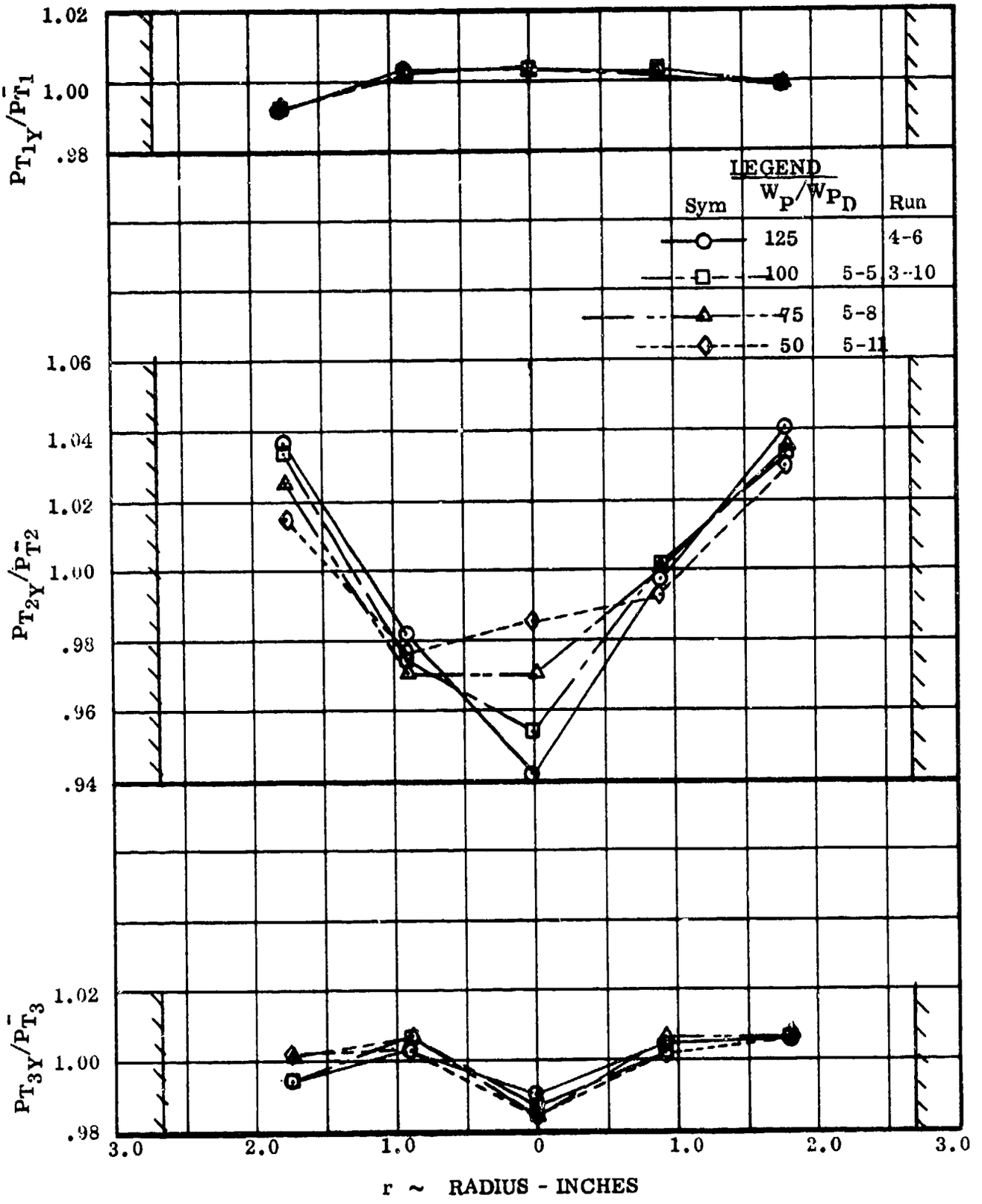

Figure 85. Effect of Primary Flow on Total Pressure Profiles, W_S/W_{S_D} = 125%

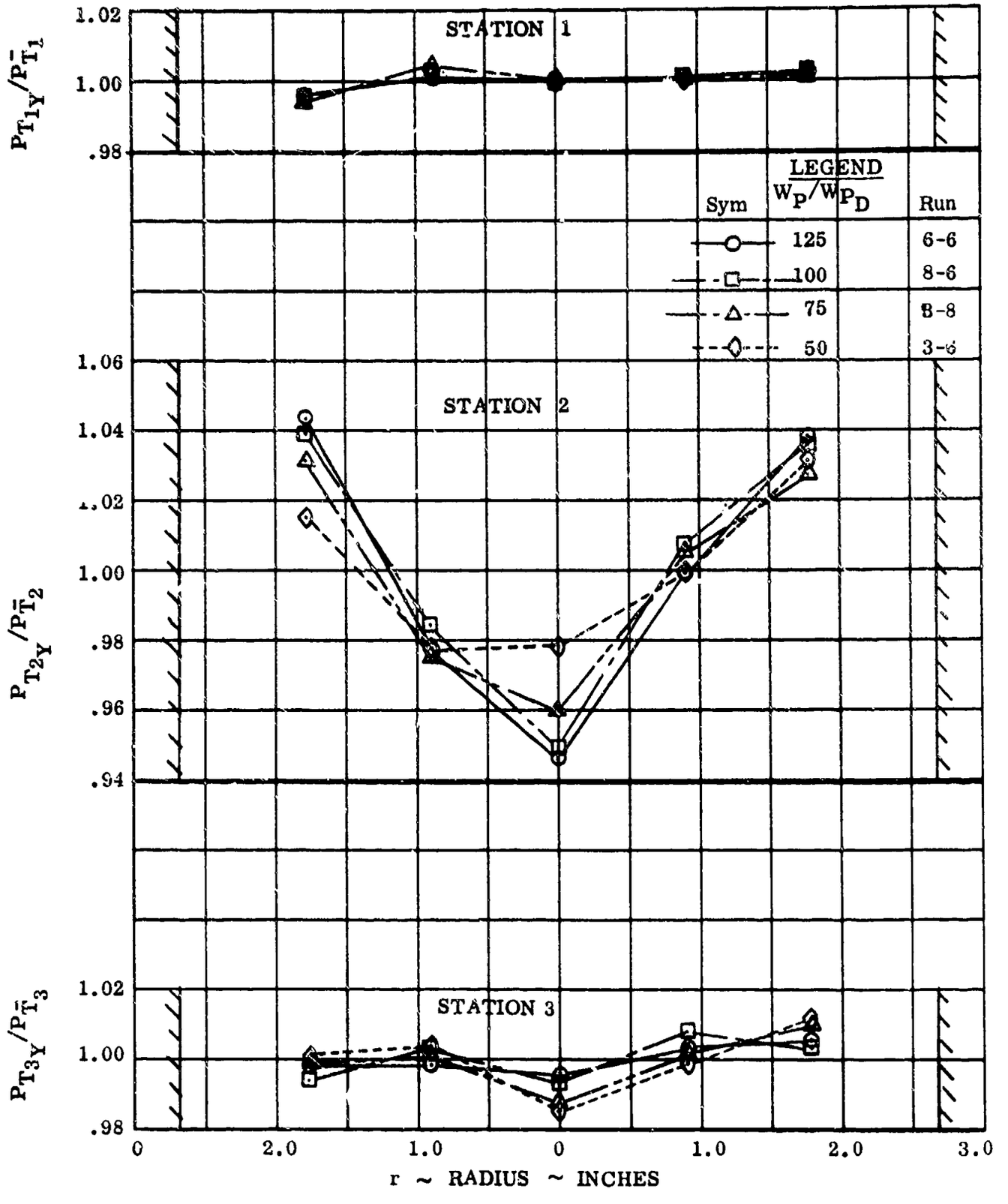

Figure 86. Effect of Primary Flow on Total Pressure Profiles, W_S/W_{S_D} = 100%

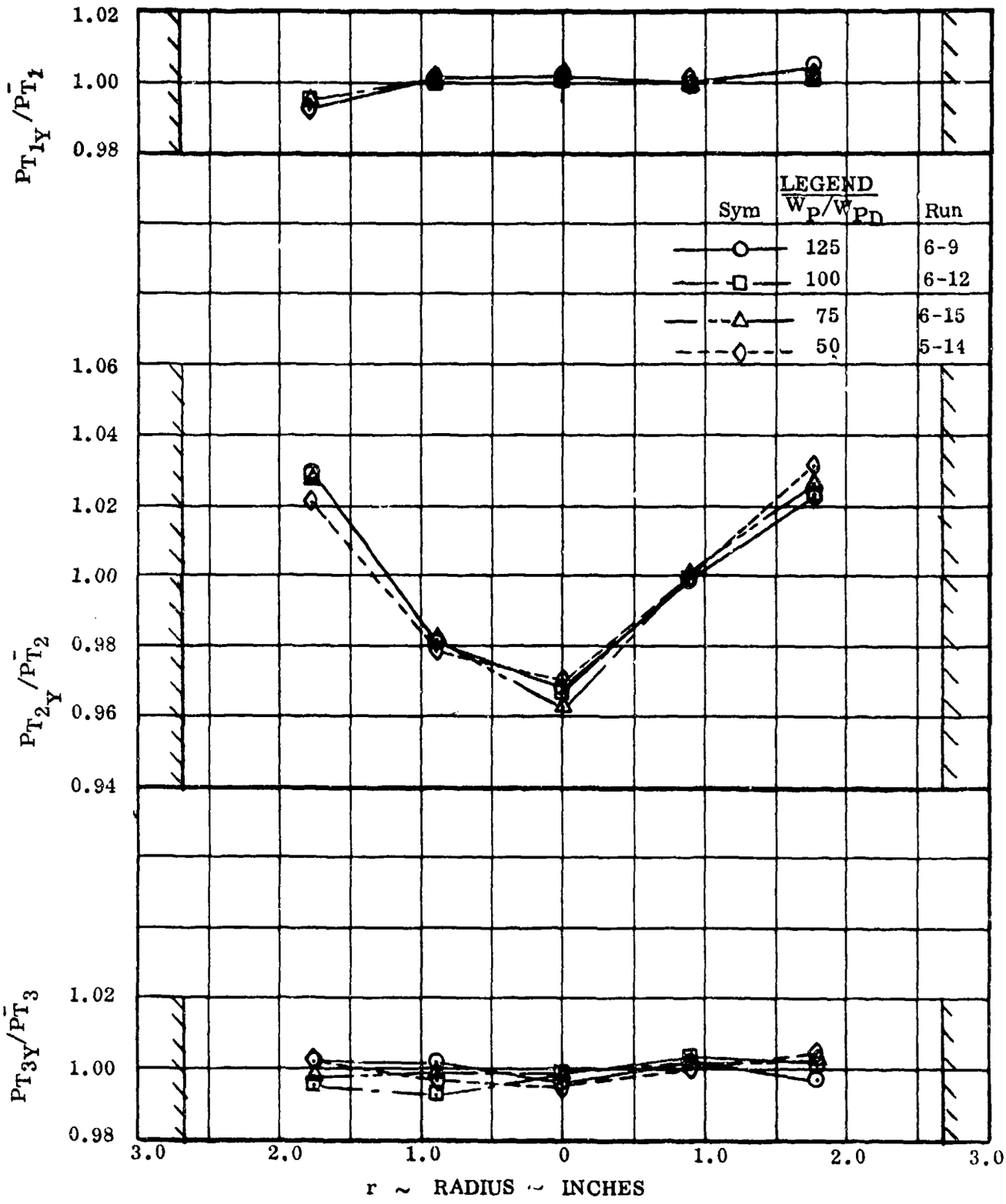

Figure 87. Effect of Primary Flow on Total Pressure Profiles, W_S/W_{S_D} = 75%

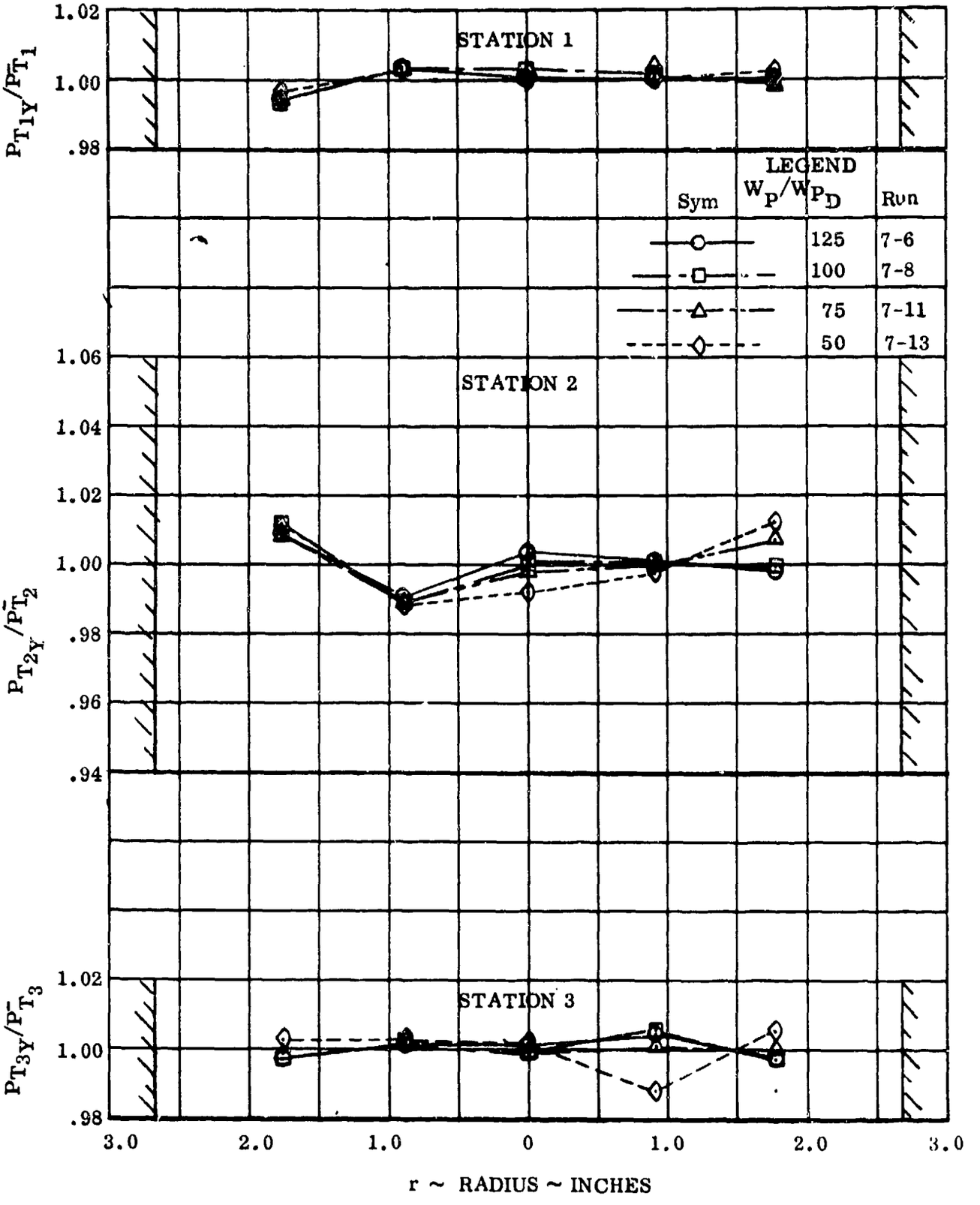

Figure 88. Effect of Primary Flow on Total Pressure Profiles, W_S/W_{S_D} = 50%

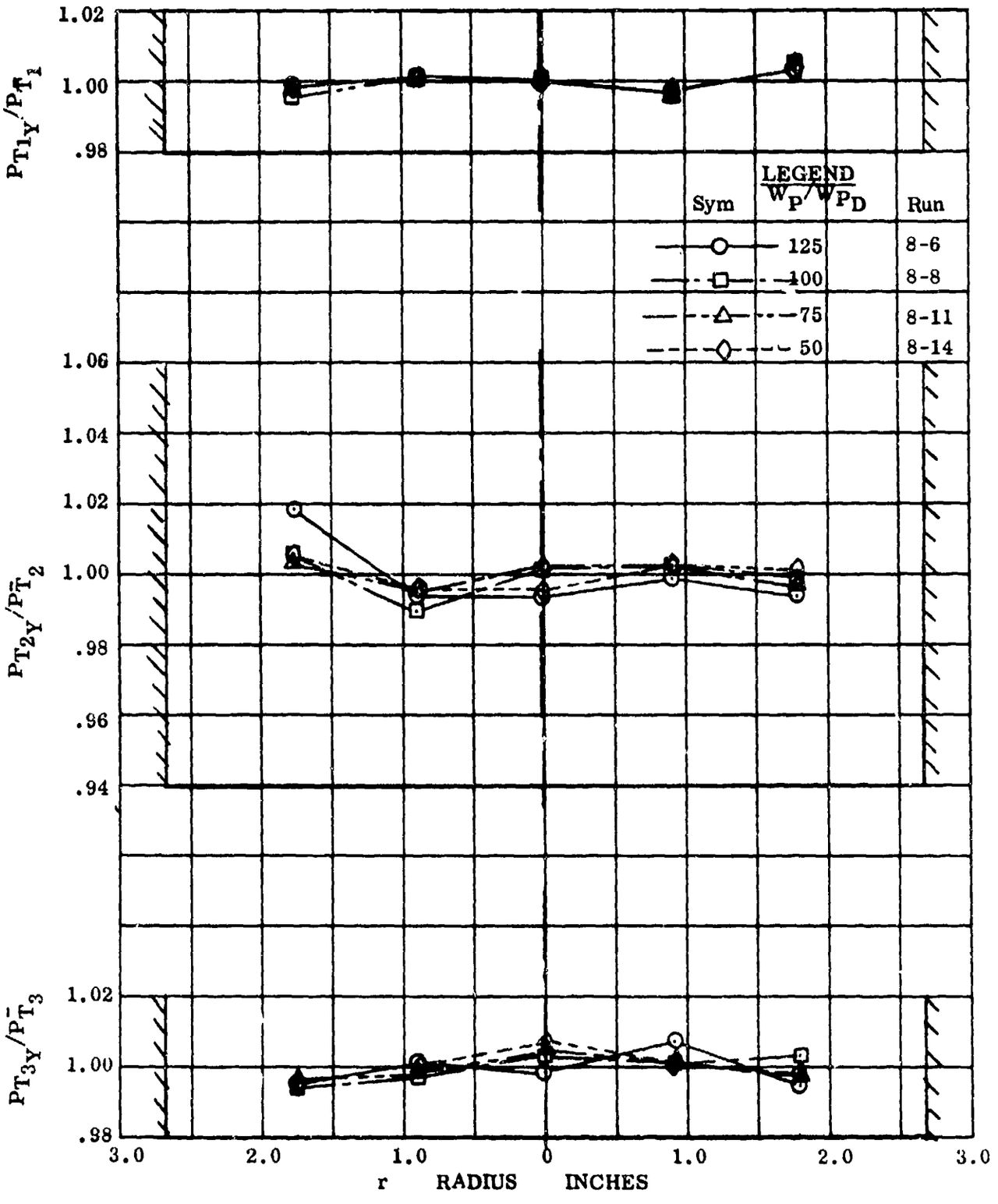

Figure 89. Effect of Primary Flow on Total Pressure Profiles, W_S/W_{S_D} = 25%

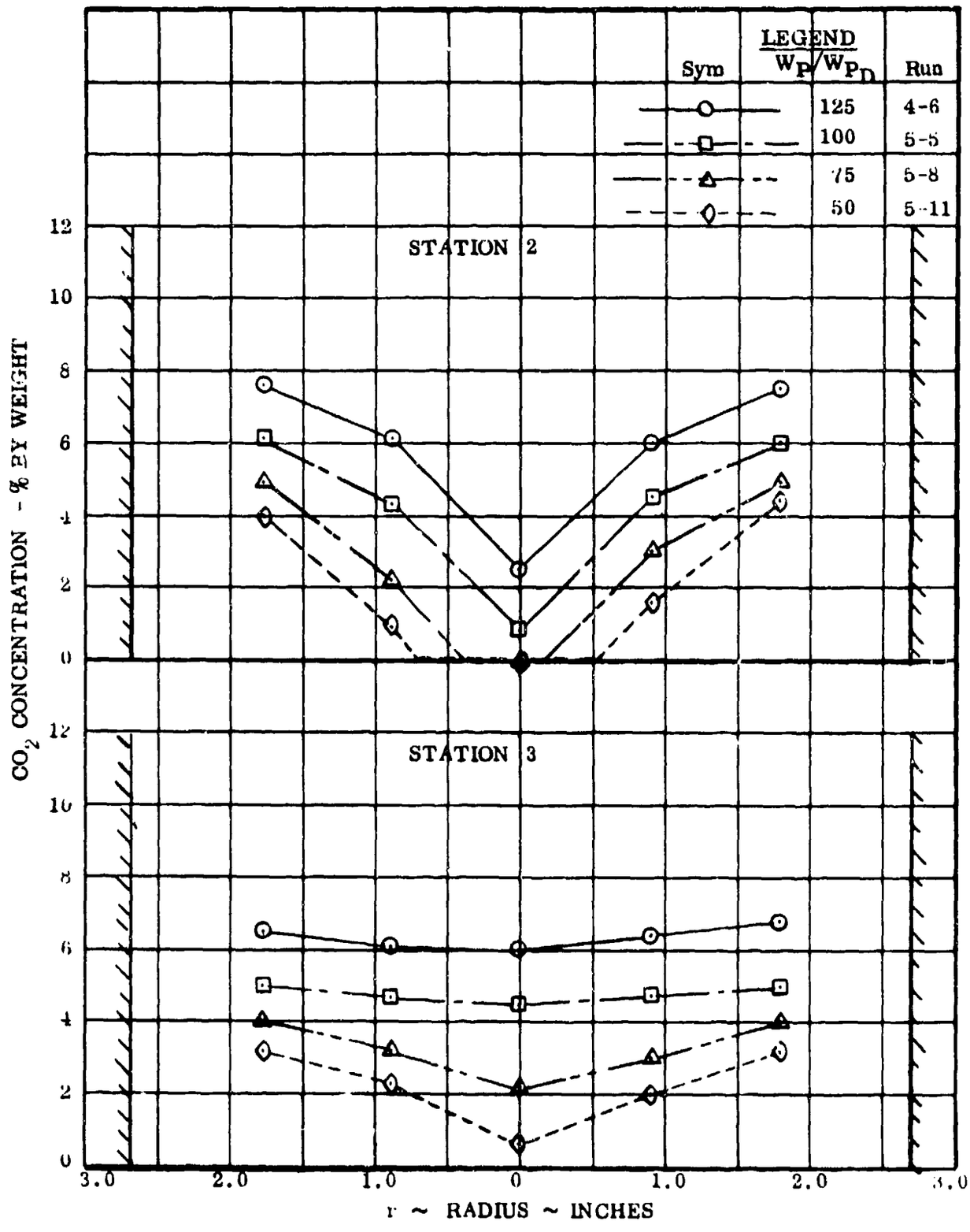

Figure 90. Effect of Primary Flow on CO_2 Concentration Distribution, W_S/W_{S_D} = 125%

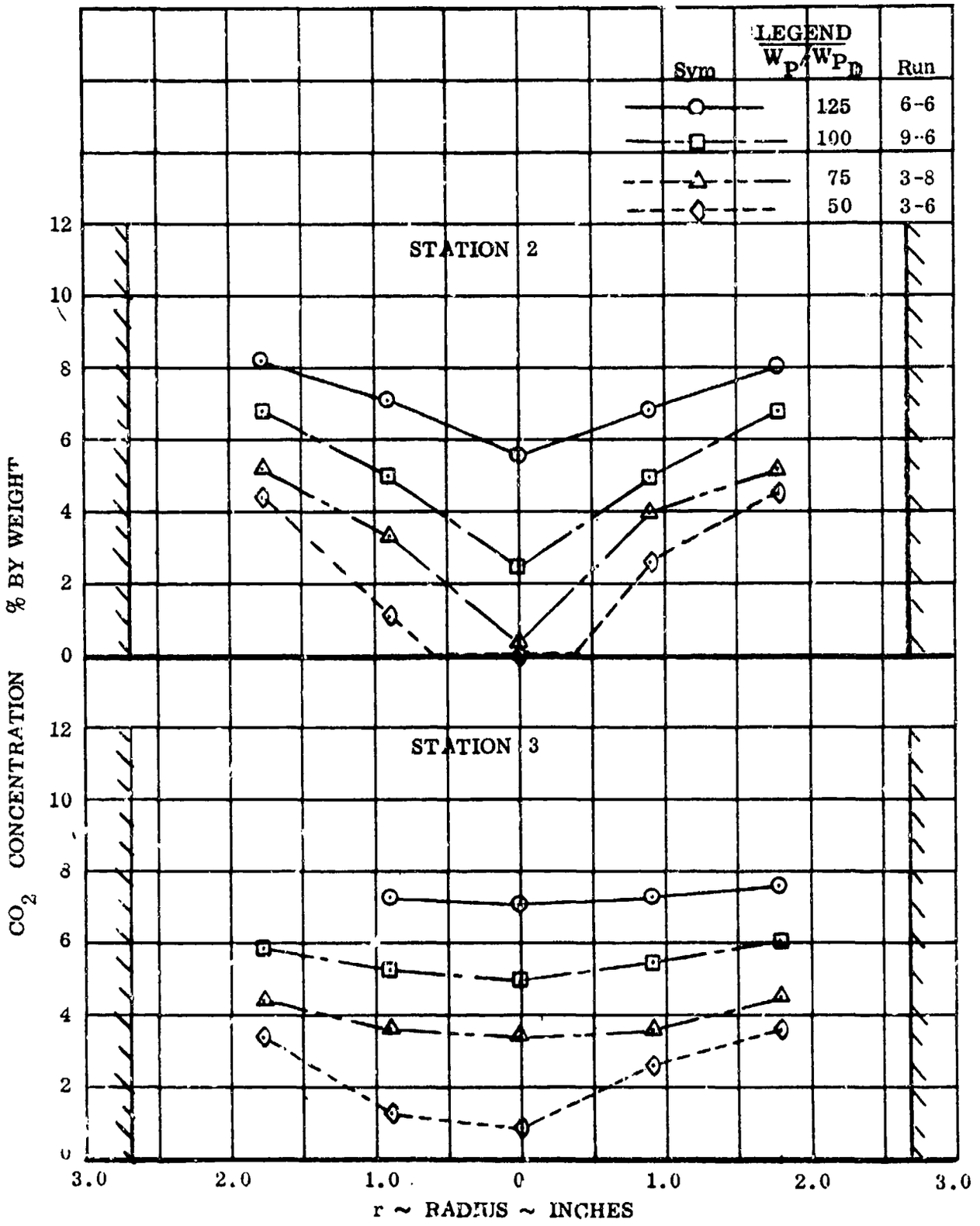

Figure 91. Effect of Primary Flow on CO_2 Concentration Distribution, W_S/W_{S_D} = 100%

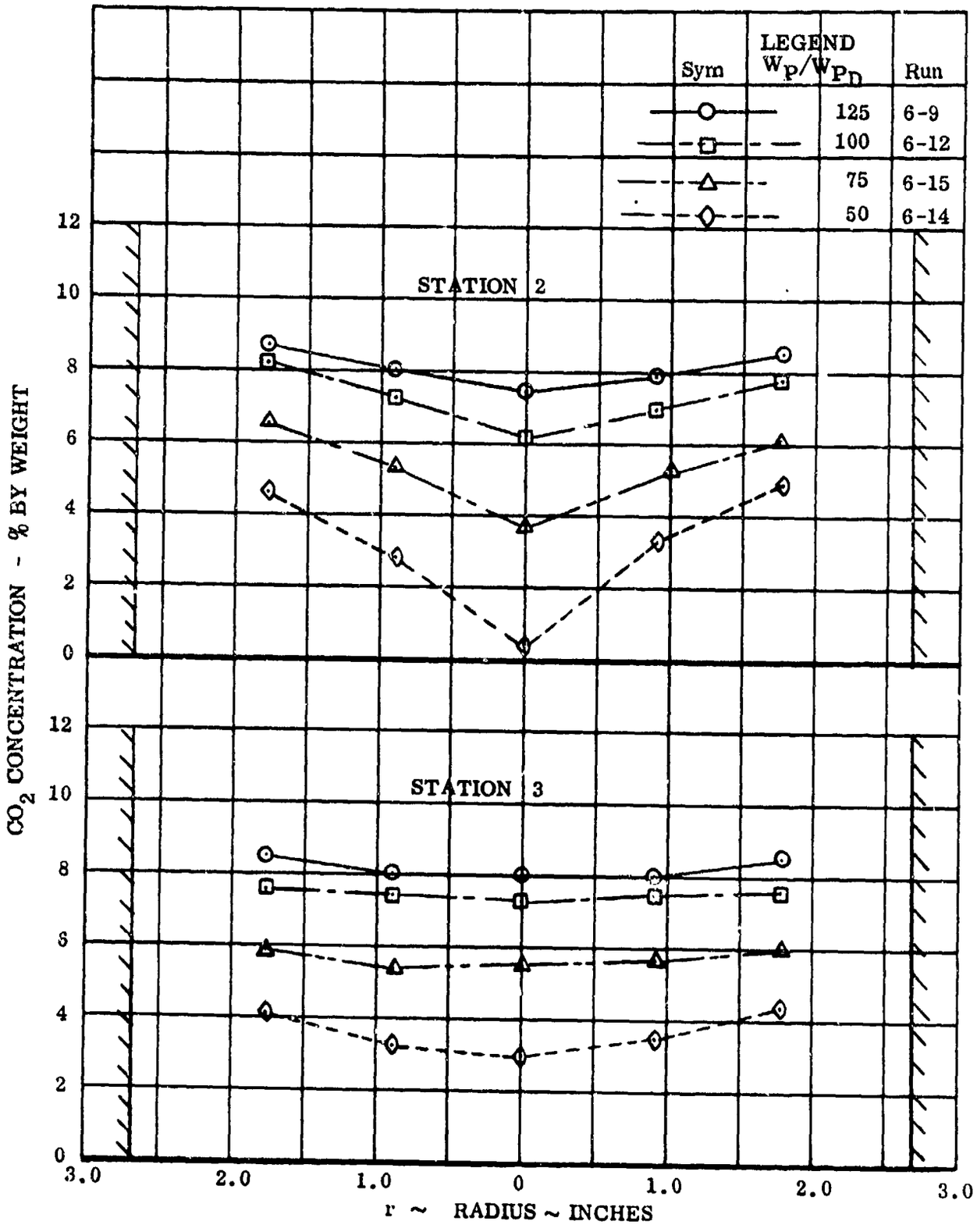

Figure 92. Effect of Primary Flow on CO_2 Concentration Distributions, W_S/W_{S_D} = 75%

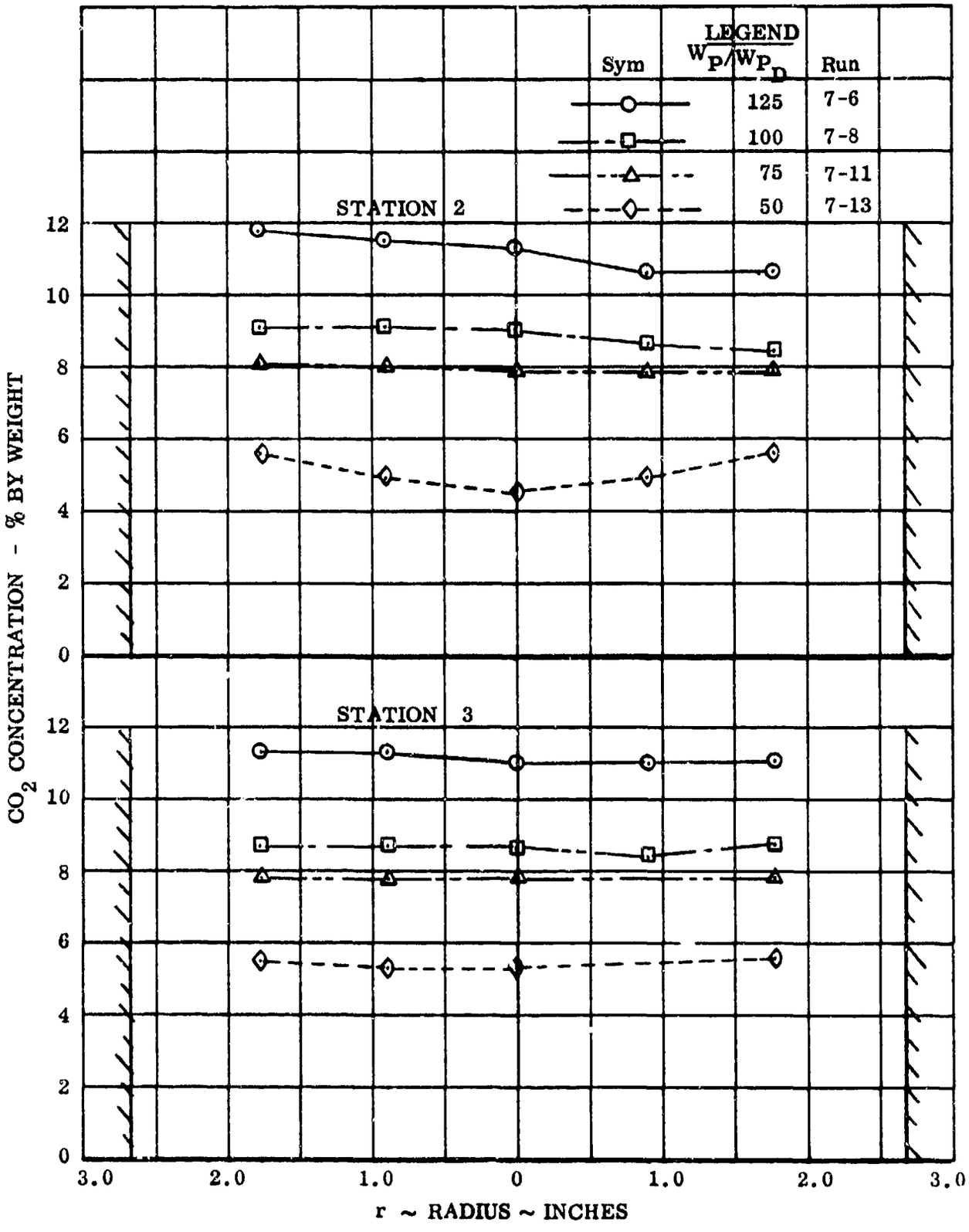

Figure 93. Effect of Primary Flow on CO_2 Concentration Distribution, W_S/W_{S_D} = 50%

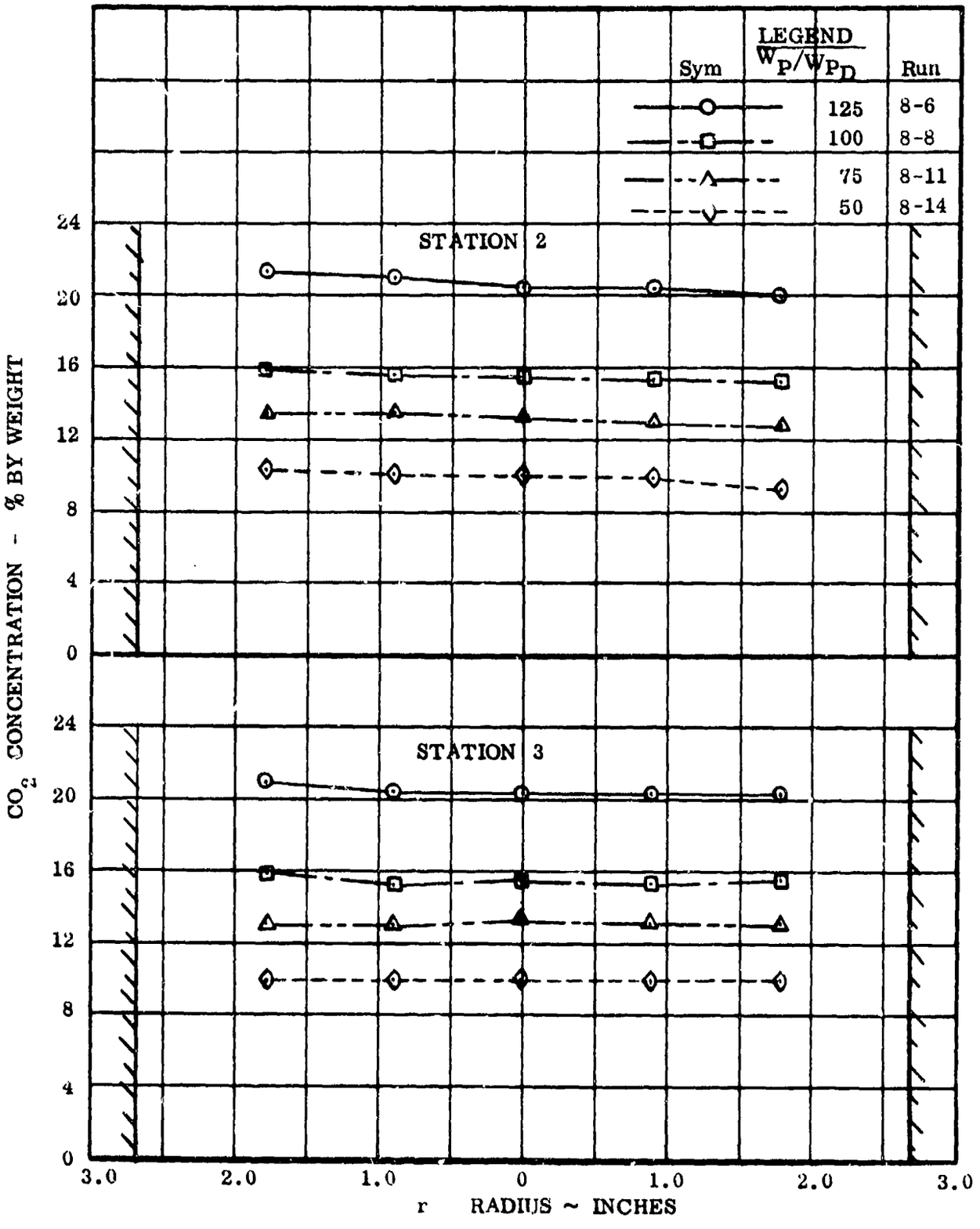

Figure 94. Effect of Primary Flow on CO_2 Concentration Distribution, W_S/W_{S_D} = 25%

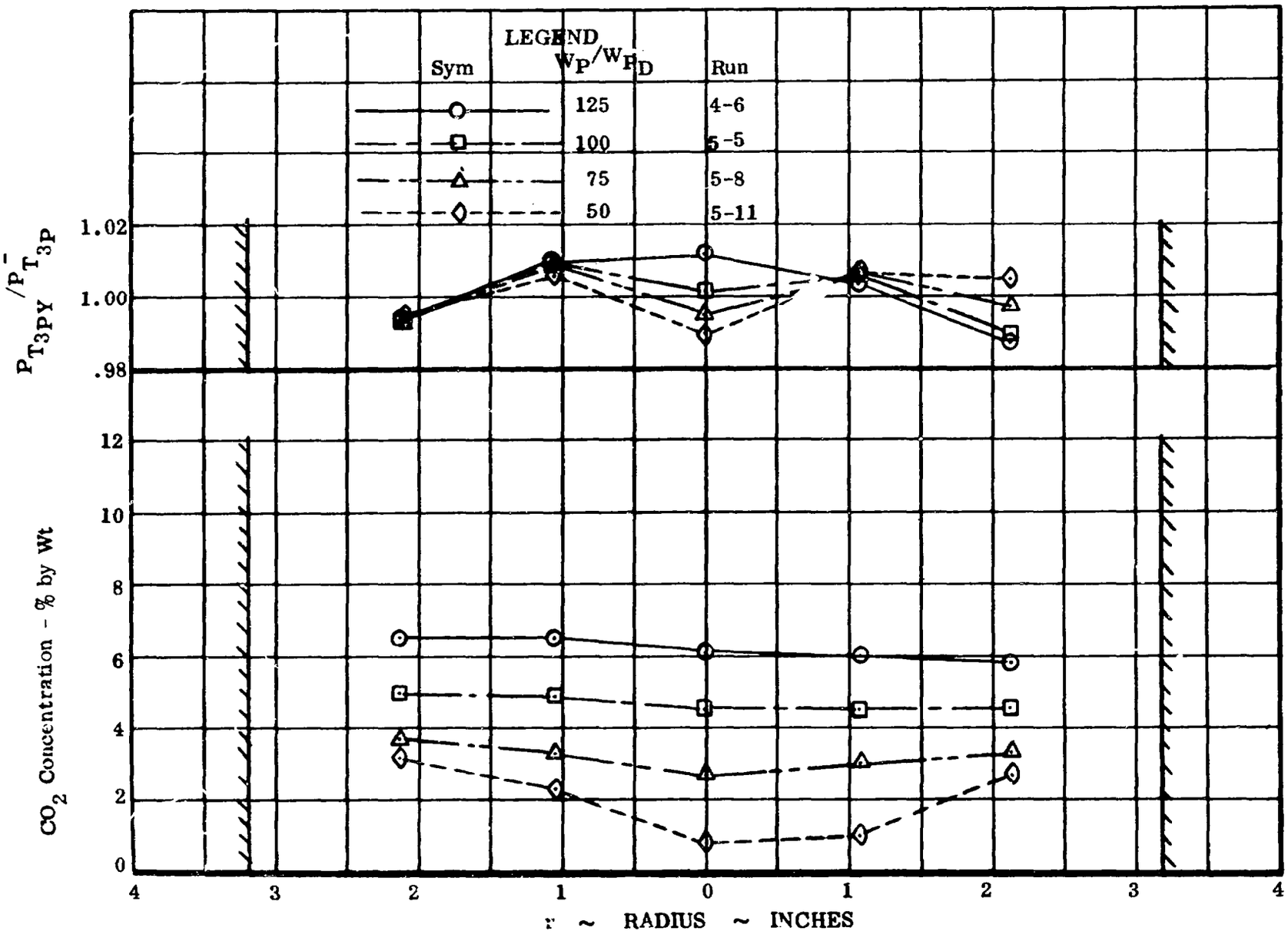

Figure 95. Diffuser Exit Total Pressure and CO_2 Concentration Distributions, W_S/W_{S_D} = 125%

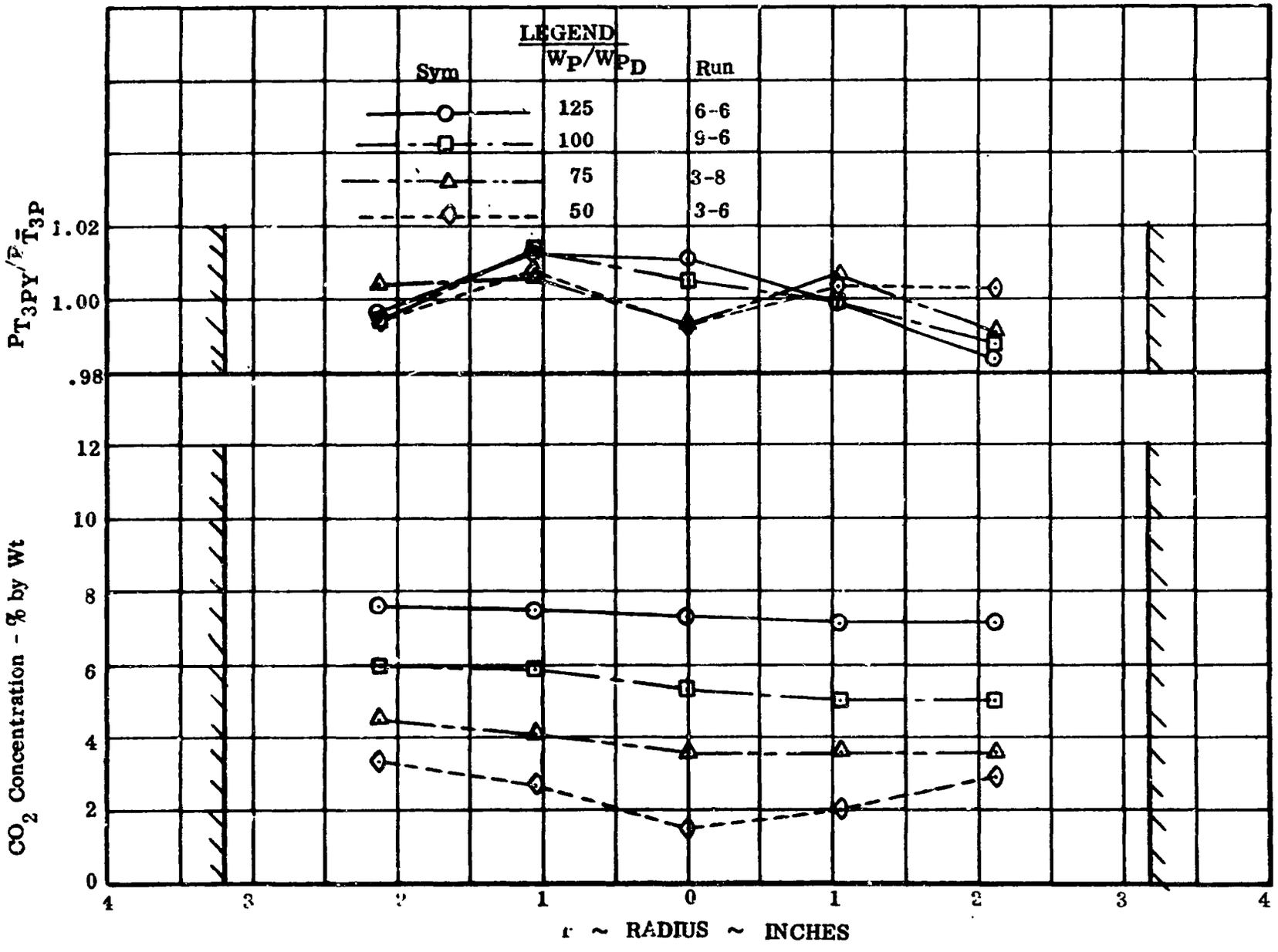

Figure 96. Diffuser Exit Total Pressure and CO_2 Concentration Distributions, W_S/W_{S_D}=100%

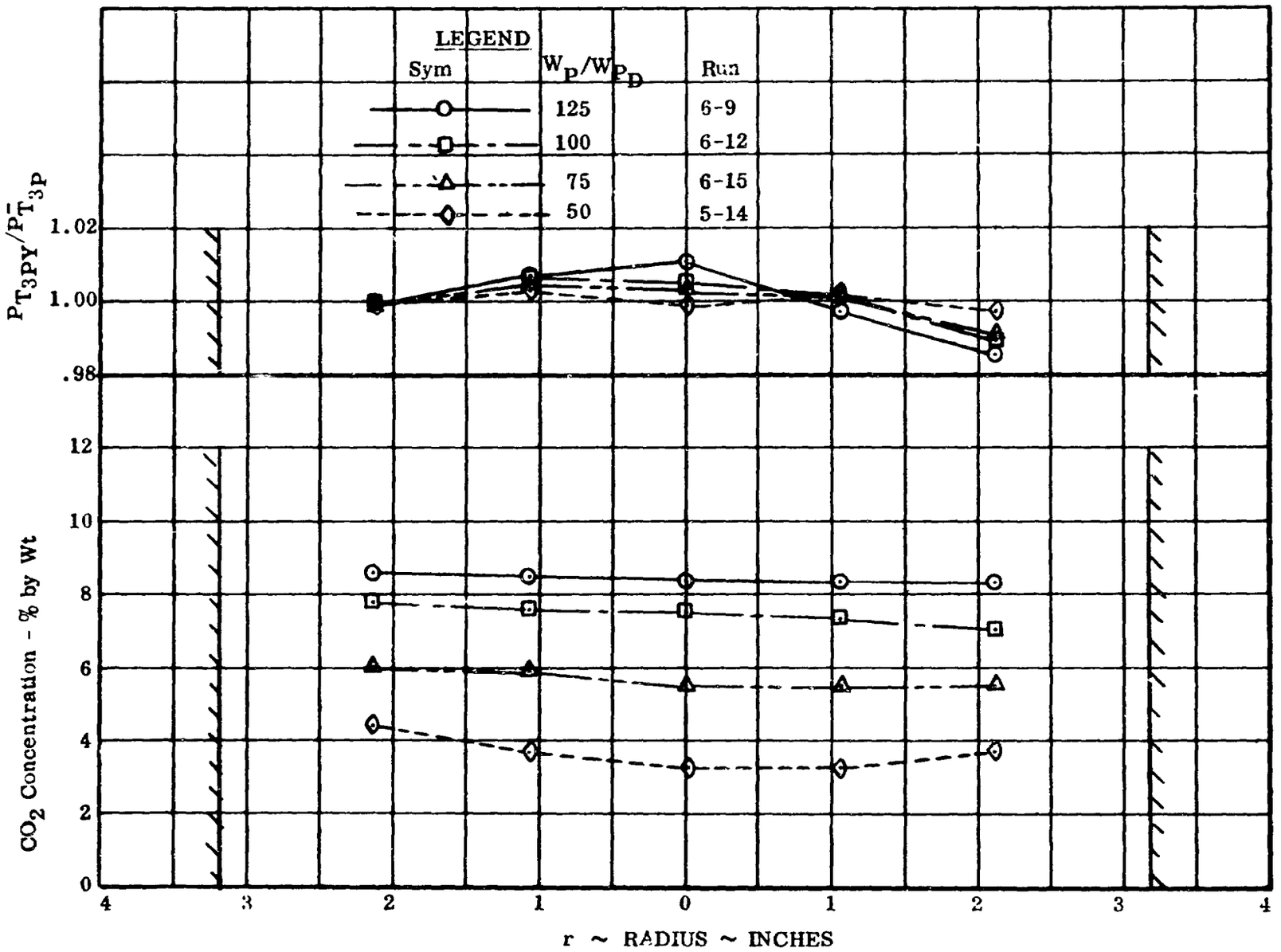

Figure 97. Diffuser Exit Total Pressure and CO_2 Concentration Distributions, W_S/W_{S_D}=75%

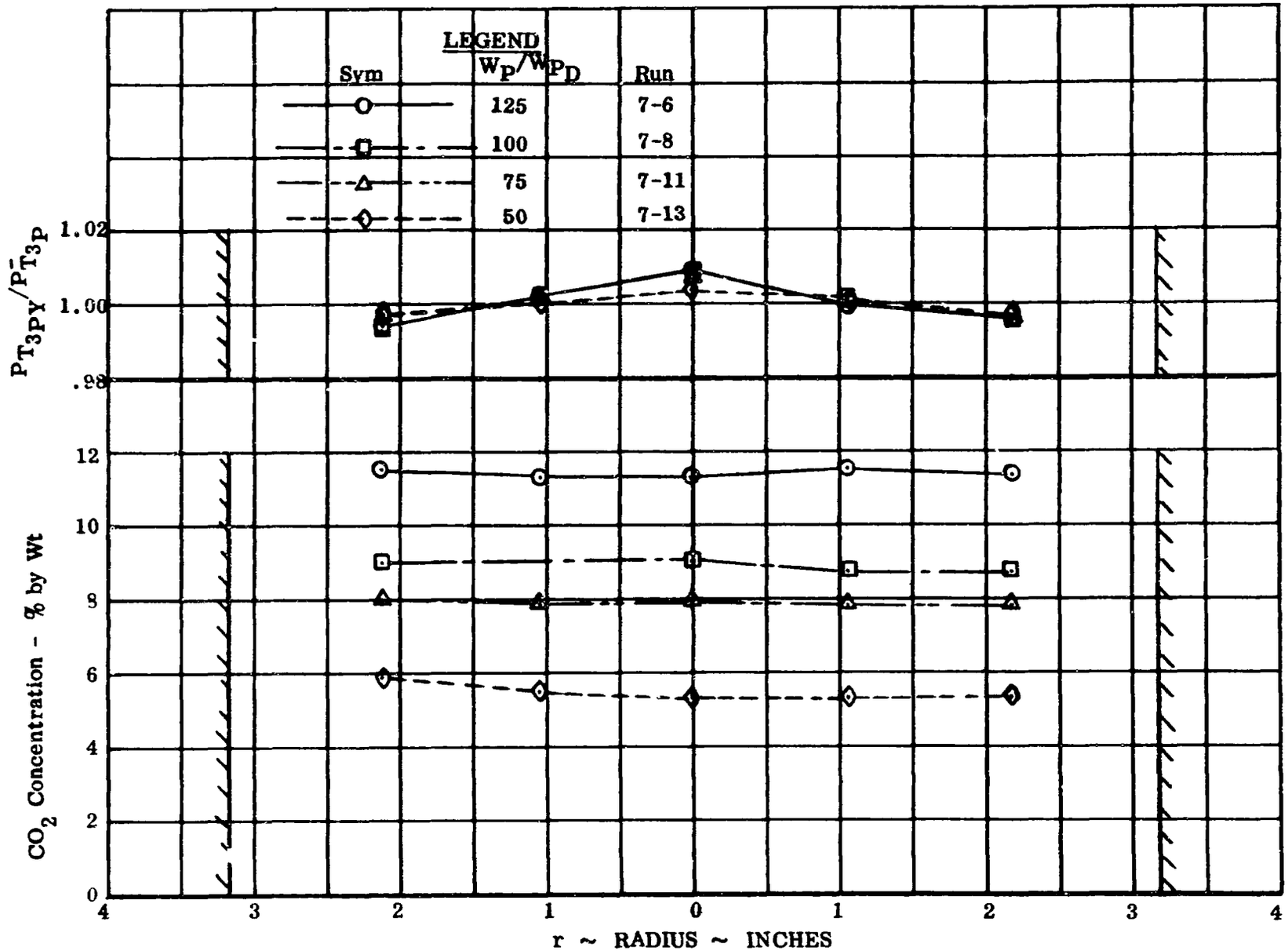

Figure 98. Diffuser Exit Total Pressure and CO_2 Concentration Distributions, W_S/W_{S_D} = 50%

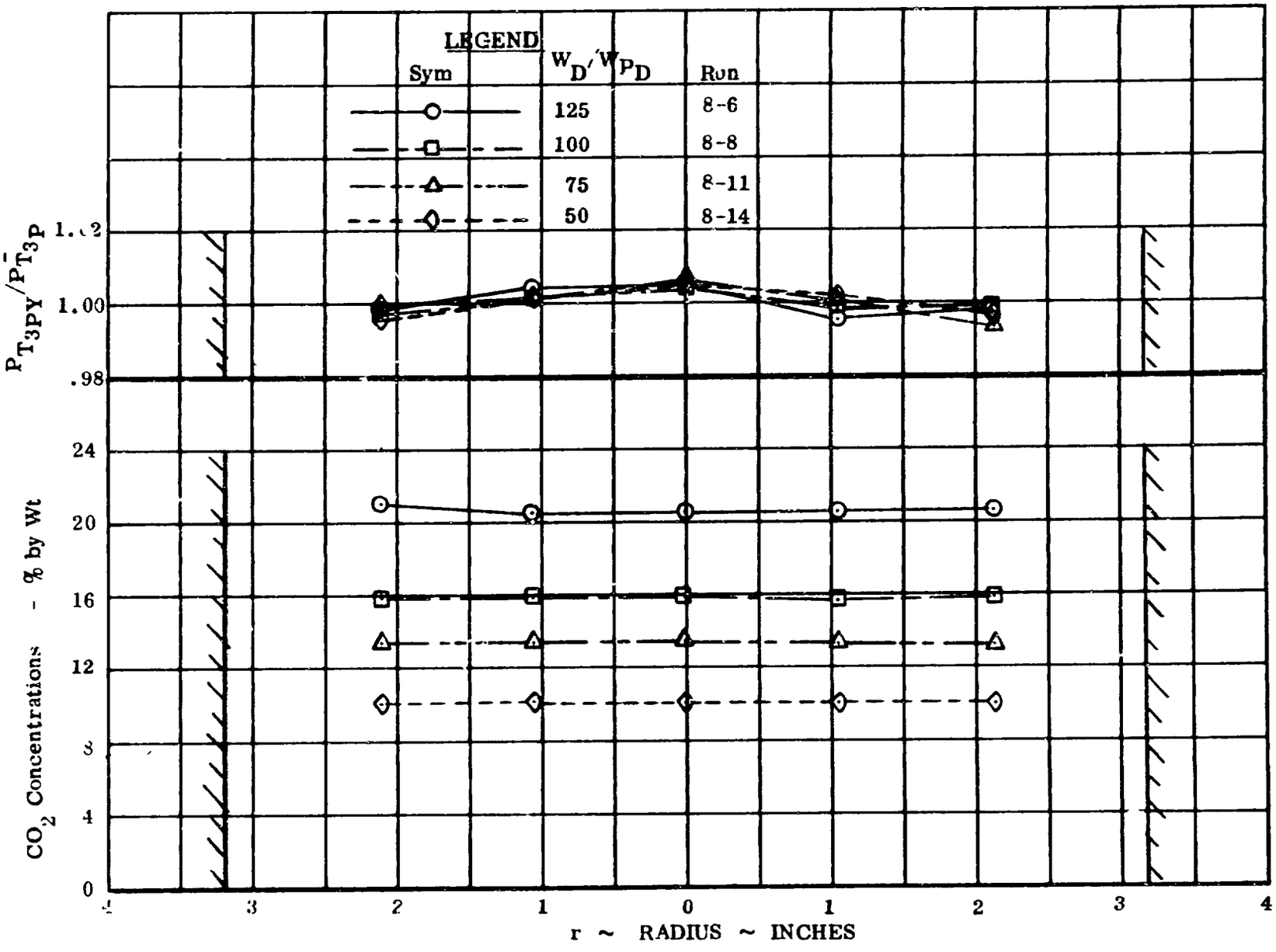

Figure 99. Diffuser Exit Total Pressure and CO_2 Concentration Distributions, W_S/W_{S_D} = 25%

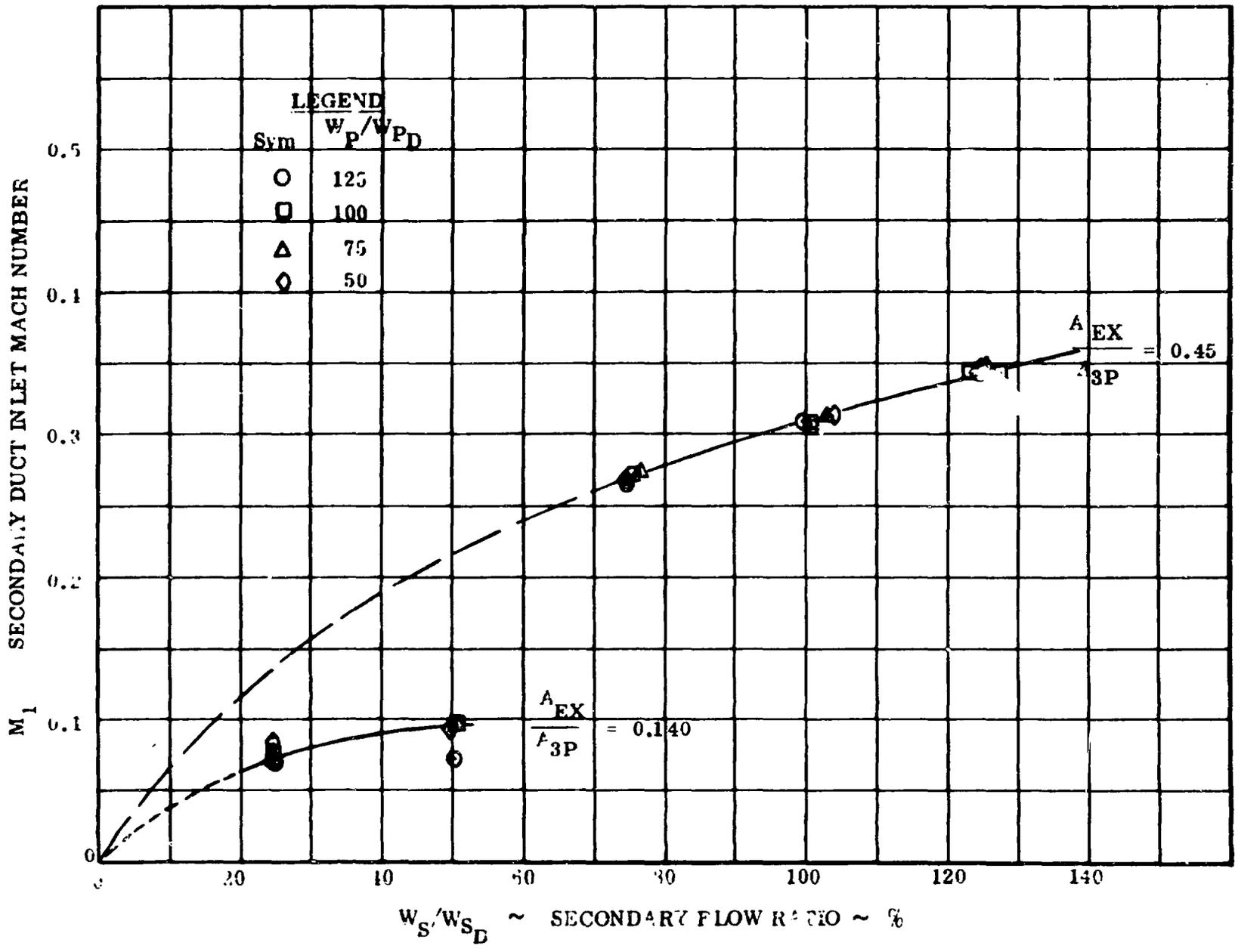

Figure 100. Ejector Inlet Mach Number Variation

APPENDIX C

TEST DATA

MODIFIED HYPERMIXING EJECTOR

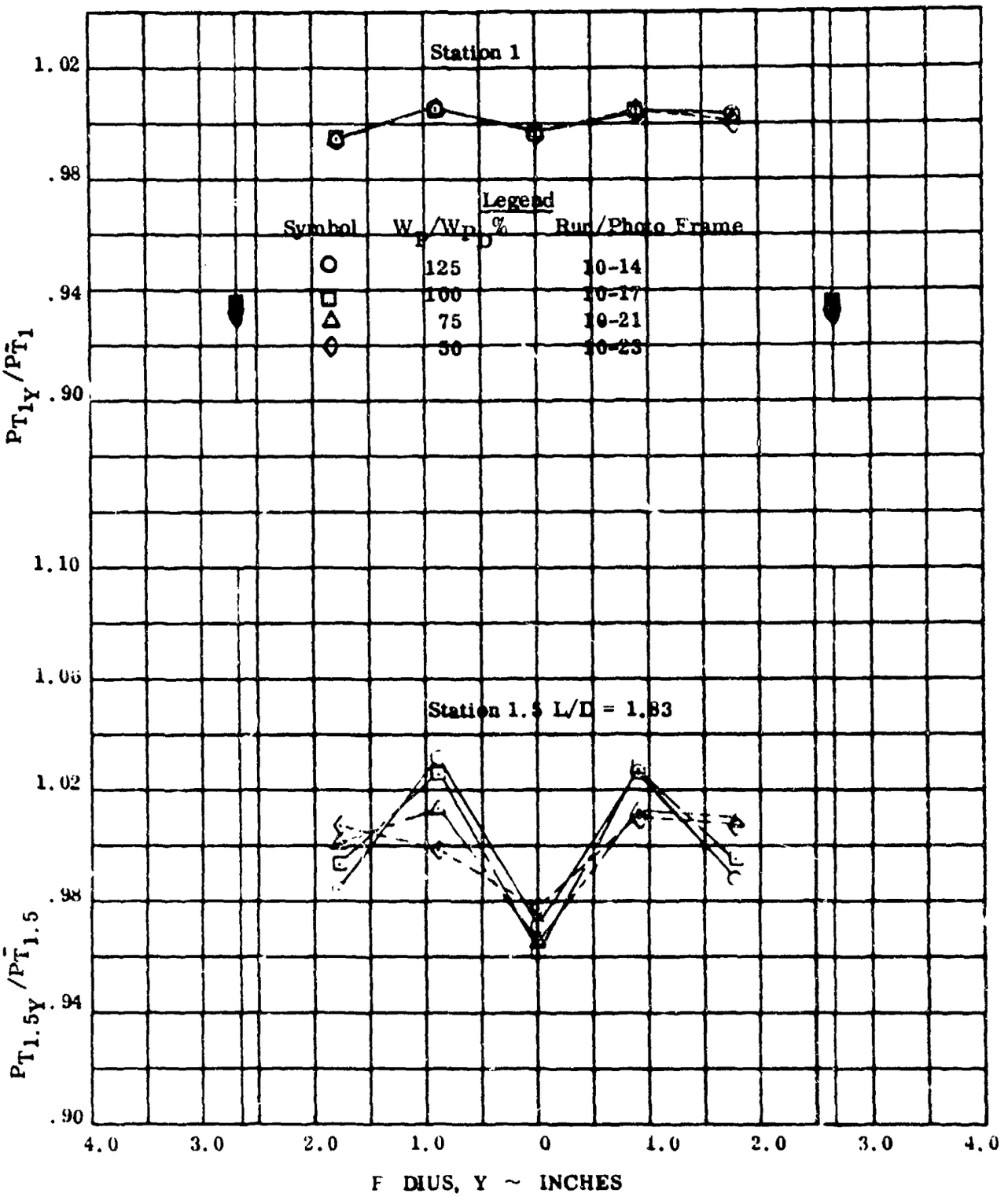

Figure 101. Effect of Primary Flow on Total Pressure Profiles, W_S/W_{S_D} = 100%

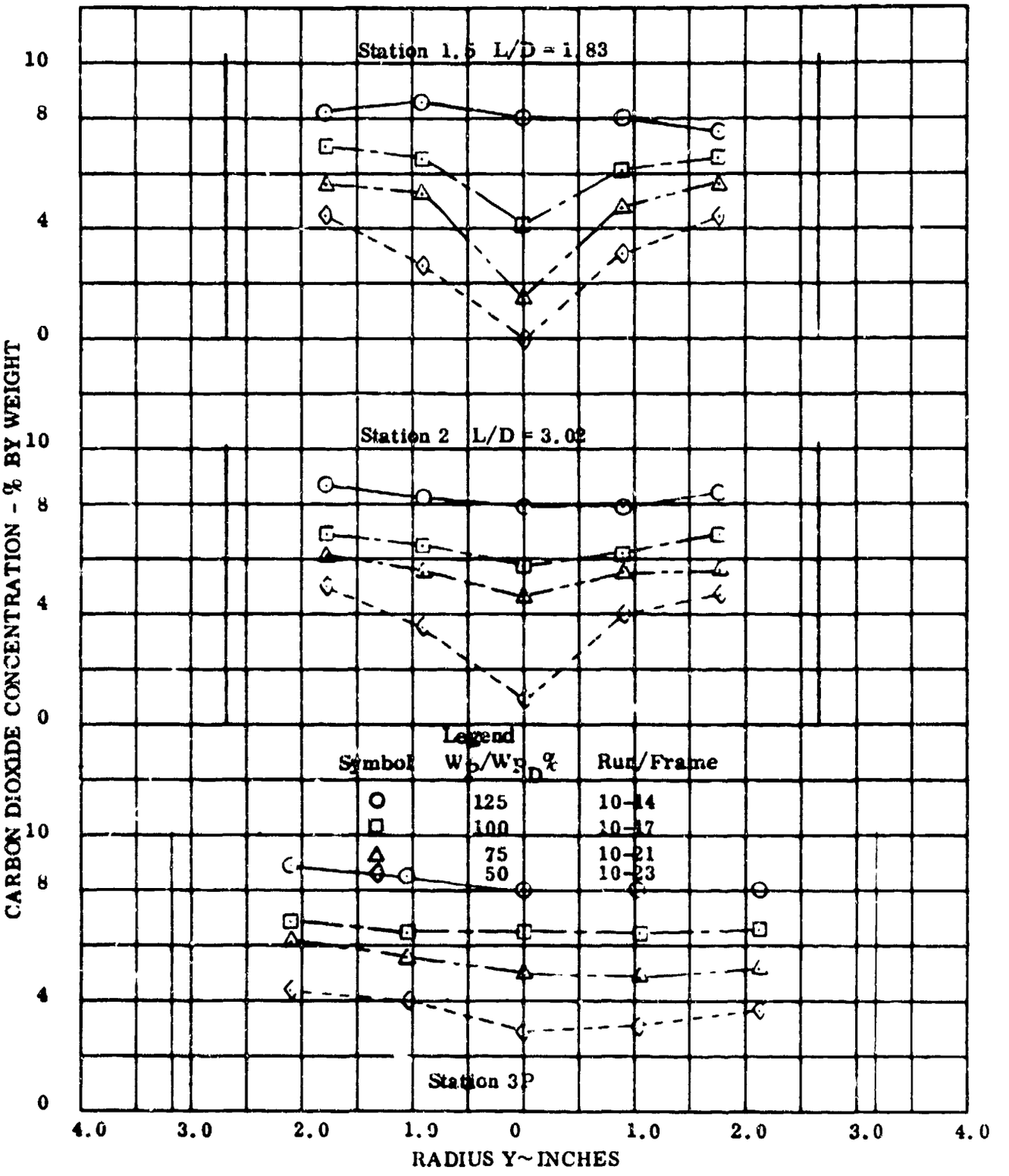

Figure 102. Effect of Primary Flow on CO_2 Concentration Distributions, $W_S/W_{S_D} = 100\%$

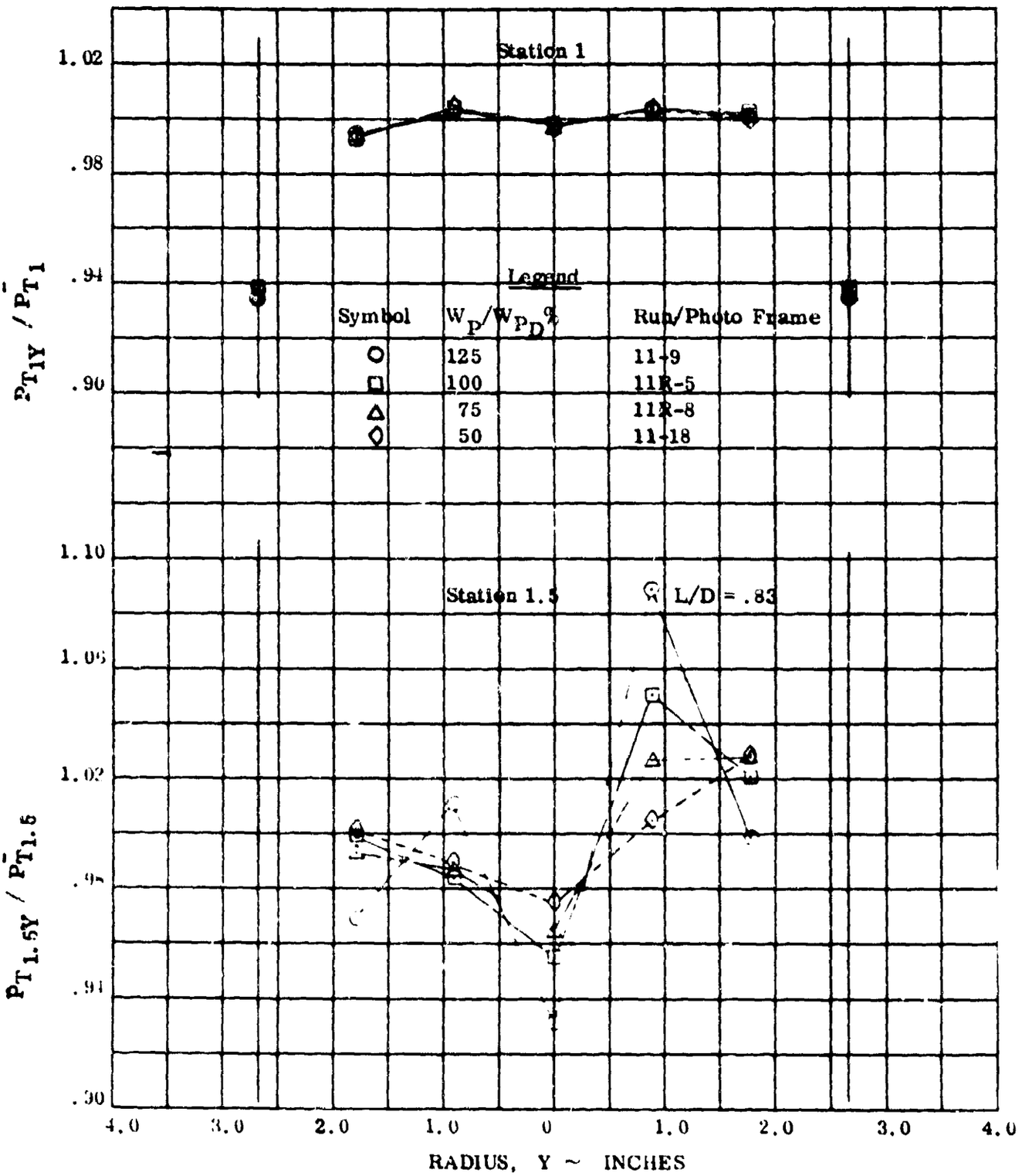

Figure 103. Effect of Primary Flow on Total Pressure Profiles, W_S/W_{S_D} = 100%

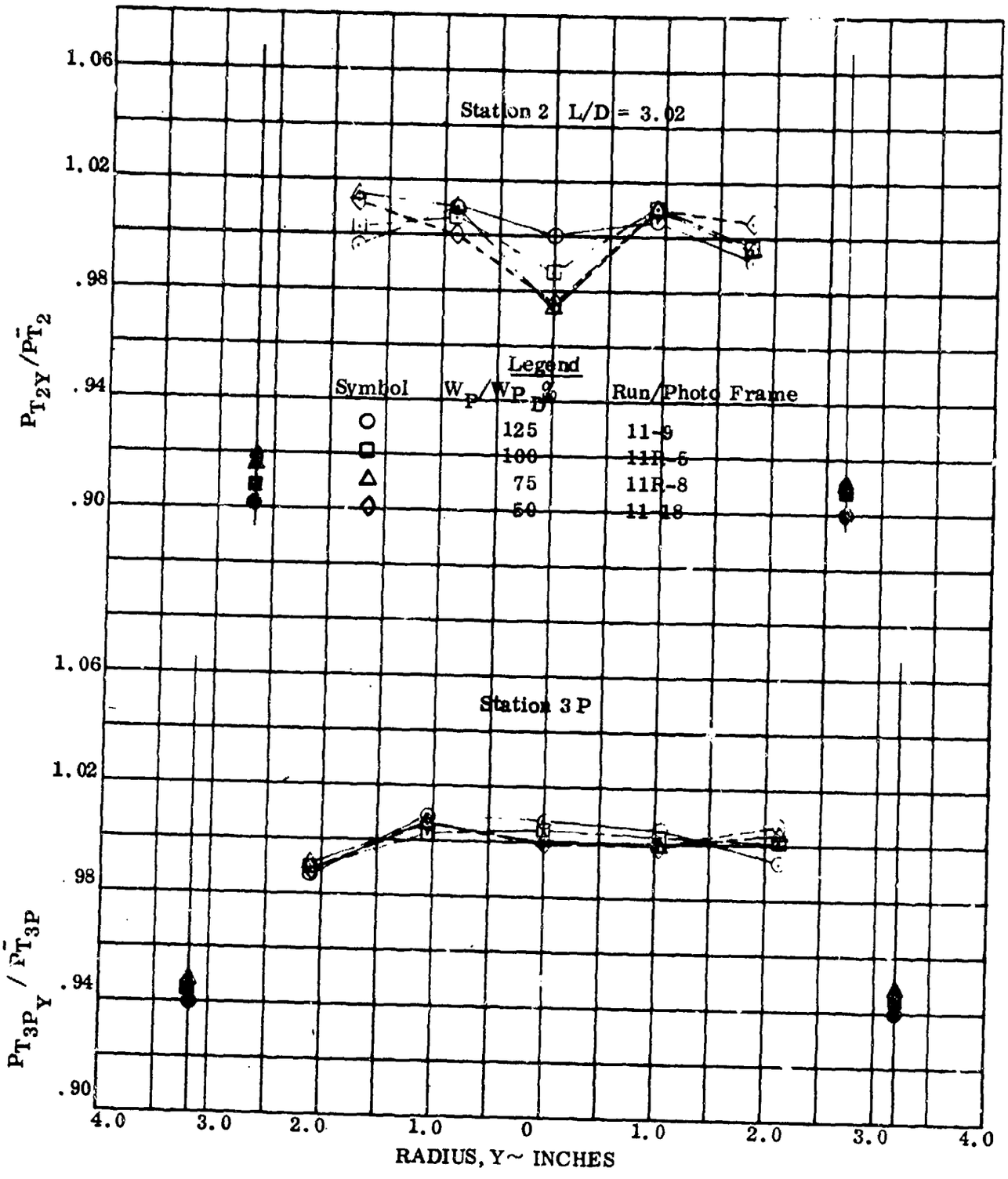

Figure 104. Effect of Primary Flow on Total Pressure Profiles, W_S/W_{S_D}=100%

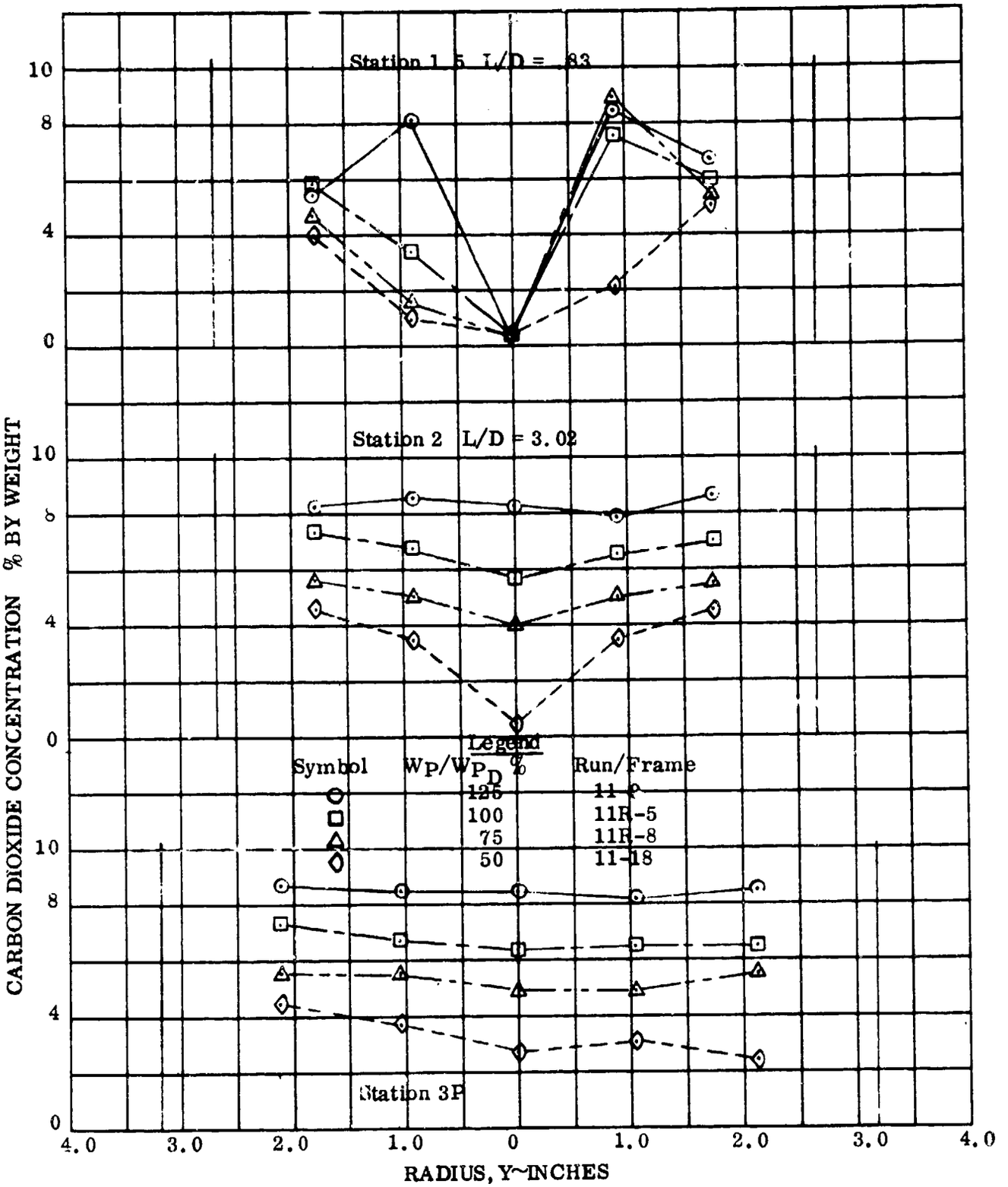

Figure 105. Effect of Primary Flow on CO_2 Concentration Distribution, W_S/W_{S_D}=100%

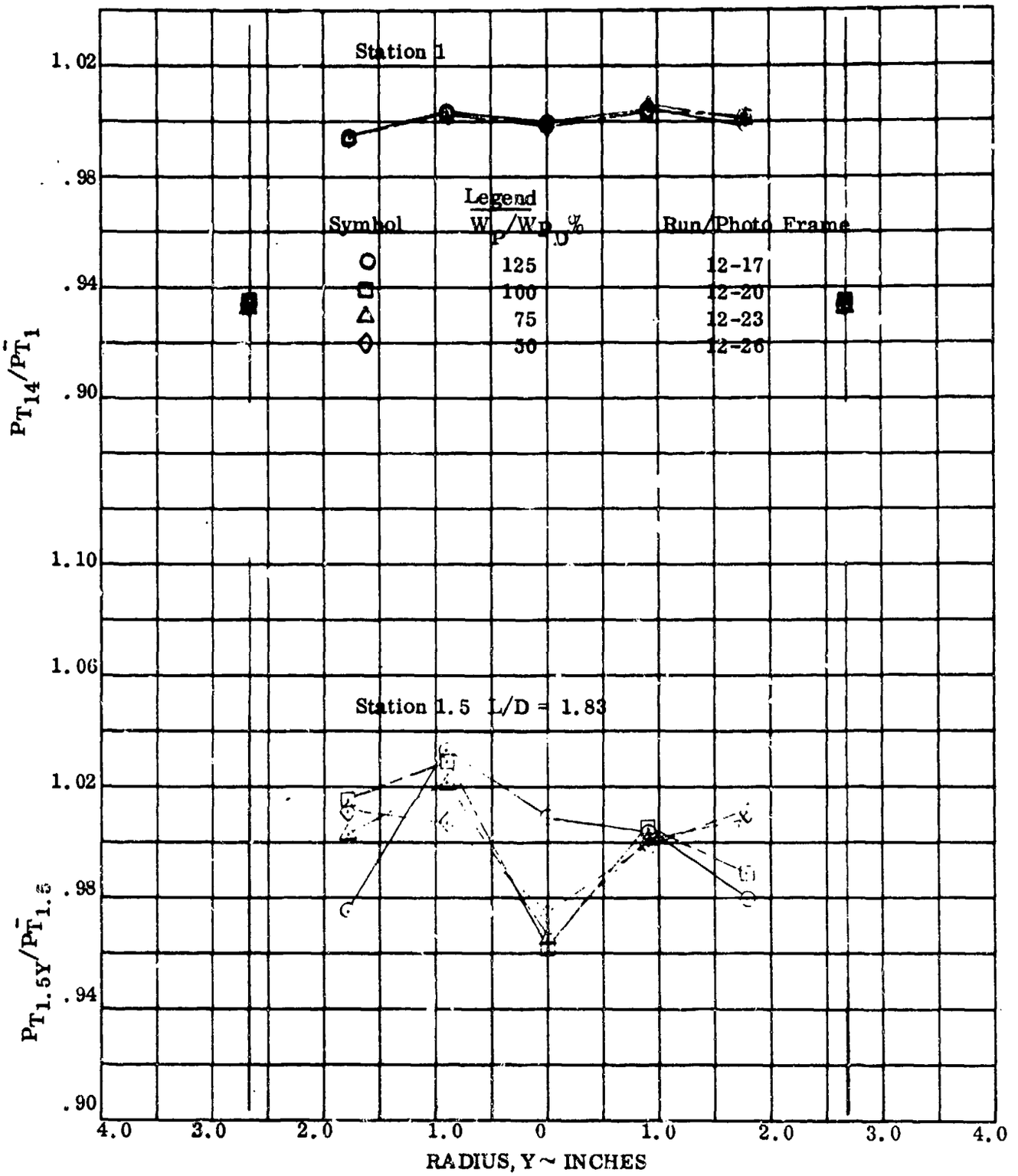

Figure 106. Effect of Primary Flow on Total Pressure Profiles, W_S/W_{S_D} = 100%

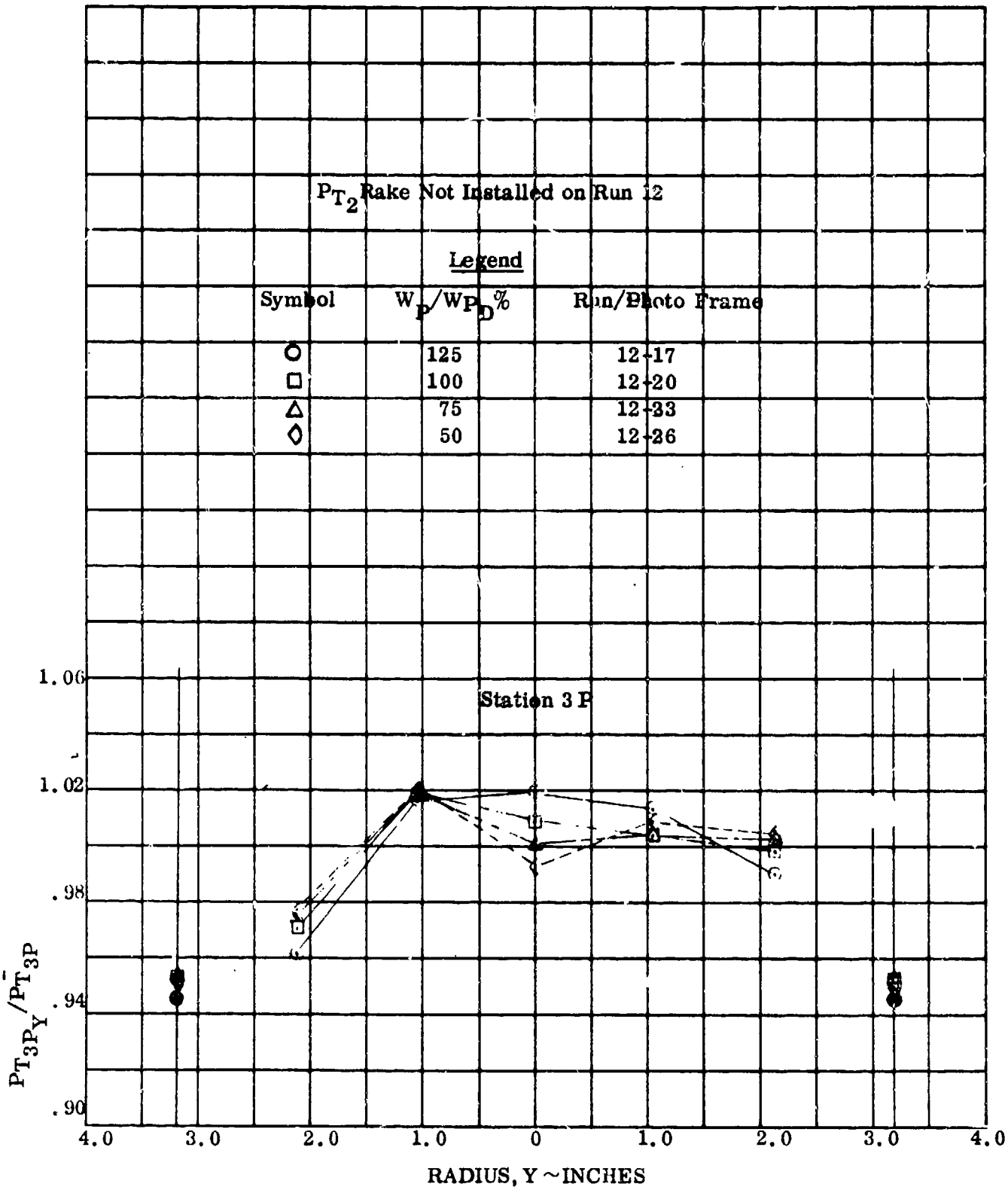

Figure 107. Effect of Primary Flow on Total Pressure Profiles, W_S/W_{S_D} = 100%

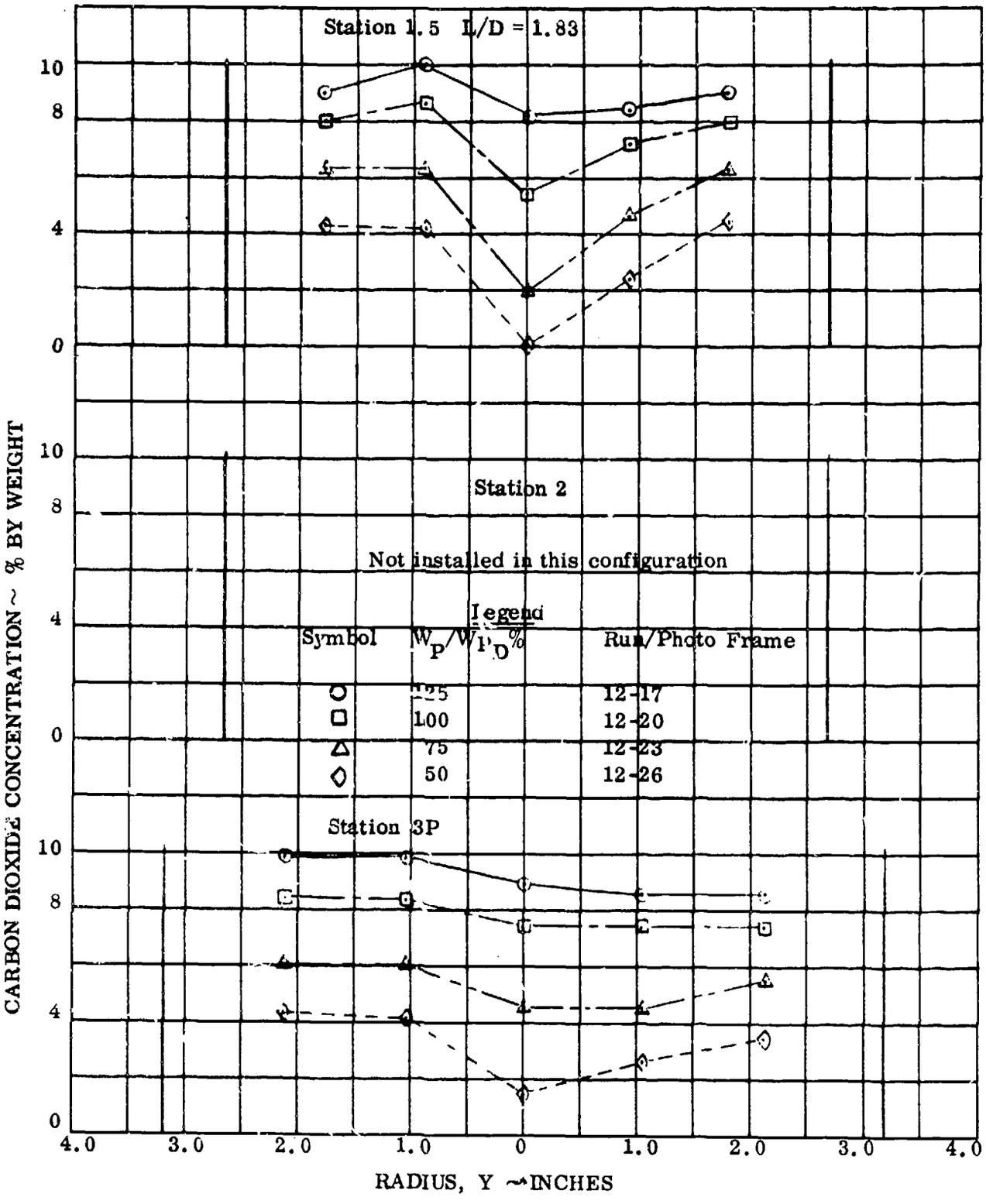

Figure 108. Effect of Primary Flow on CO_2 Concentration Distribution, W_S/W_{S_D}=100%

LIST OF SYMBOLS

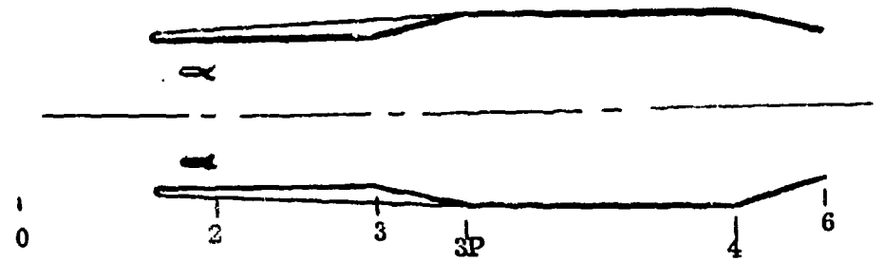

ENGINE STATION NOTATION

0	Freestream
2	Mixer Inlet
3	Mixer Outlet or Diffuser Inlet
3P	Diffuser Outlet
4	Combustor Outlet
6	Exit Nozzle Throat

NOMENCLATURE

A	Area; (A^* = Area at Mach 1.0)
a	Speed of sound
C_D	Flow discharge coefficient
C_p	Specific heat at constant pressure
D	Diameter; mixer divergence area ratio, $\left(\frac{A_3}{A_2+A_P}\right)$
F	Thrust
g	Gravitational constant
H	Enthalpy
h	Altitude
L	Length
M	Mach number
$C_{F_{NJ}}$	Net Jet Thrust Coefficient, $F/q_\infty A_4$

LIST OF SYMBOLS

P	Pressure
R	Gas constant
SFC	Specific fuel consumption
SPC	Specific propellant consumption
SLS	Sea level static conditions
T	Temperature
V	Velocity
W	Weight flow
W_S/W_P	Secondary to primary flow ratio
q_o	Freestream dynamic pressure, $\frac{1}{2} \rho_o V_o^2$
Greek Symbols	
γ	Ratio of specific heats
η	Component process efficiency
ρ	Density
ϕ	Fuel equivalence ratio
θ	Mixing process spread angle
Subscripts	
a	Air
A/B	Afterburner
C	Combustion
D	Drag
E	Exit
f	Fuel
g	Gas
M	Mixer
m	Mass
NJ	Net jet
P	Primary
S	Secondary
T	Total condition

☆ U S GOVERNMENT PRINTING OFFICE 1975—657 630/1